OFFICE OF INDUSTRIAL RESEARCH

TO STUDY-OF-THE-ART TECHNIQUES TO IMPROVE SIDELOBE CHARACTERISTICS OF SMALL EARTH-STATION REFLECTOR ANTENNAS

May 1982

OFFICE OF RESEARCH ADMINISTRATION

The University of Manitoba, Winnipeg, Manitoba, Canada R3T 2N2

TO STUDY-OF-THE-ART TECHNIQUES TO IMPROVE SIDELOBE CHARACTERISTICS OF SMALL EARTH-STATION REFLECTOR ANTENNAS

May 1982

TO STUDY STATE-OF-THE-ART TECHNIQUES TO IMPROVE SIDELOBE CHARACTERISTICS OF SMALL EARTH-STATION REFLECTOR ANTENNAS

DSS File No. 03SU.36001-1-3247
Contract Serial No. OSU81-00450

Submitted to

COMMUNICATION RESEARCH CENTRE

by

L. SHAFAI
Principal Investigator

O. ABOUL-ATTA
A. ITTIPIBOON
M. S. A. SANAD
A. A. M. SEBAK

May 1982

TABLE OF CONTENTS

		Page
I	SUMMARY	ii
II	INTRODUCTION	1
III	DESIGN CONSIDERATIONS	3
IV	COMMON SIDELOBE REDUCTION TECHNIQUES	7
V	FORMULATION OF SYMMETRIC REFLECTOR FIELD WITH CENTRAL AND STRUT BLOCKAGE	12
	(a) Unblocked Reflector	12
	(b) Aperture Blockage	15
	(c) Formulation of the Strut Blocking Equations	16
	(d) Central Blockage	21
	(e) Total Reflector Field	22
VI	COMPUTED PATTERNS FOR SYMMETRIC REFLECTOR	23
	(a) Reflector Performance with CRC Feed	23
	(b) Accurate Computation of Strut Scattering ($\cos^m\theta$ distribution)	25
VII	POSSIBLE TECHNIQUES FOR SIDELOBE REDUCTION	35
	(a) Aperture Field Phase Shifting	36
	(b) Dielectric Loading of Struts	38
	(c) Non-circular Strut Cross-Sections	41
	(d) Non-metallic Struts	43
VIII	ANTENNA NOISE TEMPERATURE	44
IX	OFFSET PARABOLIC REFLECTOR ANTENNA	48
	(a) The Mathematical Model	49
	(b) Depolarization Performance of Offset Reflector Antennas	50
	(c) Sidelobes of Offset Reflectors	51
X	PERFORMANCE OF REFLECTOR ANTENNAS WITH A CIRCULARLY POLARIZED FEED	56
	(a) Axisymmetric Reflector	56
	(b) Offset Reflector	57
XI	CONCLUSIONS AND RECOMMENDATIONS FOR FUTURE WORK	59
REFERENCES		62

I SUMMARY

The objectives of this work was to study the performance of both symmetric and offset reflectors with aperture blockage and recommend possible methods for sidelobe reduction. The statement of the contract work, required the performance study within 500 MHz band for reflector of 0.6 m to 1.8 m aperture diameters. Our study indicates that the variation of the patterns within the band is small and the provided data give an adequate understanding of the problem. Furthermore, the generation of data for requested range means an excessive computation, which would not provided additional information. Thus, we have provided representative data to indicate the performance of both reflectors adequately.

Initially, mathematical models are established, that enables us to compute the radiation patterns of both symmetric and offset reflectors. The blockage effects are also modelled by selecting circular strut cross-sections. Computed patterns are then provided for both CRC feed and $\cos^m\theta$ feed patterns. For CRC feed both plane wave and spherical shadowing are considered and the performance of the symmetric reflector is studied. It is shown that the effect of the blockage is most severe for a tapered illumination and the sidelobe levels of a symmetric reflector is generally high due to central and strut blockage. However, by selecting small strut diameters sidelobe levels of in order of -30 dB can be obtained.

Various possible methods for reducing the sidelobes of a symmetric reflector are then studied. One method which promises good performance

is recommended. It involves loading the reflector surface by narrow strips of appropriate thickness, just under each strut. The physical optics current were used to calculate the performance of the loaded reflectors. It is shown that, within this modelling accuracy, the reflector gain can be increased and the sidelobe levels can be reduced even below those of the unblocked reflector. It was then recommended that this method be verified by experiment.

The offset reflector is also studied. It is shown that its cross-polar and sidelobe levels can be reduced by proper selection of the reflector parameters and the feed taper. Since this geometry does not suffer from feed and the strut blockage, it can be designed to have a super-sidelobe level patterns and a good cross-polar performance.

The performance of both reflectors with a circularly polarized feed is also studied. In general, this performance for the co-polar radiation is the same for both linear and the circular polarization. However, the cross-polar radiation due to a circularly symmetric feed is higher for the symmetric reflector. The offset reflector does not produce a cross-polar radiation, but squints the beam. For the selected reflector parameters the beam squint is shown to be negligible.

II INTRODUCTION

For small earth-station antennas, the front-fed paraboloid is a distinctly economic choice. This system consists of a paraboloidal reflector with a feed system located at its focal point. The most common system is the symmetric paraboloid, which is normally selected due to the ease of fabrication of the reflector and low cross polarization of the radiated field. In this configuration, however, the feed must be supported by struts, which cause shadowing effect on the reflector. In an alternative system the reflector consists of an offset paraboloid. While its fabrication is, normally, more difficult than a symmetric one, its feed can be supported by struts away from the reflector aperture and consequently does not suffer from the blockage effects.

Neglecting the blockage effects, the performance of front-fed symmetric paraboloids depends entirely on the feed system. The feed performance, therefore, dictates the performance of the antenna system with a symmetric paraboloid. With an offset system, however, the reflector parameters, such as its offset angle and f/D affect the antenna gain and its cross-polar radiation. In general, the performance of an aperture antenna depends on the aperture field distribution. In the case of a symmetric paraboloid this aperture distribution is determined by the radiation field of the feed, but for an offset reflector the asymmetry of the reflector also affects the aperture field. With a symmetric feed radiation pattern, the aperture field of an offset reflector is therefore asymmetrical and results in an inherent

cross-polar radiation level. To compensate for this reflector effect the primary feed radiation pattern must therefore be asymmetric.

In this report we intend to study the performance of both symmetric and offset front-fed reflectors. The case of an offset reflector is simpler, since it involves only the reflector and the feed systems. In the case of symmetric paraboloids, however, the feed and its support structure decide on the system performance. Investigation of the reflector performance with a given feed primary pattern is again simple and have been studied extensively. The effects of the support structures on the reflector pattern is, on the other hand, much more difficult to analyze. Thus, although a symmetric reflector is simpler and more economic to fabricate, the evaluation of its performance is normally not very accurate.

The case of a symmetric paraboloid will be studied first. Following a brief literature review, we will formulate the radiation from a symmetric reflector including all blockage effects. For different support structures we will then study the system performance to evaluate the antenna gain and its pattern sidelobe levels. The possibility of reducing the pattern sidelobe levels will be considered next. The performance of the system with non-metallic struts will also be studied. The gain and sidelobe levels of an offset reflector will be considered in a separate section and its advantage and disadvantages over a symmetric reflector will be discussed. The report will be concluded with a discussion of the results and recommendations for future work.

III DESIGN CONSIDERATIONS

In design of both symmetric and offset paraboloids the main objectives are: high efficiency, low sidelobe levels, low cross-polarization and pattern control. While in an offset reflector these objectives can be controlled by a proper selection of the reflector parameters and the feed design, in a symmetric system the effect of the central and the strut blockage must also be considered. In this section we will discuss these design objectives briefly and will point out the main parameters affecting them.

High Efficiency: Parameters affecting the efficiency of a reflector antenna are: the aperture distribution, the spillover power of the feed, the edge diffraction, the cross-polarization and the feed and strut blockage. Ideally, a uniform aperture distribution gives the highest aperture efficiency. However, a uniform aperture distribution results in an excessive spillover power and high edge diffractions at the reflector rim. A practical feed, therefore, must generate a quasi-uniform aperture distribution with sharp signal drop near the edge of the reflector. Also, in a symmetric reflector to reduce the cross-polar radiation the primary feed pattern must be a rotationally symmetric one. In an offset reflector it must have a certain degree of asymmetry to compensate the asymmetry generated by the reflector. It will be shown later that by selecting a proper reflector geometry this requirement can normally be removed and a low cross-polar feed can also be used for an offset reflector. In summary, a highly efficient front-fed paraboloid can be designed by a proper design of the feed system.

Low Cross-polarization: Although in a symmetric reflector the cross-polarization can be controlled by the feed design, the overall system cross-polarization depends on the feed support blockage. The scattering by the struts causes the cross-polarization, which in general will depend on the configuration of the struts and their cross-sectional geometry. In general, both feed design and the strut geometry must be considered in the cross-polar performance of the system. In the offset system the combined effect of the feed and the reflector geometry affects the cross-polar performance and both effects must be considered.

Pattern Control: In a front-fed paraboloid the control of both near-in sidelobes and far-out sidelobes is the most essential design objective. The near-in sidelobes depend on the aperture distribution and the strut blockage. Both parameters must be considered in a symmetric reflector, but in an offset system the aperture field distribution is the only deciding parameter.

Near-in Sidelobes: The aperture efficiency and the sidelobe levels of different aperture distributions have been studied by many investigators, and a good description of the topic can be found in reference [1]. However, for practical feeds the aperture field due to the primary patterns can be approximated by [2]

$$E^{ap}(\alpha) = \cos\left[\frac{\alpha-\alpha_1}{1-\alpha_1}\cos^{-1}C\right], \quad \alpha_1<\alpha<1$$

$$= 1 \qquad\qquad 0<\alpha<\alpha_1$$

Where C is a constant defining the edge illumination (C_{db} = 20 log C) and α is the distance on the aperture. For various values of α_1 and the edge illumination the expected aperture efficiency and the first sidelobe levels are shown in Figure (1). Since for larger values of α_1, the aperture illumination is closer to uniform aperture distribution the expected aperture efficiencies approach 100% with increasing value of α_1. On the other hand, the sidelobe levels increases with α_1, approaching the level of -17.6 dB for a uniform distribution.

The effect of the aperture blockage is normally difficult to generalize, but normally reduces the aperture efficiency and increases the sidelobe level. In general, the effect of the aperture blockage is most severe for lower edge illuminations. Figure (2) shows the effect of the central blockage on the sidelobe levels. It is evident that, the percentage of blocked area is the deciding parameter on the sidelobe level. However, the most important information to note is that, for a blocked aperture the level of the sidelobes depend predominantly on the percentage blocking, rather than the initial edge illumination: that is, the effect of aperture blockage is smaller for higher edge illuminations and larger for lower edge illuminations. This means that in a symmetric reflector lowering the edge illumination may not result in a lower sidelobe level. This is an important property, since lowering the edge illumination reduces the aperture efficiency and for a symmetric reflector may not result in a lower sidelobe level. In practice a compromize must be made between the aperture efficiency of the antenna and its sidelobe level.

Far-out Sidelobes: The far-out sidelobes of a reflector depend on the edge diffracted field, the scattering field of the struts and the spillover power of the feed. While both spillover power of the feed and the edge diffraction effects can be controlled by the feed design, the strut scattering depends primarily on the strut geometry. Normally, the total scattered power by the struts cannot be eliminated, but to reduce the far sidelobe levels one may distribute the scattered power over a wide angular region. This may be achieved by forming the strut shape to scatter the aperture blockage field at different directions, from different sections of the strut.

IV COMMON SIDELOBE REDUCTION TECHNIQUES

Reduction of sidelobe levels in a reflector antenna have been the object of many investigations for reduction of interference and the antenna noise temperature. The problem has received an accelerated attention in recent years, with the use of geostationary satellites for point-to-point communication. However, the material in open literature is scarce and the existing techniques seldom provide satifisfactory degree of sidelobe level reduction. In this section, we intend to review commonly used techniques to improve the sidelobe levels of small earth station antennas.

Generally, the technique can be divided into two categories: techniques for reduction of near-in sidelobes and those for improving far-out sidelobes.

Near-in sidelobes: The most common method to lower the level of near-in sidelobes of a reflector antenna is the reduction of the edge illumination of the reflector using heavily tapered aperture illuminations. This method transfers the sidelobe problem back to the design to the reflector feed. Although, it is the most effective means of sidelobe control, it is most useful for an offset reflector with no aperture blockage. In a symmetric reflector, both central and strut blockage deteriorate the sidelobe levels, the degree of which depends on the percentage of the blocked area. As figure (2) of the previous section indicates the level of the sidelobes increases with the blockage and for large aperture blockage approaches that of a uniformly illuminated aperture. For a symmetric reflector, therefore, a tapered

aperture illumination is only an effective means of sidelobe reduction when the aperture blockage can be made small. In small reflector antennas this is a difficult task, since the diameter of the supporting struts is limited by the mechanical strength and the size of the central blockage is dictated by the feed diameter. One therefore expects that, the tapered aperture distribution can be more effective for large diameter reflectors. A disadvantage of this method of sidelobe control is the effect of tapered illumination on the antenna gain factor. Although, it improves the feed spillover power, it also tend to reduce the reflector gain factor.

Sidelobe levels may also be controlled by controlling the reflector aperture distribution. One such method has been used by Han [3], utilizing absorbing materials to block the reflection from selected regions of the reflector, Figure 3. This method is a generalization of the aperture tapering, but does not provide a practical method for sidelobe control. It causes gain reduction due to the loss of effective aperture size and does not overcome the problem of sidelobe deterioration due to feed and strut blockage. Practically, it is difficult to utilize, since the environmental effects on the absorbing material limits its useful life.

The most effective way of reducing the near-in sidelobes of a symmetric reflector has therefore been the elimination of the strut blockage. For a front-fed paraboloids this can be achieved by utilizing centrally supported feeds. Unfortunately, such feeds have poor radiation characteristics and result in lower antenna gain factor and higher cross-polarization level.

Far-out Sidelobes: The level of far-out sidelobes affects the antenna noise temperature and has received increasing attention in recent years, with continuous improvement in the performance of low noise amplifiers. Dominant parameters affecting the level of far-out sidelobes are the reflector edge illuminators, causing edge diffraction, feed spillover power and the wide angle strut scattering. Similar to the case of near-in sidelobes the level of edge diffracted fields can be reduced by tapering the aperture illumination. Additional means of reducing the edge diffracted fields are the modifications in the edge geometry using large diameter edge curves, with an additional benefit of increasing the reflector mechanical strength, utlilizing corrugated reflector edges and coating the reflector edge with a lossy dielectrics. The latter case of dielectric rim loading has been studied by Chung and Naito [4]. Its usefulness is, however, questionable due to environmental effects. Rim corrugation adds to the cost of the reflector and has not found wide spread application in practice. The most common approach is, therefore, curving the reflector edge, which is simpler to achieve and adds to the reflector strength. For extremely low sidelobe reflectors the most useful approach is the use of absorber-lined tunnels. The reflector is placed in a cylindrical tunnel, the inner wall of which is covered with absorbing material to eliminate the side radiation field [5]. Although, this method is a very effective one it can only be used in special purpose antennas. A modification of this approach uses metallic cylindrical collars on the reflector, which can be used economically and has found common use in high performance reflectors.

The only disadvantage of this method of far-out sidelobe control is the effect of the metallic collar on the near-in sidelobes. Because, the metallic collar reflects the incident radiation of the feed, these reflected fields eventually radiate in the direction of the near-in sidelobes, and consequently raising their level. In practice one therefore must optimize the rim geometry to reduce its effect on the first few reflector sidelobes.

The feed spillover power affects the sidelobe levels in the direction of the reflector rim, where the feed illumination is still high. A natural way of reducing this effect is the use of low edge illumination and designing feeds with rapid pattern tapering beyond the reflector rim. Its effect can, additionally, be reduced using the cylindrical reflector collar.

The effect of the supporting struts on the far-out sidelobes generally manifests itself in the direction of the scattering cone of the struts. The angle of the scattering cone is approximately equal to the strut angle with reflector axis, causing large sidelobes around 100° to 120° off-axis directions. Because the analysis of the strut scattering is a very difficult problem, its affects on the reflector sidelobes have been ignored until quite recently. During 1981 antennas and propagation symposium, two separate methods of investigating strut effects on the sidelobes were reported. Thielen [6] has used experimental approach to study the strut effect. He has then used two separate methods to reduce the strut effects on the sidelobes levels. In Figure (4) he has used continuously curved struts to distribute the strut scattered power over a wide angular range. In Figure (5), on the

other hand, he utilized metallic pieces mounted on the strut to reduce the scattered power. Using these methods he has measured a reduction of about 6 dB in the sidelobe level along the scattering cone angle, Figure (6).

In a similar study, Hwang and Han [7] have used a complex strut cross-section to reduce the strut scattering and to distribute the scattered power over a wide angular region. Figure (7) shows its strut geometry and the measured reflector patterns.

A novel method of sidelobe reduction has also been reported by savac antenna, Figure (8). It utilizes two planar plates on the reflector to reduce the side radiation. These plates have an additional use of shortening the strut length, which subsequently results in a smaller strut diameter. It is expected that these plates will reduce the far-out sidelobes beyond about 20 degrees off axis. However, no experimental or computed patterns for this antenna are reported and further work is required to evaluate their effect on the reflector pattern and then search for an optimum configuration for the plates.

V FORMULATION OF SYMMETRIC REFLECTOR FIELD WITH CENTRAL AND STRUT BLOCKAGE

(a) Unblocked Reflector

For computation of the reflector field near the main axis, the physical optics analysis provides a convenient approach. To develop the method we assume the incident feed pattern illuminating the reflector to be in the following form in a coordinate system which is defined in Figure (9).

$$\bar{E}_{inc} = \frac{e^{-jk\rho}}{\rho} \left[a_1(\theta')\sin\phi'\bar{a}_{\theta'} + d_1(\theta')\cos\phi'\bar{a}_{\phi'}\right] \tag{1}$$

$$\bar{H}_{inc} = \frac{1}{\eta}(\bar{a} \times \bar{E}_{inc}) = \frac{e^{-jk\rho}}{\eta\rho} \left[a_1(\theta')\sin\phi'\bar{a}_{\phi'}, -d_1(\theta')\cos\phi'\bar{a}_{\theta'}\right] \tag{2}$$

These are the far-zone field of a circular aperture excited in the m=1 azimuthal mode. The E-plane is the yz-plane and H-plane is the xz-plane. The polar patterns $a_1(\theta')$ and $d_1(\theta')$ are assumed to be such that most of the energy is radiated toward the reflector and very little energy is radiated in the half-space $z>0$. Furthermore to assure continuity of the field when $\theta'=\pi$ it is necessary that

$$d_1(\pi) = -a_1(\pi). \tag{3}$$

Application of equation (2) shows the geometrical-optics current density on the front of the reflector to be

$$\bar{J}_S = \frac{2}{\eta}\frac{e^{-jk\rho}}{\rho}\{C_x\bar{a}_x + C_y\bar{a}_y + C_z\bar{a}_z\} \tag{4}$$

where

$$C_x = -\sin\frac{\theta'}{2}\sin\phi'\cos\phi'\,[a_1(\theta') + d_1(\theta')] \tag{5}$$

$$C_y = -\sin\frac{\theta'}{2}\,[a_1(\theta')\sin^2\phi' - d_1(\theta')\cos^2\phi'] \tag{6}$$

$$C_z = -\cos\frac{\theta'}{2}\sin\phi' a_1(\theta'). \tag{7}$$

The principal component of current is the y-component because the field is polarized in the yz-plane. The cross-polarized x-component is zero in the principal planes. By making the feed pattern axially symmetric; i.e.,

$$d_1(\theta') = -a_1(\theta') \text{ for } \theta'_0 \leq \theta' \leq \pi \tag{8}$$

we then have

$$\bar{J}_S = \frac{2e^{-jk\rho}}{\eta\rho}\{-\sin\frac{\theta'}{2}\,\bar{a}_y - \cos\frac{\theta'}{2}\sin\phi'\bar{a}_z\}a_1(\theta') \tag{9}$$

and the cross-polarized component of surface current has been eliminated.

Similarly, the ray-optical reflected field may be computed from

$$\bar{E}_{REFL} = -\bar{E}_{INC} + 2(\bar{n}\cdot\bar{E}_{INC})\bar{n} \tag{10}$$

yielding

$$\bar{E}_{REFL} = \{\frac{e^{-jk\rho}}{\rho}\}\{\bar{a}_x\sin\phi'\cos\phi'(a_1+d_1) + \bar{a}_y\,(a_1\sin^2\phi' - d_1\cos^2\phi')\} \tag{11}$$

This field propagates rectilinearly parallel to the z-axis producing the focal plane field

$$\bar{E}_{APER} = \frac{e^{-j2kF}}{\rho} \{\bar{a}_x \sin\phi' \cos\phi' (a_1+d_1) + \bar{a}_y (a_1 \sin^2\phi' \bar{d}_1 \cos^2\phi')\} \qquad (12)$$

where

$$\begin{aligned} \phi' &= \tan^{-1}(y/x) \\ \theta' &= \tan^{-1}(\sqrt{x^2+y^2} \;/\; [-F + \frac{x^2+y^2}{4F}]) \\ \rho &= 2F = 2F/(1-\cos\theta'). \end{aligned} \qquad (13)$$

In the next section this aperture field will be used to determine the scattered field of the feed supporting struts.

The far-zone fields radiated by the currents induced on the scatterer are from equation

$$\bar{E}(P) = -\frac{j\omega\mu}{4\pi} \frac{e^{-jkR}}{R} \int [\bar{J}_S - (\bar{J}_S \cdot \bar{a}_R)\bar{a}_R] \, e^{j\bar{k}\rho \cdot \bar{a}_R} \, dS. \qquad (14)$$

If J is approximated by the geometrical current density in equation (4), then the resulting physical-optics approximation of the field, after necessary manipulations becomes

$$E_\theta(P) = jkF\sin\phi \frac{e^{-jkR}}{R} \int_{\theta_0}^{\pi} \frac{e^{-jk\rho(1-\cos\theta\cos\theta')}}{(1-\cos\theta')} \{a_1\cos\theta[J_0(\beta)-J_2(\beta)]$$

$$-d_1\cos\theta[J_0(\beta) + J_2(\beta)] - 2j\sin\theta \operatorname{ctn}\frac{\theta'}{2} J_1(\beta)a_1\}\sin\theta'd\theta' \quad (15)$$

$$E_\phi(P) = jkF\cos\phi \frac{e^{-jkR}}{R} \int_{\theta_0}^{\pi} \frac{e^{-jk\rho(1-\cos\theta\cos\theta')}}{(1-\cos\theta')} \{a_1[J_0(\beta) + J_2(\beta)]$$

$$-d_1[J_0(\beta) - J_2(\beta)]\} \sin\theta'd\theta' \quad (16)$$

where $\beta = k\rho\sin\theta\sin\theta'$.

(b) Aperture Blockage

The presence of an object in front of a reflector antenna will cause significant changes in its radiation patterns. In general, these objects may be classified as either large centrally located objects such as a subreflector or a feed horn, which are essential to the operation of the antenna, or long thin cylindrical struts used for mechanical support of the central object, Figure 10.

In this section expressions for the computation of the strut scattered field are given. The effect of the central blockage will be discussed later. For simplicity only cylindrical struts are considered, so that analytic expressions can be developed. For struts of arbitrary cross-sections the problem must be solved numerically, which require excessive computer and personnel time and could not be attempted in this work. However, the conclusions derived from cylindrical struts will be extended to arbitrary shape ones and will be provided later.

(c) Formulation of the Strut-Blocking Equations

The geometry of a single, perfectly conducting strut is shown in Figure 11, where the strut axis lies in the plane $\phi' = \phi_0$. The (cylindrical) strut lies entirely on one side of the z-axis with, at most, one end touching the z-axis. The x'-y'-z' coordinate system is centered at the paraboloid prime focus, with the z'-axis directed away from the reflector along its axis of symmetry. The strut lies at an angle $\alpha(-90<\alpha<90)$ with respect to the r'-axis, which is perpendicular to z' in the plane $\phi' = \phi_0$. The end of the strut axis lying closer to the z' axis has coordinates (r'_1, z'_1), and the other end has coordinates (r'_2, z'_2), where $r'_1 \geq 0$, $r'_2 > 0$, $r'_1 < r'_2$ and

$$\alpha = \tan^{-1}\left[\frac{z'_2 - z'_1}{r'_2 - r'_1}\right] \tag{17}$$

The right-handed x"-y"-z" coordinate system is shown in Figure 12, with its origin located at the nearer end of the strut (r'_1, z'_1), the z"-axis lying along the strut, and the x"-axis lying in the r'-z' plane; i.e., in the plane $\phi' = \phi_0$. Also shown in the figure is the incident plane wave emerging from the reflector (transit mode) with $\bar{k} = ka_{z'}$; i.e., in the positive z'-direction. An oblique view of the x"-y"-z" system is shown in Figure 13, with the angle $\phi"$ measured about the z"-axis, in the x"-y" plane, from the x"-axis.

(C-1) E-Polarization

In this section the strut will be assumed to have a circular cross-section. Furthermore, initially it will be assumed that the

E-vector of the incident plane-wave lies in the plane $\phi' = \phi_0$ as indicated in Figure 12. Under these conditions the currents induced on the cylinder (neglecting end effects because $L >> \lambda$) will flow entirely in the z"-direction. Then the scattered field due to the strut currents is

$$E(P) = -\frac{j\omega\mu}{4\pi}\left(\frac{\bar{e}^{jkR}}{R}\right)\int_0^{2\pi} a\,d\phi'' \int_0^{L} dz'' \{J_{Sz''}[a_{z''}]_{trans}\, e^{jk\bar{\rho}\cdot\bar{a}_R} \quad (18)$$

where P is a field point with coordinates R,0,ϕ, R is the distance from the origin 0 to the field point, ρ is the vector from 0 to the integration point, $\bar{a}$ is a unit vector from 0 to P, and only the transverse (to $\bar{a}$) components of the current contribute to the scattered field. For a plane wave incident at an angle α the induced curent is given by

$$J_S = \bar{a}_{z''}\left(\frac{2E_0}{n\pi ka\cos\alpha}\right)e^{-jk\sin\alpha z''} \sum_{n=-\infty}^{+\infty} (j)^{-n}\frac{e^{jn\phi''}}{H_n^{(2)}(ka\cos\alpha)} \quad (19)$$

Insertion of (19) into (18) and evaluation of the ϕ"-integral yields

$$\bar{E}(P) = \left(\frac{jk}{2\pi}\right)\left(\frac{e^{-jkR}}{R}\right)e^{jP_0}\{\bar{\varepsilon}_0\ IFRE(D,\delta,\alpha)\}\ 2a \int_{r'_1}^{r'_2} E_A(r')e^{jkr'A_0}\,dr' \quad (20)$$

where

$$\bar{e}_0 = [\cos\theta\cos(\phi-\phi_0) - \tan\alpha\sin\theta]\,\bar{a}_\theta - \sin(\phi-\phi_0)\,\bar{a}_\phi$$

$$P_0 = (kz'_1 - kr'_1\tan\alpha)(\cos\theta - 1)$$

$$A_0 = \sin\theta\cos(\phi-\phi_0) + \tan\alpha(\cos\theta-1)$$

$$B = \sin\alpha\sin\theta\cos(\phi-\phi_0) - \cos\alpha\cos\phi \qquad (21)$$

$$C = \sin\theta\sin(\phi-\phi_0)$$

$$D = \sqrt{B^2 + C^2}$$

$$\delta = \tan^{-1}\left[\frac{-C}{-B}\right]$$

$$\mathrm{IFRE}(D,\delta,\alpha) = -\frac{1}{ka\cos\alpha}\sum_{n=-\infty}^{+\infty} e^{jn\delta}\,\frac{J_n(kaD)}{H^{(2)}(ka\cos\alpha)} \qquad (22)$$

The remaining integral has been transformed to an integral of $E_A(r')$ the <u>focal-plane</u> E-field in the r'-direction, times the phase factor $e^{jkr'A_0}$.

When $\theta = 0$; i.e., P lies on the z'-axis (boresight axis), (22) reduces to

$$\bar{E}(R,0,0) = \left(\frac{jk}{2\pi}\right)\left(\frac{e^{-jkR}}{R}\right)\tilde{a}_{r'}\ 1FR_E\ 2a\int_{r'_1}^{r'_2} E_A(r')\,dr' \qquad (23)$$

where IFR_E is the E-polarization IFR (induced field ratio) of a circular cylinder obtained from (20) and (22) with $\theta=0$. Except for the IFR_E factor, (23) is the field of the rectangular aperture defined by the projection of the strut on the x'-y' plane as shown in Figure (14). Thus, in the optical limit of $IFR_E \to -1$, (23) reduces to the classical null-field result. However, for typical strut widths of the order of a wavelength, IFR_E is far from -1, and a considerably different result is obtained.

Equation (20) also provides more precise angular information about the strut tilt than does the conventional "flat" shadow

representation. For example, since $E_A(r')$ is constant-phase in the focal plane, the integral in (20) is maximum in those directions (θ,ϕ) for which $A_0 = 0$. Thus, from A_0 in (21), it is shown that local maxima of the scattered field occur along the contour

$$\cos(\phi_{MAX} - \phi_0) = \tan(\theta_{MAX}/2)\tan\alpha \ . \tag{24}$$

(C-2) H-Polarization

The procedures of the previous section will again be followed, but this time with a component of the H-vector lying along the strut. For $\alpha = 0$, both axial and circumferential components of surface current will be induced. Then the scattered field is

$$\bar{E}(P) = -\frac{j\omega\mu}{4\pi}\left(\frac{e^{-jkR}}{R}\right)\int_0^{2\pi} a\,d\phi'' \int_0^{L} dz'' \left\{J_{S\phi''}\left[\bar{a}_\phi\right]_{trans} + J_{Sz''}\left[\bar{a}_{z''}\right]_{trans}\right\} e^{-jk\bar{\rho}\cdot\bar{a}_R} \ . \tag{25}$$

From two-dimensional circular cylinder theory, the two components of current are:

$$J_{S\phi''} = \left(\frac{2jH_0}{\pi ka}\right) e^{-jk\sin\alpha z''} \sum_{n=-\infty}^{\infty} (j)^{-n} \frac{e^{jn\phi''}}{H_n^{(2)'}(ka\cos\alpha)} \tag{26}$$

$$J_{Sz''} = -\left(\frac{2jH_0}{\pi ka}\right) e^{-jk\sin\alpha z''} \left(\frac{\sin\alpha}{ka\cos^2\alpha}\right) \sum_{n=-\infty}^{\infty} n(j)^{n} \frac{e^{jn\phi''}}{H_n^{(2)'}(ka\cos\alpha)} \tag{27}$$

The z"-component of current, which vanishes when $\alpha = 0$, causes the H-polarization result to be significantly more complicated than the E-polarization.

Inserting (26) and (27) into (25) and evaluating the ϕ"-integral yields

$$\bar{E}(P) = \left(\frac{jk}{\pi}\right)\left(\frac{e^{-jkR}}{R}\right) e^{jP_0} \{\bar{e}_c \, IFRH(D,\delta,\alpha) +$$

$$\left[\frac{\bar{e}_s}{kaD} - (\bar{a}_\theta e_\theta + \bar{a}_\phi e_\phi)\frac{\sin\alpha}{ka\cos^2\alpha}\right] JFRH(D,\delta,\alpha)\} \cdot$$

$$\cdot 2a \int_{r'_1}^{r'_2} \eta H_A(r') e^{jkr'A_0} dr' \qquad (28)$$

where

$$\bar{e}_c = \bar{a}_\theta [\sin\delta\cos\alpha\sin\theta + \sin\delta\sin\alpha\cos\theta\cos(\phi-\phi_0) - \cos\delta\cos\theta\sin(\phi-\phi_0)]$$

$$+ \bar{a}_\phi[-\sin\delta\sin\alpha\sin(\phi-\phi_0) - \cos\delta\cos(\phi-\phi_0)] \qquad (29)$$

$$\bar{e}_s = \bar{a}_\theta[\cos\delta\cos\alpha\sin\theta + \cos\delta\sin\alpha\cos\theta\cos(\phi-\phi_0) + \sin\delta\cos\theta\sin(\phi-\phi_0)]$$

$$+ \bar{a}_\phi[-\cos\delta\sin\alpha\sin(\phi-\phi_0) + \sin\delta\cos(\phi-\phi_0)] \qquad (30)$$

$$\bar{e}_\theta = \cos\alpha\cos\theta\cos(\phi-\phi_0) - \sin\alpha\sin\theta \qquad (31)$$

$$\bar{e}_\phi = -\cos\alpha\sin(\phi-\phi_0) \qquad (32)$$

$$IFRH(D\,\delta,\alpha) = -\frac{1}{ka\cos\alpha} \sum_{n=-\infty}^{+\infty} e^{jn\delta} \frac{J_n'(kaD)}{H_n^{(2)'}(ka\cos\alpha)} \qquad (33)$$

$$JFRH(D,\delta,\alpha) = -\frac{1}{ka\cos\alpha} \sum_{n=-\infty}^{+\infty} jne^{jn\delta} \frac{J_n(kaD)}{H_n^{(2)'}(ka\cos\alpha)} \qquad (34)$$

The final factor in (28) is an integral of $H_A(r')$, the focal-plane H-field in the r'-direction.

When $\theta=0$, JFRH is identically zero, and (28) becomes

$$\bar{E}(R,0,0) = -\left(\frac{jk}{2\pi}\right)\left(\frac{e^{-jkR}}{R}\right)\bar{a}_{\phi_0}\ IFR_H\ 2a \int_{r'_1}^{r'_2} \eta H_A(r')dr' \qquad (35)$$

where IFR_H is the H-polarization IFR of a circular cylinder obtained from (28) with $\theta=0$. Except for the IFR_H factor, (35) is the field of the rectangular aperture shown in Figure (14).

(d) Central Blockage

A centrally located object, such as a feed or a subreflector, causes scattering of the reflector field, which can be considered as a combination of the shadowing effect on the main reflector and the edge diffracted fields. For small scatterers the contribution of the edge diffraction to the total field is negligible and the central blockage field can be obtained accurately using the geometrical shadowing. The effect of the geometrical shadowing can easily be accounted for by modifying the integration range in the formulation of the main reflector fields. That is, in equations (15) and (16) one only needs to carry out the numerical integration form θo to $\pi-\delta\theta$, where $\delta\theta$ is the half angle subtended by the central blockage from the reflector centre. Assuming the central blockage radius as rc, this angle is given by $\delta\theta = \tan^{-1}(rc/F)$.

(e) Total Reflector Field

An addition of the strut fields, in equations (20) and (28), to the reflector fields, in (15) and (16), gives the total radiated field of a symmetric paraboloid. For an arbitrary polarization of the aperture field, with respect to the struts, a combination of both (15) and (16) must be used, with a proper vectorial addition. Similarly, for multiple strut support the overall strut field must be considered.

In the foregoing sections the strut scattered field was obtained analytically for a cylindrical strut. Similar expressions for struts of arbitrary cross-section can be obtained and, in general, a numerical method such as the moment method must be utilized. Since, the given expressions will provide adequate information for the strut effects on the reflector pattern, the case of struts with arbitrary cross-section is not considered. Furthermore, the generation of adequate data using numerical methods is costly and time consuming and could not be attempted in this phase of the work. A brief description of such cases will be given in a later section.

VI COMPUTED PATTERNS FOR SYMMETRIC REFLECTOR

Based on the mathematical model developed in the previous section for the reflector, central blockage and the strut field, the expected reflector patterns for several cases have been computed. This section presents few selected data. Initially, we have used the CRC feed [14], as the primary source for the reflector and the results are obtained for various strut geometries and the reflector sizes. Following this section a simplified feed model in the form of $\cos^m\theta$ illumination is selected and the expected co-polar and cross-polar behaviours of different strut configurations are studied. A modification in the reflector surface to generate an appropriate phase change for the strut field is then proposed and its effect on the improvement of the reflector gain and the sidelobe levels are examined. Other strut geometries such as: dielectric coated struts, dielectric struts and conducting struts of arbitrary cross-sections are also considered. Finally, the reflector noise temperature and its G/T are also computed.

(a) Reflector Performance with CRC Feed

Using CRC feed as the illuminating source the reflector patterns are computed for three different strut geometries, a J-hook, a tripod configuration and finally a quad-strut geometry. Initially, the case of a J-hook is considered. The reflector diameter for all cases is kept at 48λ, with $f/D = 0.375$ and the orientation of the strut and its mounting location on the reflector is modified. The geometry of

the J-hook is shown in figure (17), which defines all parameters and the dimensions of the CRC feed and its radiation patterns are shown in Figures (15) and (16). The computed patterns are shown in Figures (18) to (26) for an E-polarized strut and in Figures (27) to (35) for an H-polarized one. In all cases the strut diameter is 1.0λ. Three different mounting locations for the strut are selected, which affect the spherical shadowing of the feed on the reflector. The general conclusions are that, the spherical shadow increases the sidelobe levels and the level of the sidelobes is higher in the plane of the struts. Note that in the present method we have used the geometrical shadowing approach to compute the blockage effect. The computed strut shadow fields are then corrected by the induced field ratio of the E-plane and the H-plane scatterer. This approach is of course approximate and results for an H-polarized strut are similar to an E-polarized one. In Section IV-b we will use the actual scattering field of the strut and thus the sidelobe levels of an H-plane strut will be shown to be somewhat lower than those of the E-plane one.

For a tripod configuration the geometry and the diameters of the selected reflectors are shown in Figure (36). The strut diameter is still 1.0λ and for all reflectors $f/D = 0.375$. For each reflector and the strut mounting location, the reflector patterns are provided in three planes of $\phi = 0, 45°$ and $90°$. Results are within expectation, the reflector gain decreases with the percentage plane wave and the spherical shadows and the level of the first side lobe level increases. The results are shown in Figures (37) to (60). No specially significant information is evident, except that a tripod configuration does not drastically increases the sidelobe levels.

Finally, we have considered the quad-strut case. Figures (61) and (70) show the geometry and Figures (62) to (74) provide the computed patterns for different reflector diameters, when the struts are mounted at the mid-point or the reflector edge. All figures show expected results. For this strut configuration the most interesting results are obtained with the geometry of figure (75). Here vertical struts are selected, which cause the most severe spherical shadows. The computed patterns are shown in Figures (76) to (83), which indicate excessive gain reduction. The sidelobe levels are also high in the principal plane. However, in the 45°-plane the sidelobes are, generally, lower than the sidelobe levels of the unblocked aperture. In fact, as Figure (79) indicates by a proper selection of the percentage shadows the sidelobe levels can be reduced considerably below that of the unblocked ones. This property of the quad-strut configuration is quite unique and, whenever possible, may be used to reduce the interference level from other sources.

(b) Accurate Computation of Strut Scattering

($\cos^m \theta$ distribution, $|a_1(\theta)| = |d_1(\theta)| = \cos^m\theta$)

In the previous section the reflector patterns were generated including both central and strut blockage. The strut blockage was computed on the basis of geometrical shadowing weighted by induced field ratios, this method gives accurate reflector patterns for small angles and only for the co-polarization component. To study the cross-polarization due to the struts we must handle the strut fields more accurately. In this section we have used the strut scattered fields

computed using strut current as shown in equations (20) and (28). Since the cross-polarization will be higher for longer struts, only the case of struts mounted on the reflector edge are considered in this section. For other cases the results can similarly be obtained, but the co-polar patterns will be similar to the results of the previous section and the cross-polar components will be lower.

In this section we have studied the sidelobe performance of a 4 ft reflector with both $\cos\theta$ and $\cos^2\theta$ patterns of the primary feed. Again, three strut geometries are considered: a single strut, a tripod configuration and a quad-strut geometry. In all cases the strut is assumed to be supported from the reflector edge, so that, full plane wave blockage of the reflector exists.

For a single strut the computed patterns are shown in Figures (84) to (88) for a $\cos\theta$ feed pattern and in Figures (89) to (93) for a $\cos^2\theta$ feed pattern. The corresponding efficiencies are listed in Tables (1) to IV. In all cases the polarization of the feed is in the y-direction, the diameter of the central blockage is 2.5λ (feed diameter) and the strut diameter is assumed to be 0.5λ. All struts are located at an angle 47° with respect to the x'-y' plane.

An examination of Figures (84) to (88) indicates that when the polarization of the feed is along the strut, the effect of the scattered field of the strut on the reflector pattern is larger. This is clear from Figure (87), where the level of the first sidelobe is higher and the overall reflector pattern has, generally, higher sidelobe levels than the pattern of Figure (84). The cross-polarization introduced by the strut is shown in Figure (85), which is quite satis-

factory and is below -52dB level. Also, comparing the results of Tables (I) and (II) it is clear that for the polarization along the strut, the blocked efficiency is lower; i.e., 80.196% compared with 80.342%.

Similar results are evident in Figures (89) to (93) for a $\cos^2\theta$ feed pattern. Again, when the feed polarization is along the strut, the blockage effect is higher and the corresponding blocked efficiency is lower; i.e., 68.88% compared with 70.0%. The cross-polarization has also similar behaviour, with a peak level about -53dB.

Comparing the results of two different illuminations, we note that as expected, for a $\cos^2\theta$ feed pattern the effect of the blockage is very significant. In fact, when the feed polarization is perpendicular to the strut, the main pattern deterioration is due to the central blockage. The struts have a minimal effect. For strut along the feed polarization, the effect of the strut in the plane normal to the strut is very high and is of the same order as the central blockage effect. For a $\cos\theta$ illumination both central and strut blocking have negligible effect on the reflector pattern. From these results we conclude that, although by strong tapering of the feed illumination ($\cos^2\theta$ feed), sidelobe levels can be lowered to around -38dB. The aperture blockage raises their level to about -30dB. In the case of $\cos\theta$ illumination the original sidelobe level of about -25dB increases to around -23dB level.

For identical feed and strut dimensions the computed results for a tripod configuration are shown in Figures (94) to (99). The polarization of the field is along the y-direction. From Figures (94)

to (96) again it is evident that blockage effect on the reflector pattern is small for a $\cos\theta$ feed pattern. In fact, provided that the struts are not along the E-plane the blockage effect of a tripod on the sidelobes, seems to be smaller than that of a single strut along the feed polarization. The blockage efficiency however is lower; i.e., 78.33% compared to 80.196%. The cross-polarization is also poor, which is indicated in Figure (95) and has a maximum level of about -40dB. Similar results are also obtained for a $\cos^2\theta$ illumination, which are shown in Figures (97) to (99). Sidelobe performance is satisfactory and increase their level slightly above that of the central blockage. The first sidelobe level is about -32dB. A major disadvantage of a tripod configuration is the generally high level of the higher order sidelobes, which although are lower than that of a single strut located along the E-plane their level is otherwise higher. The computed efficiencies, for this configuration are shown in Tables V and VI. They are, as expected, lower than those of a single strut and for two assumed illuminations are 78.33% and 67.06%, respectively.

Figures (100) to (103) show the computed patterns for a quad-configuration. Again, the dimensions of the feed and struts are the same as before and strut lengths are assumed to be the full length of the aperture. Furthermore, for the computed data two struts are assumed along the feed polarization. Therefore, the sidelobe levels, indicated in these figures, are the maximum levels that one generally should expect. Deterioration of the pattern in the principal E-plane is most severe for higher order sidelobes. But the cross-polarization

is satisfactory at about -52dB. The computed efficiencies are shown in Tables VII and VIII.

To indicate the effect of strut diameter on the reflector pattern Figures (104) and (105) are also included, which are respectively for tripod and quad-strut configurations. In both cases the strut diameter has been increased to one λ and the illumination is due to a $\cos\theta$ feed pattern. For the tripod geometry the level of the first sidelobe is almost unaffected, odd sidelobe levels have been reduced and the even sidelobes are raised. For a quad-strut case, in Figure (105), the shape of the pattern has remained the same, but its level has increased almost uniformly. It is therefore clear that the diameter of the strut has a strong effect on the pattern of a good configuration, but generally does not affect the results of a tripod geometry. Corresponding efficiencies are shown in Tables IX and X, which indicate lower percentages than those for a 0.5λ strut.

TABLE I

Efficiencies of a Single Strut, Strut Perpendicular to the E-plane Feed Feed Diameter = 2.5λ, Strut Diameter = 0.5λ, Reflector Diameter = 48λ, cos θ Illumination

Spillover	5.69%
Unblocked η_0	82.803%, G_0 = 42.75 dB
Blocked η_B	81.342%, G_B = 42.67 dB

TABLE II

Efficiencies of a Single Strut, Strut Along the E-plane Dimensions Same as Table I, cos θ Illumination

Spillover	5.69%
Unblocked η_0	82.803%, G_0 = 42.75 dB
Blocked η_B	80.196%, G_B = 42.61 dB

TABLE III

Efficiencies of a Single Strut Perpendicular to the E-plane Dimensions Same as Table I, $\cos^2\theta$ Illumination

Spillover	0.84%
Unblocked η_o	71.61%, G_o = 42.12 dB
Blocked η_B	70.0%, G_B = 42.02 dB

TABLE IV

Efficiencies of a Single Strut Along the E-plane Dimensions Same as Table I, $\cos^2\theta$ Illumination

Spillover	0.84%
Unblocked η_o	71.61%, G_o = 42.12 dB
Blocked η_B	68.88%, G_B = 41.95 dB

TABLE V

Efficiencies of a Tripod Dimensions Same as Table I, cos θ Illumination

Spillover	5.69%
Unblocked η_o	82.803%, G_o = 42.75 dB
Blocked η_B	78.33%, G_B = 42.51 dB

TABLE VI

Efficiencies of a Tripod Dimensions Same as Table I, $\cos^2\theta$ Illumination

Spillover	0.84%
Unblocked η_o	71.61%, G_o = 42.12 dB
Blocked η_B	67.06%, G_B = 41.83 dB

TABLE VII

Efficiencies of a Quad-Strut Dimensions Same as Table I, cos θ Illumination

Spillover	5.69%
Unblocked η_o	82.80%, G_o = 42.75 dB
Blocked η_B	77.12%, G_B = 42.44 dB

TABLE VIII

Efficiencies of a Quad-Strut Dimension Same as Table I, $\cos^2\theta$ Illumination

Spillover	0.84%
Unblocked η_o	71.61%, G_o = 42.12 dB
Blocked η_B	65.89%, G_B = 41.76 dB

TABLE IX

Efficiencies of a Tripod Feed Diameter = 2.5λ, Strut Diameter = 1.0λ, Reflector Diameter = 48λ, cos θ Illumination

Spillover	5.69%
Unblocked η_o	82.80%, G_o = 42.75 dB
Blocked η_B	74.7%, G_B = 42.3 dB

TABLE X

Efficiencies of a Quad-Strut, Data Same as Table IX

Spillover	5.69%
Unblocked η_o	82.8%, G_o = 42.75 dB
Blocked η_B	72.34%, G_B = 42.16 dB

VII POSSIBLE TECHNIQUES FOR SIDELOBE REDUCTION

In Section IV we presented computed data for the effects of central and strut blockage on the reflector sidelobe levels. It was found that for a single strut geometry, such as a j-hook, the sidelobe levels are generally satisfactory as long as the strut is not located along the E-plane. The results for a tripod were also satisfactory. However, for a quad-strut geometry the situation was quite different. When struts were supported on the reflector edge, blocking the entire length of the aperture, the overall patterns were poor and for the E-plane struts all near-in sidelobes had very high levels. On the other hand, supporting these quad-struts at an appropriate location on the reflector the spherical shadow generated proper phase for the scattered field to cancel the reflector generated sidelobes. That is, although the principal plane patterns still had poor sidelobe levels, the 45°-plane patterns actually had lower sidelobes than the unblocked reflector pattern. This property of a quad-strut configuration provides a convenient means of reducing the sidelobes, provided it can be used in a practical situation. The disadvantages of this method of sidelobe reduction is that: (1) spherical shadowing reduced the antenna efficiency considerably, (2) in many practical applications aligning the reflector at a 45°-plane is not practical. Nevertheless, a quad-strut configuration has this interesting property and, whenever possible it can be used as a very low sidelobe antenna to reduce interference from adjacent satellites.

In this section we intend to consider alternative approaches to lower the reflector sidelobe levels. The proposed methods are studied analytically and the geometries are modelled approximately. It is therefore expected that the computed data be approximate and their accuracy must be examined experimentally. In particular, even if the method may be found satisfactory by the experiment, the optimization of the proposed geometries must be carried out experimentally.

(a) Aperture Field Phase Shifting

Generally, scattered field of a conductor has a phase difference with the incident field by about 180°. This phase reversal is total for large scatterers, but always is around 180°. For this reason, the scattered fields due to the feed and the struts tend to reduce the axial gain of the reflector and raise the level of the first sidelobe. For larger angles off the reflector axis both magnitude and the phase of the scattered fields cause the pattern deterioration. From this property of the scattered field one therefore can expect that, any method that can be used to reverse the phase of the illuminating field of the blocked area, it may remedy the sidelobe deterioration of the antenna. Here we intend to explore one possibility. We propose to use metallic strips on the reflector surface, just under each strut, so that, the reflecting surface is raised by the thickness of the strip. In this manner, the field illuminating the central blocking feed and struts will travel shorter distance and consequently the field illuminating the blockage will have a phase difference with the aperture field. If the thickness of the strips is selected properly

this phase difference will compensate for the phase reversal due to struts and feed and their scattered field will become in phase in the axial direction. Thus, the effect of the blockage scattered field can be used beneficially to enhance the gain and to reduce the sidelobe levels, rather than to increase them.

For quad-strut geometry the configuration of the strips on the reflector is shown in Figure (106). To study the effects of this reflector modification on the reflector patterns, we consider only the strips under the struts. Thus, the central blockage will still exist and the computed patterns will indicate the effect of strut blockage only. To simplify the analysis we assume the current distribution on the strips to be the physical optics currents. This assumption is a crude one, since the width of the strips is small and their current distribution is not exactly close to the physical optics current. Nevertheless, it will provide a reasonable answer to the problem at hand. For a precise analysis one must use the actual current on the strips. With the assumed physical optics currents on the strip we have computed the new reflector patterns and the strut scattered field. The generated data were examined for various strip thickness and an optimum thickness for each strut configuration was found. It was realized that a thickness of between 0.3λ to 0.4λ generally gives a satisfactory result.

For a tripod configuration the representative patterns for a strip thickness of 0.35λ are shown in Figure (107), where a $\cos\theta$ feed illumination was assumed and the strut diameter was 0.5λ. It is evident that the sidelobes are reduced considerably and the pattern

first sidelobe is lowered below that of unblocked aperture. The corresponding efficiencies are shown in Table XI, which show an enhancement of the gain and the efficiency.

For a quad-strut configuration the computed patterns for two strip thickness are shown in Figures (108) and (109). For a 0.3λ strip thickness, Figure (108) shows a useful reduction of the sidelobe below that of the unblocked aperture and an enhancement of the gain. Figure (109) on the otherhand, indicates a reduction of the higher order sidelobes at the expense of the first sidelobe and the gain. The corresponding efficiencies are shown in Tables XII and XIII.

From these data it is clear that, loading the reflector surface with appropriately selected conductors improves the antenna gain and overcomes the problem of the aperture blockage. With a properly selected conductors one can, in fact, improve the reflector patterns over that of the unblocked reflector. However, as it was pointed out, this analysis is approximate and the optimized strip thicknesses may not in practice be optimum. The correct strip dimension must in practice be found experimentally. This analysis only serves the purpose of indicating that the blocked aperture patterns can be improved considerably by loading the reflector surface.

(b) Dielectric Loading of Struts

As an alternative method of sidelobe reduction the dielectric loading of struts is also considered. This approach may be used in two different ways, one to lower the scattering cross-section of the struts and the other to use the dielectric loading to cause a phase shift in

TABLE XI

Efficiencies of a Loaded Reflector Tripod Struts, Data Same as Table V
Strip Thickness = 0.35 λ

Spillover	5.69%
Unblocked η_o	82.8%, G_o = 42.75 dB
Blocked η_B	81.13%, G_B = 42.66 dB

TABLE XII

Efficiencies of a Loaded Reflector Quad-Struts, Data Same as Table VII

Spillover	5.69%
Unblocked η_o	82.8%, G_o = 42.75 dB
Blocked $\eta_{B'}$	80.85%, G_B = 42.65 dB, strip thickness = 0.35λ
Blocked η_B	76.85%, G_B = 42.42 dB, strip thickness = 0.45λ

the scattered field. The first approach is useful whenever the polarization of the field can be fixed with respect to the strut directions. Normally, the E-plane struts scatter field more efficiently. Thus, to reduce the strut effects one may use dielectric loading to minimize the strut scattering. In the second method one may select dielectric dimensions to cause a proper phase relationship between the reflector and the strut fields. An extensive investigation is carried out to study both cases [9] and few selective data will be presented in this report.

For the E-plane struts selecting proper dielectric thickness minimizes the scattering cross-section. The degree of the reduction in the scattered field depends on the strut diameter and normally improves for larger strut diameters. Figures (110) to (112) show the variation of the strut scattering cross-section with strut diameter, the dielectric thickness and the permittivity of the dielectric. For each configuration there always exists a dielectric thickness that minimizes the scattering. The strut therefore becomes almost invisible. In these figures, a is the strut radius, b is the outer radius of the coated strut and ε_r is the dielectric permittivity. As a reference, the scattering cross-section of an H-polarized strut with the dielectric loading is also shown in Figure (113). It shows that for this case the scattering cross-section increases with the dielectric thickness and generally deteriorates an already satisfactorily low scattering. Thus, the reduction of the scattering by a dielectric loading is useful if the strut direction can be controlled and only the E-plane struts are coated. Otherwise the reduction of the

scattering by the E-plane struts may be compensated by the increase in the scattering of the H-plane ones.

Dielectric loading of the struts to modify the phase of the scattered field was also studied extensively [9]. For few selected data the computed amplitude and phase of the forward scatterd field are shown in Figures (114) and (115). These figures indicate that with a single coating the phase of the scattered field can not, in general, be changed adequately to become in phase with the incident field. However, because the reflector axial field is usually a real number, a phase difference of about 270° may not reduce the reflector gain, or raise the first sidelobe level appreciably. Thus, by a proper selection of the dielectric thickness one may move the scattered and the incident field phase differences for both E and H-polarizations to around 270°. In this manner both struts types can be coated by the same dielectric to improve the reflector gain and the sidelobe levels. However, this method has few disadvantages that make its usefulness questionable, (1) dielectric materials on struts are unreliable due to focusing of sun and the possibility of melting, or other environmental effects (2) the improvement in the reflector patterns may not be satisfactory. For these reasons no representative data for reflectors with coated struts is obtained.

(c) Non-circular Strut Cross-sections

In the previous sections the strut cross-section was assumed circular, so that, their scattered field can be obtained analytically. This analytic solution enabled us to generate a reflector field more

conveniently. However, from a mechanical point of view it is advantageous to select other cross-sections, such as square or rectangle that has better bending characteristics. For these arbitrary strut cross-sections the scattered field can not, in general, be found analytically and a numerical method must be used.

From geometrical optics one expects that, reducing the shadowing of the strut on the reflector should reduce the blockage effect. However, for practical strut cross-sectional dimensions of small earth-stations, the actual strut effect is considerably different from the geometrical shadowing effect. This is mostly true for the E-plane strut, where the strut scattering scross-section approaches infinity as the strut thickness approaches zero. That is, an infinitely thin strip still scatters a sufficiently large field, for the E-polarized case, to cause large sidelobes. A major disadvantage of non-circular struts is their generation of high cross-polarization level. While, these struts may, in certain cases, affect the co-polar sidelobes by a lesser amount, they will generate much larger cross-polar fields. For this reason we have selected circular struts for the present investigation. In addition, the computation of non-circular strut field requires excessive personnel and computer time and could not be attempted in this work. However, we could expect that by a proper selection of strut cross-sectional dimension one may obtain improved sidelobe levels. Based on our experience with scattering from various shaped objects we expect this improvement to be relatively small.

(d) Non-metallic Struts

In investigation of scattering from dielectric rods we see that their scattering cross-section has an oscillating behaviour, indicating the resonance phenomenon. This means that, by selecting an appropriate rod diameter we may reduce the strut scattered field to levels lower than those of the conducting ones. However, dielectric rods are, generally, good scatterers also for the H-polarization of the incident field. Thus, while using dielectric rods may reduce the scattered field of the E-plane struts, they will increase the scattered field of the H-plane ones. In practice, therefore, the overall scattered field of dielectric struts may not be smaller than that of conducting ones.

Dielectric struts also have additional disadvantages in aging and other environmental effects. For small earth-stations a major problem lies in the focusing of sun on the struts, which in the dielectric rod case will certainly cause a complete failure of the strut. Provided these disadvantages can be tolerated, non-circular directric strut may be selected to provide proper phasing of its scattered field with the field of the reflector. In such a case the shadowing by the strut can be used as an advantage to improve both reflector gain and sidelobe level. However, for all above reasons we do not recommend non-metallic struts and a detailed analysis of their blocking effect has not been carried out in this work.

VIII ANTENNA NOISE TEMPERATURE

For an earth-station antenna normally the gain-to-noise temperature ratio G/T_A represents the figure of merit of the antenna. The antenna noise temperature is the total noise received by the antenna, which reflects the contribution of the noisy ground, the atmosphere and the overall space noise. The distribution of the noise, as a function of the antenna location and the elevation angle, is normally obtained experimentally. Using this noise distribution at the desired frequency the total antenna noise temperature can be computed from

$$T_A(\psi) = \frac{1}{4\eta} \int_0^{\pi} \int_0^{2\pi} G(\theta',\phi')T(\theta',\phi')\sin(\theta')d\theta'd\phi'$$

where

$T(\theta',\phi')$ = distribution of the apparent temperature within field of view

$G(\theta',\phi') = 4\eta\, p(\theta',\phi')/P_T$

$P(\theta',\phi')$ = power radiated per unit angle in the direction (θ',ϕ')

P_T = total power delivered to the loss less antenna

ψ = elevation angle of the antenna main beam.

The apparent average noise temperature $\bar{T}(\theta'\phi')$ can, in most applications, be assumed symmetric about the local zenith, which can simplify the ϕ' integration in the above equation. At the required 12 GHz frequency this apparent noise temperature can be described by the following relationship [13].

$$T(\theta'\phi')=T(\theta') = \begin{cases} [3.6/\cos\theta'] + 1.8 & 0 \leq \theta' \leq 88.57 \\ 290 - 100.66(90-\theta) & 88.56 \leq \theta' \leq 90 \\ 290 & 90 \leq \theta' \leq 180 \end{cases}$$

Using this relationship the antenna noise temperature can be computed by the integration of the above equation. However, it requires considerable computation time to determine the expected antenna noise temperatures at all antenna elevation angles. The detail of the method are indicated in [15] and is omitted here for brevity. Since in the present analysis we have considered a large number of antenna configurations, the evaluation of the noise temperature of all cases and for several antenna elevation angles is beyond the scope of this report. Instead we will provide few sample computed data to compare the expected antenna noise temperatures. Table XIII shows the results for an antenna elevation of 50°, whereas Tables XIV and XV show the data for elevation angles 30° and 10°, respectively. In all cases the antenna diameter is 48λ and a quad-strut configuration is selected to give the lowest possible G/T_A values. For other configurations the expected values will fall between those of the unblocked aperture and the quad-strut case.

TABLE XIII

Antenna Noise Temperature and G/TA for a Symmetric Reflector
Antenna Elevation = 50°
Antenna Diameter = 48λ

Case No.	TA,°K	G/TA,dB
1	39.0	26.52
2	21.9	28.36
3	34.5	27.27
4	14.7	30.34
5	30.1	27.97
6	9.9	32.17

Case Description

1 - 4 struts (ϕ_o=0,90,180,270) $\cos\theta$ distribution
2 - 4 struts (ϕ_o=0,90,180,270) $\cos^2\theta$ distribution
3 - 4 struts (ϕ_o=0,90,180,270) $\cos\theta$ distribution 0.4λ strip corrected reflector
4 - 4 struts (ϕ_o=0,90,180,270) $\cos^2\theta$ distribution 0.4λ strip corrected reflector
5 - unblocked reflector $\cos\theta$ distribution
6 - unblocked reflector $\cos^2\theta$ distribution

TABLE XIV

Antenna Noise Temperature and G/TA of a Symmetric Reflector
Antenna Elevation = 30°
Antenna Diameter = 48λ

Case No.	TA,°K	G/TA,dB
1	40.1	26.41
2	28.0	27.29
3	35.6	27.13
4	18.95	29.24
5	30.23	27.95
6	13.3	30.94

TABLE XV

Antenna Noise Temperature and G/TA of a Symmetric Reflector
Antenna Elevation = 10°
Antenna Diameter = 48λ

Case No.	TA,°K	G/TA,dB
1	56.4	24.93
2	48.7	24.89
3	51.9	25.5
4	40.2	25.97
5	46.9	26.04
6	34.55	26.74

IX OFFSET PARABOLIC REFLECTOR ANTENNA

The offset-parabolic reflector antenna offers a number of advantages over its axisymmetrical counterparts. The offset reflector antenna avoids aperture blocking effects which will result in gain reduction and an increase in the sidelobe levels. It also implies the small coupling between the primary feed and the reflector. This suggests that the primary feed can essentially be matched independent of the reflector.

These advantages of the offset reflector antenna are the results of the arrangements of the primary feed and its supporting structure away from the region of the highest aperture field intensity. The amount of the aperture blockage and the reflector reaction can be reduced by a proper selection of the offset angle θ_o and the angular aperture θ^*, which enables the feed and its supporting structure be out of the aperture field region. Under this condition, the scattered field of the feed and its supporting structure due to blockage will not exist. The sidelobe levels are thus the result of the aperture field radiation characteristic and the diffracted field at the edge of the reflector due to the direct incident field from the feed. The latter will generally control the far-out sidelobe levels provided that the sidelobes and the backlobes of the feed itself are very small.

The main disadvantage of the offset reflector antennas is the increase in the peak cross-polarization levels, as compared to its axisymmetric counterparts, when illuminated by a linearly polarized

feed. When the reflector is illuminated by a feed with a circularly polarized field, there is no cross-polarized component being induced. However, the direction of the maximum radiation will be shifted.

The sidelobe level control will result mainly from the feed imposed taper illumination on the reflector. The polarization of the feed will have very little effect on the sidelobe levels. The sidelobe levels and the peak cross-polarization levels can be controlled simultaneously using a matched feed instead of a conventional horn feed. The detailed studies of the sidelobe level control are given in this chapter.

(a) The Mathematical Model

A number of well established techniques are available, which can be used to determine the far-field of offset paraboloidal reflectors [10]-[12]. The best known of these techniques are the current distribution and the aperture field methods. Because the first method was used to evaluate the field of an axisymmetric reflector, it will also be used to study the performance of an offset one.

The geometry of an offset reflector is shown in Figure (116), where θ_o is the reflector offset angle, θ^* is the half aperture angle seen from the focal point and F is the focal length of the parent parabola. Utilizing the physical optics currents the reflector secondary field can be computed from

$$E^s = \frac{-j\omega\mu}{2\pi r} e^{-jkr} \int_s (n \times \bar{H}_i) \exp(jk\bar{\rho} \cdot a_r) \, ds \qquad (36)$$

where $\bar{H}_i$ is the magnetic field of the illuminating feed, n is the unit normal to the reflector and a_r is the unit positional vector of the far field point. The radial vectors $\bar{\rho}$ and $\bar{r}$ are defined in Figure (116) and the integration is over the reflector surface. Using the third definition of Ludwig the expected Co and cross-polar field near the reflector axis can be computed from [10]

$$\begin{matrix} Ep \\ Eq \end{matrix} = \frac{-j\omega\mu}{2\pi r} e^{-jkr} \begin{matrix} -(1+\cos\theta)\sin\theta\cos\phi & -\cos\theta\sin^2\phi + \cos^2\phi \\ \cos\theta\cos^2\phi - \sin^2\phi & (1+\cos\theta)\sin\phi\cos\phi \end{matrix} \begin{matrix} I_x' \\ I_y' \end{matrix} \quad (37)$$

where E_p and E_q are the Co and the cross-polar components and

$$I_A = \int_s (n \times \bar{H}i) \cdot A \exp(jk\bar{\rho} \cdot a_r) ds \quad (38)$$

the unit vector A representing x' and y', respectively. Once the feed radiation field $\bar{H}_i$ is defined the reflector patterns can be computed numerically. The detail of the work are omitted for brevity and can be found elsewhere [10] and [11].

(b) Depolarization Properties of Offset Reflector Antennas

It has been known that if a paraboloid reflector antenna is fed by a linearly polarized feed which is not a balanced feed [1], the antenna will radiate energy in both copolar and cross-polar directions. For the offset paraboloid reflector, this depolarization always occurs even though it was fed by a balanced feed [12]. This depolarization effects originate entirely from the offset between the fed and the reflector axis, and vanishes only when the offset angle becomes zero.

The peak cross-polar levels radiated in the plane of the asymmetry ($\phi = \pi/2$) and as a function of the offset-reflector parameters θ_o and θ^* are determined by Chu and Turrin [15], are shown in Figure (117) for a feed pattern of 10 dB edge illumination. Increasing the taper to 20 dB reduces the maximum cross polarization only by about 1 dB. From these results, it is evident that the peak value of the reflector cross-polarization is dependent very largely upon the offset angle θ_o and the angular aperture θ^*, while it is relatively insensitive to the feed imposed illumination taper. The polarization loss-efficiency as a function of the offset reflector parameters θ_o and θ^* are computed by Dijk, et al., [14] and are shown in Figure (118). From these results, it is clear that the loss of the aperture efficiency from depolarization tends to be small for values of θ_o and θ^* less than 45°, but it can become significant for large angles.

(c) Sidelobes of Offset Reflectors

Because an offset reflector does not suffer from the aperture blockage, its sidelobe levels depend on the feed illumination and the reflector parameters. In addition, it was mentioned, in the previous section that the cross-polar radiation level depend primarily on the reflector offset and the aperture angles. Thus, for a design of a reflector with satisfactory sidelobes and the cross-polarization an understanding the relationship between all these parameters is mandatory. Assuming a linearly polarized balanced feed with no cross-polarization, the computed sidelobe levels and the cross

polarizations are shown in Figure (119). The reflector aperture angle is selected as $\theta_0=\theta^*+5°$, to provide adequate clearance for the feed. This figure indicates data for a -10dB edge illumination with a subscript one and those for a -20 dB edge illumination with a subscript two. It is evident that decreasing the edge illumination does not affect the cross-polarization significantly. However,the sidelobes levels depend strongly on the field taper and decrease significantly for a -20 dB edge illumination. An interesting result to note is that, for both illuminations the sidelobe levels are identically the same, in both planes of symmetry and asymmetry, as long as the reflector offset angle is less than 30°. Also, for this range of the offset angle, the reflector generated cross-polarization is below -30dB level.

From the above discussion it is clear that an offset reflector with $\theta_0 \leq 30$ degrees can satisfactorily be used with a simple primary feed, without the necessity of using a dual mode matched feed, to lower the reflector depolarization. However, selecting $\theta_0 < 30°$ means longer focal length and inconvenience for the feed support. Thus, choosing $\theta_0 = 30°$ $(\theta^* = 25°)$ provides a satisfactory design parameter for the reflector. With these reflector parameters one can therefore select an appropriate feed illumination to achieve the desired sidelobe levels.

In the remaining part of this section we have used the above reflector parameters to study the sidelobe levels of the antenna as a function of the feed radiation pattern. Similar to the case of an axisymmetric paraboloid discussed in the last section we will model the

feed pattern by a $\cos^m\theta$ distribution ($|a_1(\theta)|=|d_1(\theta)|=\cos^m\theta, 0\leq\theta\leq\frac{\pi}{2}$). Since the offset reflector aperture angle of 25° is much less than that of a symmetric reflector the useful values of m to provide satisfactory gain factor are relatively larger.

Figures (120) to (123) show the computed radiation patterns for an offset reflector with a 24λ projected aperture diameter. The frequency is 12 GHz and Figures (120) and (121) give the results for three different values of m and for an α-polarized feed. As expected, the pattern shapes are almost identical in both planes. Figures (122) and (123) show the results for a y-polarized feed, with results identical to the x-polarization cases. Figures (124) to (132) show the results for two different frequencies, namely, 11.3 GHz and 12.3 GHz. Because, the feed patterns are assumed the same, the reflector patterns are unchanged, indicating negligible effect of the offset configuration on the patterns. The computed cross-polarizations at 12. GHz are shown in Figures (133) to (138). The effects of the feed illumination, the frequency and the feed polarization seems negligible on the peak cross-polar levels, which are above -29 dB level.

Summarizing the results Figures (139) and (140) show the level of the reflector sidelobe as a function of m, the feed illumination parameter. Since the gain factor of the reflector reduces with an excessive aperture tapering a compromize between the gain and the sidelobe levels must in practice be made. However, as Figure (141) shows the reduction of the reflector gain for m larger than its optimum value is not too significant. From these analysis we conclude

that an offset reflector with a gain factor larger than 70% can be designed simply to meet any sidelobe levels between -21dB to -35 dB. Selecting the reflector offset and aperture angles respectively at 30° and 25° also ensures the cross-polarization at about -30dB level, by utilizing a simple scalar feed.

Noise temperature of an offset antenna is usually lower than that of an axisymmetric one, due to the fact that it has no aperture blockage and also the feed system, normally faces the cold sky. For the latter reason the contribution of the feed spillover to the antenna noise temperature is generally much lower. For two diffferent feed illuminations m=12 and m=22 and a reflector with a 48λ aperture size the expected noise temperature data are computed approximately and are listed in Table XVI.

TABLE XVI

Antenna Noise Temperature G/T_A of an Offset Reflector Antenna
Aperture = 48λ

Feed Illumination / Antenna Elevation	m=12		m=22	
	TA,°K	G/TA,dB	TA,°K	G/TA,dB
50°	18.4	29.83	8.1	33.2
30°	20.5	29.36	11.8	31.6
10°	41.9	26.26	35.9	26.77

X PERFORMANCE OF REFLECTOR ANTENNAS WITH A CIRCULARLY POLARIZED FEED

(a) Axisymmetric Reflector

Generally, an axisymmetric reflector antenna, excluding the strut blockage, has a performance independent of the feed polarization. However, strut scattered field is dependent on the feed polarization and as such its performance for linear and circularly polarized feed will differ. The reception of circularly polarized signal has been discussed by Sinclair [16]. He has shown that, the voltage generated at the terminal of a circularly polarized antenna is given by

$$V = h_\theta E_\theta + h_\phi E_\phi \tag{39}$$

where h_θ and h_ϕ are the polarization vectors of the circularly polarized antenna and E_θ and E_ϕ are the polarization vectors of the signal. Using equation (39) one can, in general, obtain the response of the antenna for an incoming elliptically polarized signal, from which one can study the co-polar and the cross-polar components of the circularly polarized antenna. Here, for a right-hand circularly polarized wave the antenna response will correspond to the co-polar components and its response to a left-hand circularly polarized wave will denote the cross-polarization. In particular, in the principal planes, $\phi=0$ and $\phi=\pi/2$, the co-polar and the cross-polar components will become the θ and the ϕ-component contributions. Thus, utilizing the data of a linearly polarized feed, one can readily obtain the circularly polarized feed co- and the cross-polar data, simply by addition and subtraction of the copolar data.

From the above discussion it is evident that the sidelobe levels of a circularly polarized feed will be the average sidelobe levels for the x and the y-polarized feeds. For a quad-strut geometry a representative data are shown in Figure (142), for a $\cos\theta$ feed pattern. These co-polar and the cross-polar data may be compared with those of a y-polarized feed given in Figures (95) and (96). The co-polar pattern has somewhat lower sidelobe levels, but the cross-polar level is considerably higher, -37 dB, compared to -53 dB. However, the cross-polar level is still satisfactory. Other antenna performance factors will be similar to the linearly polarized case, since the difference between the co-polar patterns is relatively small.

(b) Offset Reflector

An offset reflector has an inherent property that, it does not produce cross-polar component with a circularly polarized feed. As a result, its co-polar patterns are similar to the case of a linearly polarized feed. For this reason its pattern for a circularly polarized feed are not included. On the other hand, an offset reflector beam shifts away from the reflector axis, due to the circular polarization. The direction of the shift is different for the right or the left hand of the polarization. This beam shift, generally known as beam squint, can be calculated from [12]

$$\psi_s = \sin^{-1}\left[\frac{\lambda \sin\theta_o}{4\pi F}\right] \qquad (40)$$

where F is the focal legnth of the reflector. To indicate the magnitude of this beam shift we assume a frequency of 12GHz, θ_o=30° and θ^*=25°. For a 48λ reflector aperture one finds.

$$F = \frac{48\lambda}{4} \frac{\cos\theta o + \cos\theta^*}{\sin\theta^*} = 50.32\lambda$$

or (41)

$$\psi_s = \sin^{-1}\left[\frac{\lambda \sin\theta o}{4\pi \times 60.32\lambda}\right] = 0.045 \text{ degree}$$

This beam shift angle is too small and is much less than the pointing accuracy of small earth-station antennas. Thus, the performance of an offset reflector with a circularly polarized feed is satisfactory provided that the above reflector parameters are selected.

XI CONCLUSIONS AND RECOMMENDATIONS FOR FUTURE WORK

In this report we have studied the performance of both symmetric and offset reflectors and examined the level of their sidelobe and the cross-polarizations. For the symmetric antenna the effects of both central blockage, due to the feed, and the strut blockage were studied for the three strut configurations of J-hook, the tripod and the quad geometry. It was shown that, in all cases, the tapering of the apertures field reduces the sidelobe level, but the blockage affects the sidelobe levels of the heavily tapered illumination more significantly. For this reason, the symmetric reflector generally has higher sidelobe levels than the offset one. The cross-polarization of both reflectors was found to be satisfactory.

Among the three strut geometries, the quad-strut was found to have a distinct feature. When the quad-struts are selected to have an appropriate spherical shadow they produce patterns, in the 45° plane, which have sidelobes lower than the unblocked reflector. Thus, whenever possible this property of a quad-configuration can be used to generate super-low sidelobe antennas. Its sidelobes, however, are high in the principal planes.

To study the cross-polarization of a symmetric reflector the current distributions on the struts were obtained, using the approximation of infinite struts. These current distributions were then used to determine the strut scattered field accurately. The cross-polar components were obtained and were found quite low.

To remedy the problem of high sidelobe of a symmetric reflector it was recommended that one may modify the reflector field illuminating the strut to generate a proper phase shift. One method to achieve this phase change was to use strips of appropriate thickness (about 0.3λ to 0.4λ) just under each strut. The computed reflector patterns indicated that, this method of aperture phase change can enhance the antenna gain and reduce the near-in sidelobes. The problem was modelled approximately, using physical optic currents on the strips. In practice this model will provide inaccurate strip curents and an experimental investigation must be carried out to study its usefulness.

The performance of an offset reflector was also studied. It was recommended that for a proper performance the offset and the reflector aperture angles must be selected less than 30° and 25°, respectively. With these parameters, the cross-polar radiation of the reflector, with asymmetric feed pattern, is below -29 dB, and its beam squint is negligible. Its sidelobe level can then be reduced to very small levels by tapering the aperture field.

The performance of both reflectors with a circularly polarized feed was also studied. It was found that in both cases the performance of the antenna for the co-polar radiation is similar to the linearly polarized case. The cross-polar radiation, however, was found to be higher.

Various other techniques for reducing the sidelobes of a symmetric reflector were also discussed. It was then concluded that the most promising approach is to load the reflector with conducting strips under each strut. Because, this method was analyzed approximately, it

is recommended that this method of sidelobe reduction be studied experimentally.

As a recommendation for future work, we feel that the loading of the reflector be studied further. In practical situations loading the reflector must be handled carefully. Attaching strips to the reflector may not perform satisfactorily, since strip currents between the strip and the reflector surface may destroy the predicted behaviour. Thus, either strips must be carefully electrically shorted to the reflector, or, other geometries such as knife edge conductors, similar to SAVAC antenna [8] be employed. In all cases the reflector performance must be evaluated, so that, the optimum configuration may be obtained.

REFERENCES

1. S. Silver, "Microwave Antenna Theory and Design", New York, McGraw-Hill, 1949.

2. P. J. B. Clarricoats, and G. T. Poulton, "High-Efficiency Microwave Reflector Antennas, A review", Proc. IEEE, Vol. 65, No. 10, pp. 1470-1505, Oct. 1977.

3. C. C. Han, "Reduction of Ground Antenna Near-in Sidelobes in the Direction of Geostationary Orbit", IEEE/Ap Symposium, pp. 310-313, Aug. 1973.

4. S. Chung and Y. Naito, "Sidelobe Control of Aperture Antenna by Dielectric Rim Loading", IEEE/Ap Symposium, pp. 236-239, June 1975.

5. R. B. Dybdal and H. E. King, "Performance of Reflector Antennas with Absorber-Lined Tunnels", IEEE/Ap Symposium, pp. 714-717, June 1979.

6. H. Thielen, "Reduction of the Strut Radiation of Reflector Antenna", IEEE/Ap Symposium, pp. 504-507, June, 1981.

7. N. Matsunaka, S. Betsudan, and T. Katagi, "Sidelobe Level Reduction by Improvement of Strut Shape", IEEE/Ap Symposium, pp. 496-499, June, 1981.

8. Savac International, Inc., "Four Element Vectored Array", Microwaves, pp. 14, Feb. 1982.

9. M. Shariatmadar and L. Shafai, "Effect of Dielectric Coating of Struts on the Reduction of Sidelobe Levels", Univ. of Manitoba, Elect. Eng. Internal Rept.

10. A. A. Zaghlool and L. Shafai, "Performance of Offset Paraboloid Reflectors with Offset Matched Feeds", Univ. of Manitoba, Elect. Eng., TR 80-8.

11. L. Shafai and O. Aboul-Atta, "Study Covering the Electrical and Mechanical Characteristics of a Transmitting Antenna", Final Report, Com. Res. Centre, Contract OSU76-00177, March 1977.

12. A. W. Rudge and N. A. Adatia, "Offset-paraboloid-reflector Antennas: A Review", IEEE proceeding, Vol. 66, No. 12, pp. 1592-1618, Dec. 1978.

13. L. Shafai and O. Aboul-Atta, "Optimum Design of a Low Noise Paraboloid Antenna", Univ. of Manitoba, Elect. Eng., TR79-5.

14. L. Shafai, "A High Performance Feed for a Low Cost Earth Terminal", Com. Res. Centre, Tech. Memorandum 59/77, Feb. 1977.

15. T. S. Chu and R. H. Turrin, "Depolarization Properties of Offset Reflector Antennas", IEEE Trans. Ant. & Propag., Vol. Ap-21, pp. 339-345, May 1973.

16. G. Sinclair, "The Transmission and Reception of Elliptically Polarized Waves", Proc. I.R.E., pp. 148-151, Feb. 1950.

FIGURES

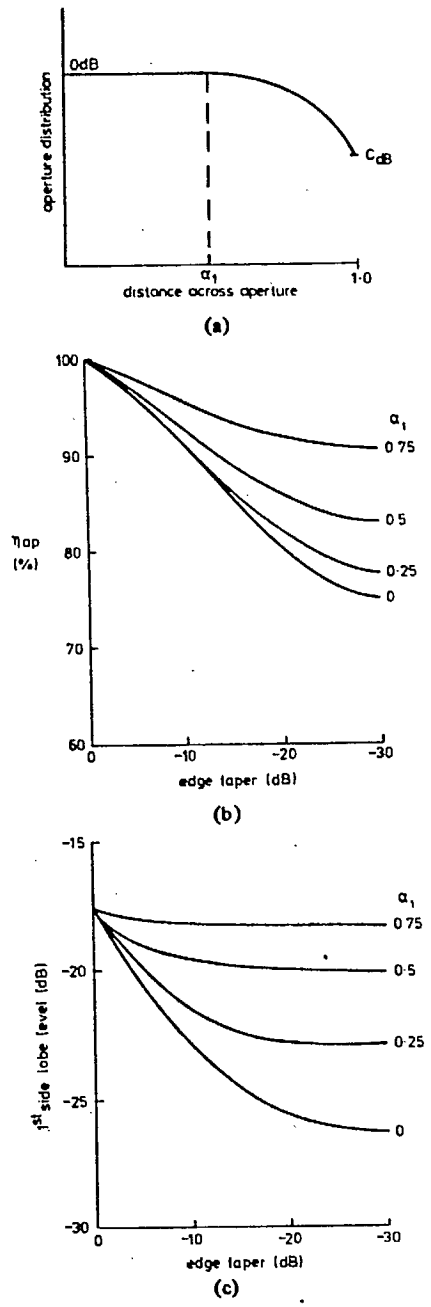

Figure 1. Effects of aperture distribution. (a) Type of aperture distribution assumed. (b) Variation of aperture efficiency with distribution parameters α, and C_{dB}. (c) Variation of first sidelobe level with α, and C_{dB}.

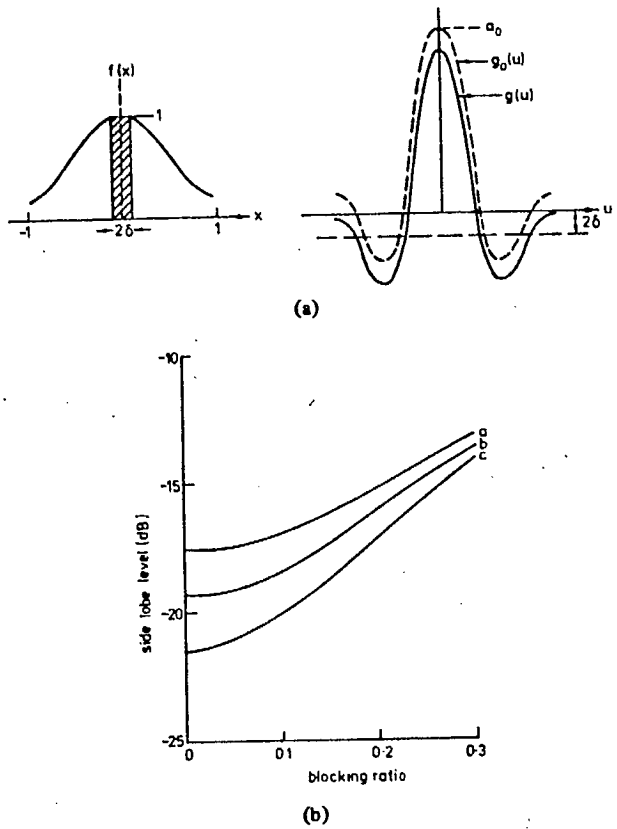

Figure 2. Effect of central blockage on sidelobe level. (a) Effect of aperture blockage (Silver [1]). (b) Variation of first sidelobe level with aperture blockage. a-uniform illumination; b-10d edge taper, $\alpha_1 = 0.5$; c-10dB edge taper; $\alpha_1 = 0.25$.

Figure 3. -Reflector with absorbers mounted.

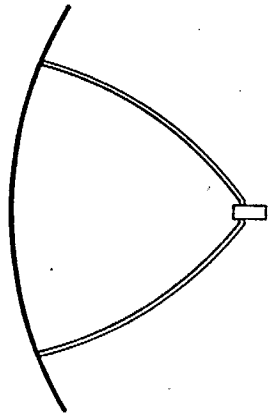

Figure 4. Paraboloidal antenna with bent struts.

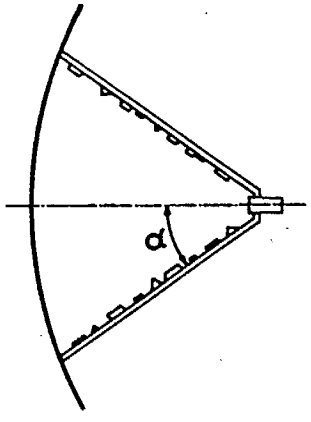

Figure 5. Paraboloidal antenna with small metal pieces attached to the feed struts.

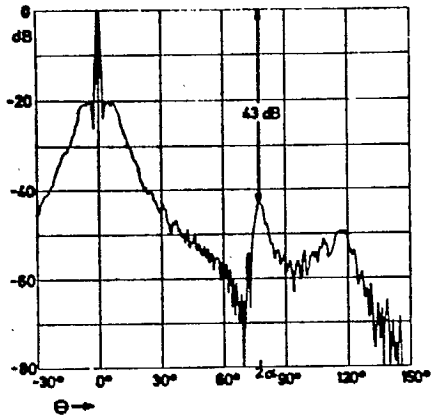

(a) Radiation pattern of a 1.5-m paraboloidal antenna having four straight struts with smooth surfaces (11.5 GH_z)

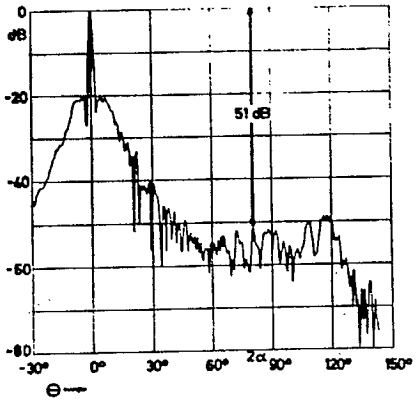

(b) Radiation pattern of a 1.5-m paraboloidal antenna whose struts have been changed according to Figure 5 (11.5 GH_z)

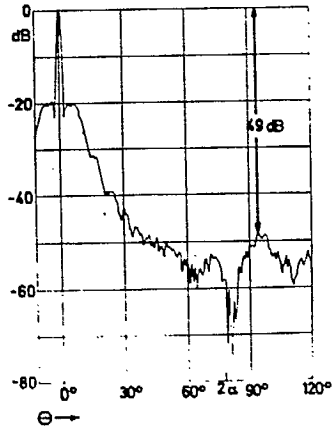

(c) Radiation pattern of a 1.5-m paraboloidal antenna with bent struts (11.5 GH_z)

Figure 6

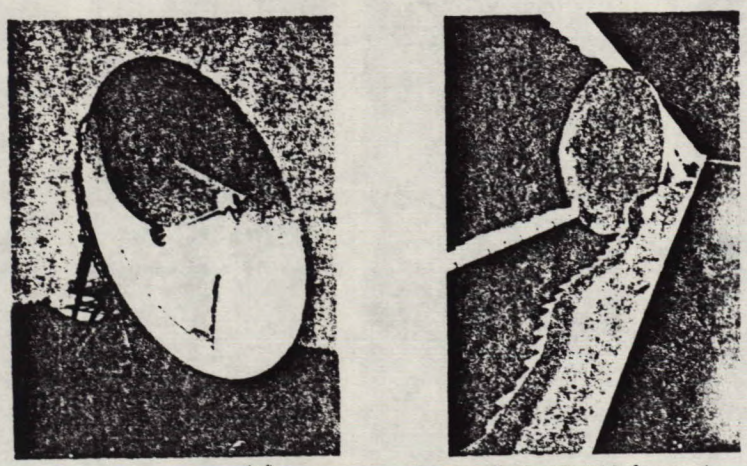

Standard "A" Earth Station Antenna Equipped With Improved Strut. (KDD, YAMAGUCHI, Japan)

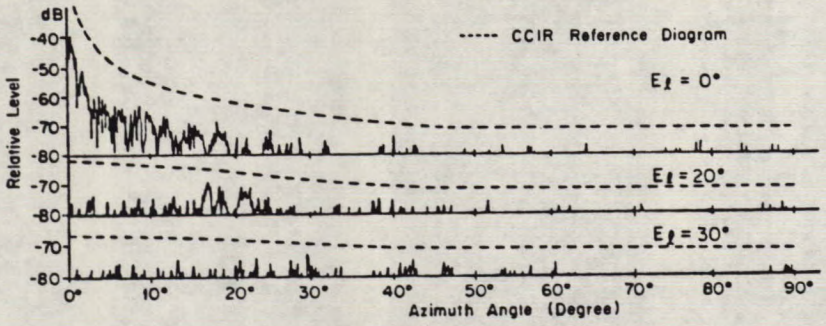

(a) In case of Improved Tripod

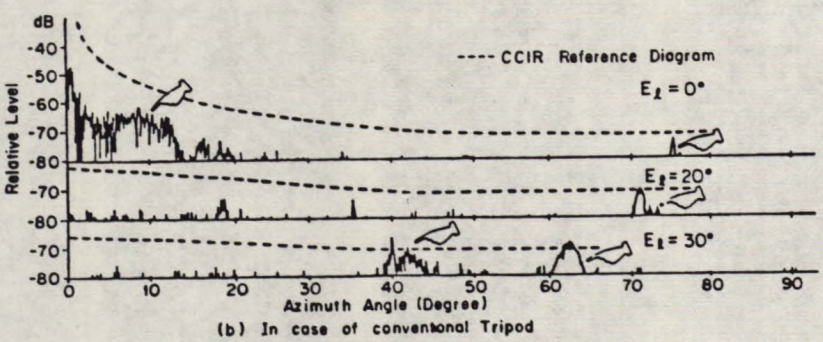

(b) In case of conventional Tripod

Effect of the Improved Strut
(Cross-polar, 6. GHz)

Figure 7

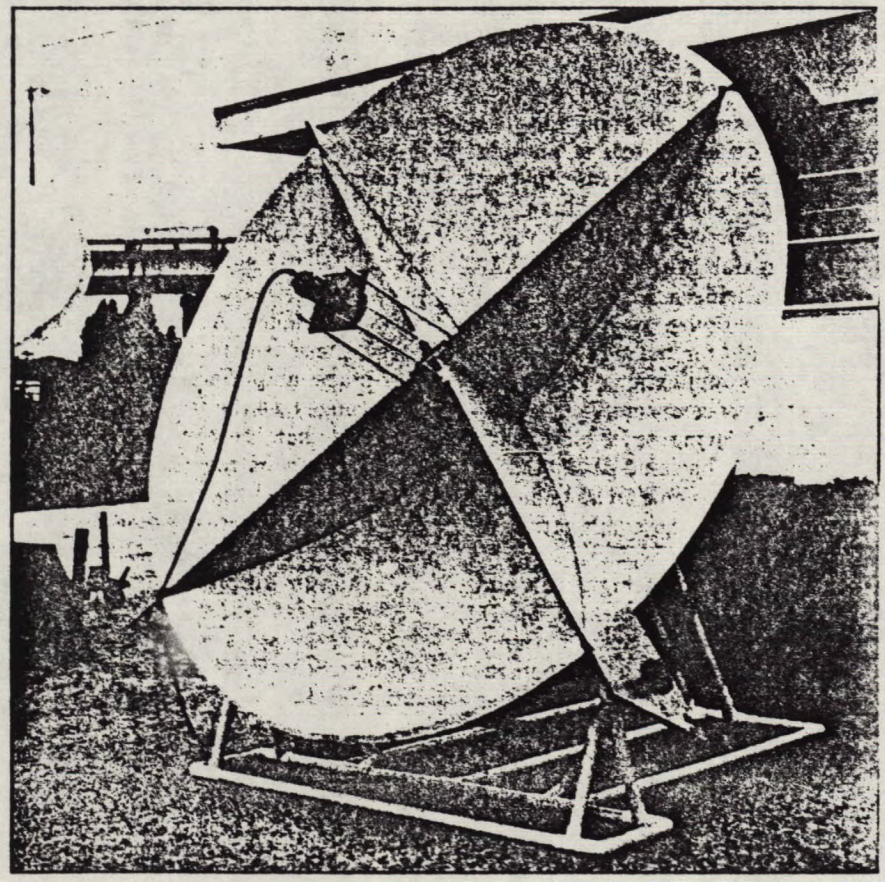

Figure 8. The SAR - 10.3 antenna, designed by SAVAC, International Inc.

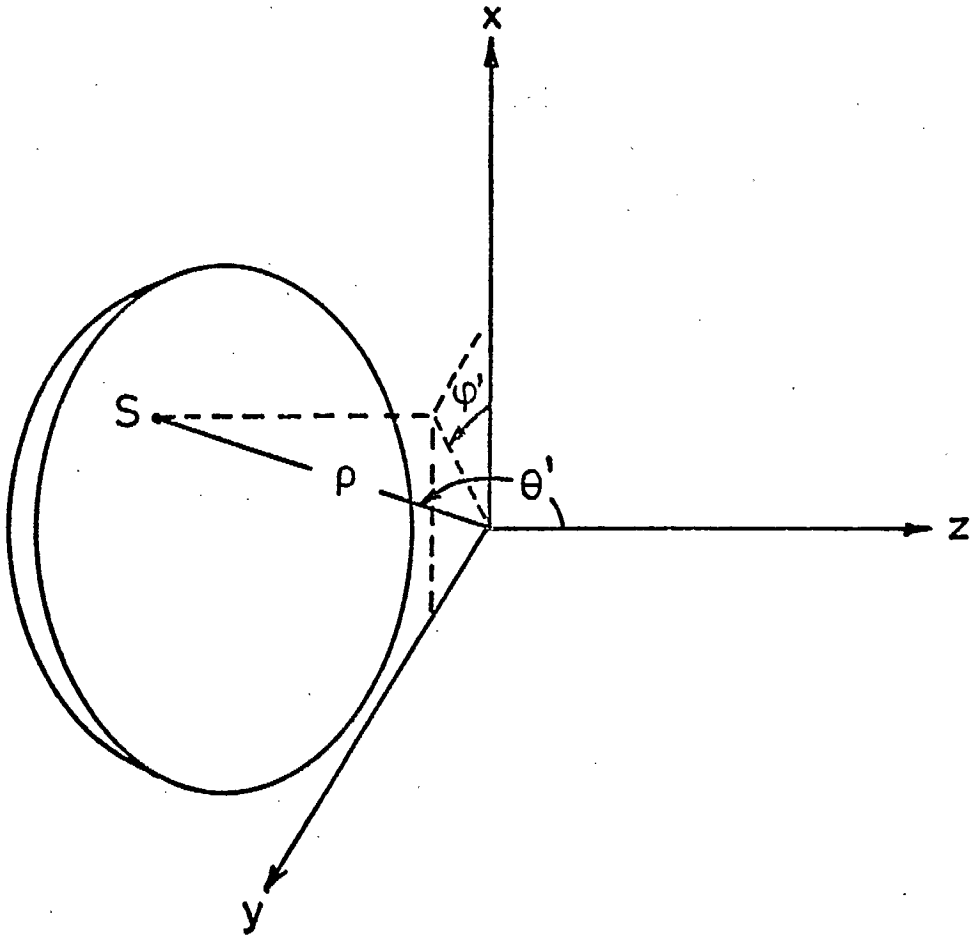

Figure 9. Paraboloid geometry

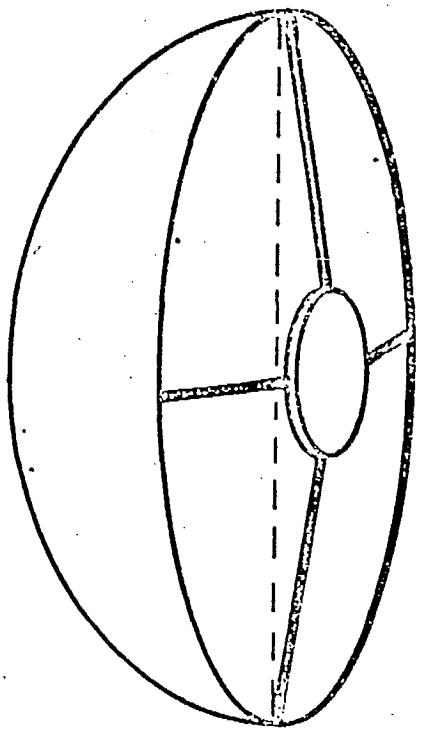

Figure 10. Geometry of typical aperture blockage of reflector antenna

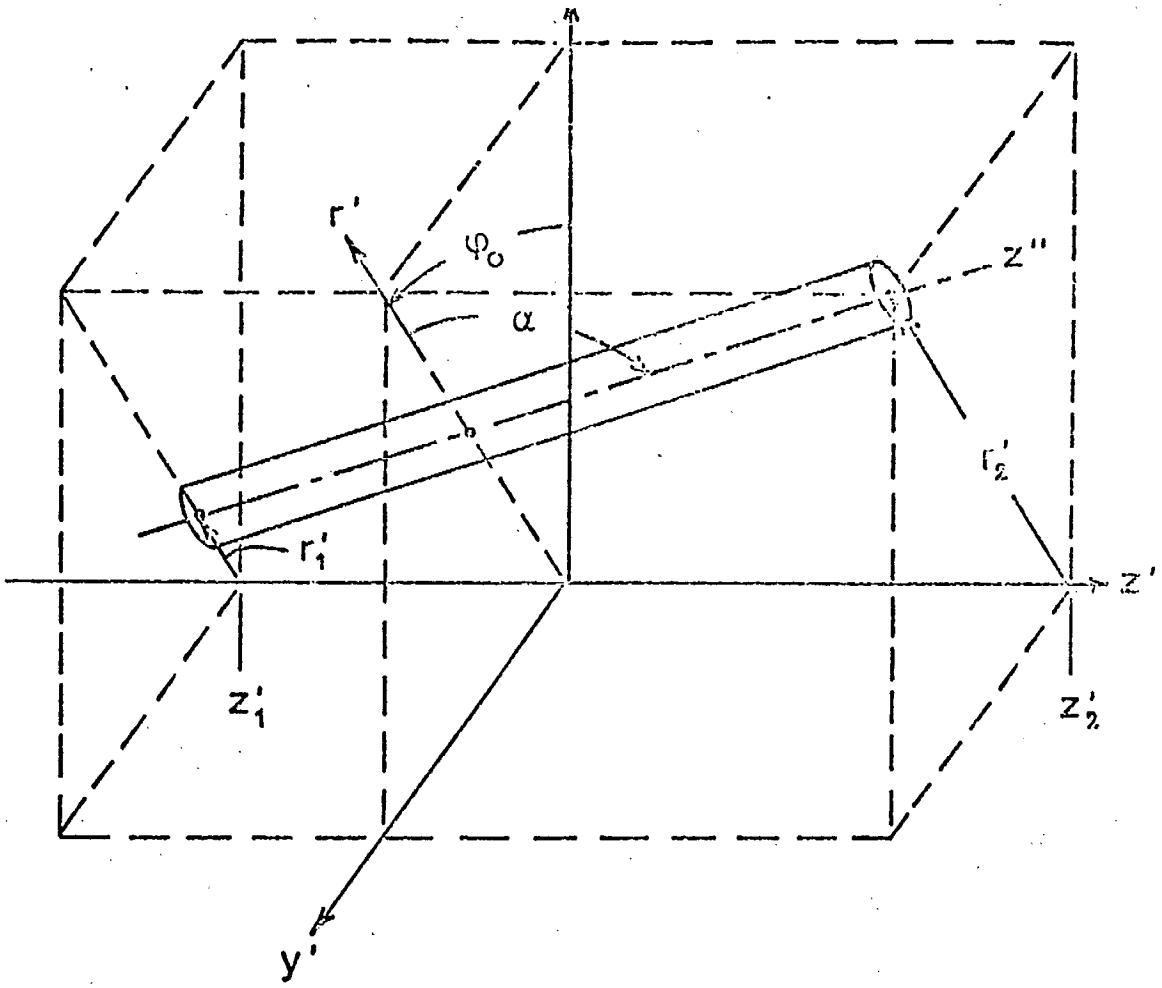

Figure 11. Strut geometry

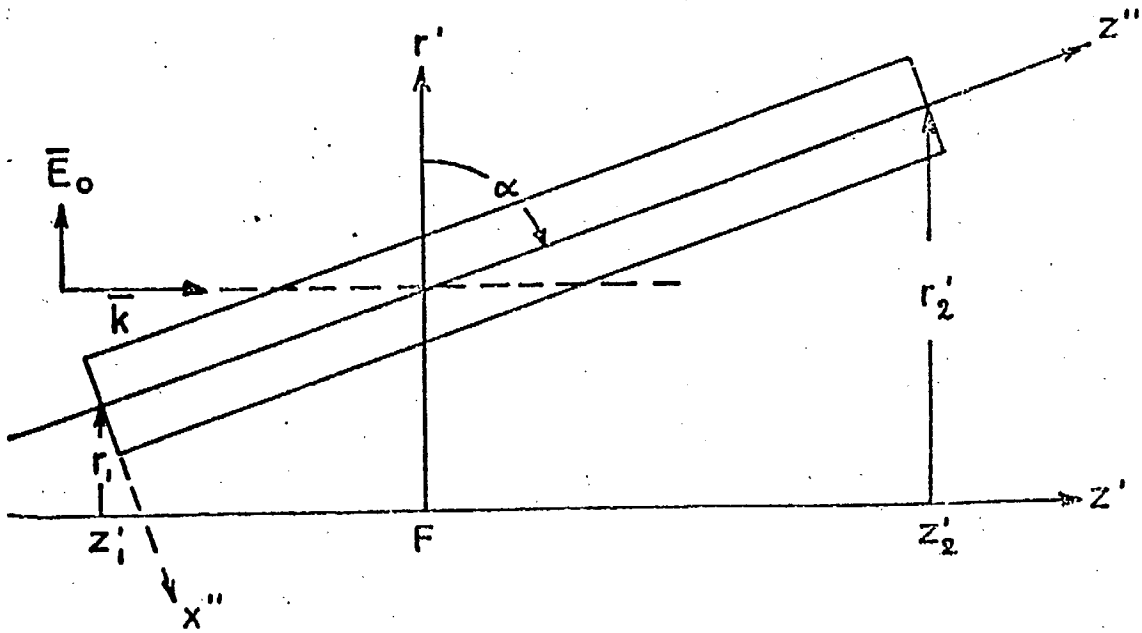

Figure 12. Relation between single-prime and double-prime coordinate systems

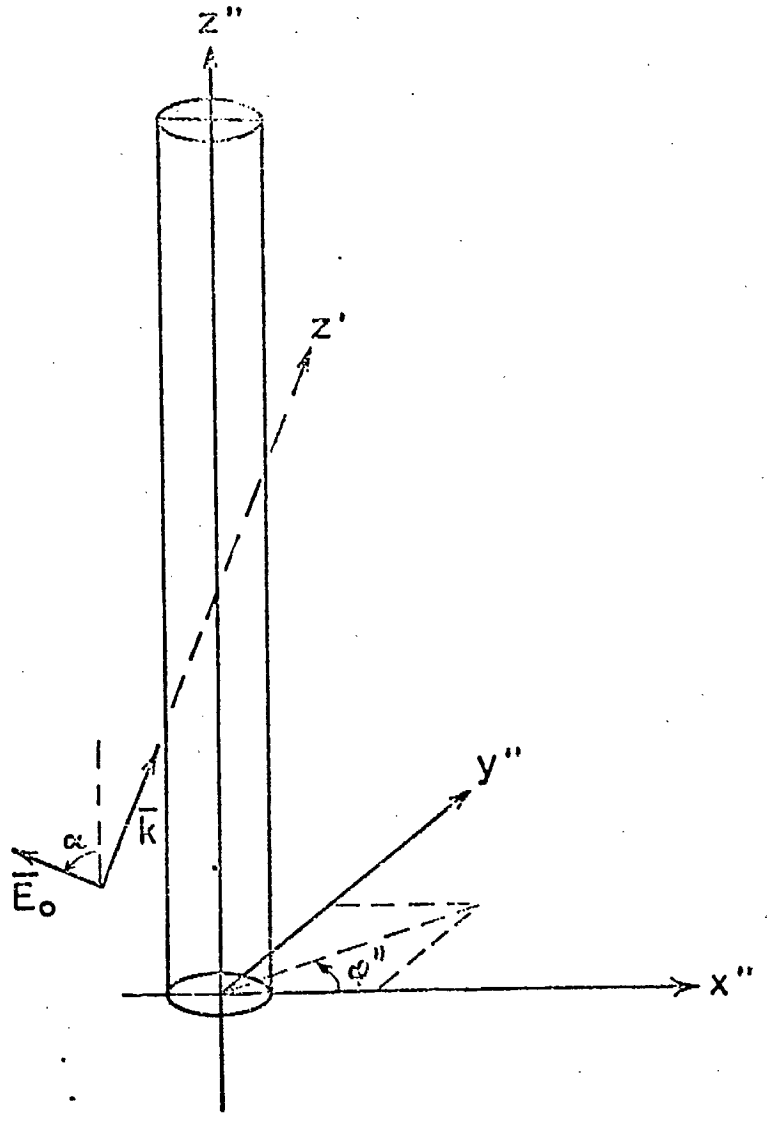

Figure 13. Oblique view of double-prime coordinate system

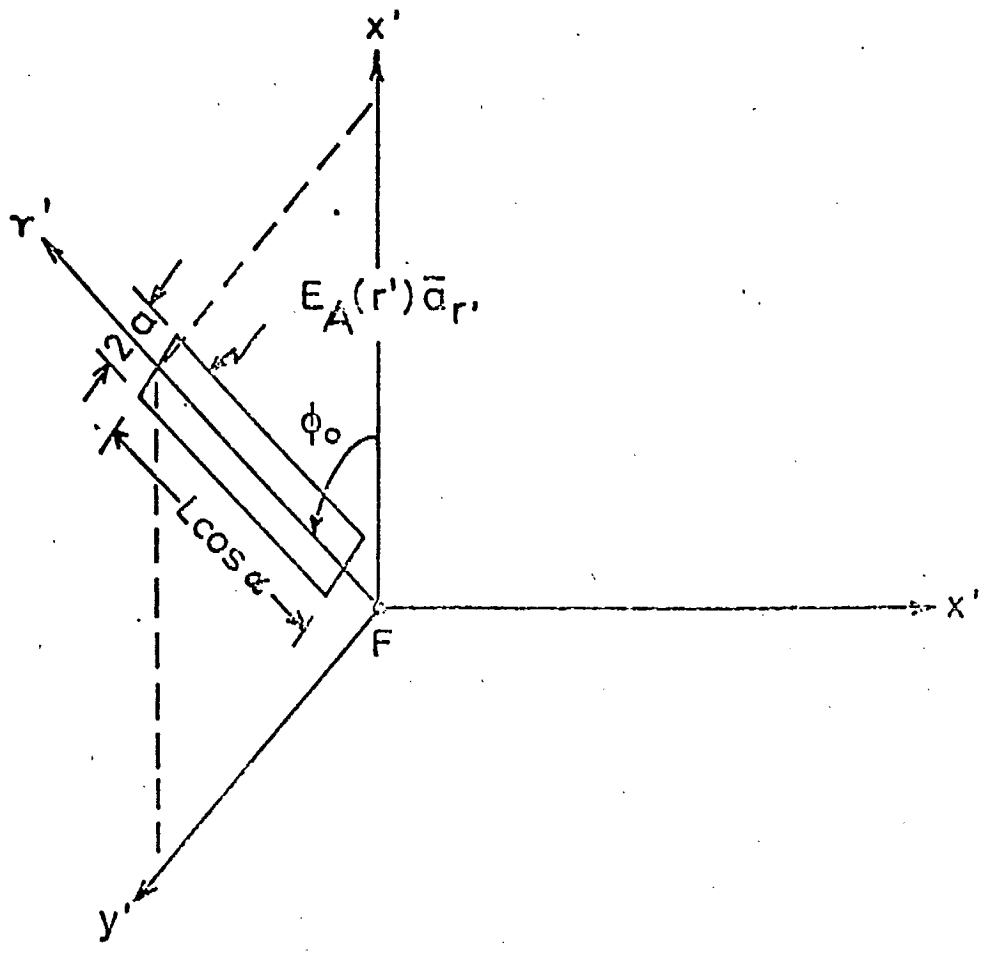

Figure 14. Equivalent aperture defined by projecting strut on x' -y' plane

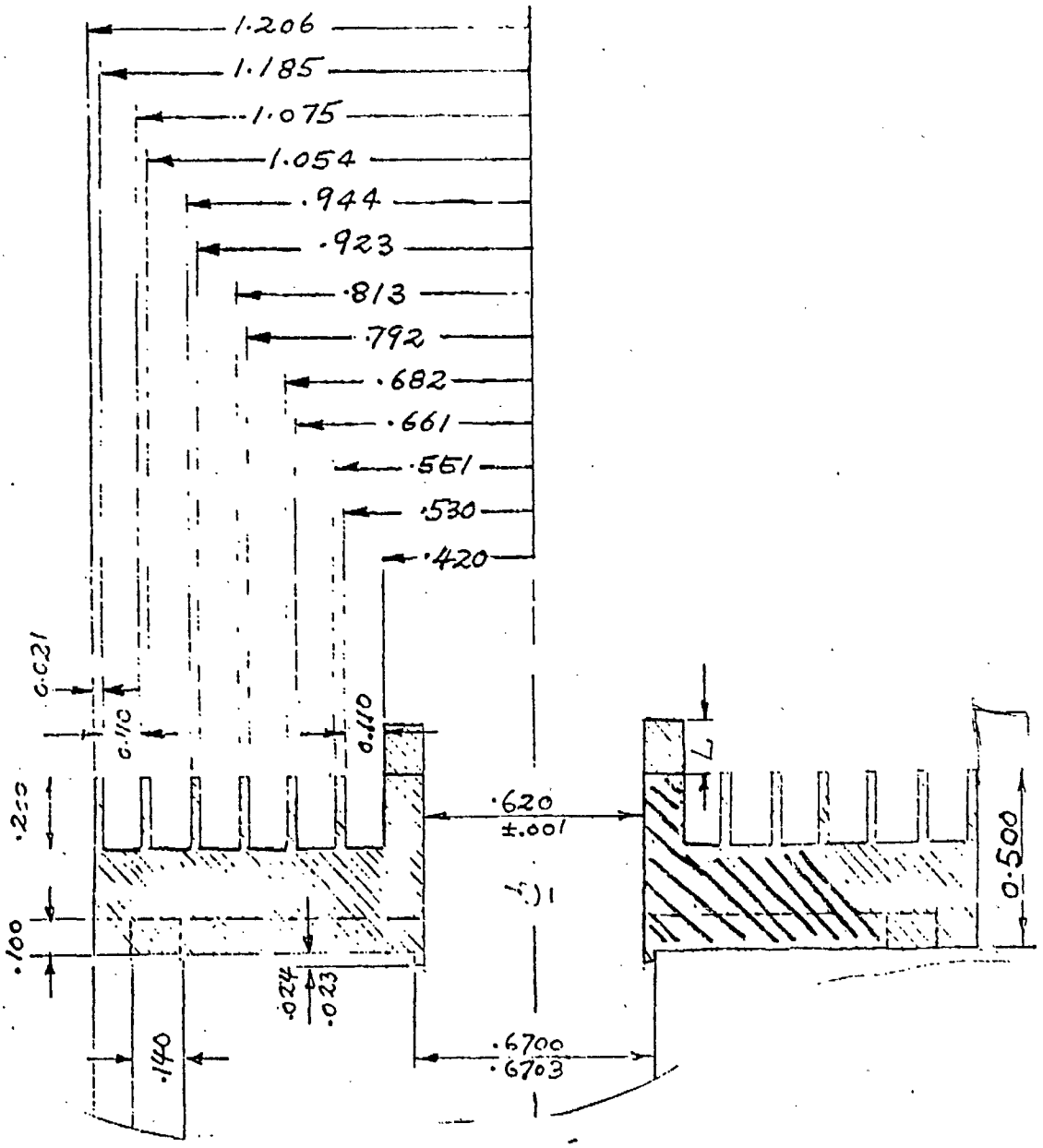

Figure 15. Corrugation geometry of CRC feed

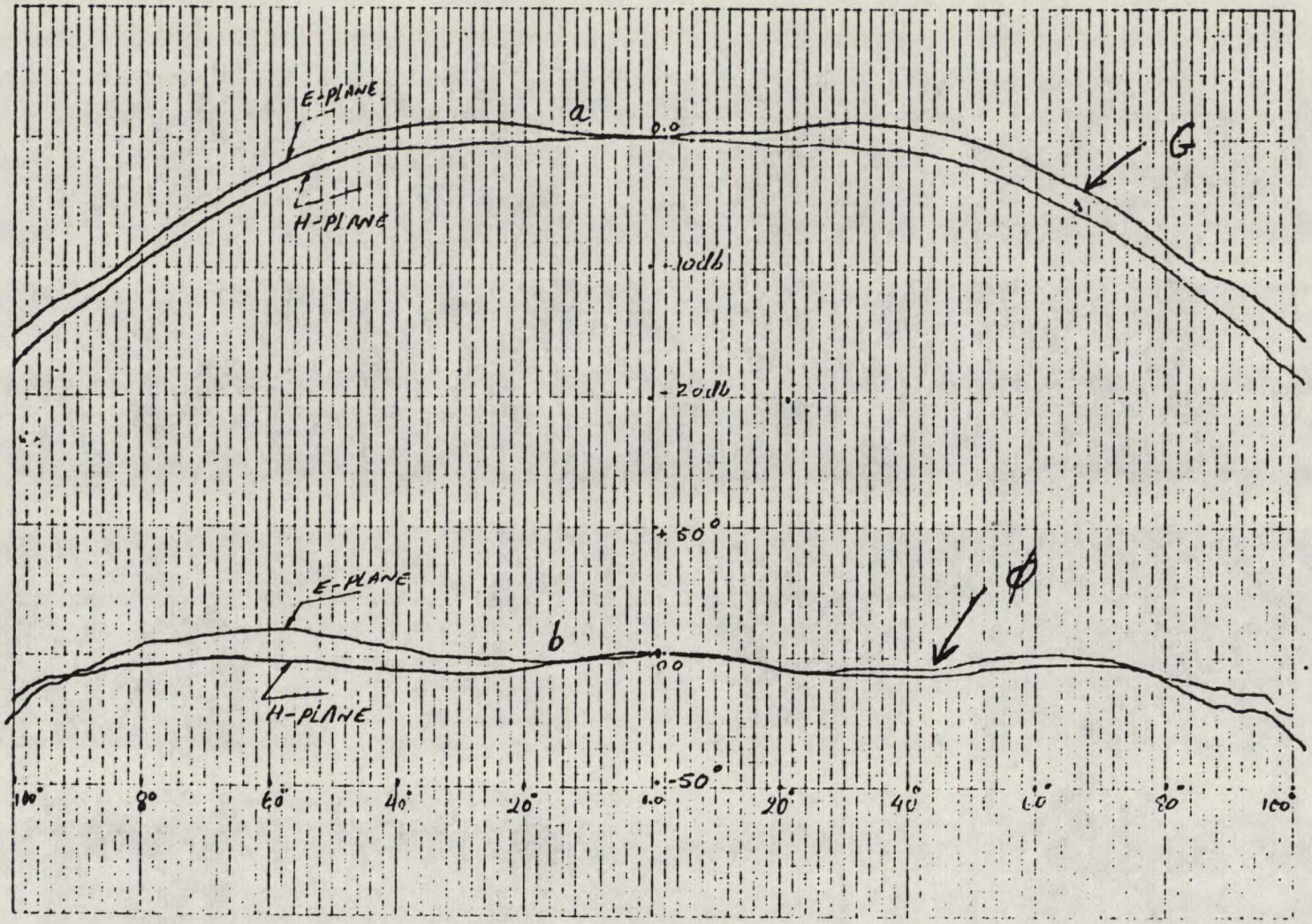

Figure 16. Radiation patterns of CRC feed

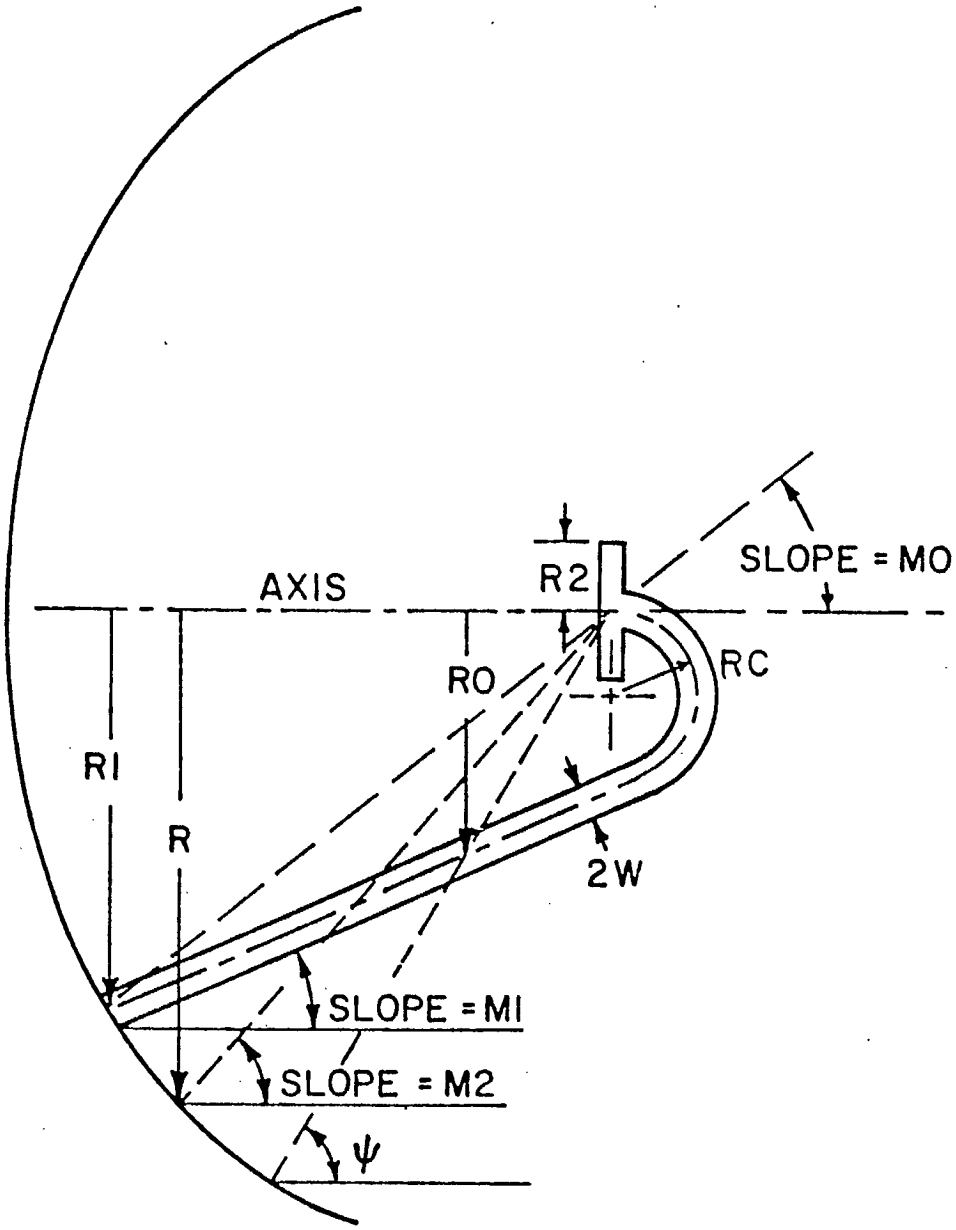

Figure 17. J - hook geometry

CASE I

J - HOOK

The following figures are given in code as:

JA XX YY

J indicates J - Hook supporting structure

A indicates the feed polarization, E or H

XX indicates the ratio of J - Hook location to the reflector radius. The maximum value is 1 which will be represented by XX equal to 10

YY indicates the angle ϕ (degree) at which the pattern is calculated

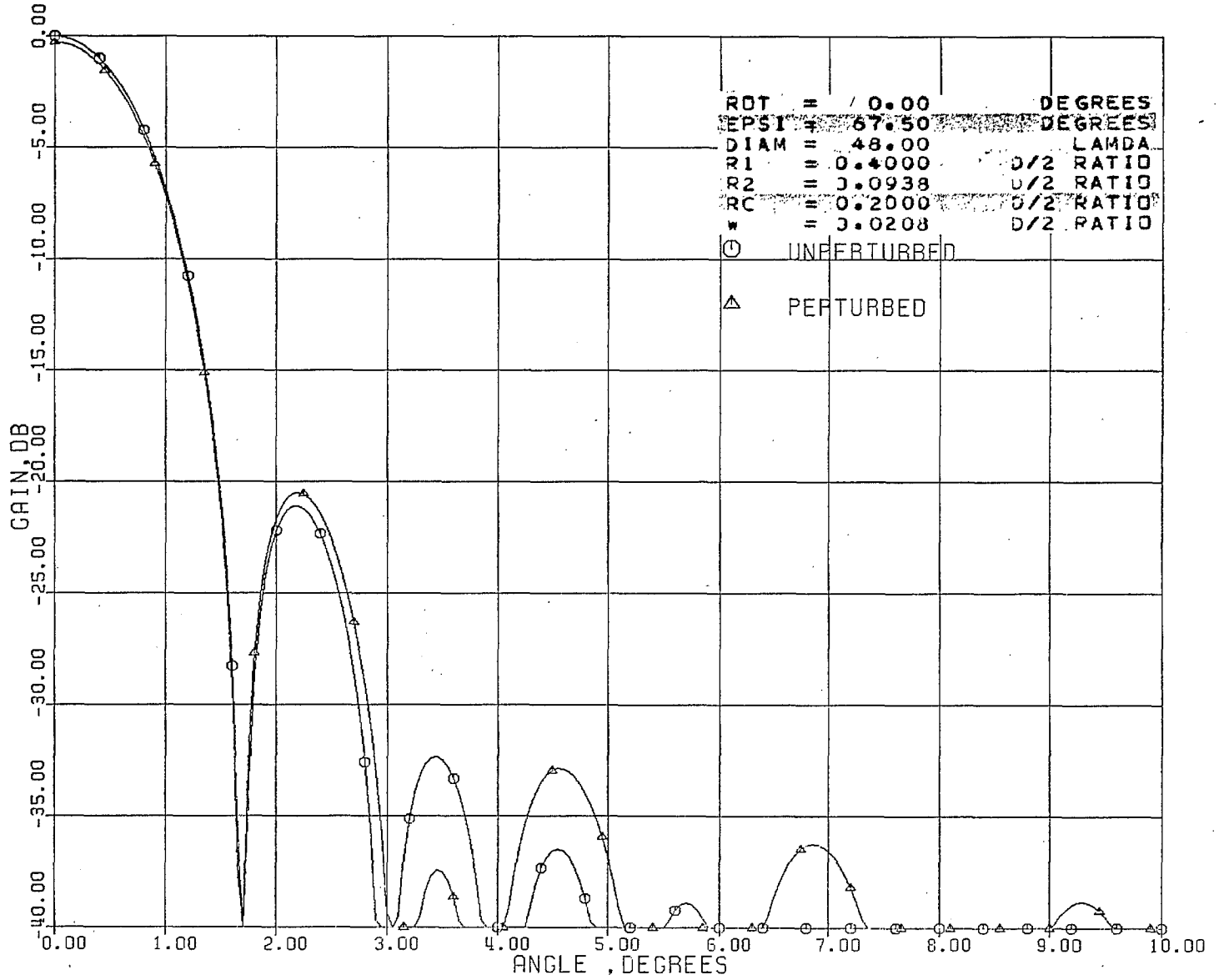

Figure 18. J - hook, E - polarization (JE 0400)

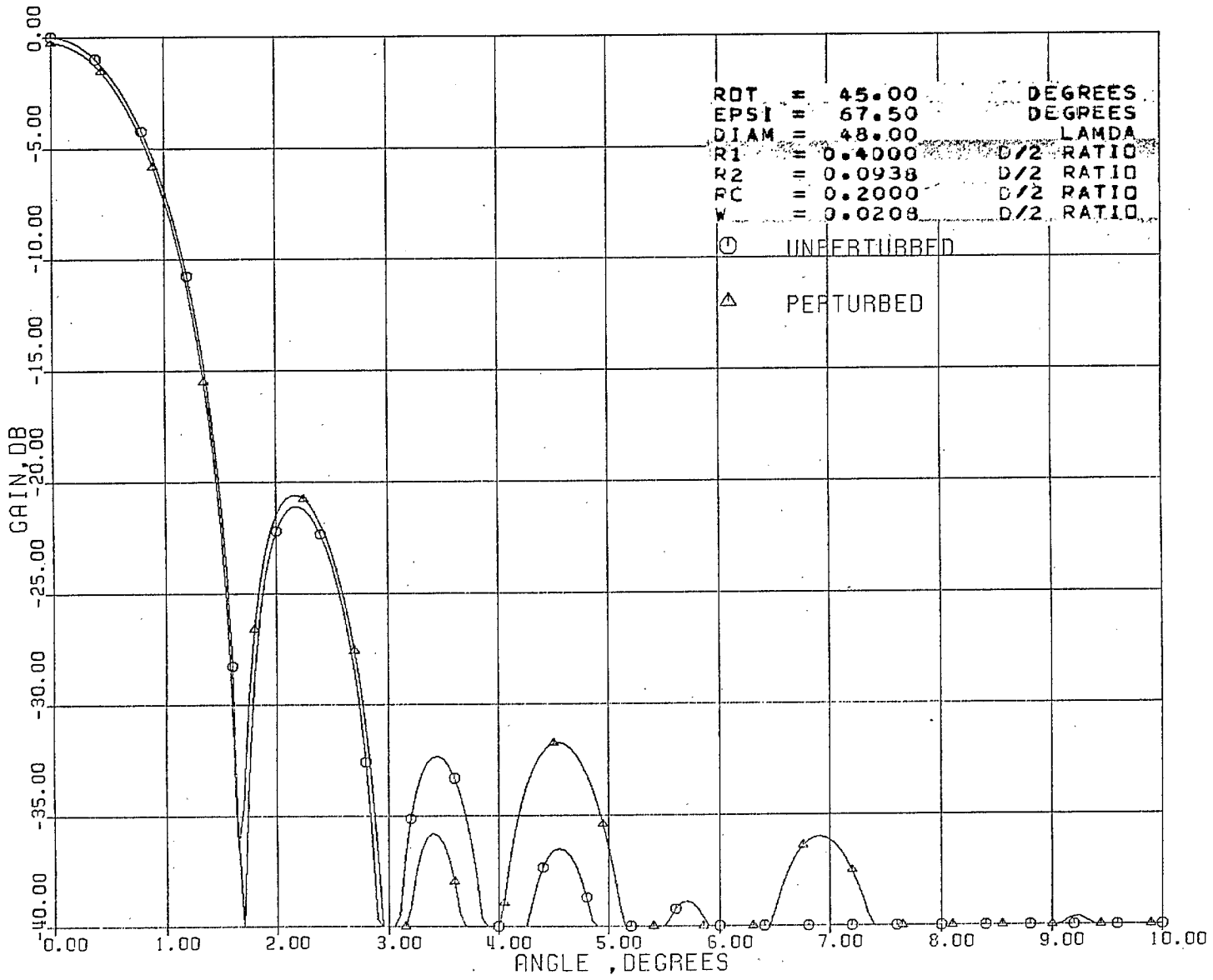

Figure 19. J - hook, E - polarization (JE 0445)

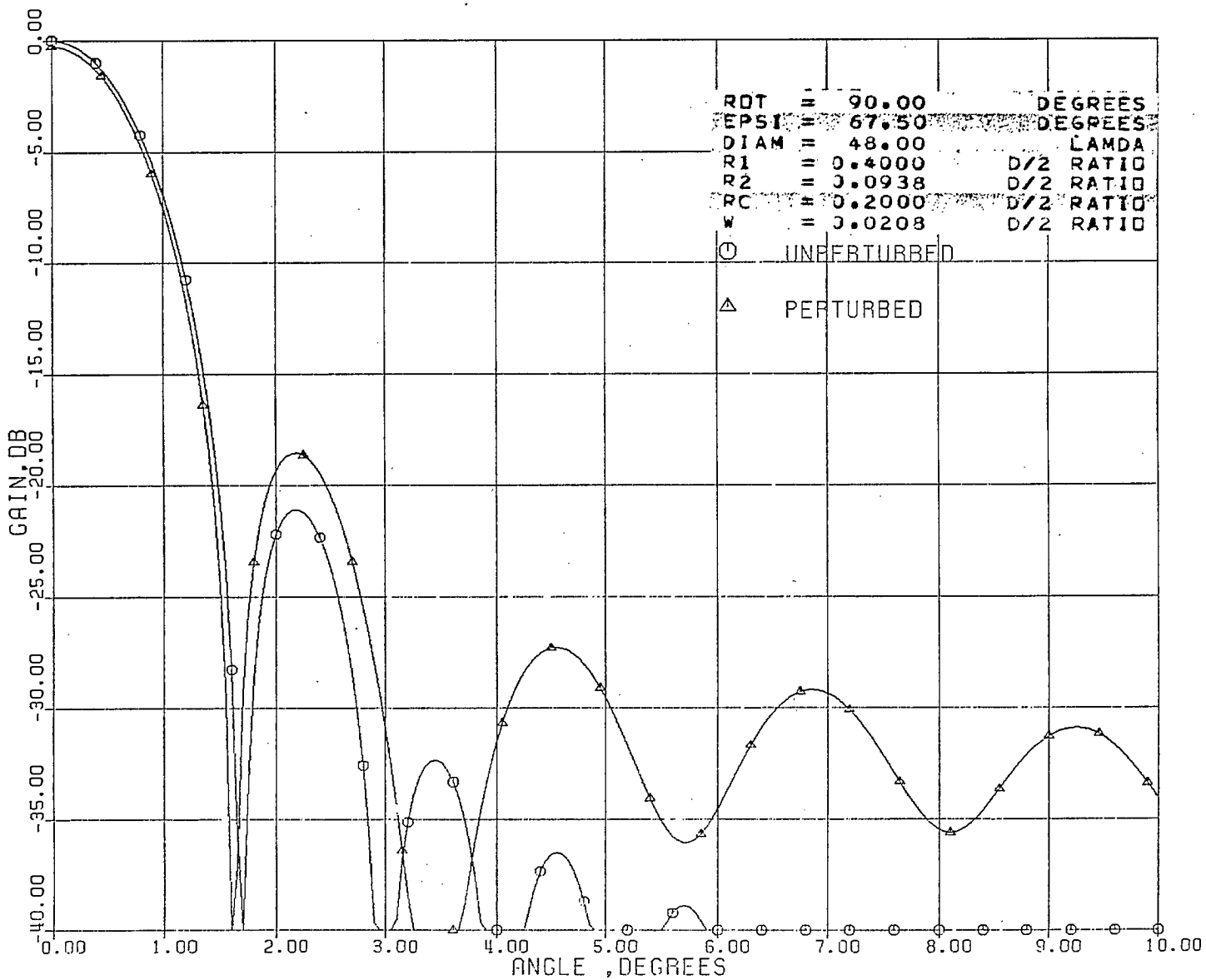

Figure 20. J - hook, E - polarization (JE 0490)

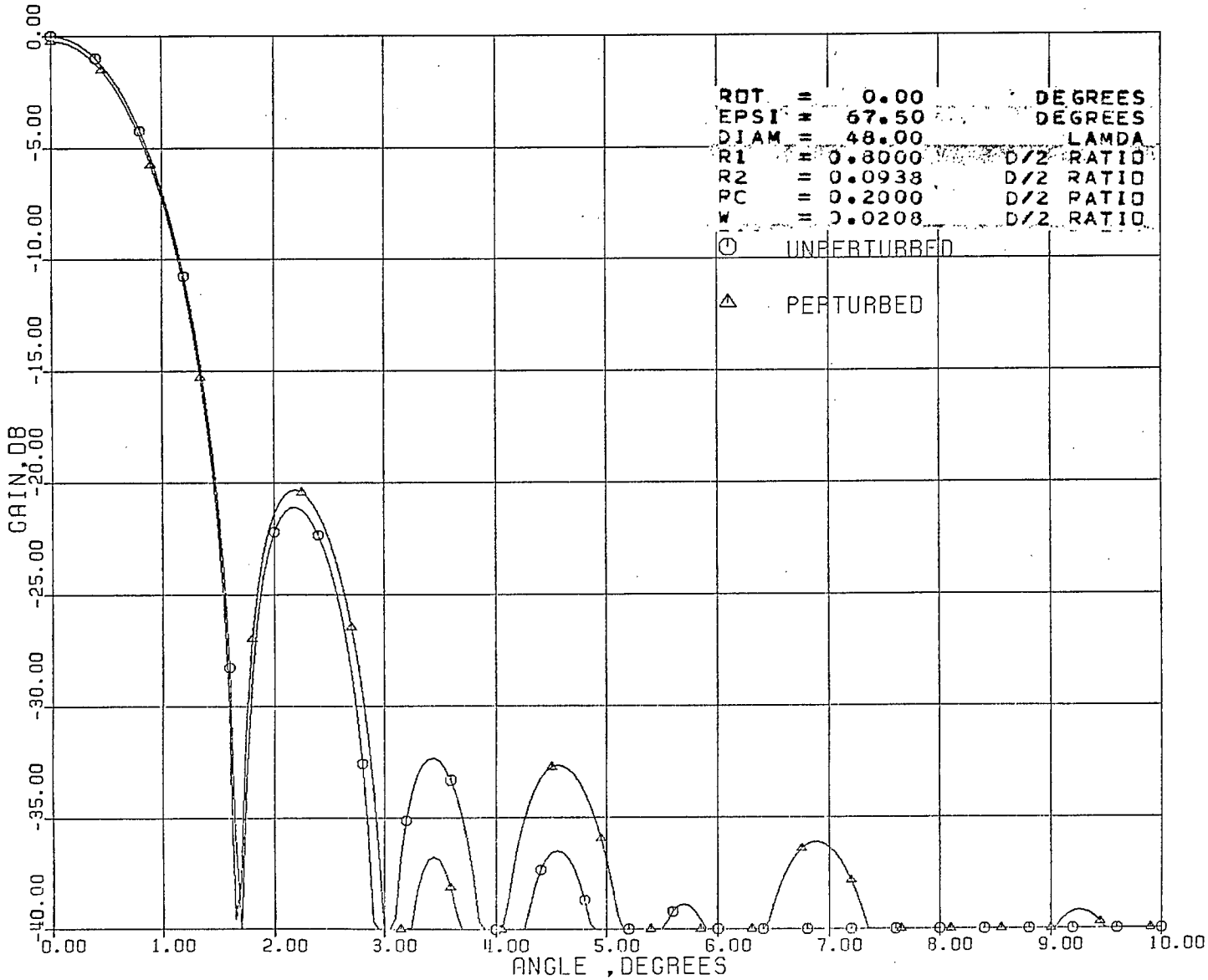

Figure 21. J - hook, E - polarization (JE 0800)

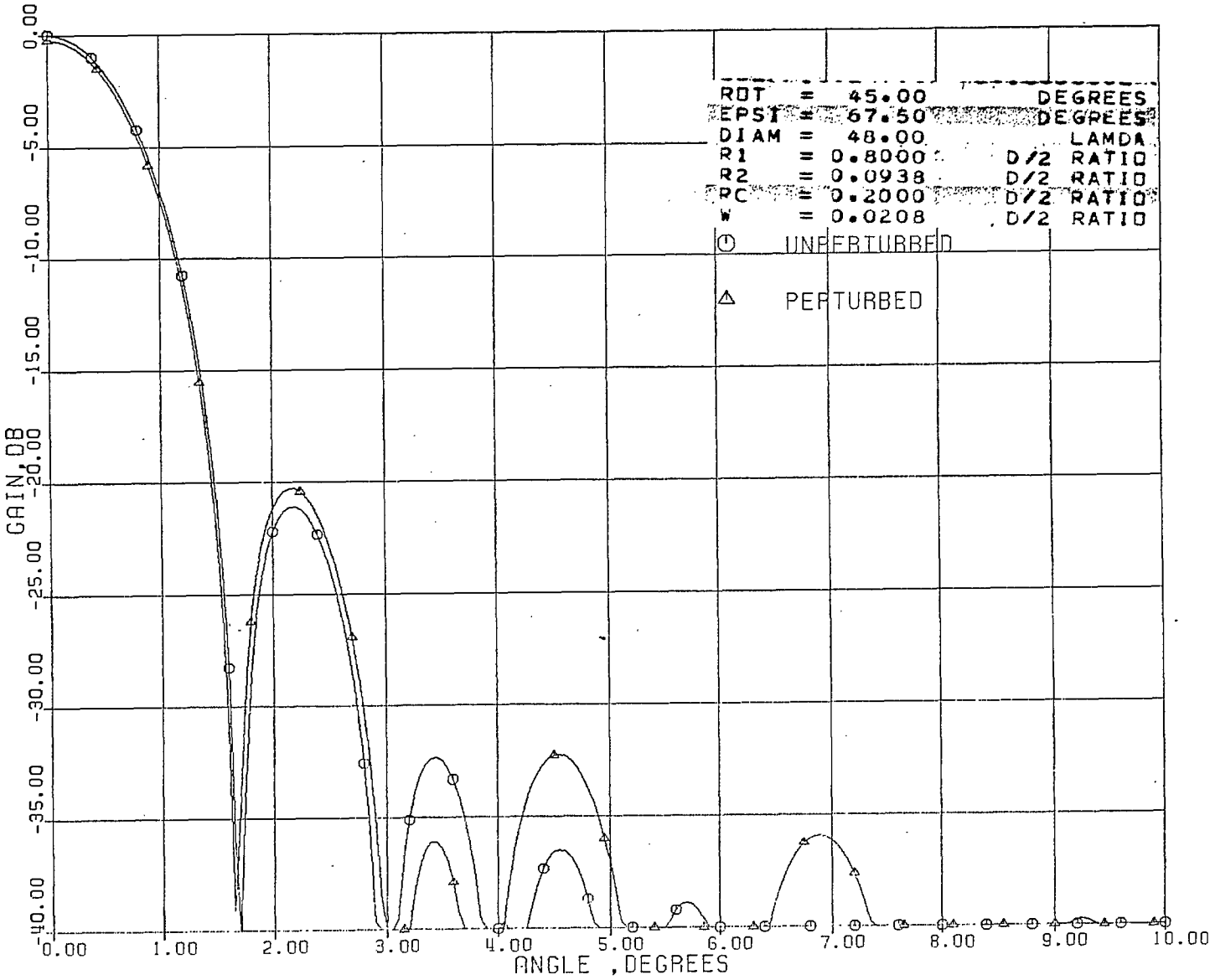

Figure 22. J - hook, E - polarization (JE 0845)

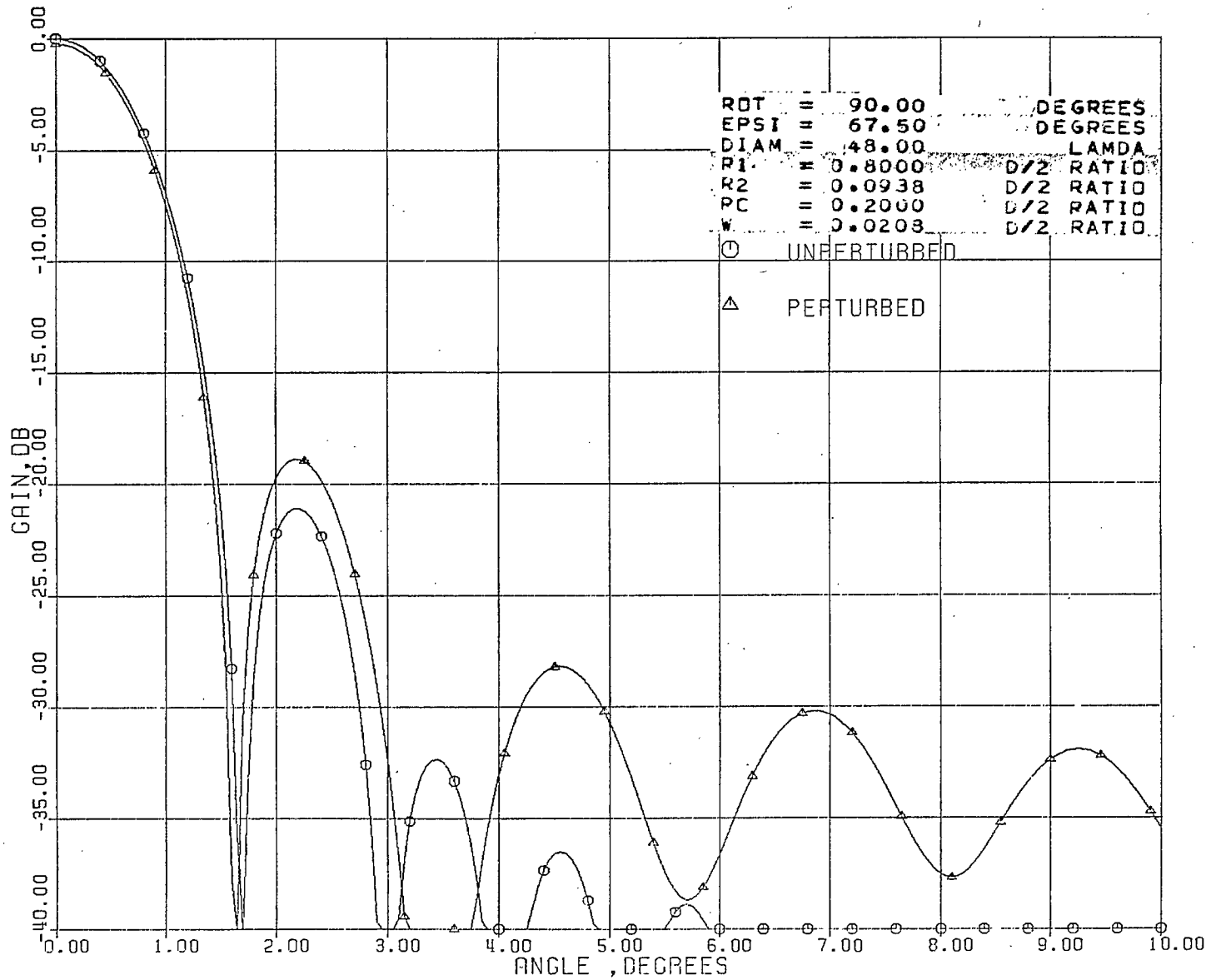

Figure 23. J - hook, E - polarization (JE 0890)

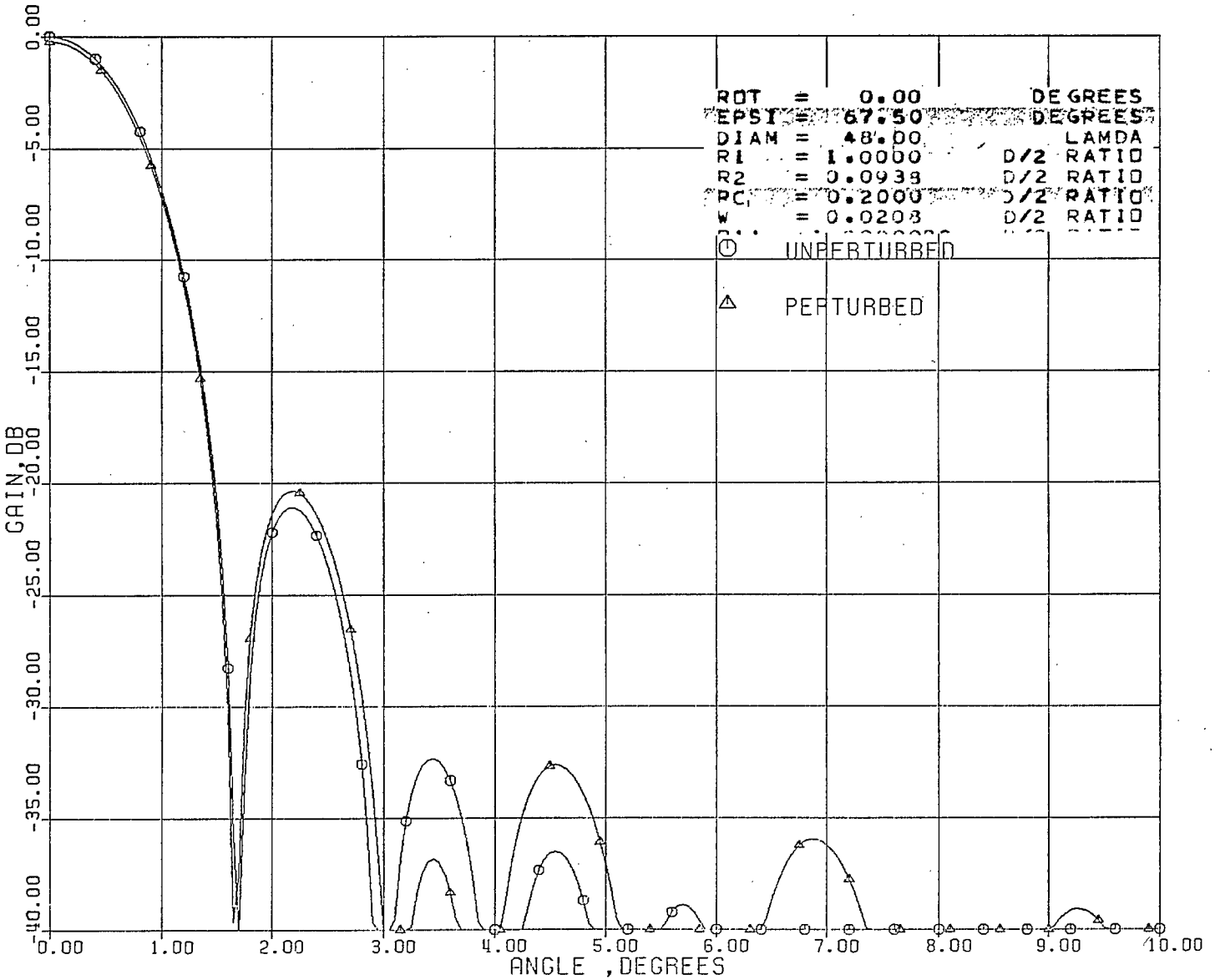

Figure 24. J - hook, E - polarization (JE 1000)

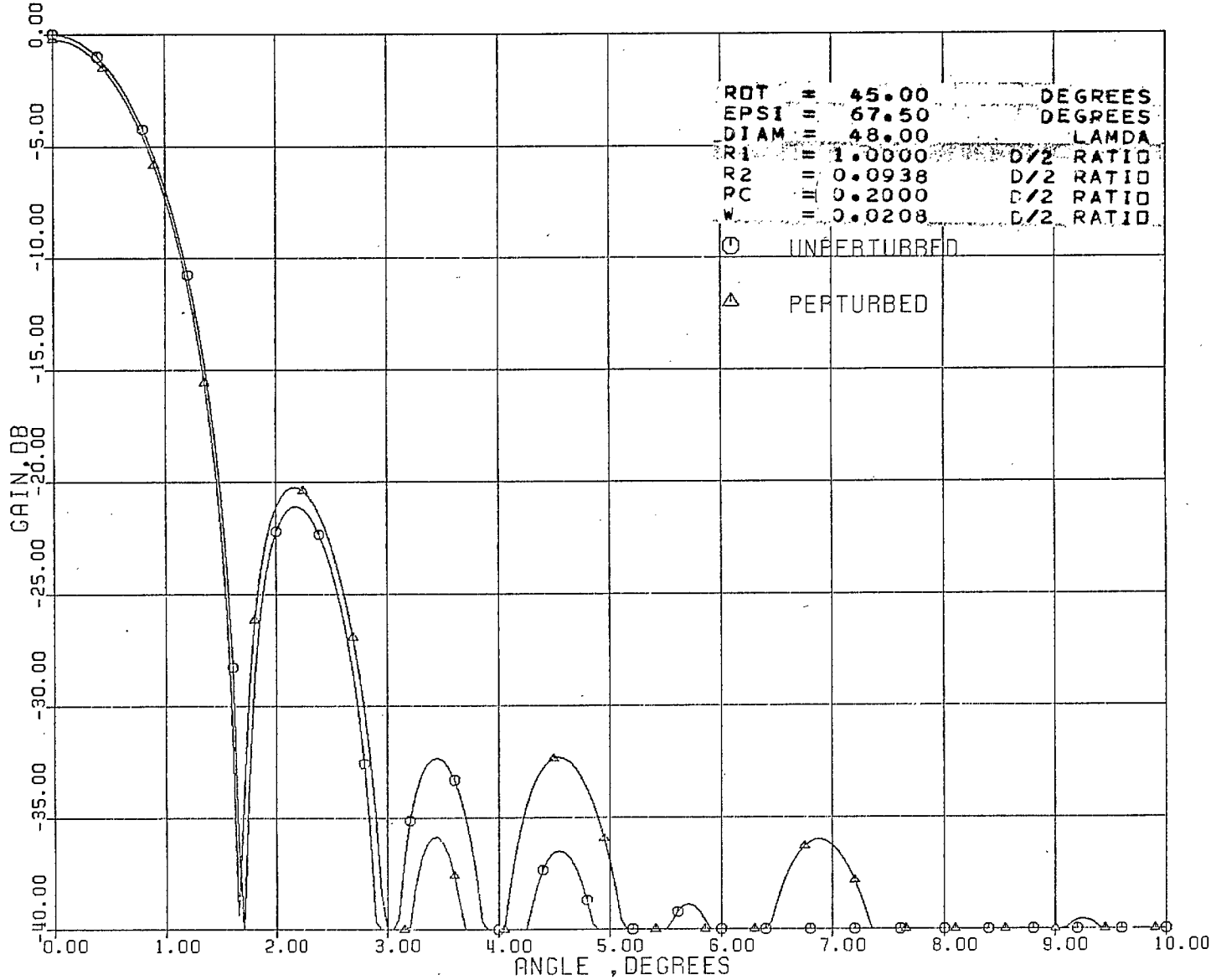

Figure 25. J - hook, E - polarization (JE 1045)

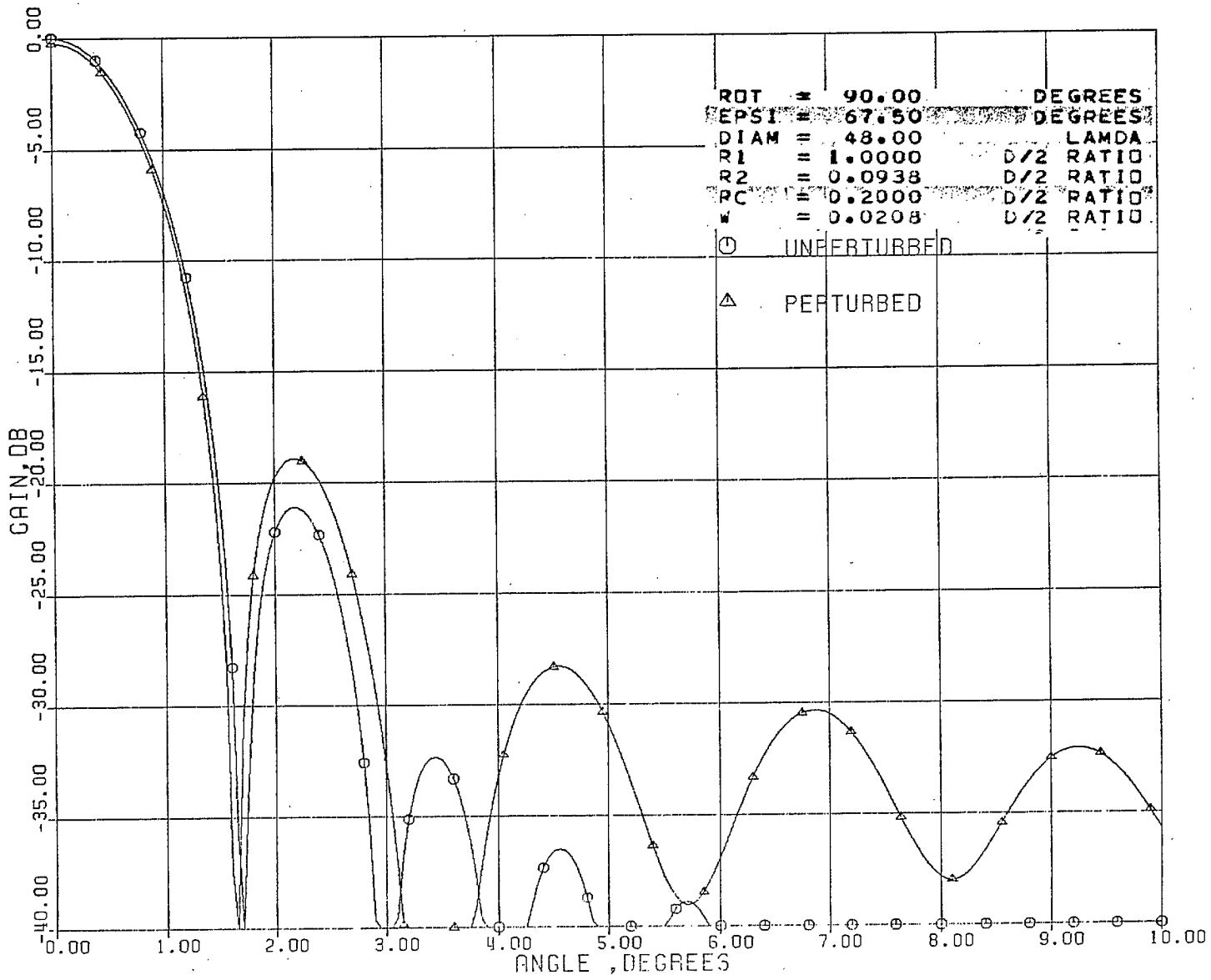

Figure 26. J - hook, E - polarization (JE 1060)

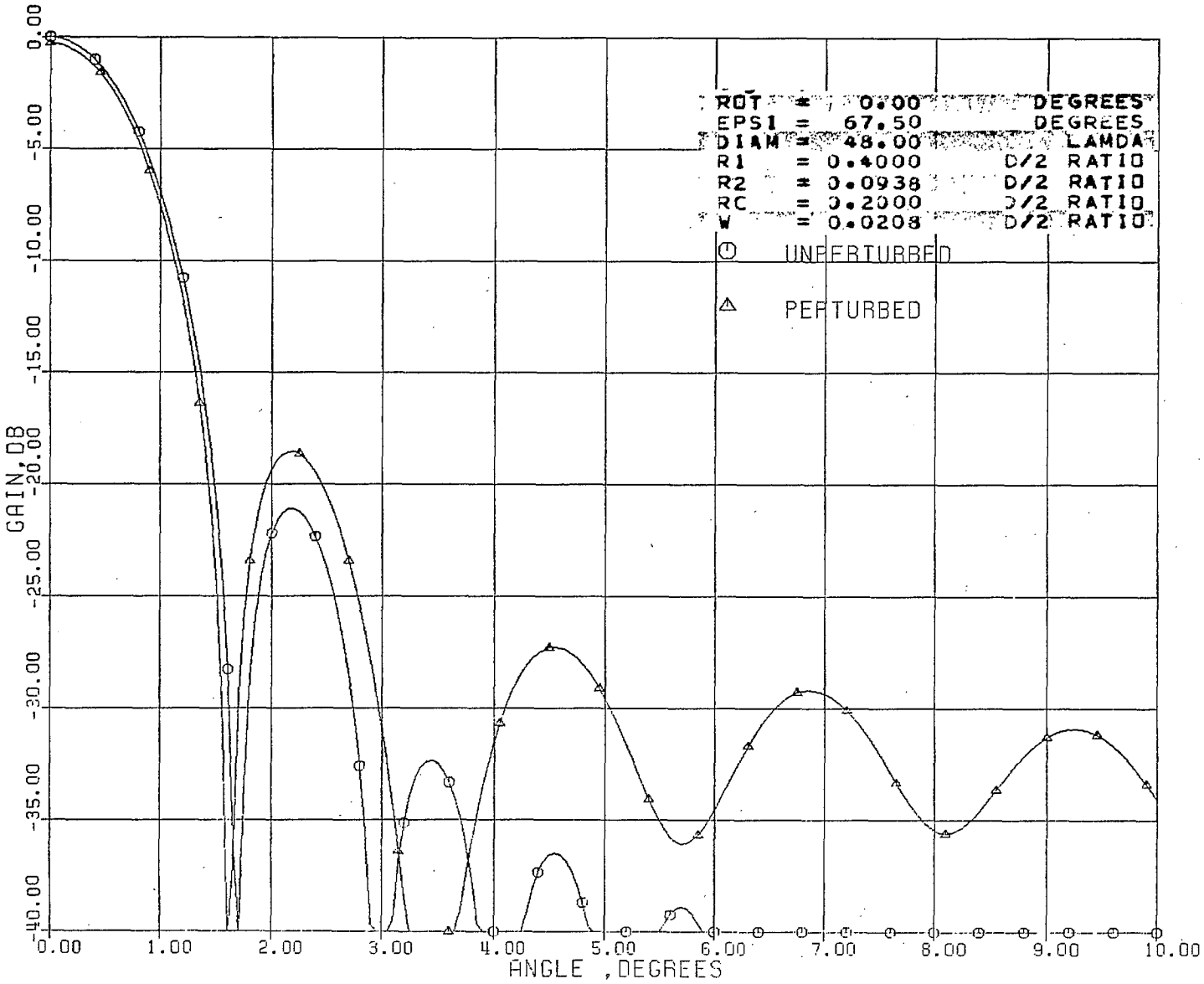

Figure 27. J - hook, H - polarization (JH 0400)

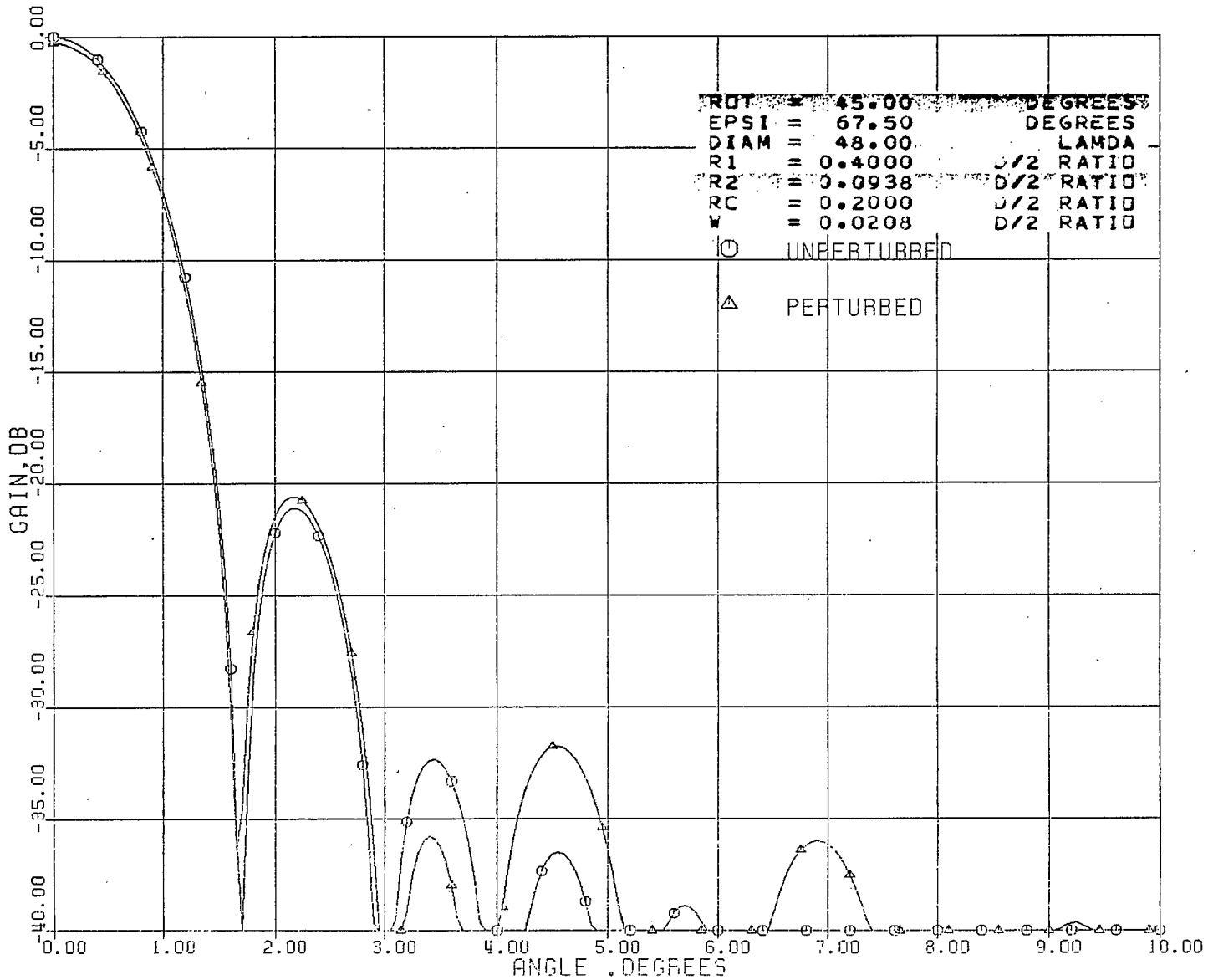

Figure 28. J - hook, H - polarization (JH 0445)

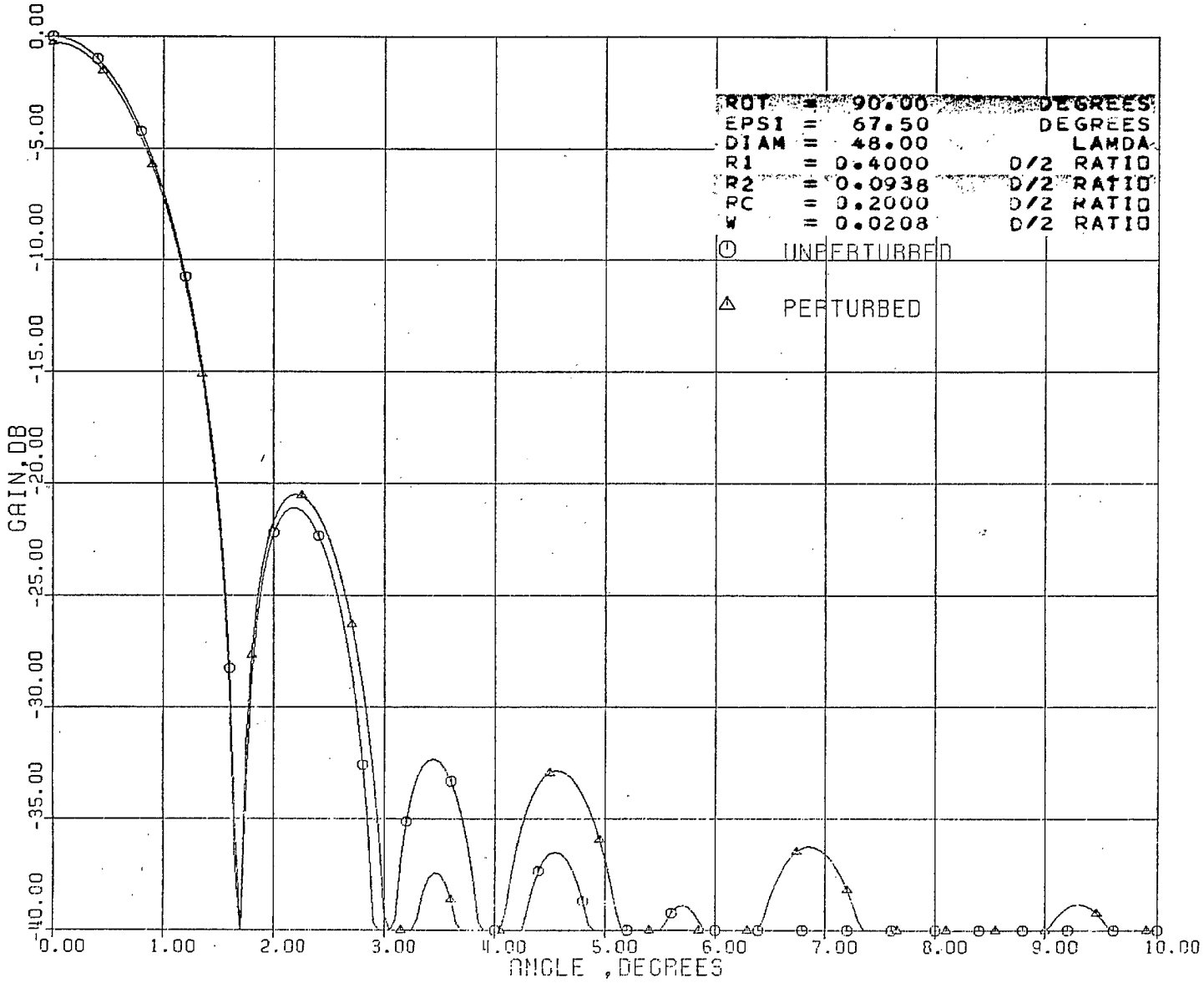

Figure 29. J - hook, H - polarization (JH 0490)

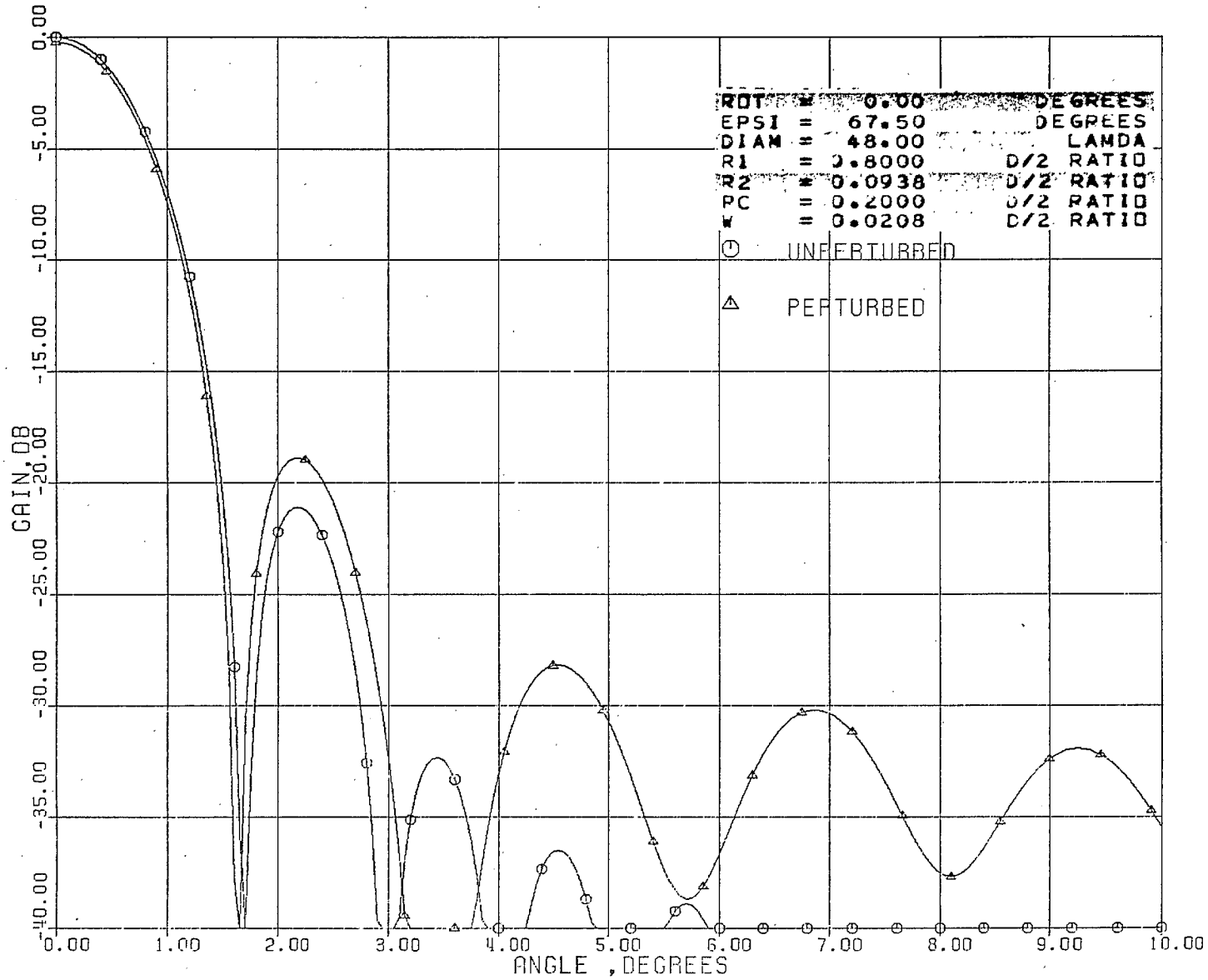

Figure 30. J - hook, H - polarization (JH 0800)

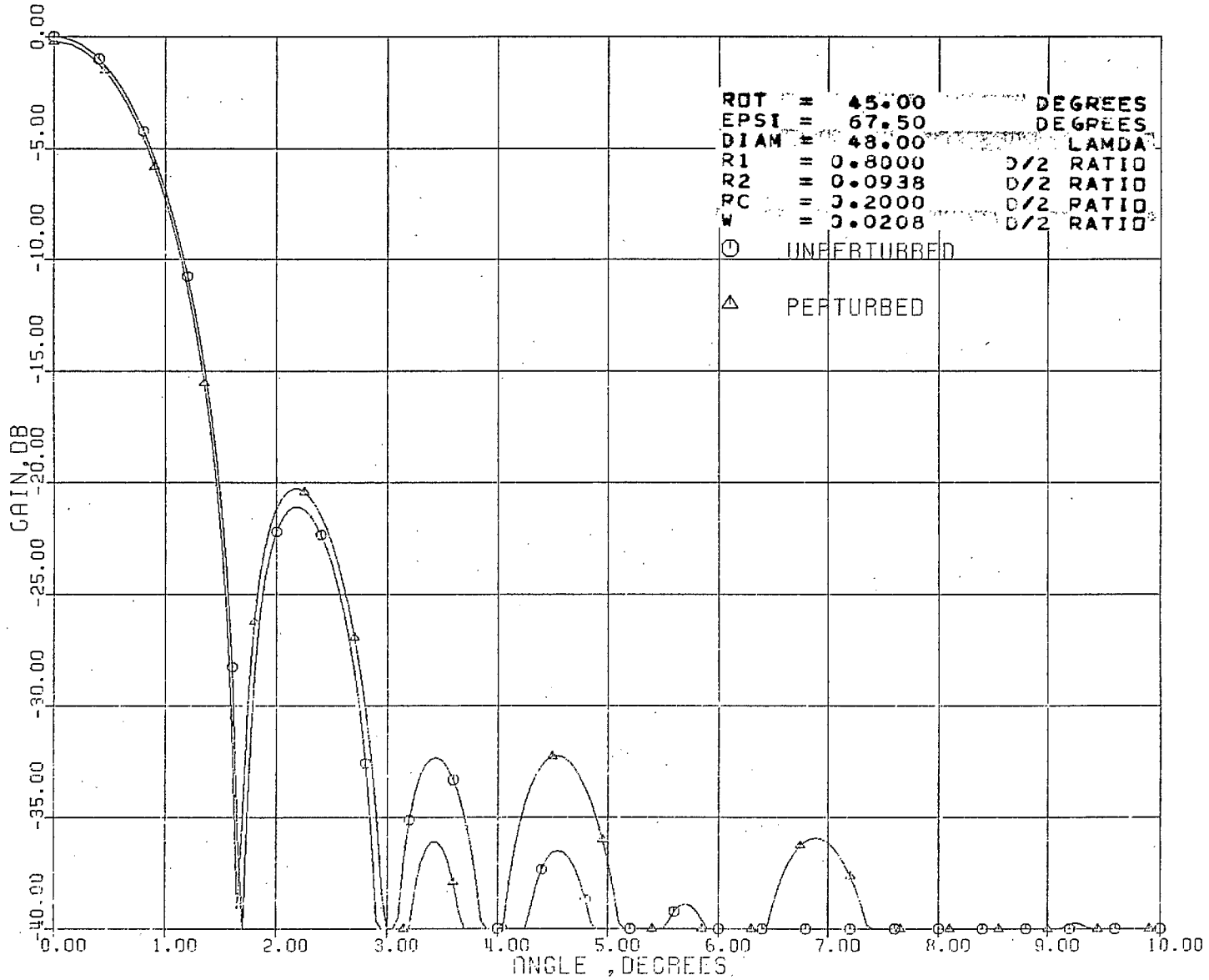

Figure 31. J - hook, H - polarization (JH 0845)

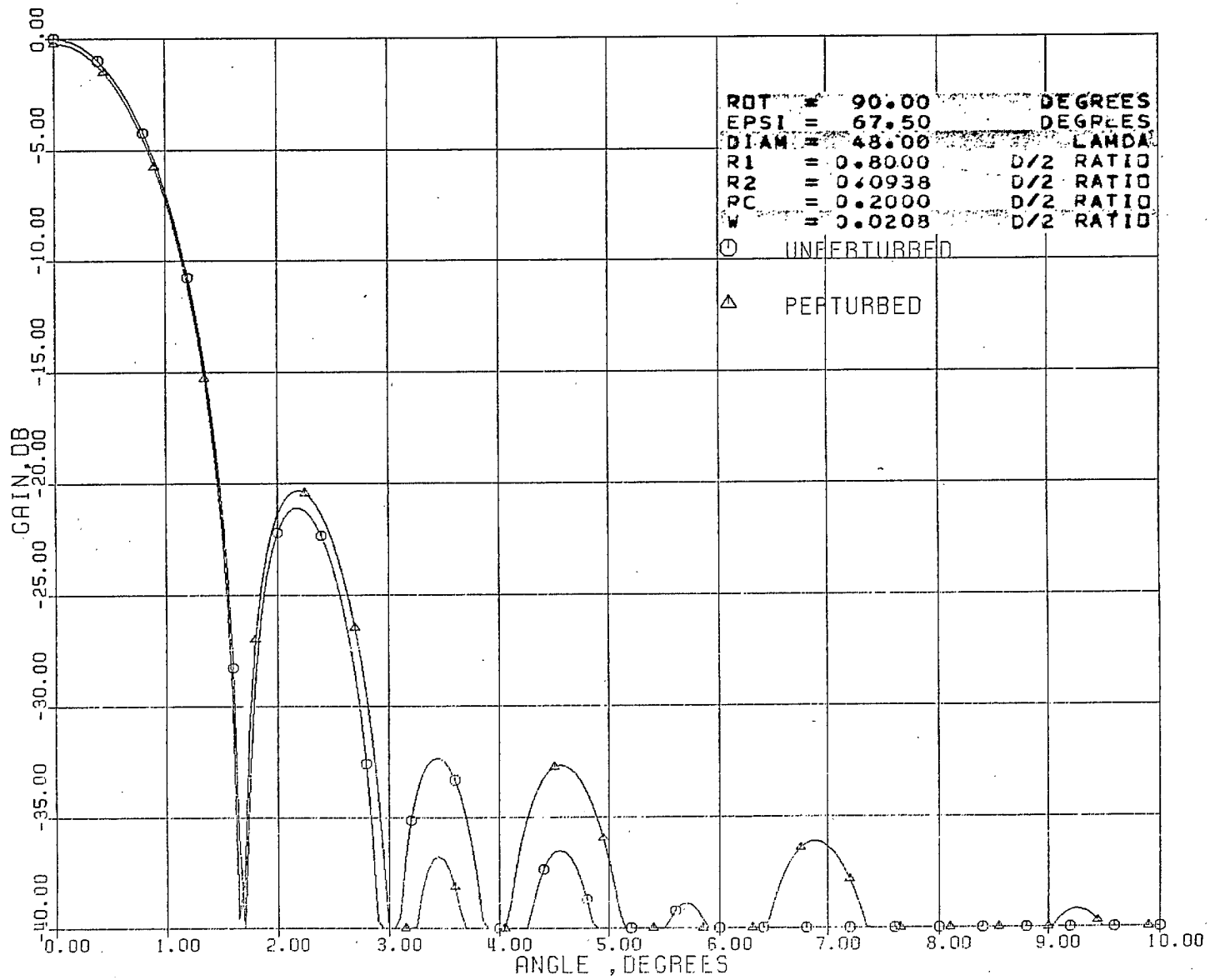

Figure 32. J - hook, H - polarization (JH 0890)

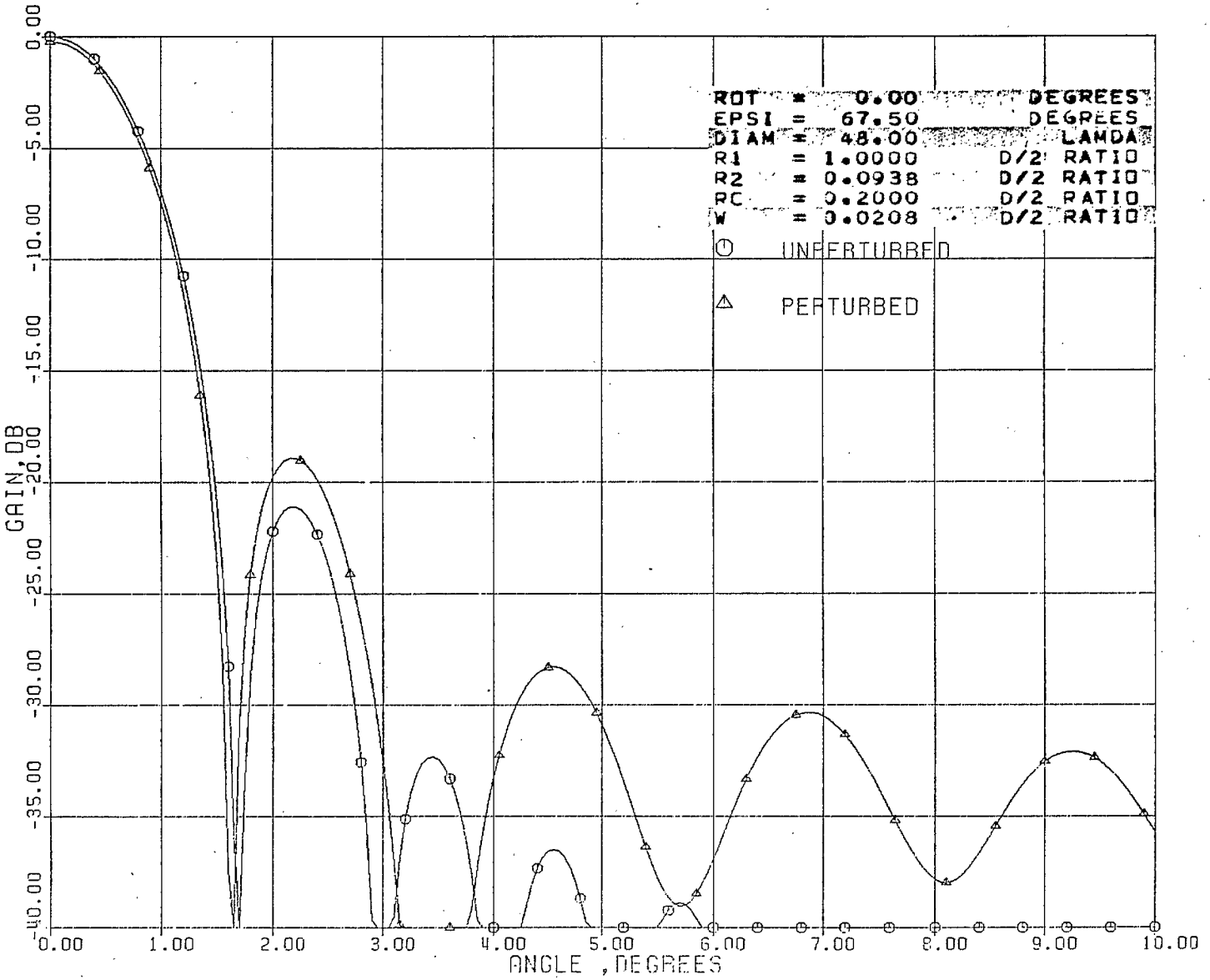

Figure 33. J - hook, H - polarization (JH 1000)

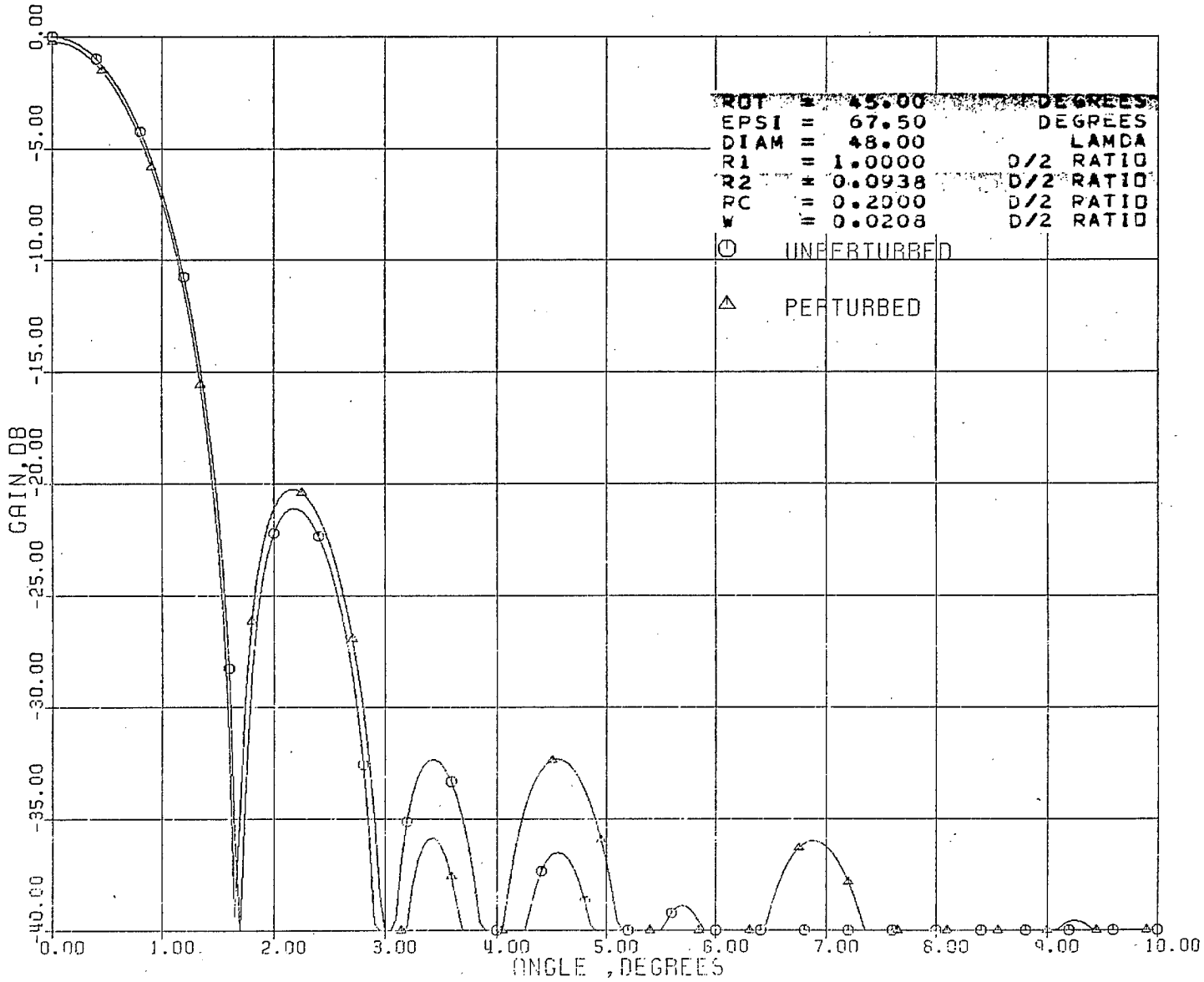

Figure 34. J - hook, H - polarization (JH 1045)

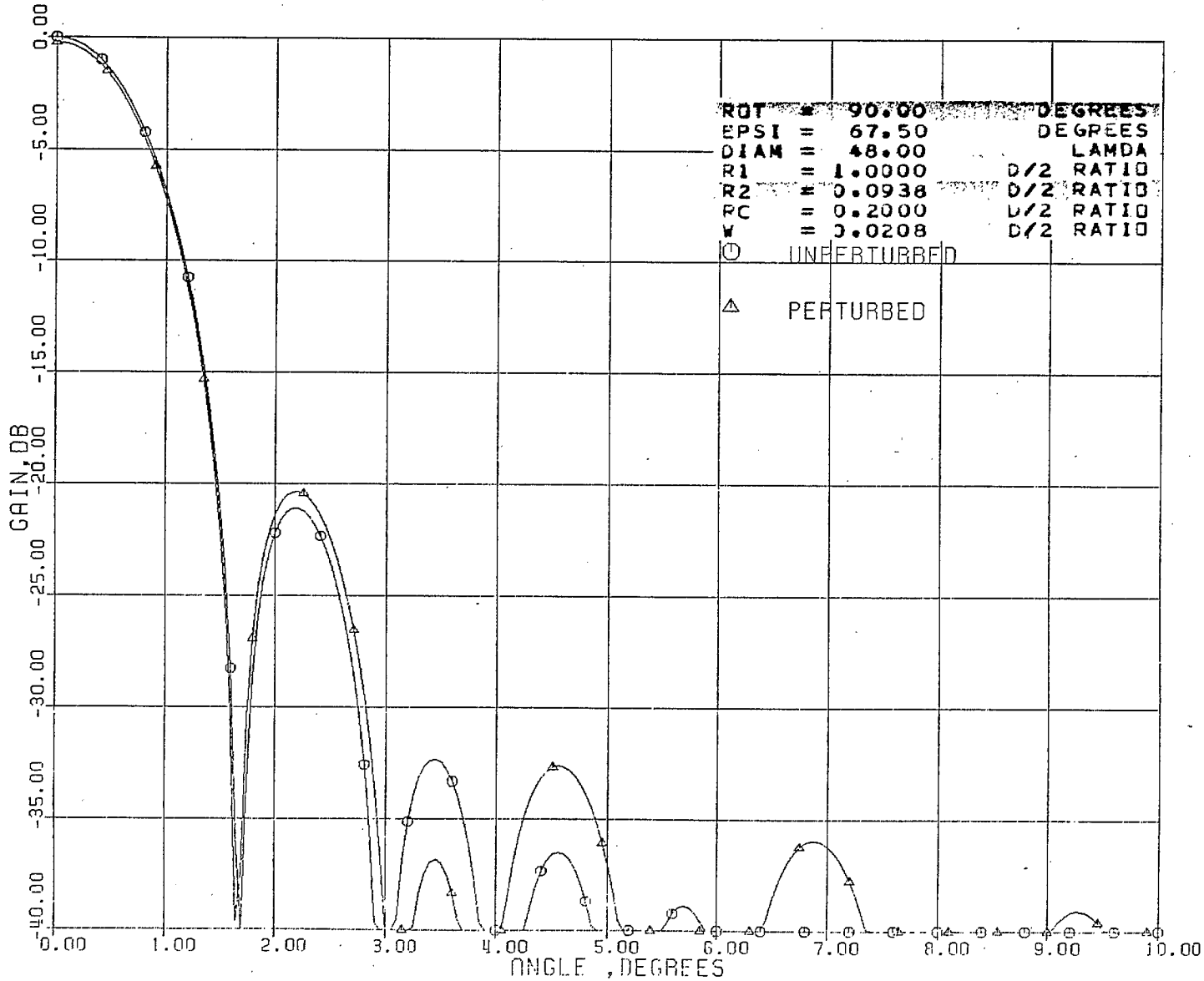

Figure 35. J - hook, H - polarization (JH 1090)

CASE II

TRIPOD AND QUAD

The following figures are given in code as:

L M XX YY

L indicates the size of reflector diameter with

A = 24λ
B = 36λ
C = 48λ
D = 72λ

M indicates the number of struts 3 or 4

XX indicates the ratio of strut location to the reflector radius. The maximum value is 1 which will be represented by XX as 10

YY indicates the angle ϕ (degree) at which the pattern is calculated

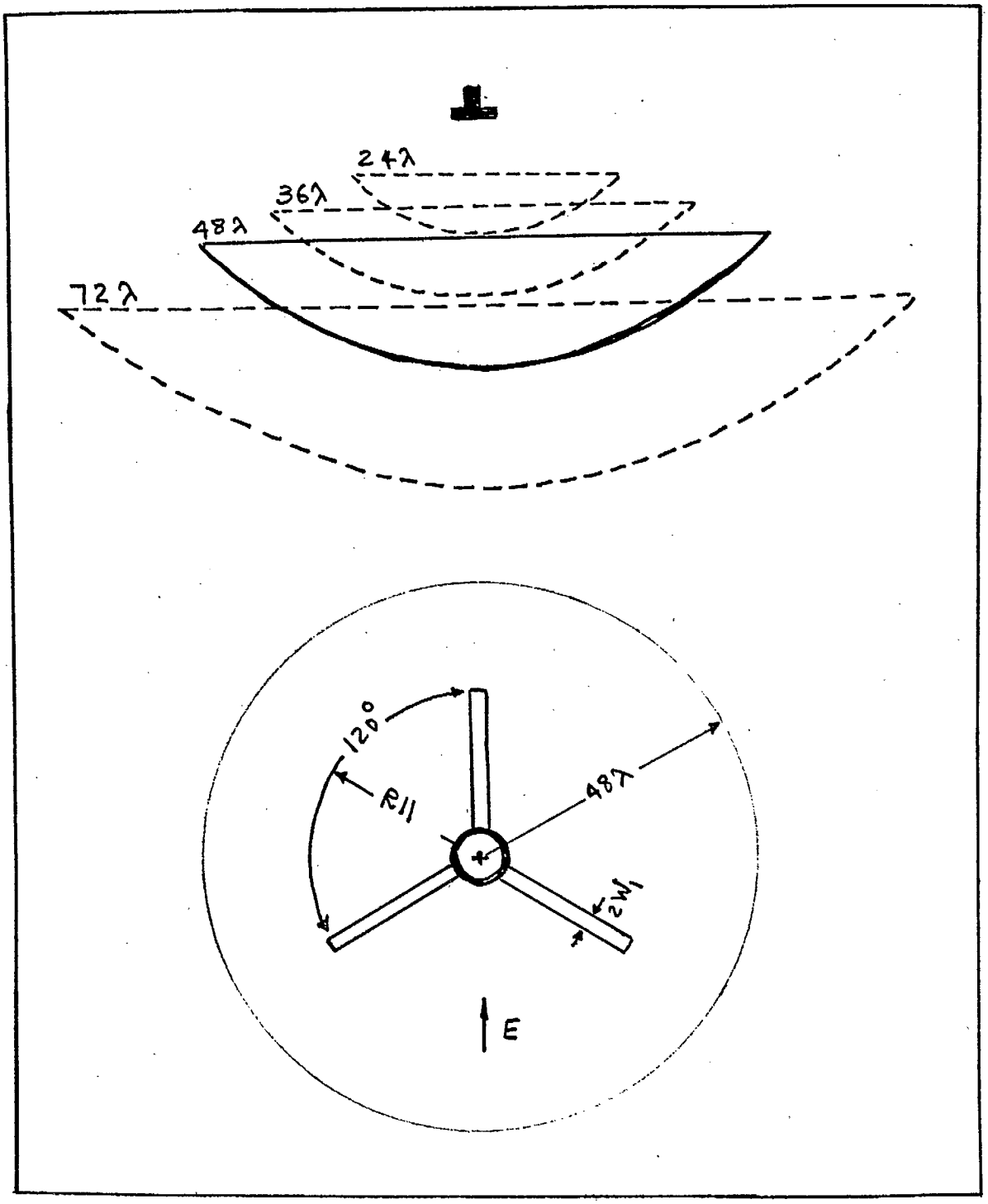

Figure 36. Tripod geometry

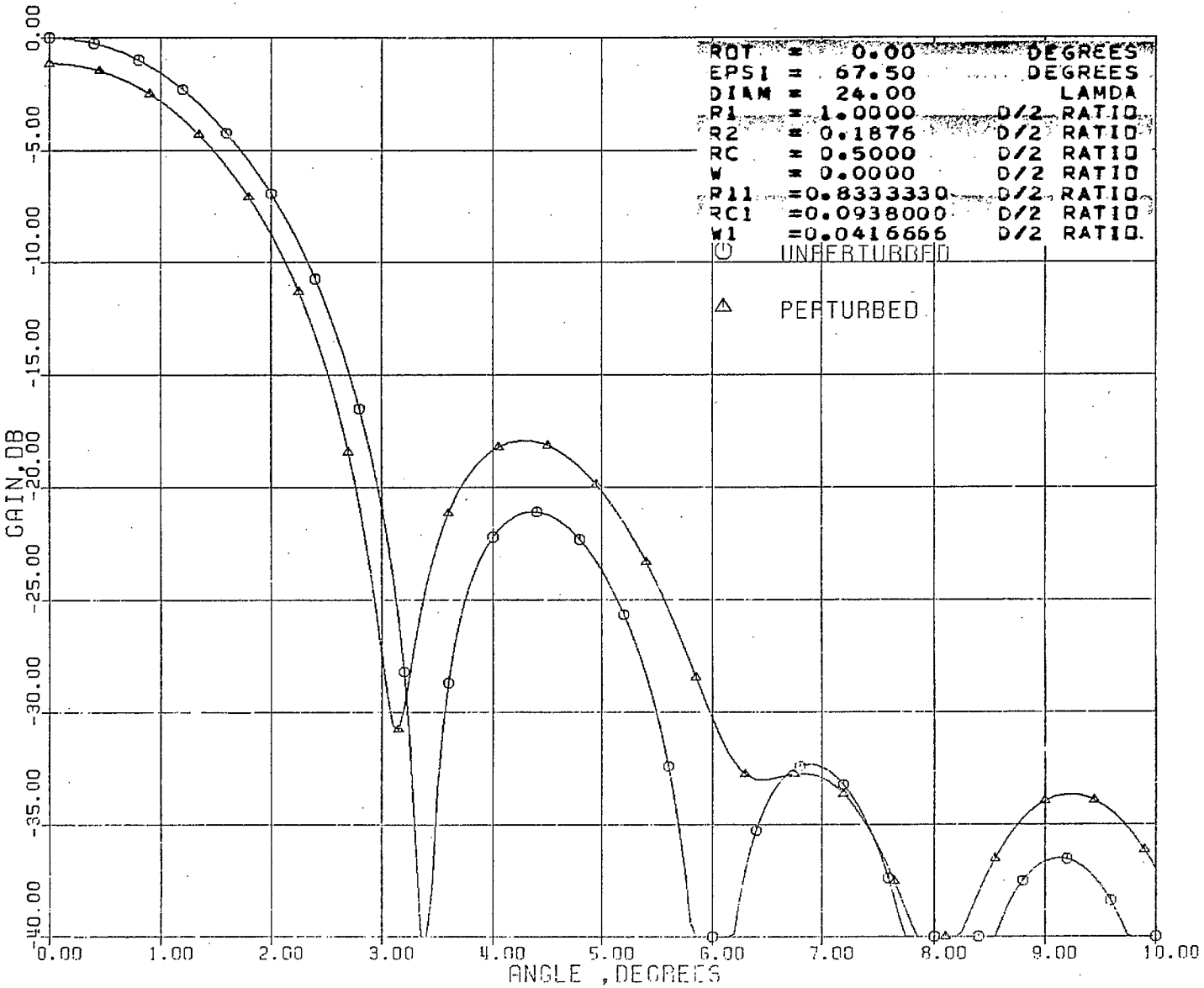

Figure 37. Radiation pattern with tripod (A30800)

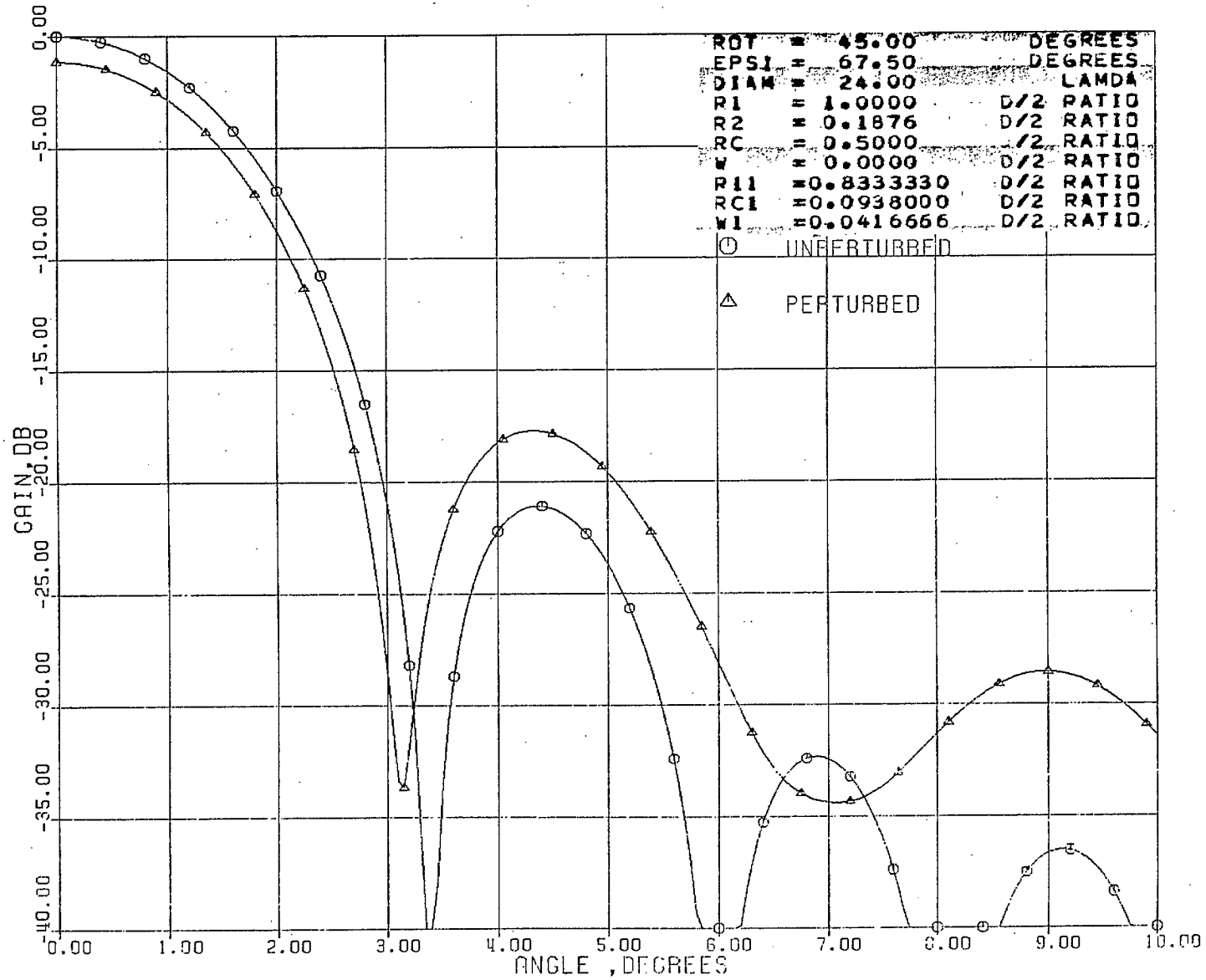

Figure 38. Radiation pattern with tripod (A30845)

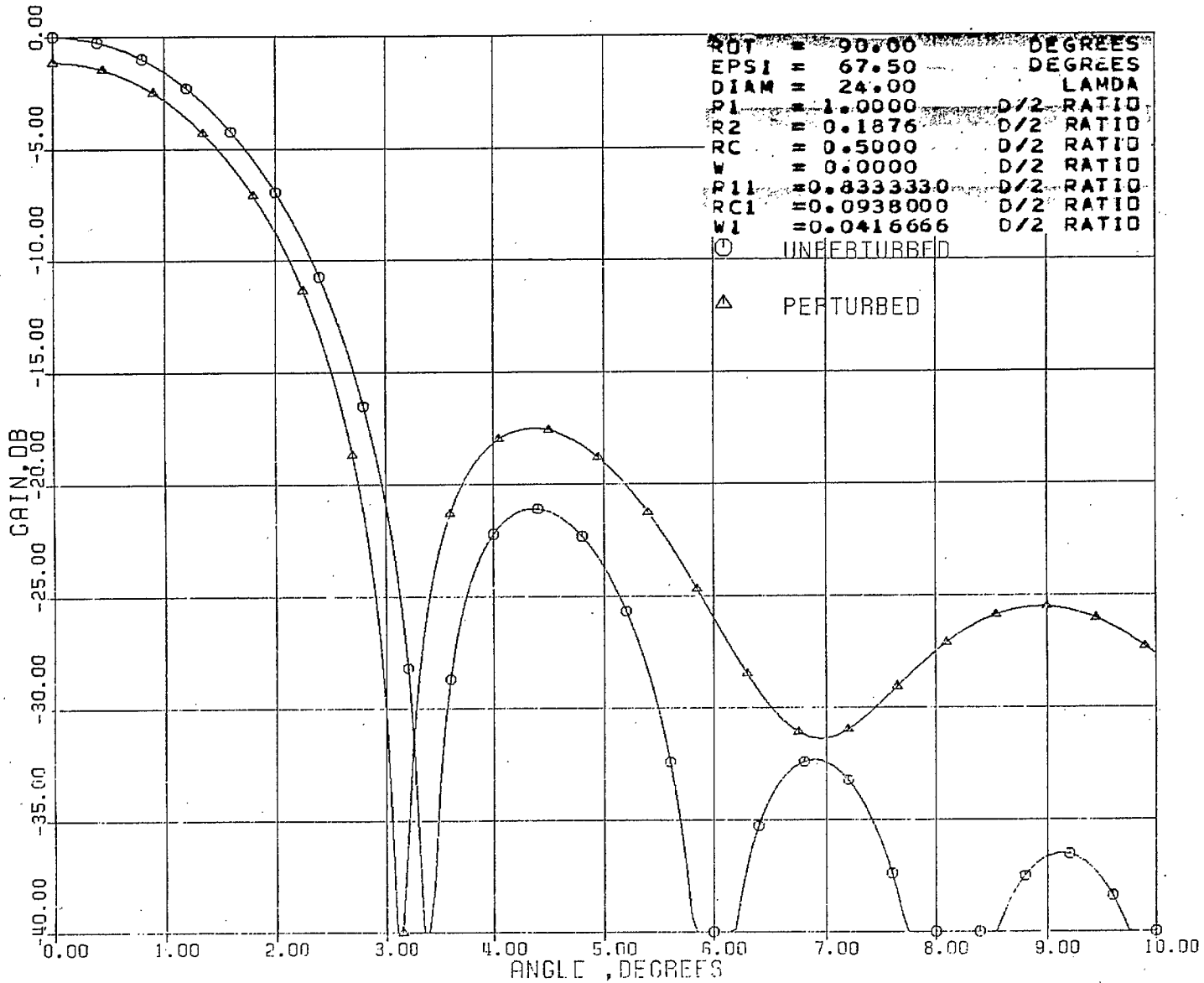

Figure 39. Radiation pattern with tripod (A30890)

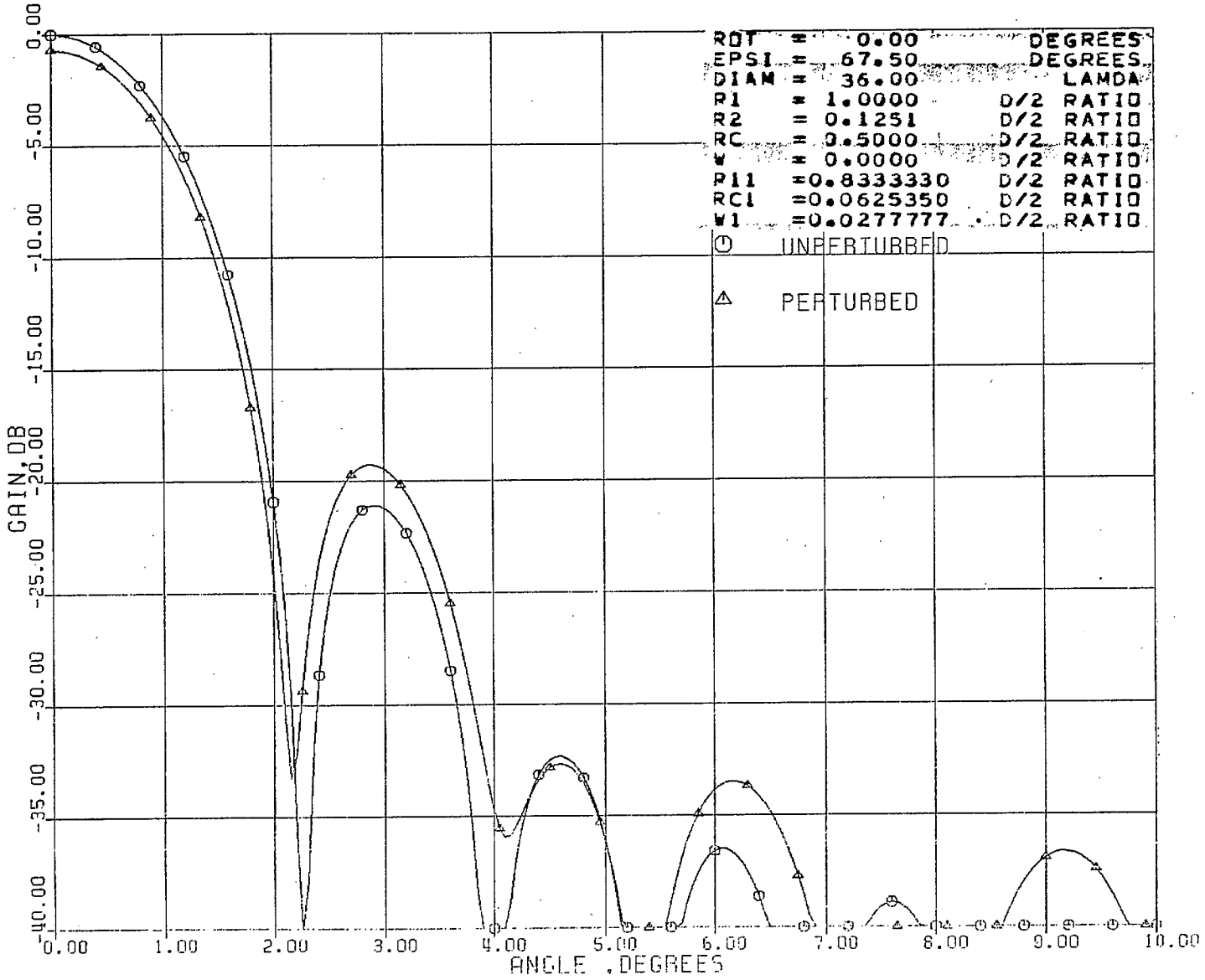

Figure 40. Radiation pattern with tripod (B30800)

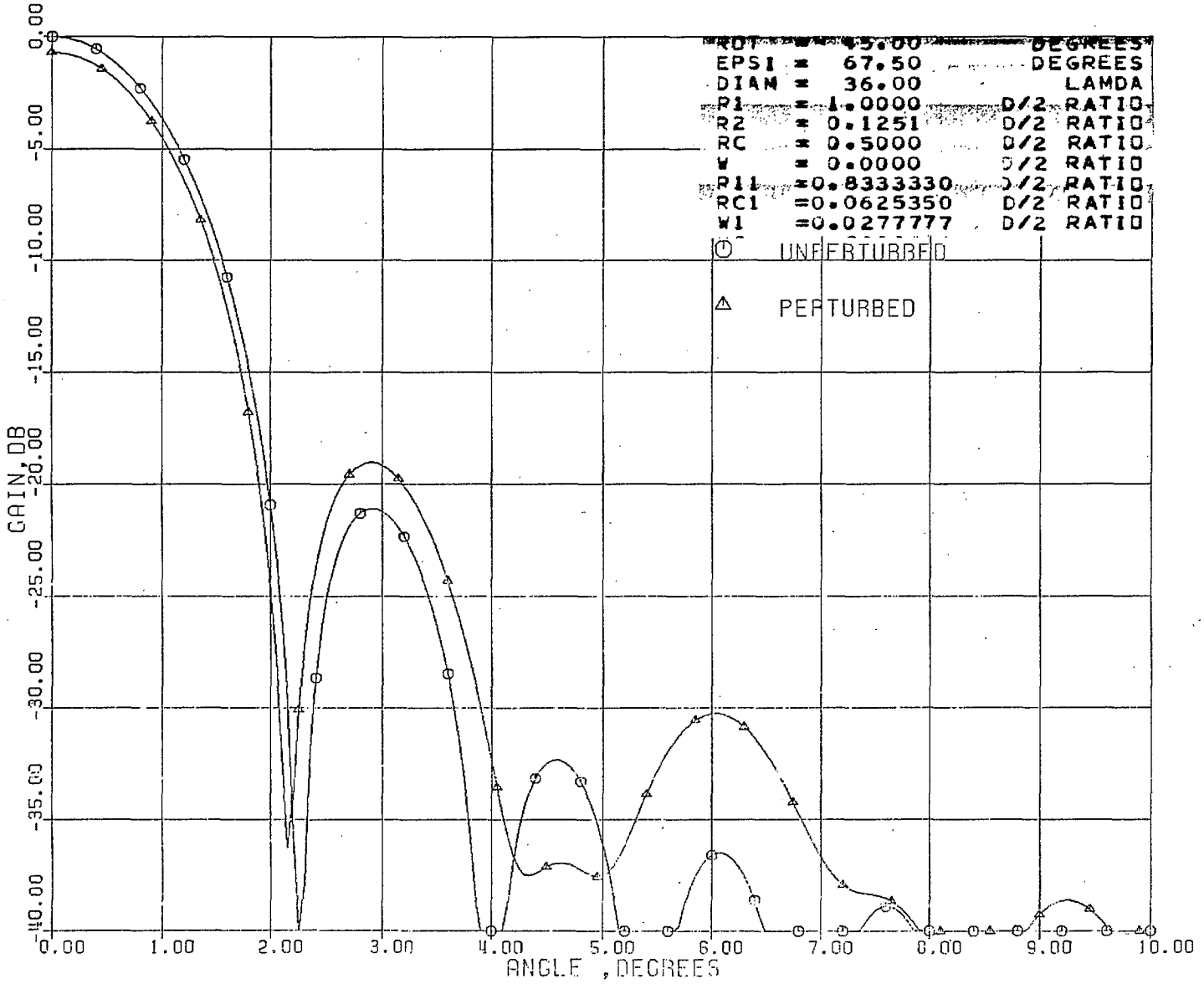

Figure 41. Radiation pattern with tripod (B30845)

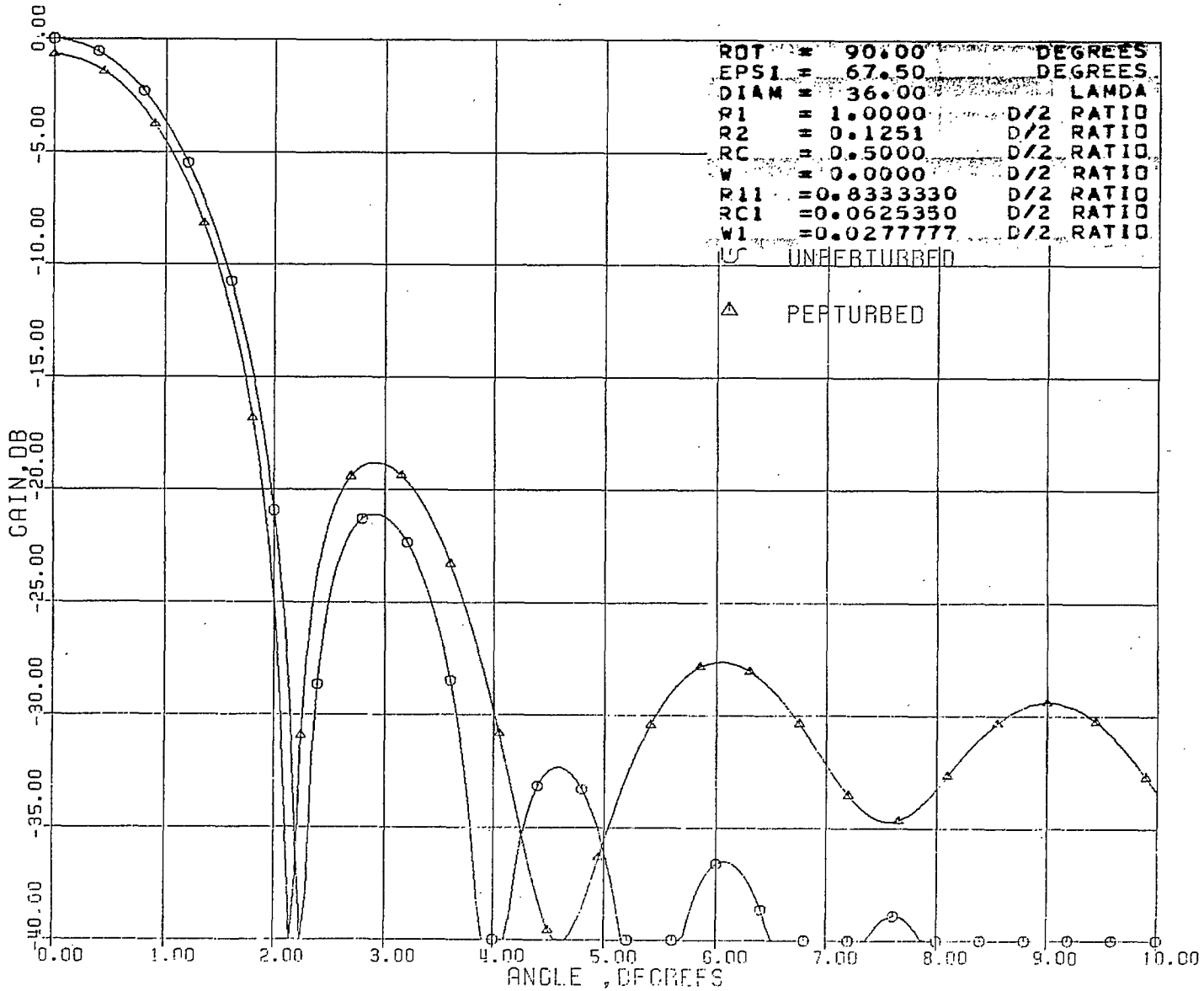

Figure 42. Radiation pattern with tripod (B30890)

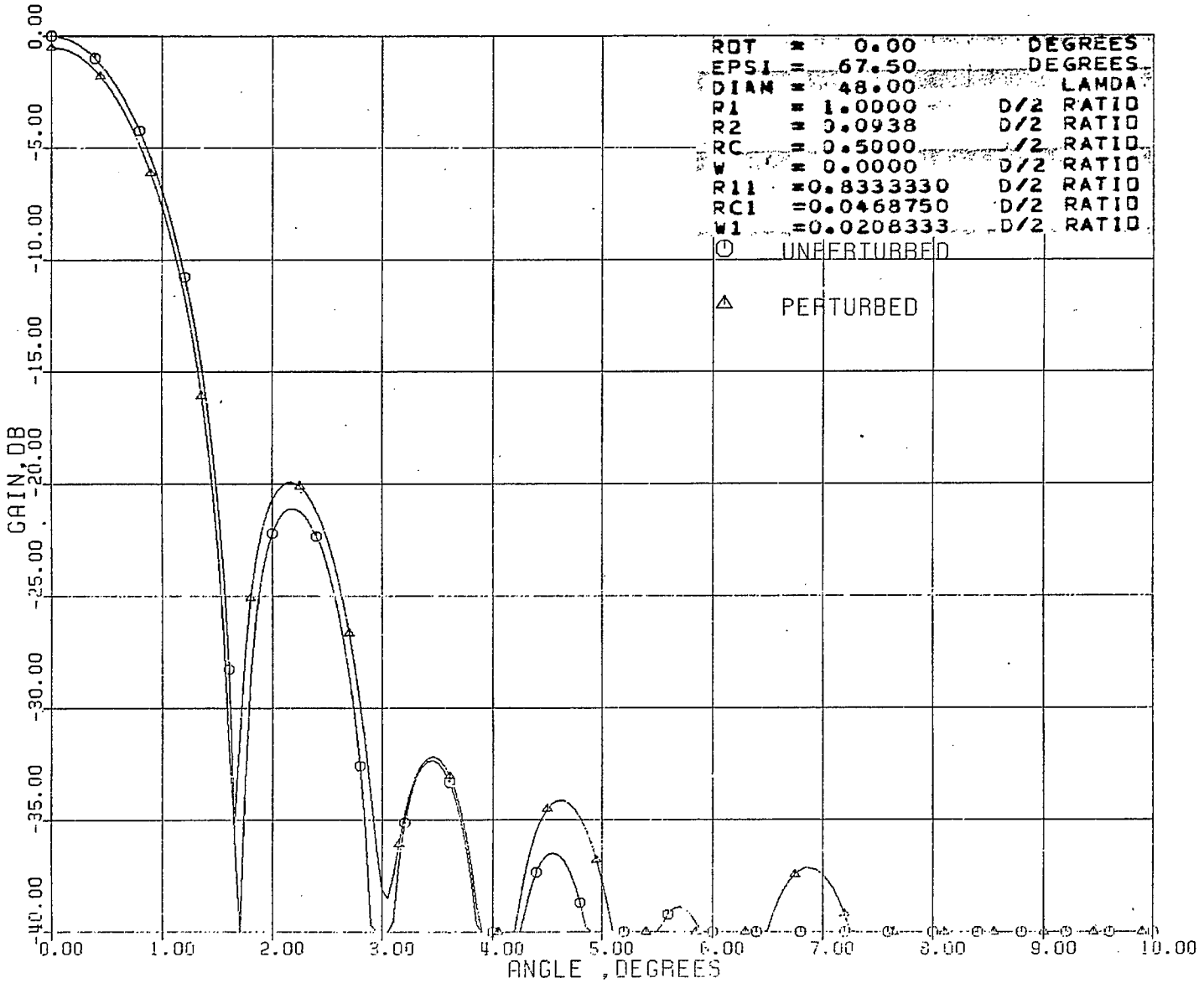

Figure 43. Radiation pattern with tripod (C30800)

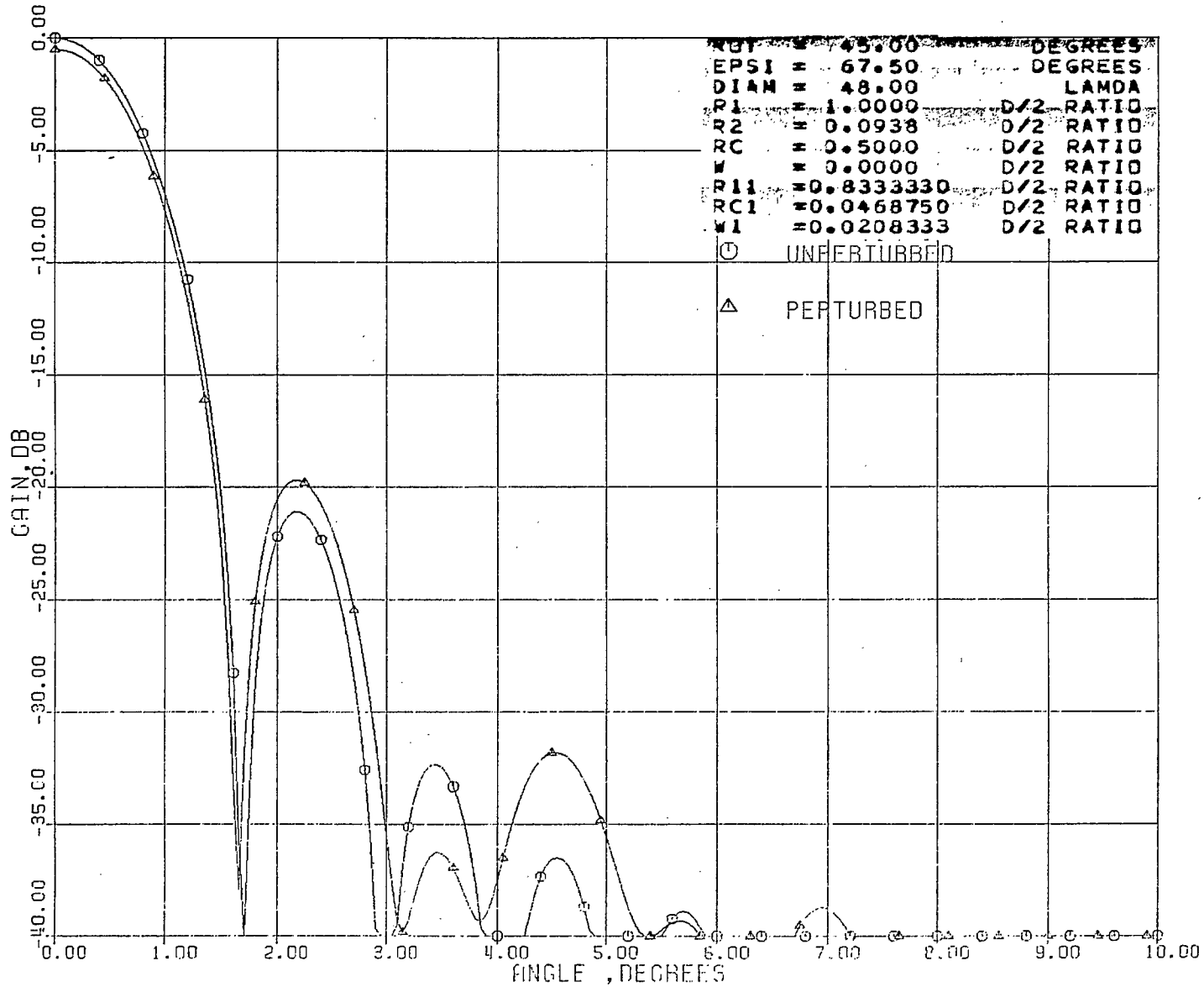

Figure 44. Radiation pattern with tripod (C30845)

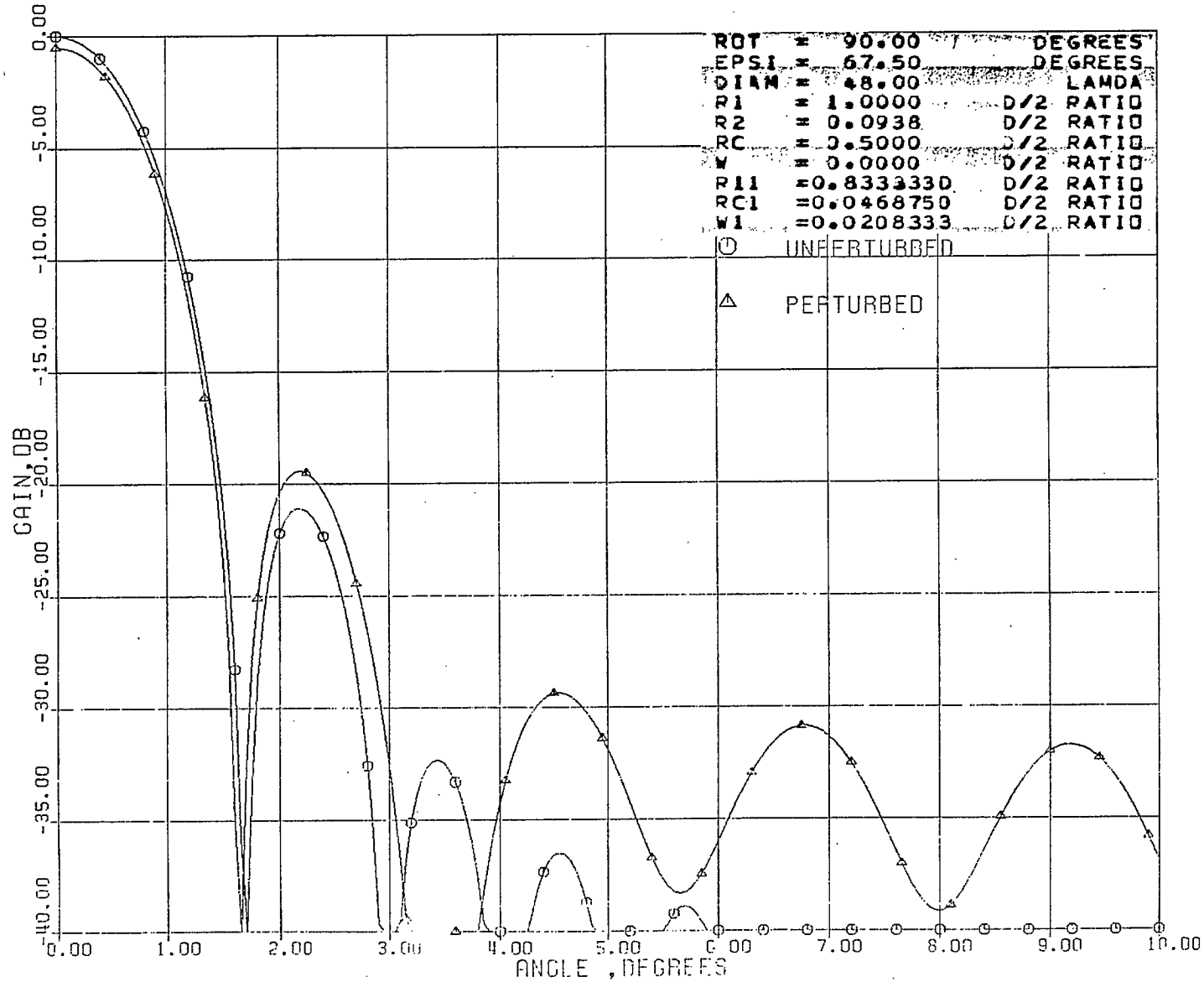

Figure 45. Radiation pattern with tripod (C30890)

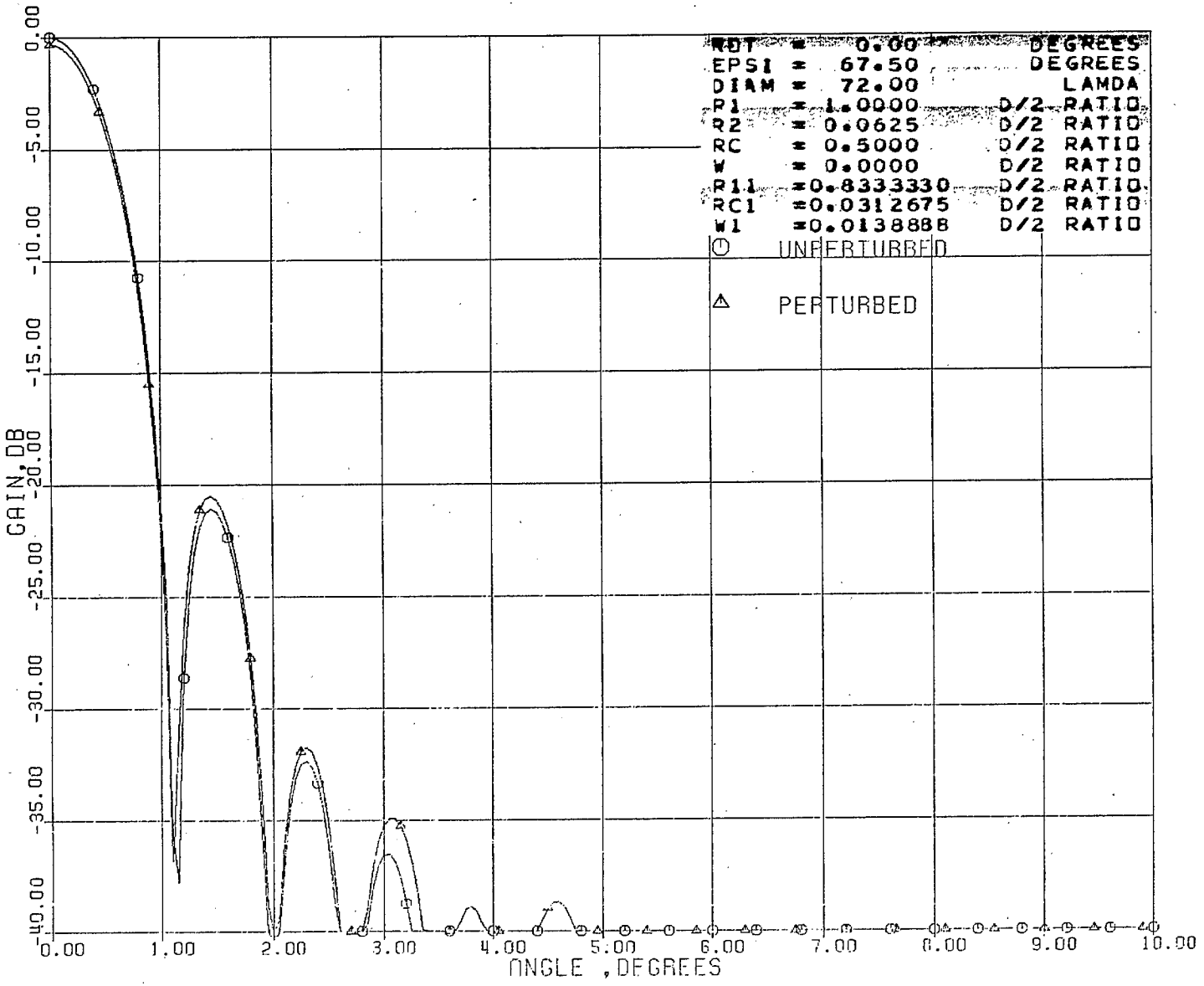

Figure 46. Radiation pattern with tripod (D30800)

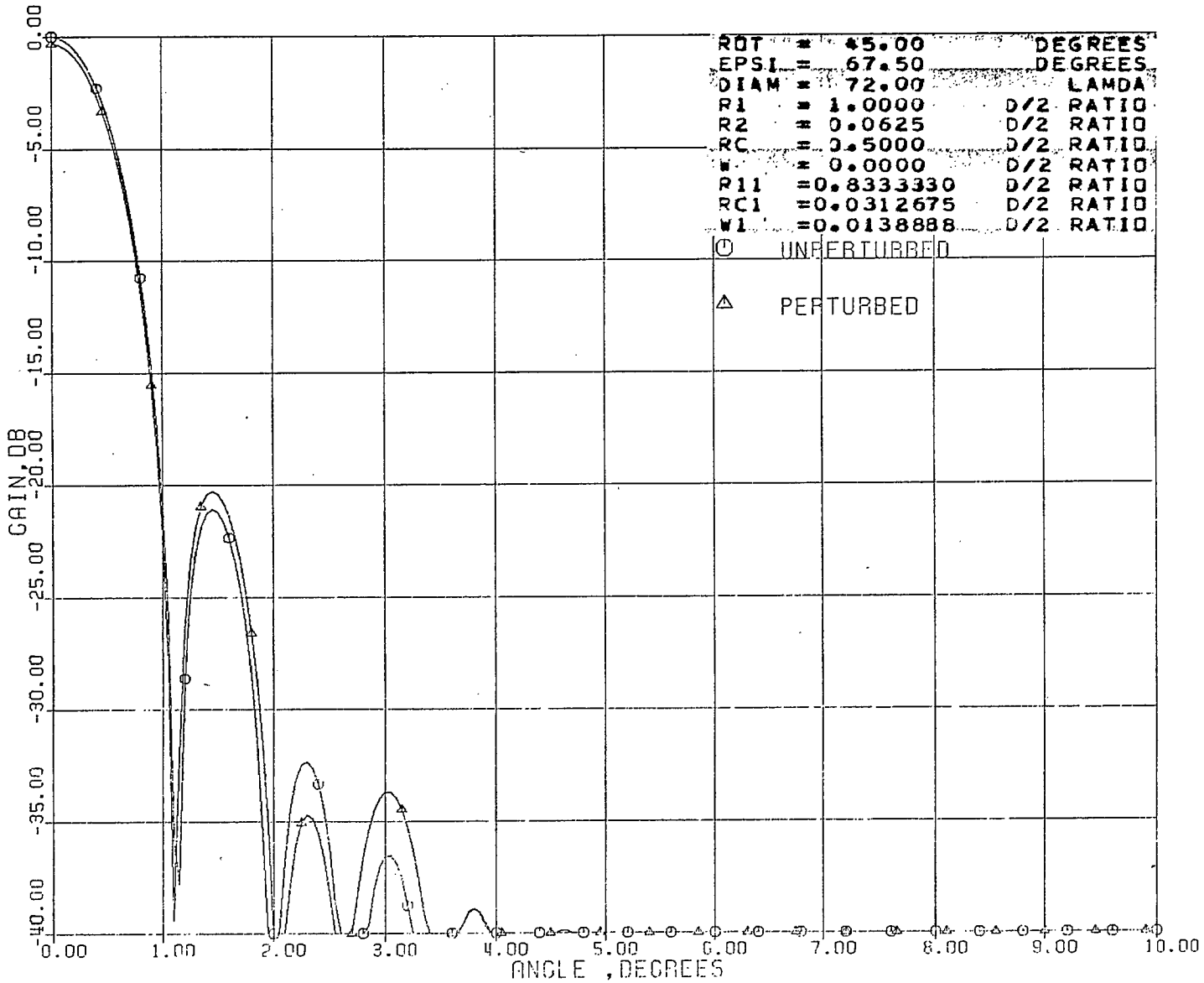

Figure 47. Radiation pattern with tripod (D30845)

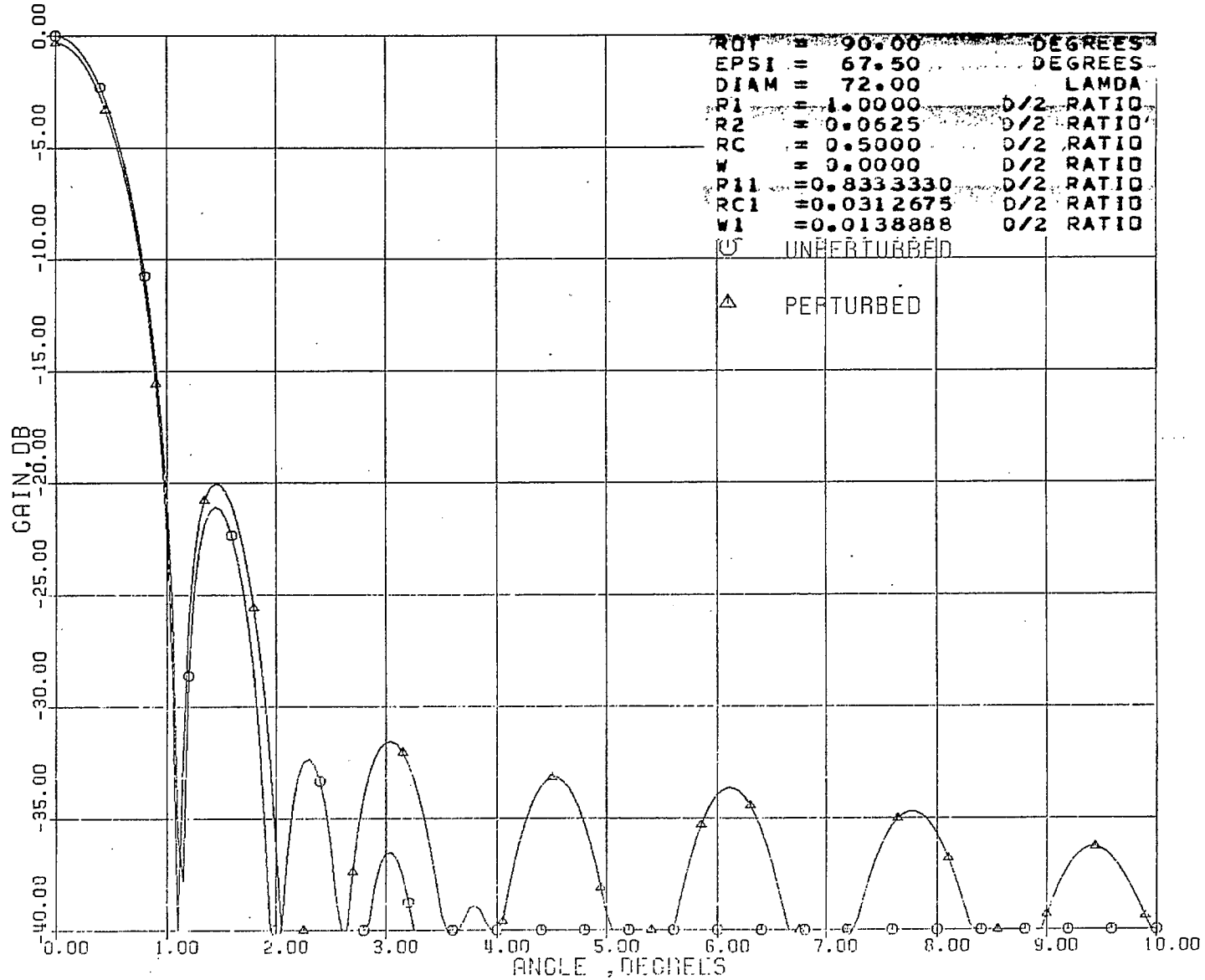

Figure 48. Radiation pattern with tripod (D30890)

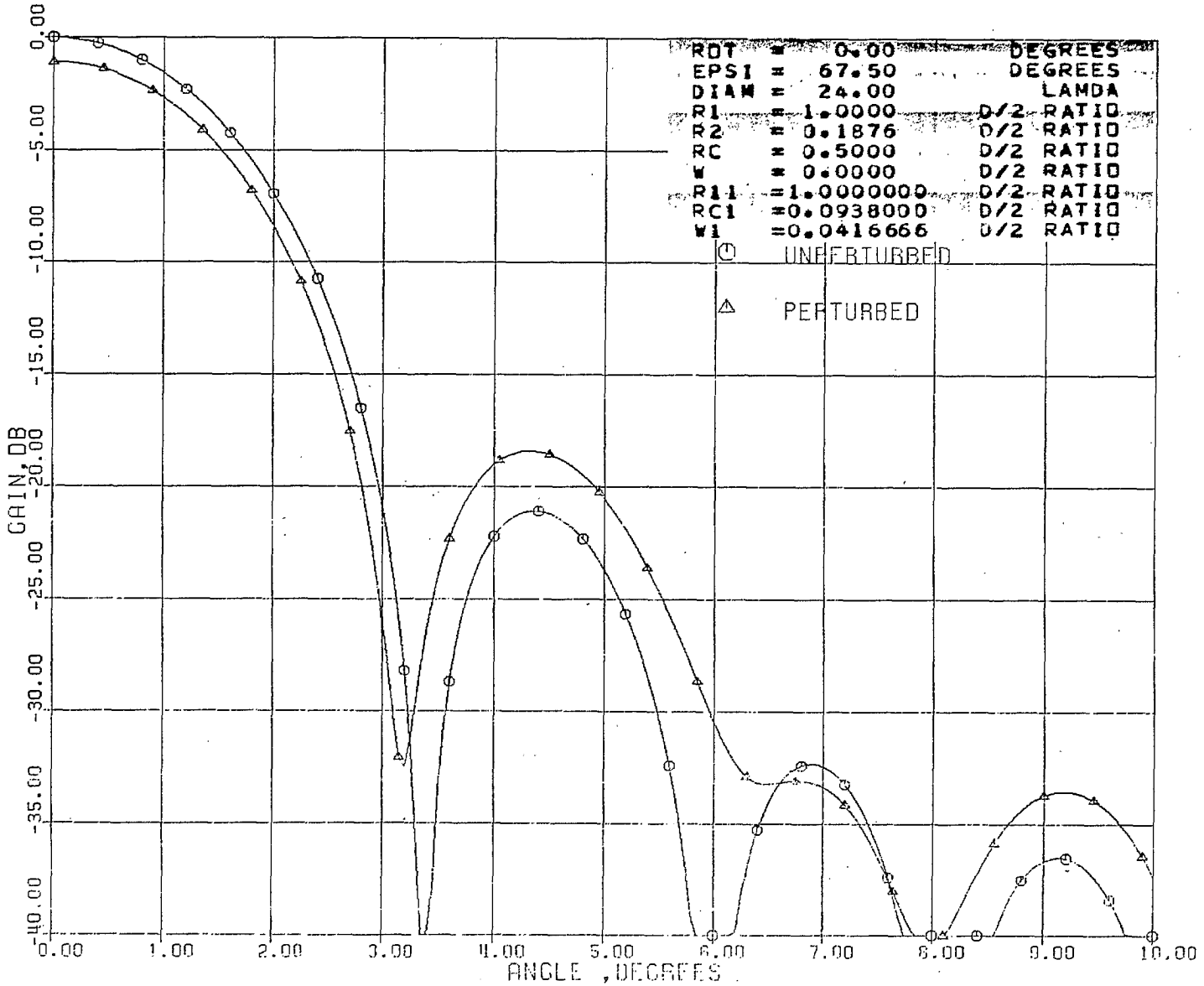

Figure 49. Radiation pattern with tripod (A31000)

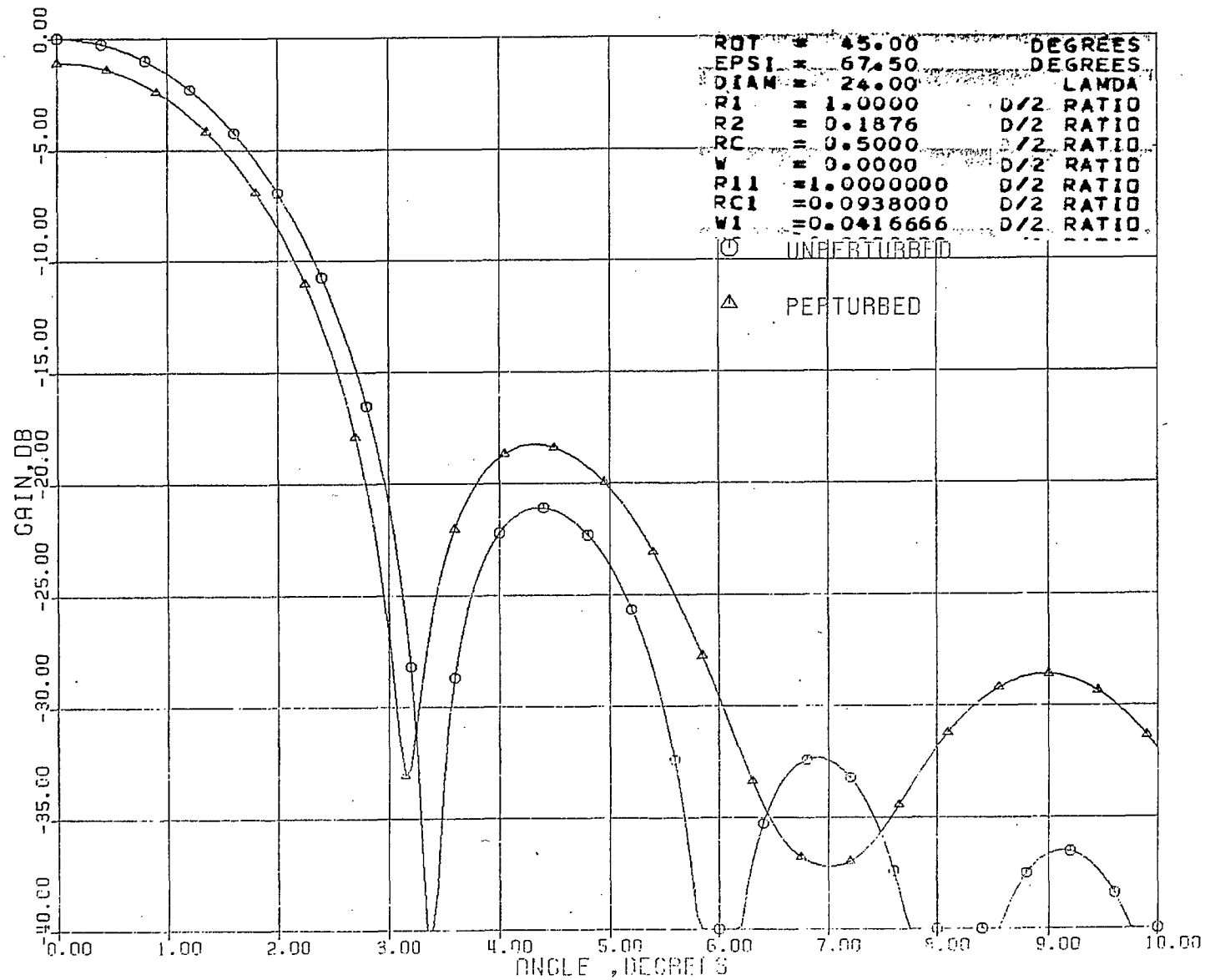

Figure 50. Radiation pattern with tripod (A31045)

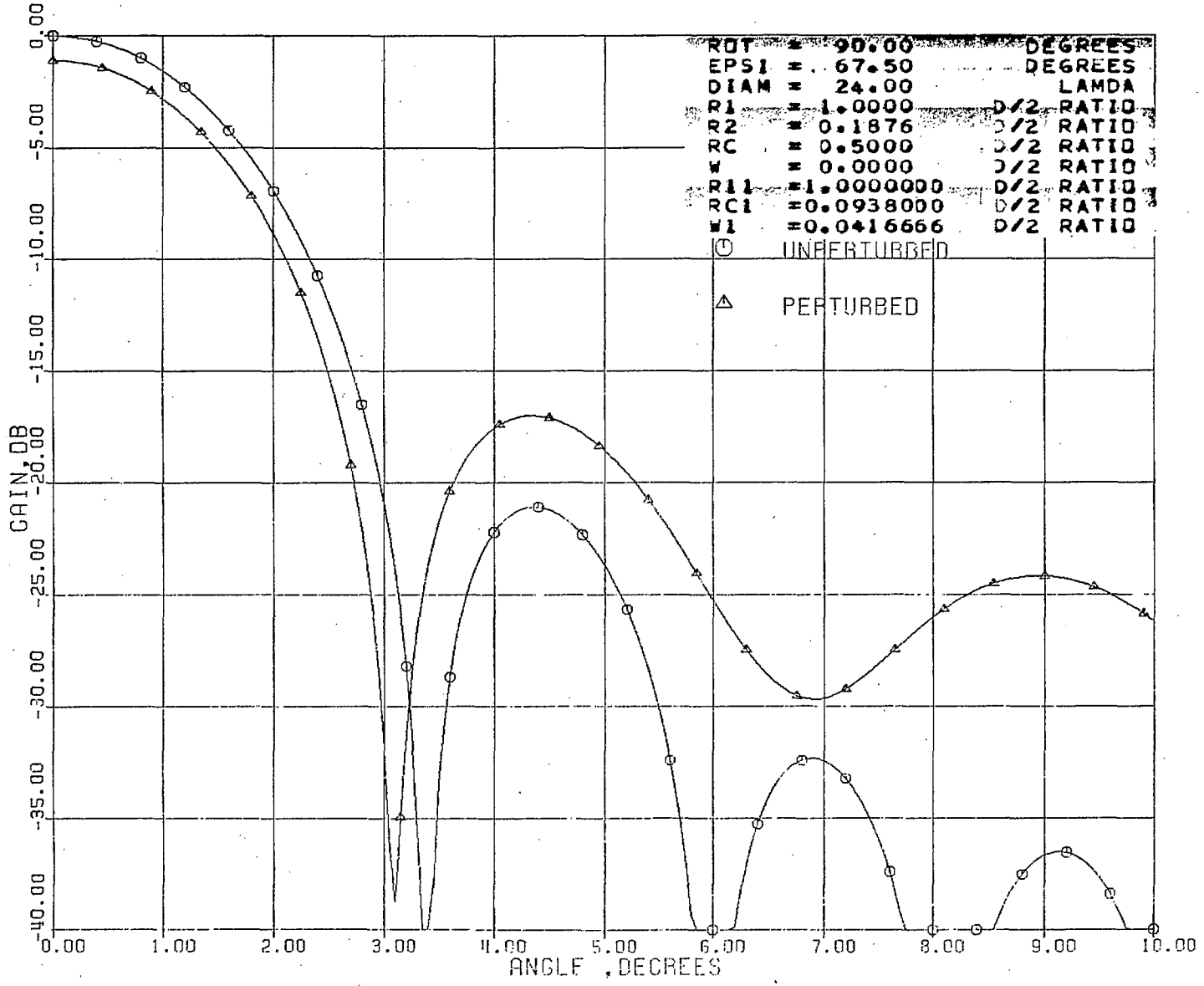

Figure 51. Radiation pattern with tripod (A31090)

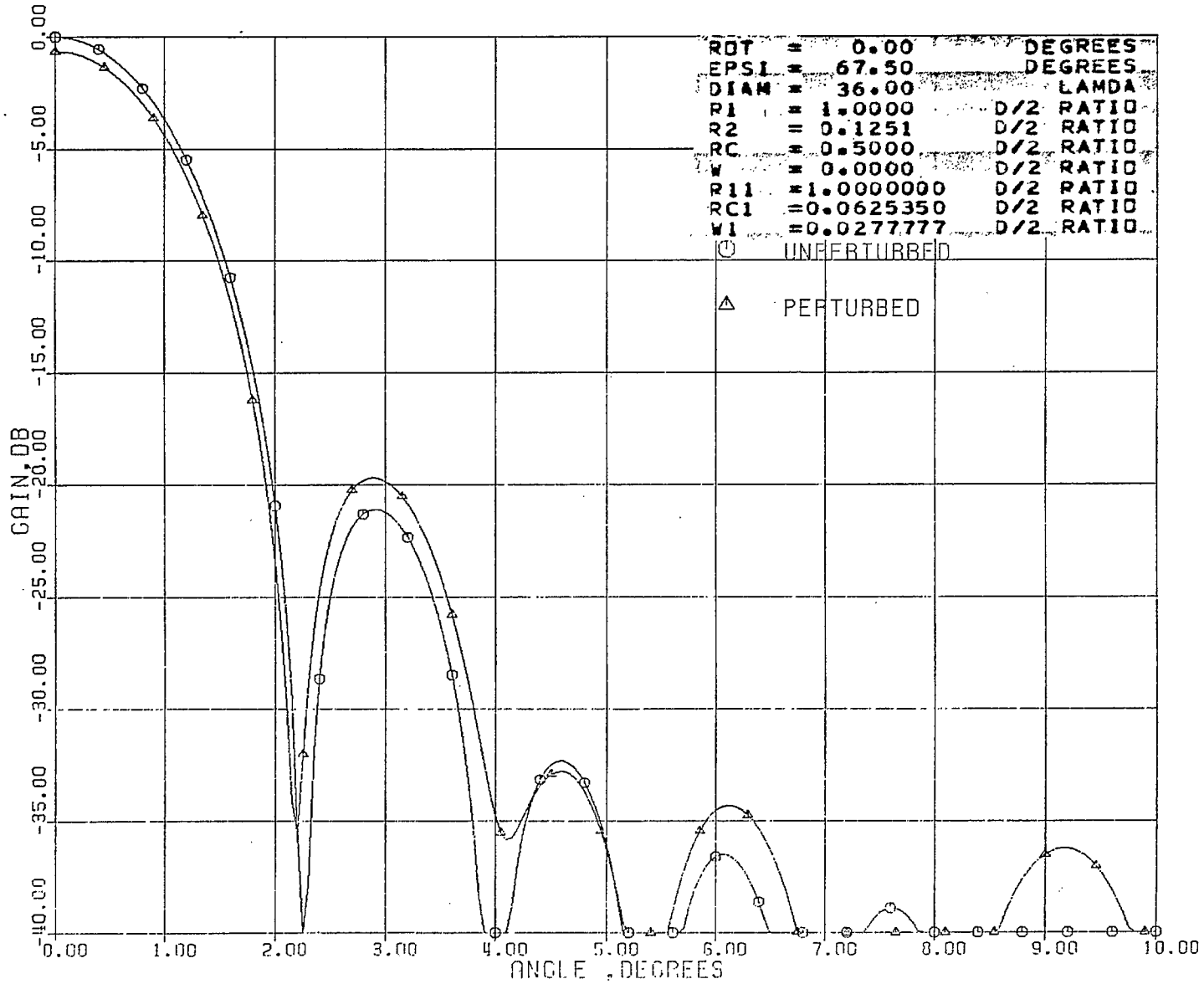

Figure 52. Radiation pattern with tripod (B31000)

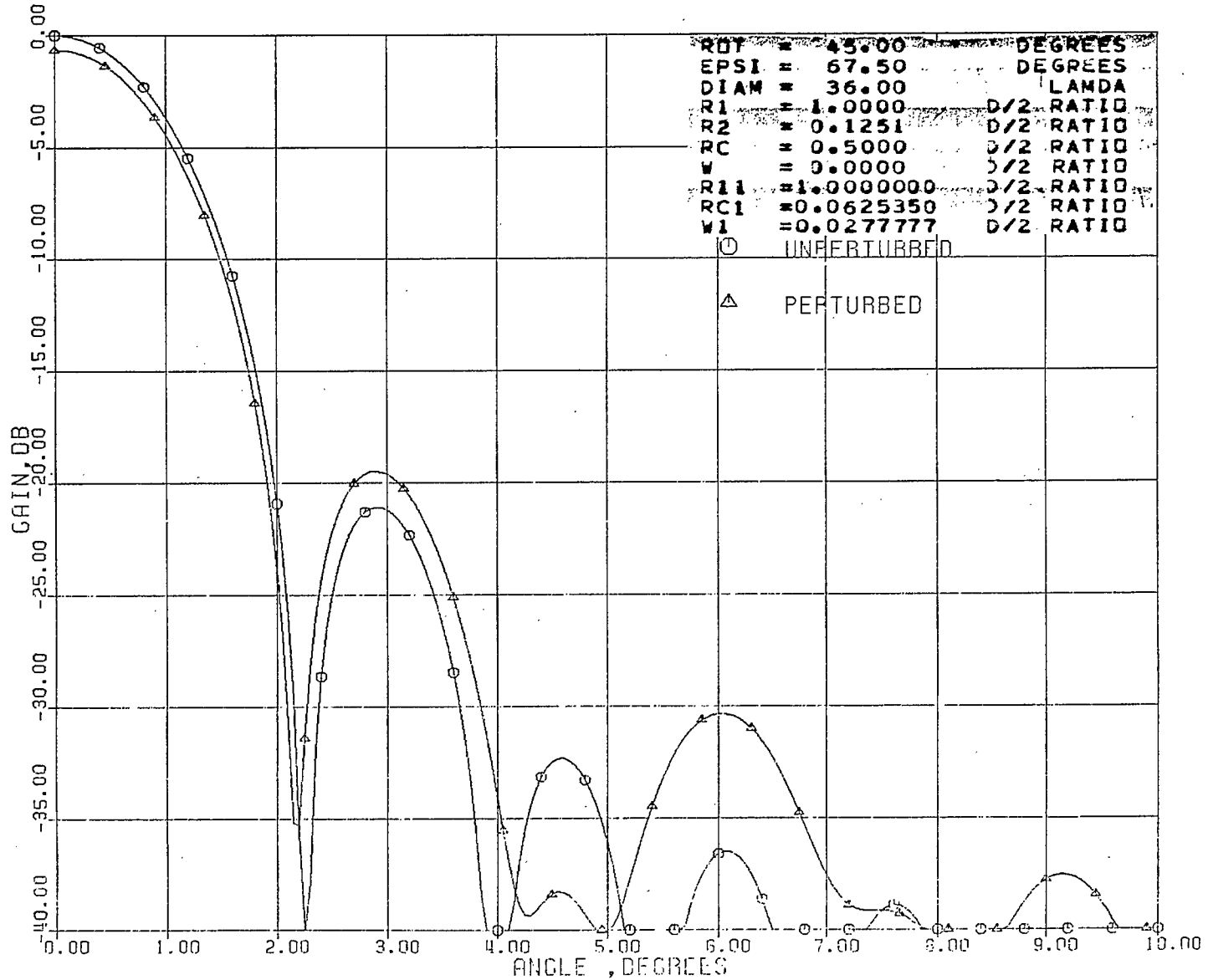

Figure 53. Radiation pattern with tripod (A31045)

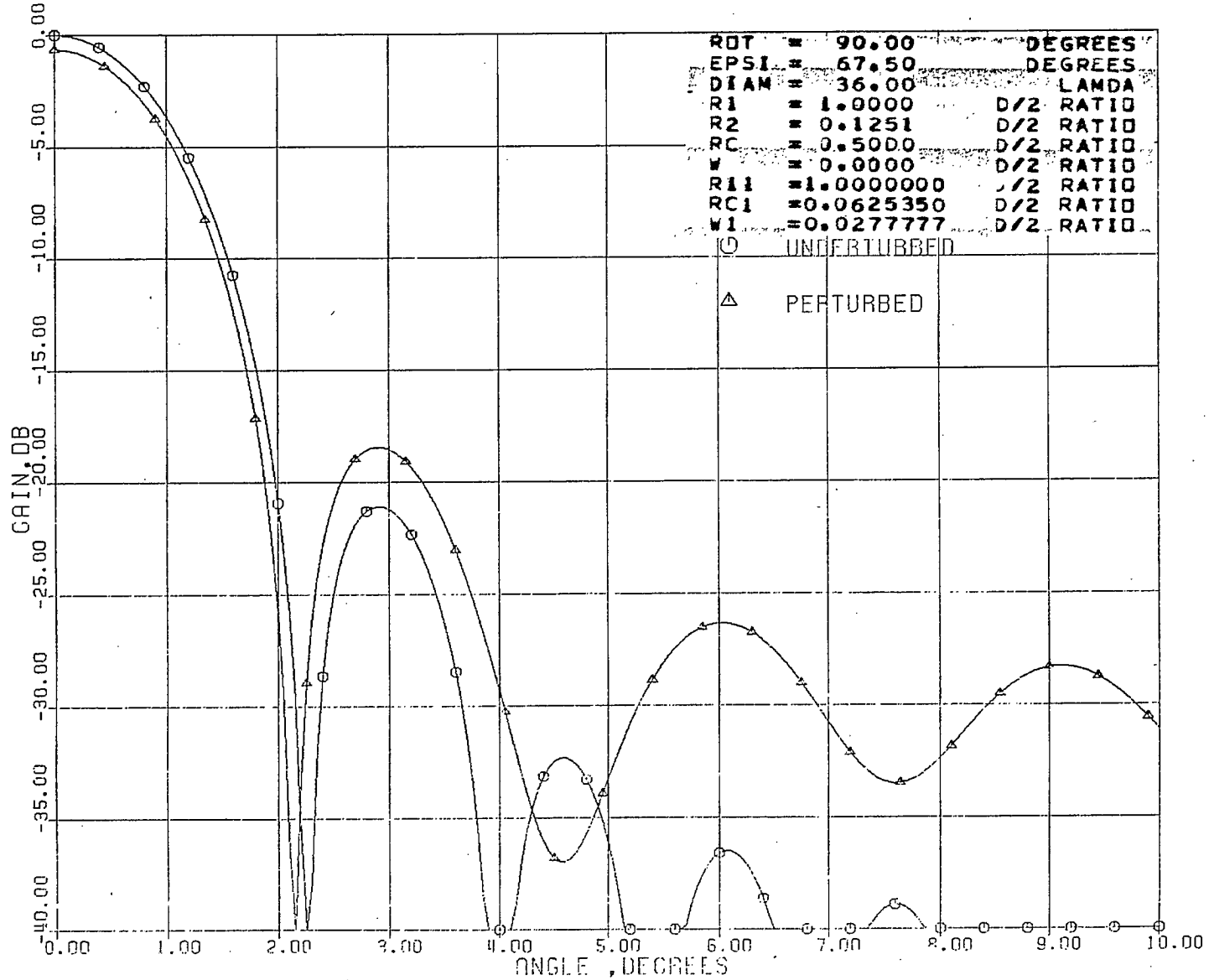

Figure 54. Radiation pattern with tripod (B31090)

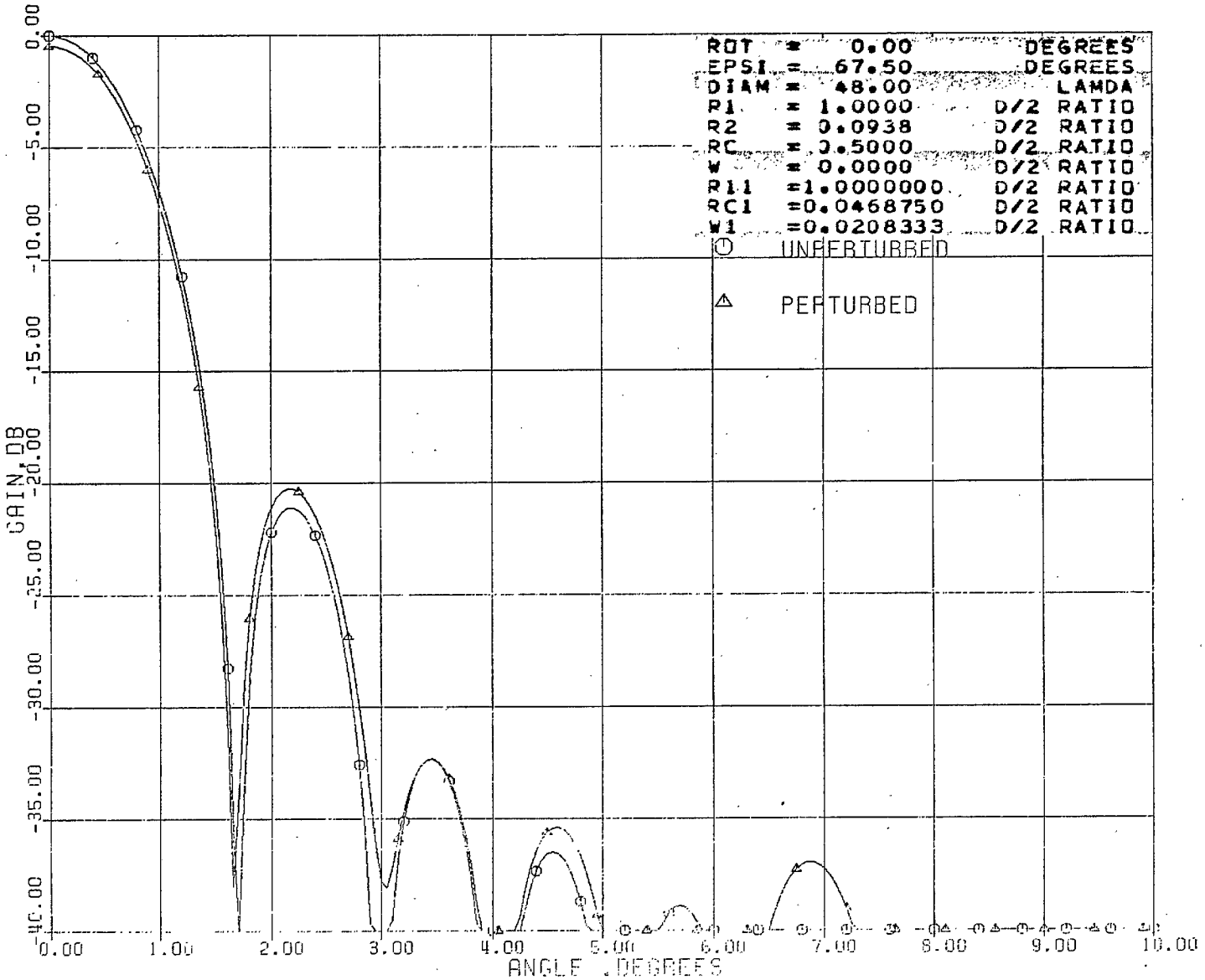

Figure 55. Radiation pattern with tripod (C31000)

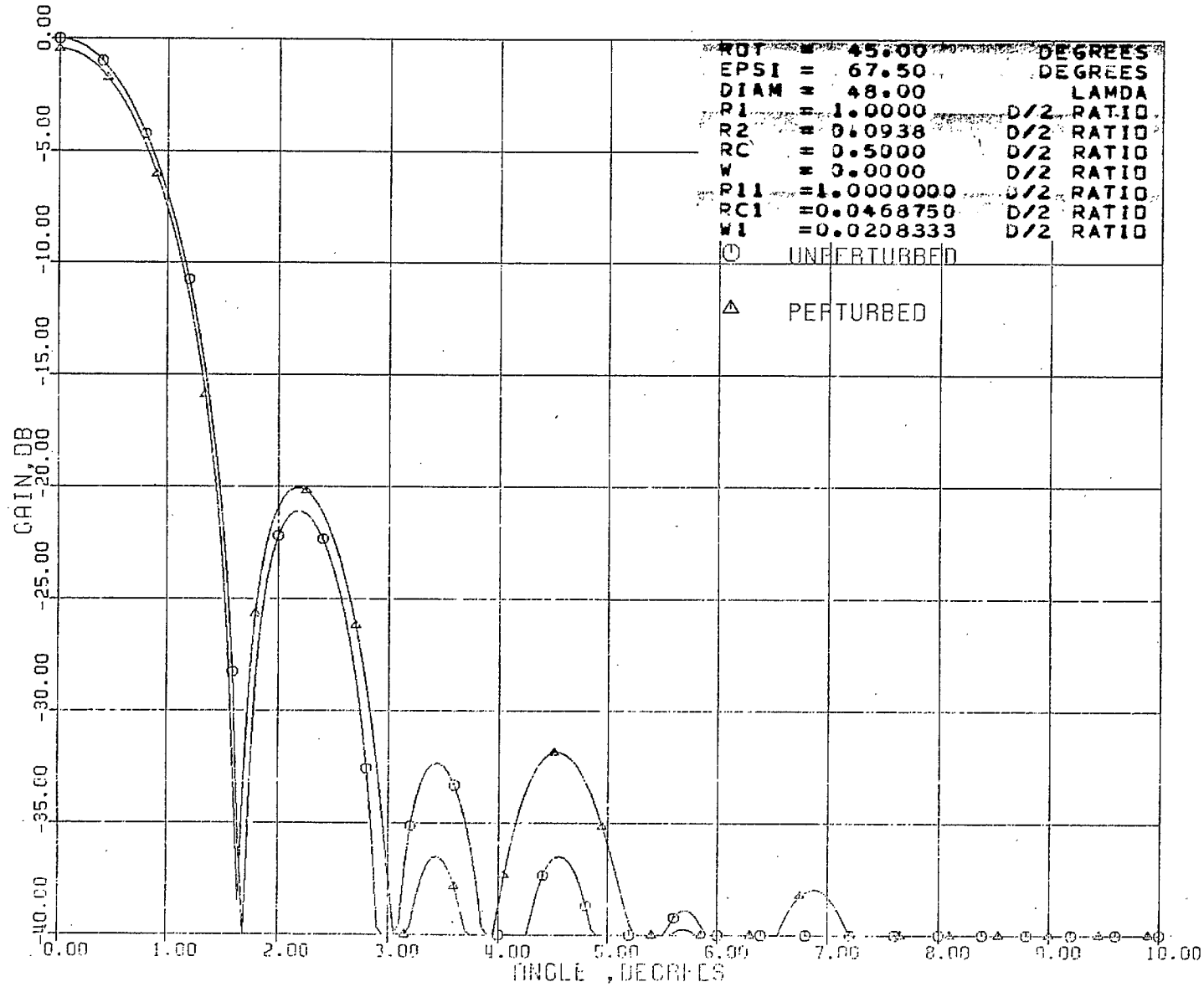

Figure 56. Radiation pattern with tripod (C31045)

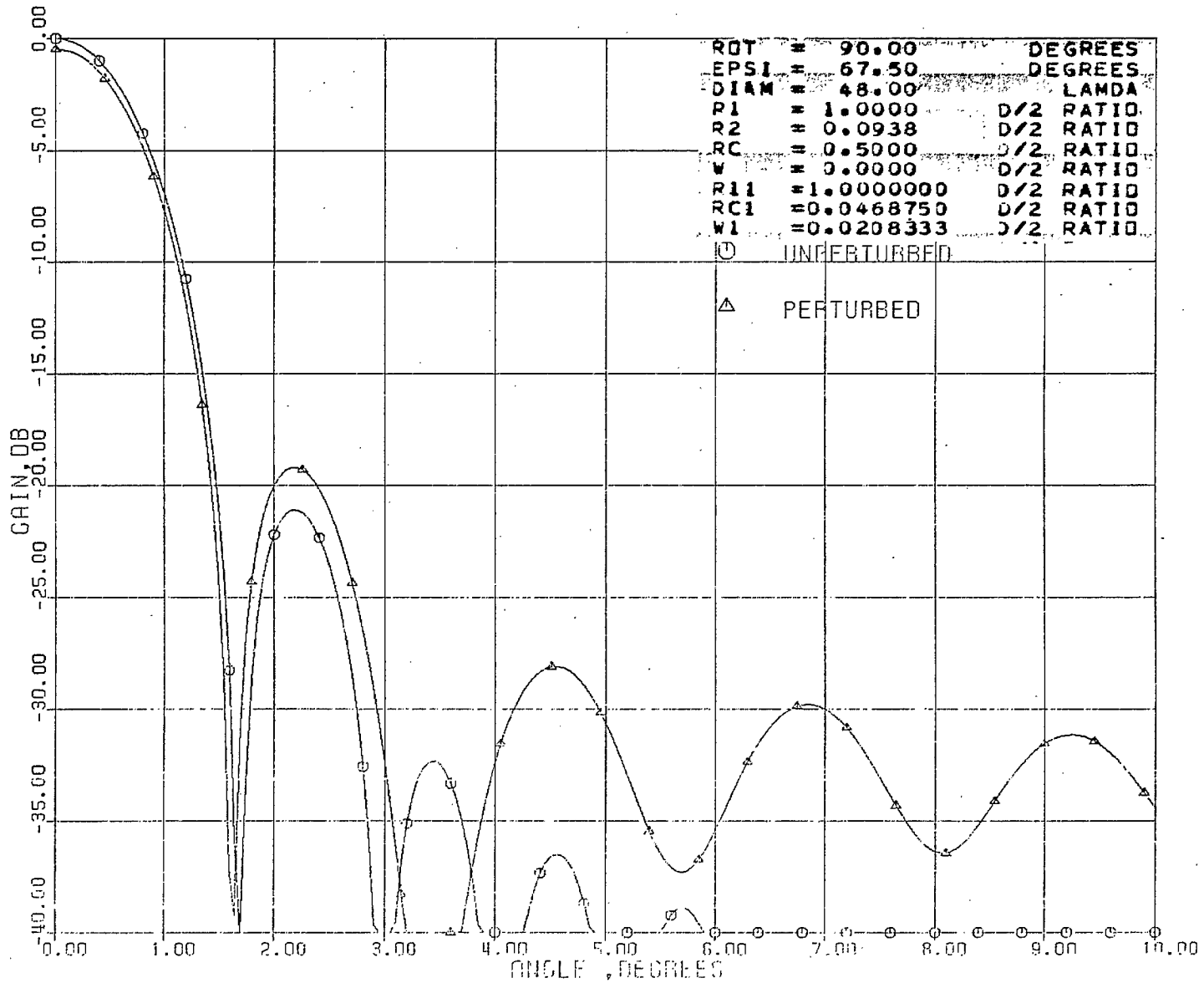

Figure 57. Radiation pattern with tripod (C31090)

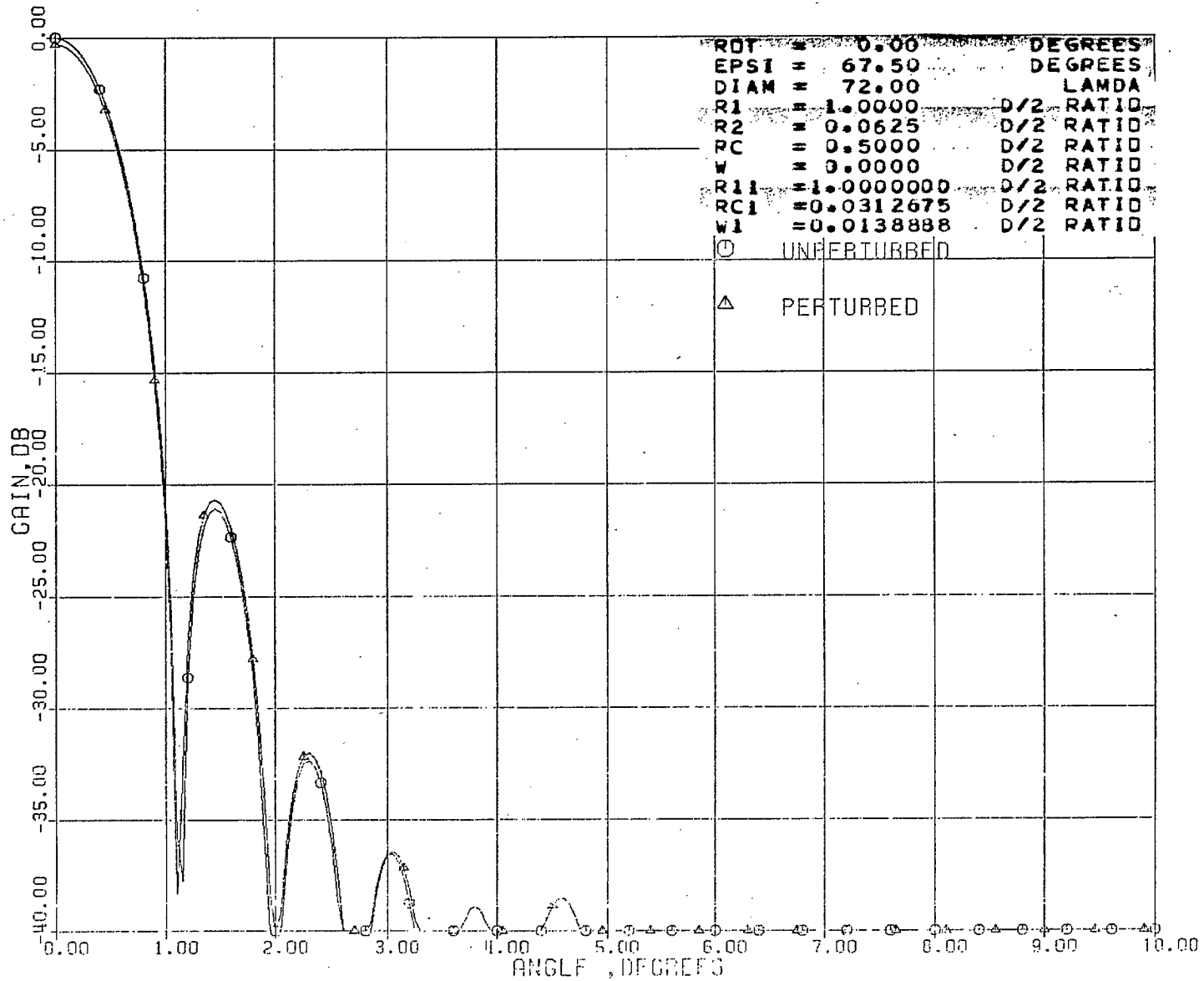

Figure 58. Radiation pattern with tripod (D31000)

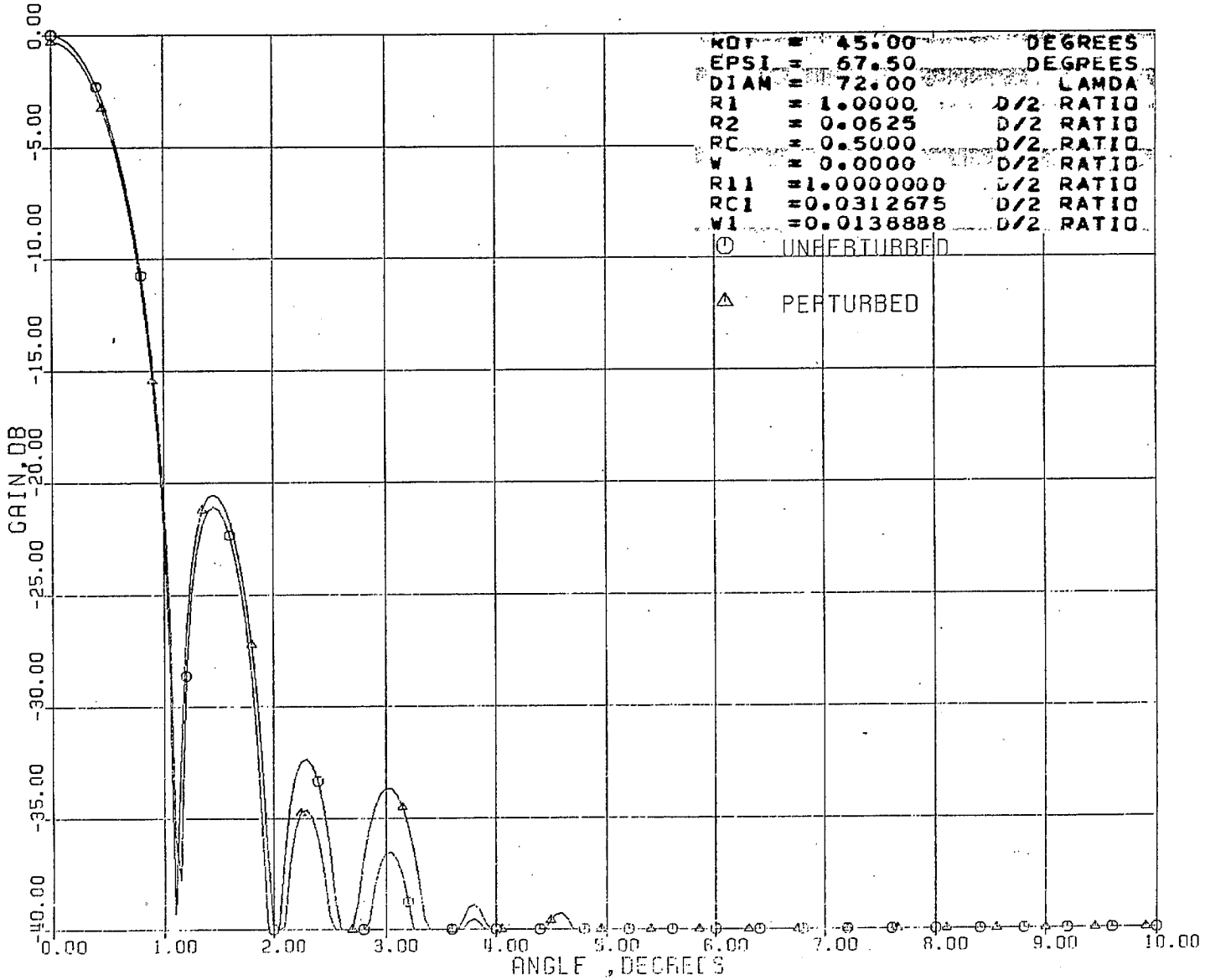

Figure 59. Radiation pattern with tripod (D31045)

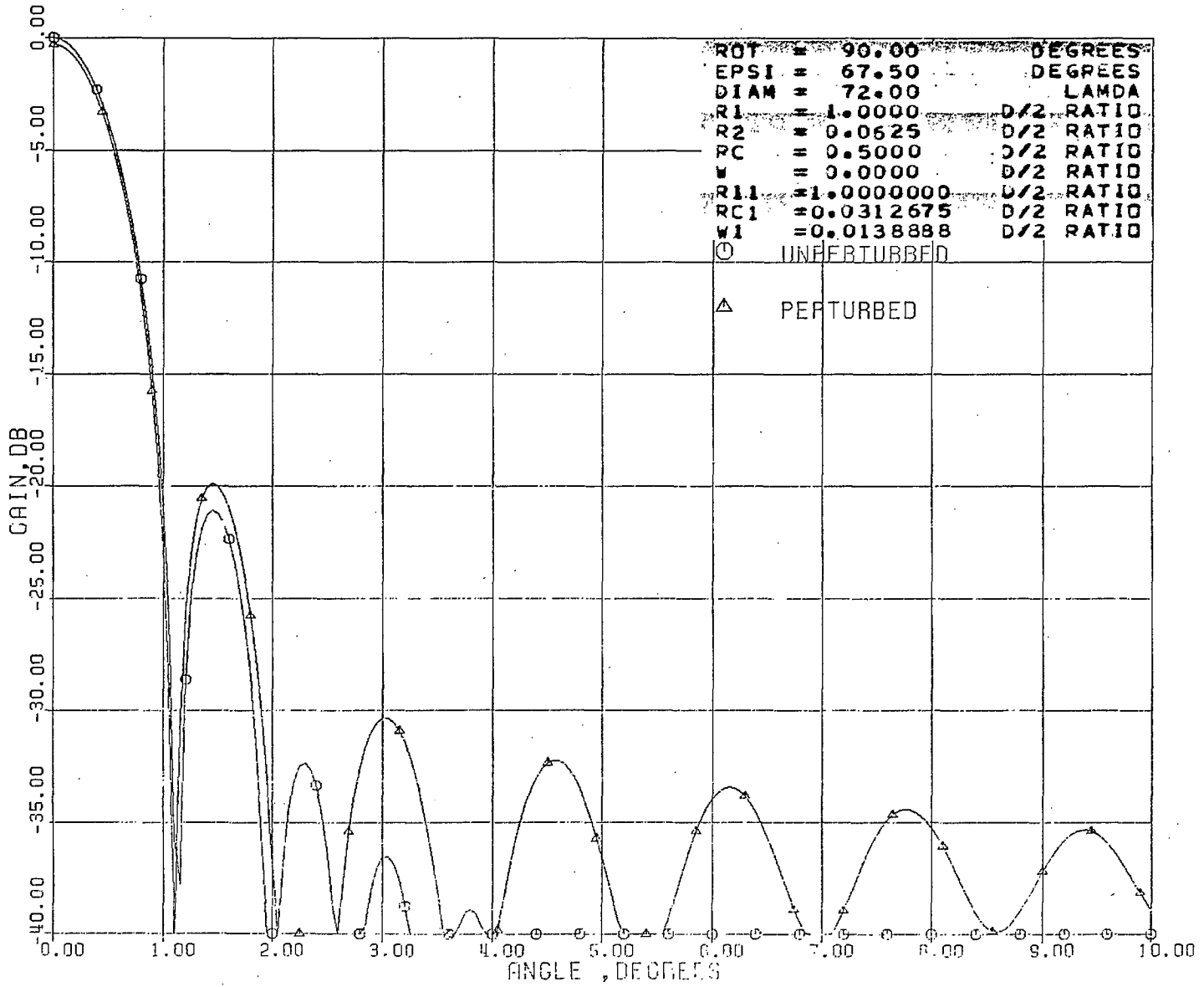

Figure 60. Radiation pattern with tripod (D31090)

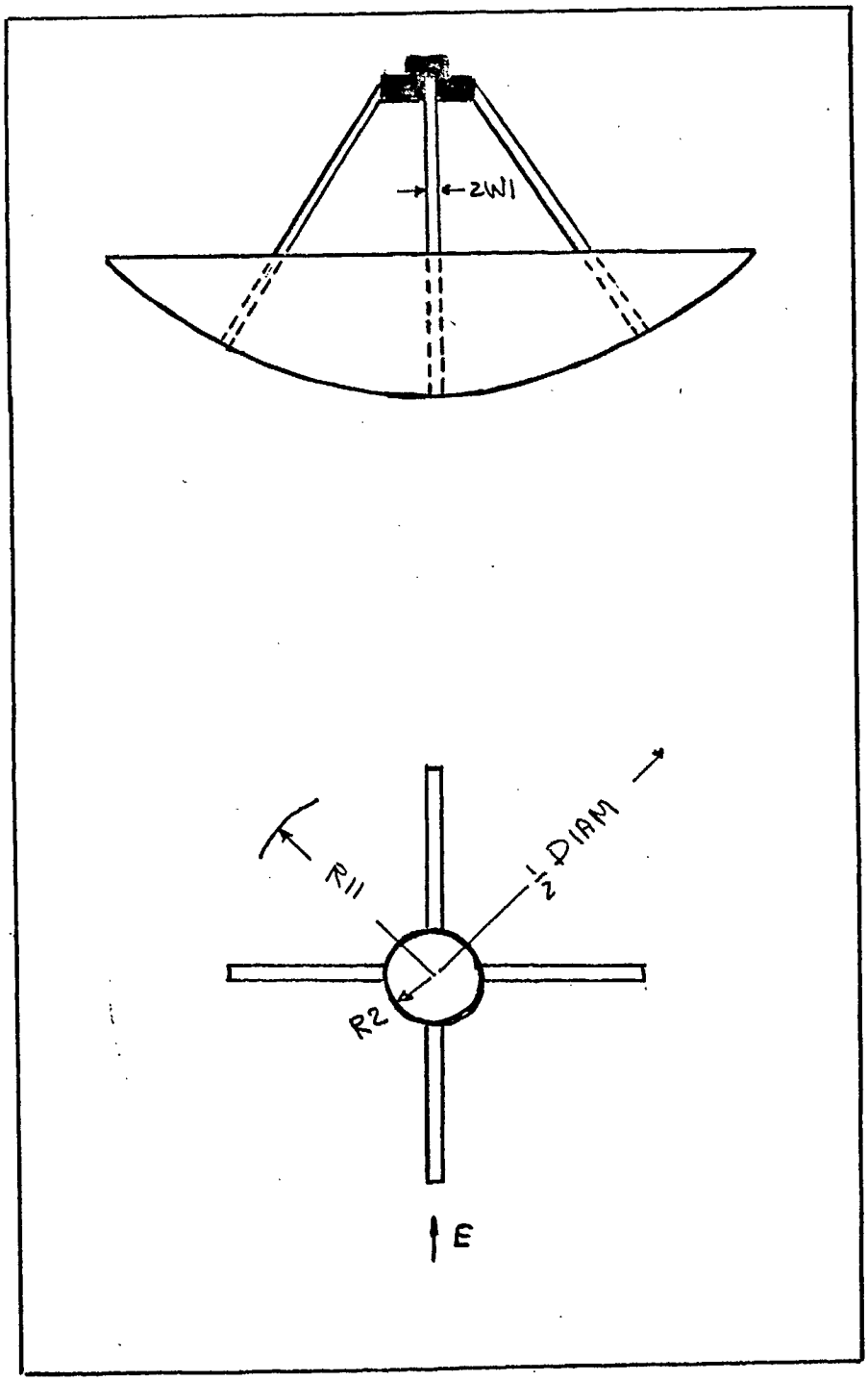

Figure 61. Quad geometry

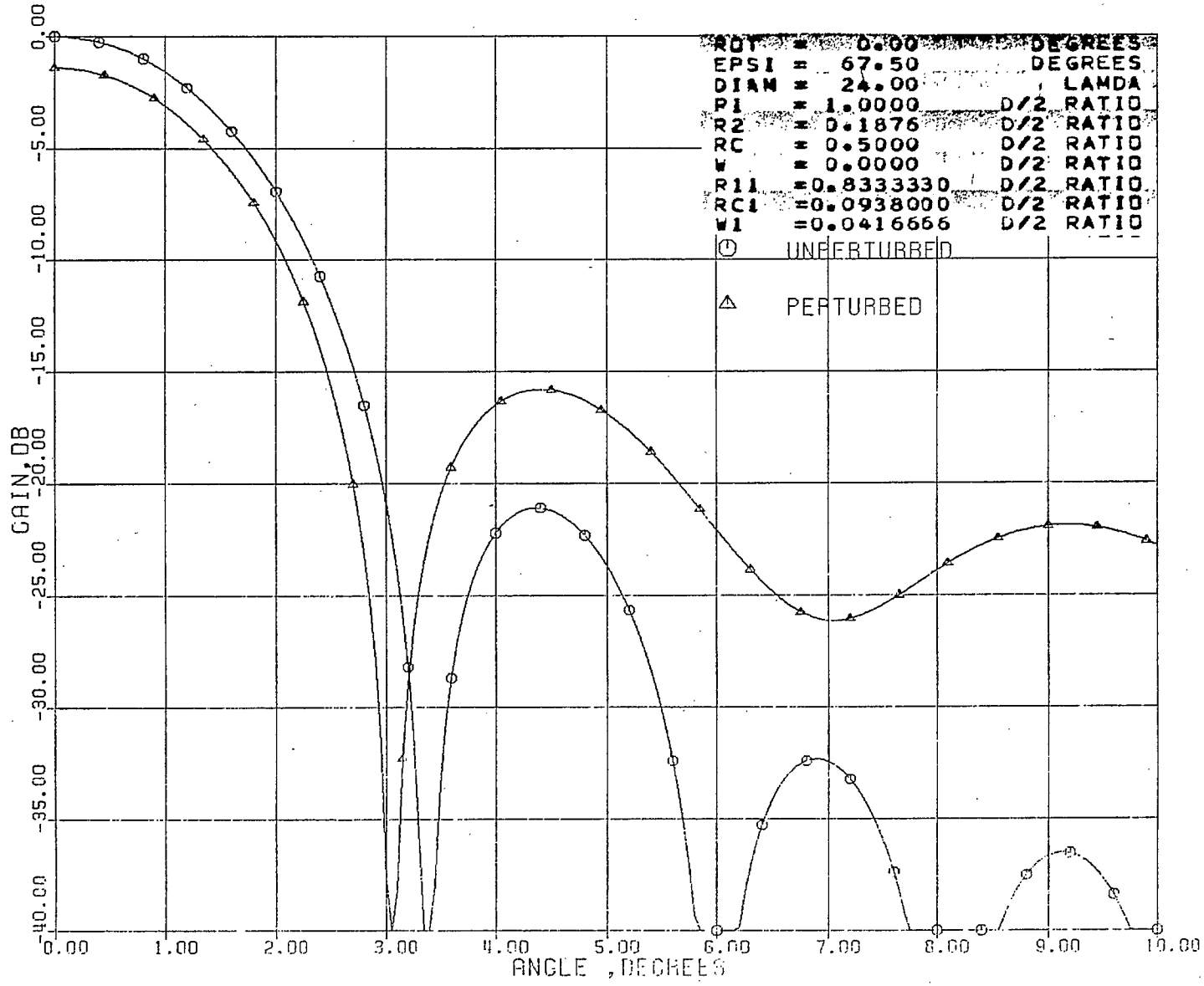

Figure 62. Radiation pattern with quad (A40800)

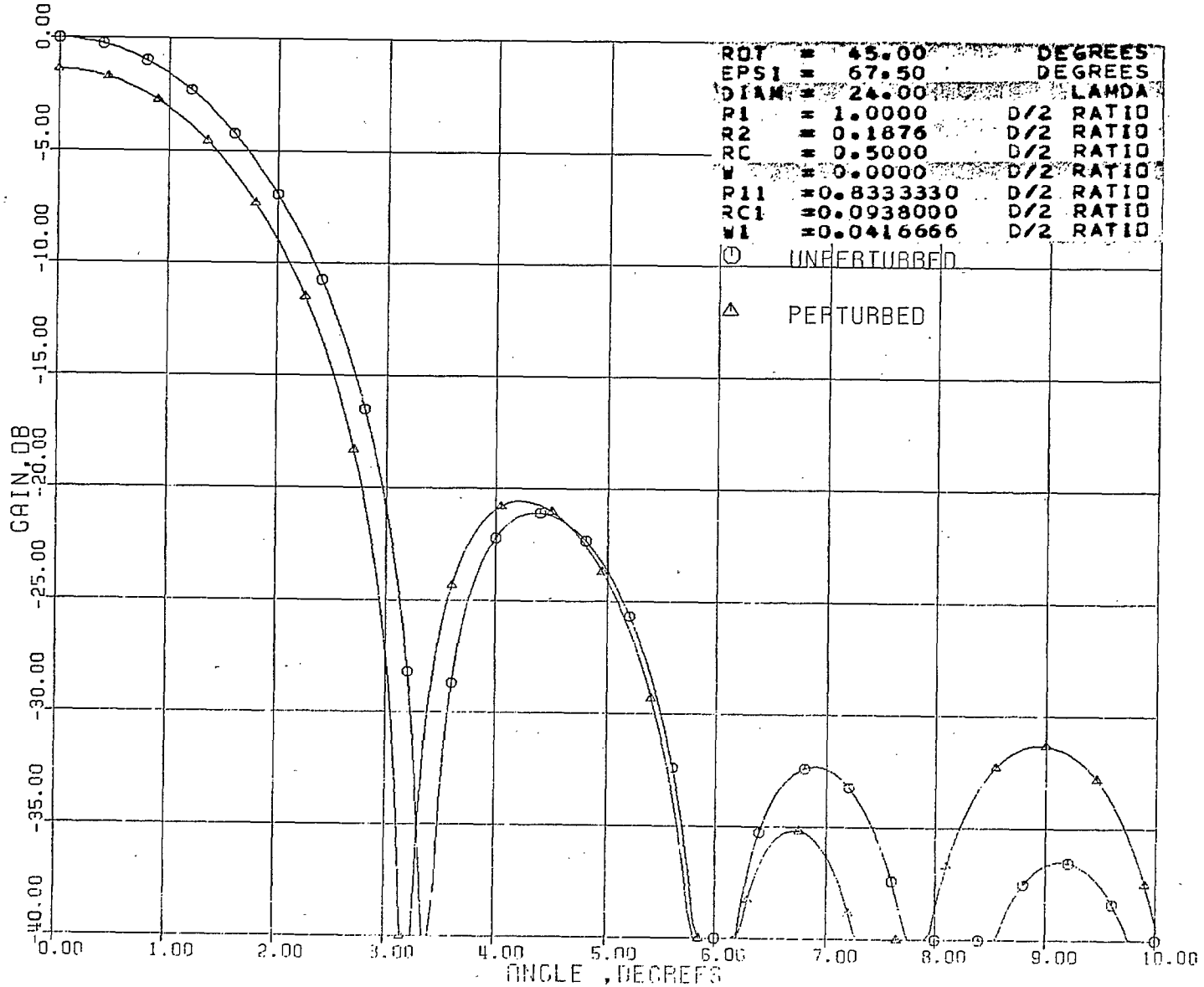

Figure 63. Radiation pattern with quad (A40845)

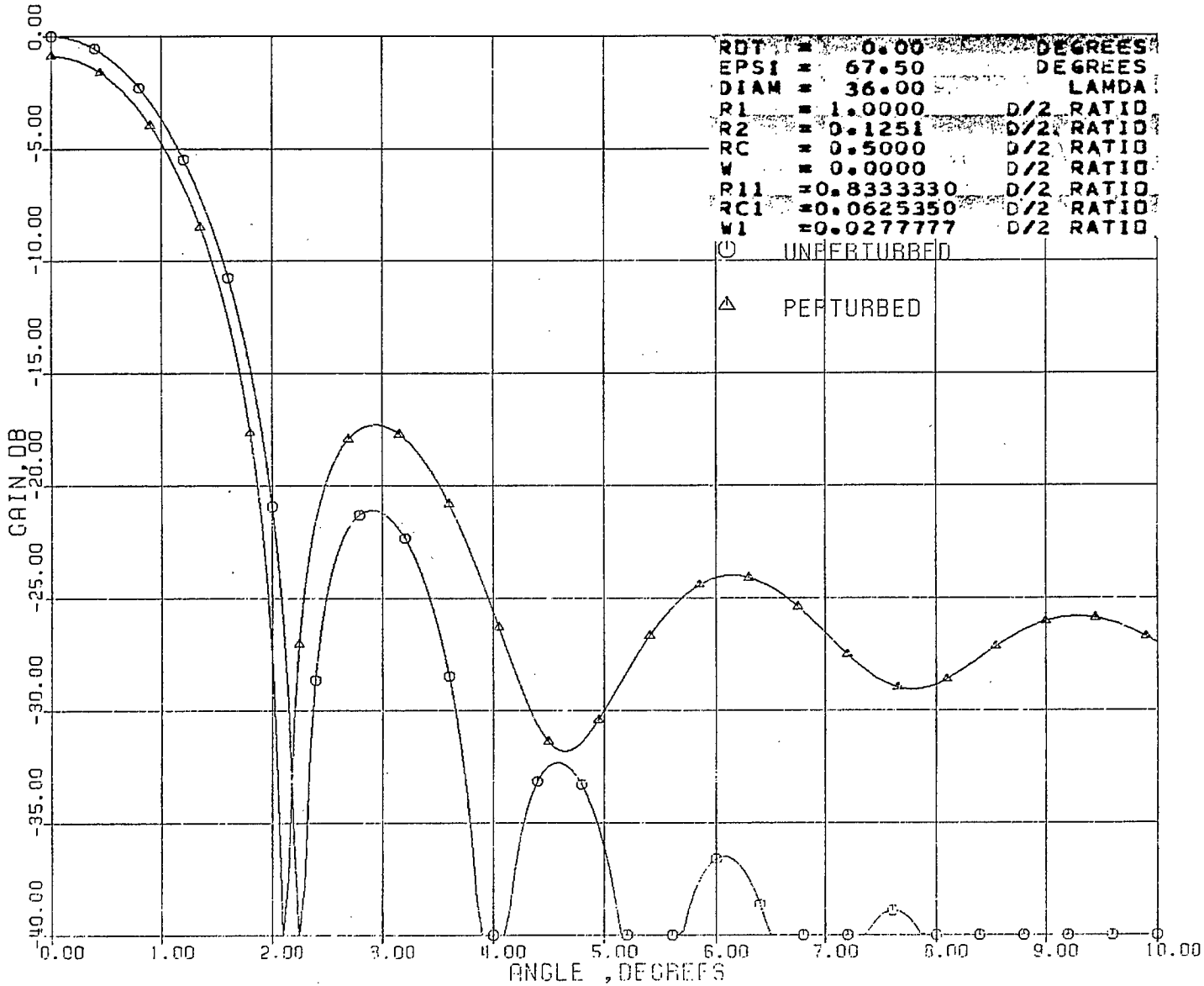

Figure 64. Radiation pattern with quad (B40800)

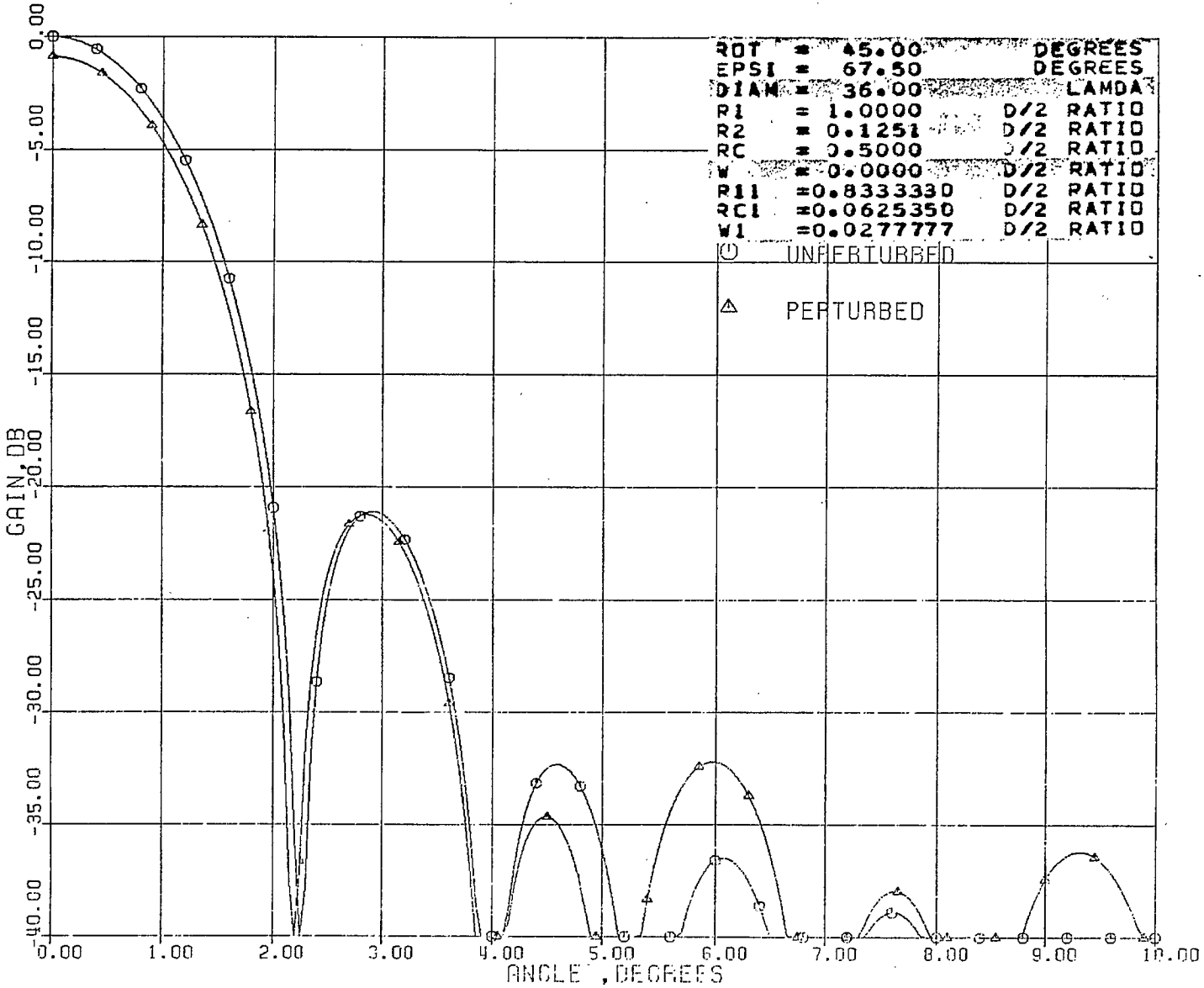

Figure 65. Radiation pattern with quad (B40845)

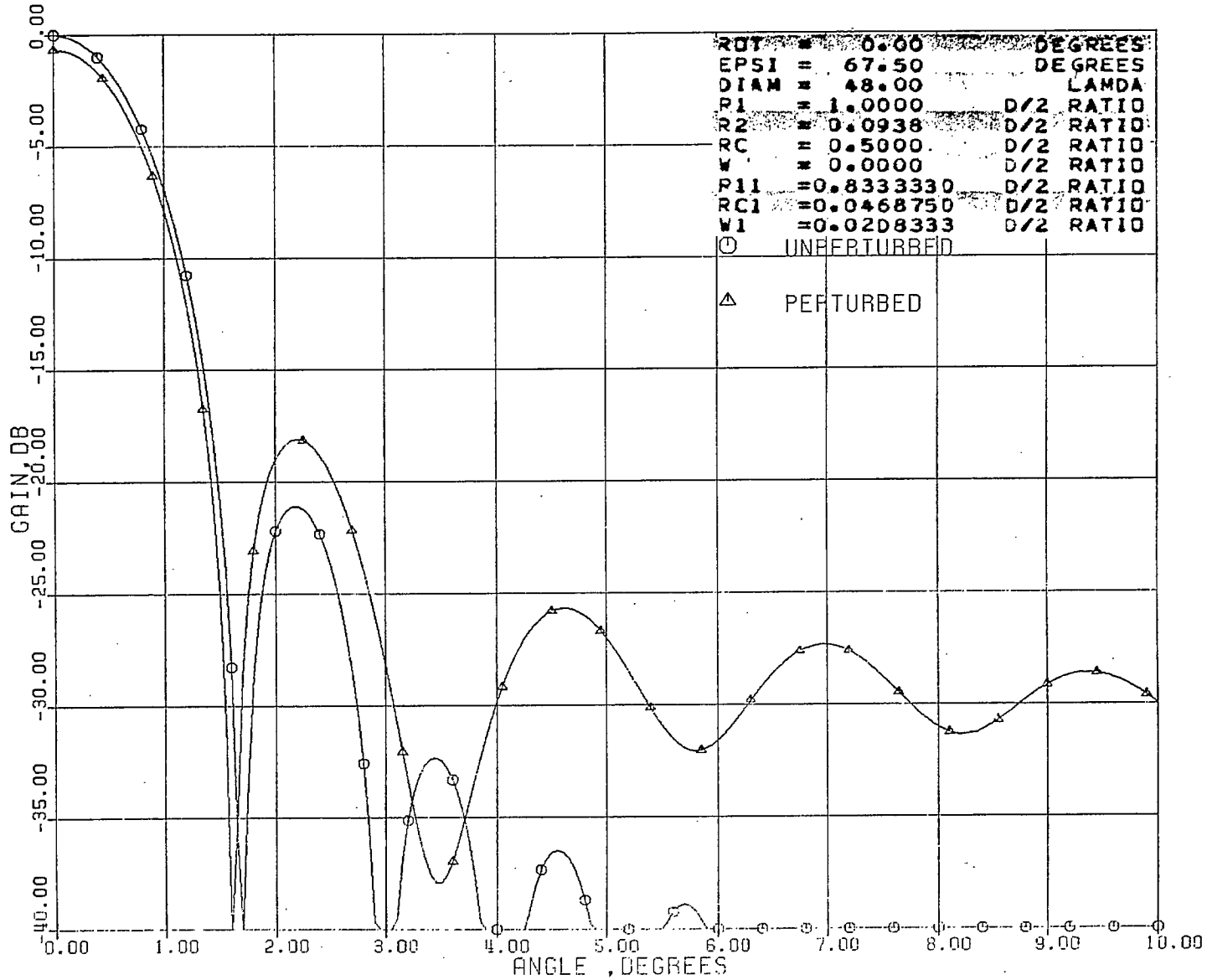

Figure 66. Radiation pattern with quad (C40800)

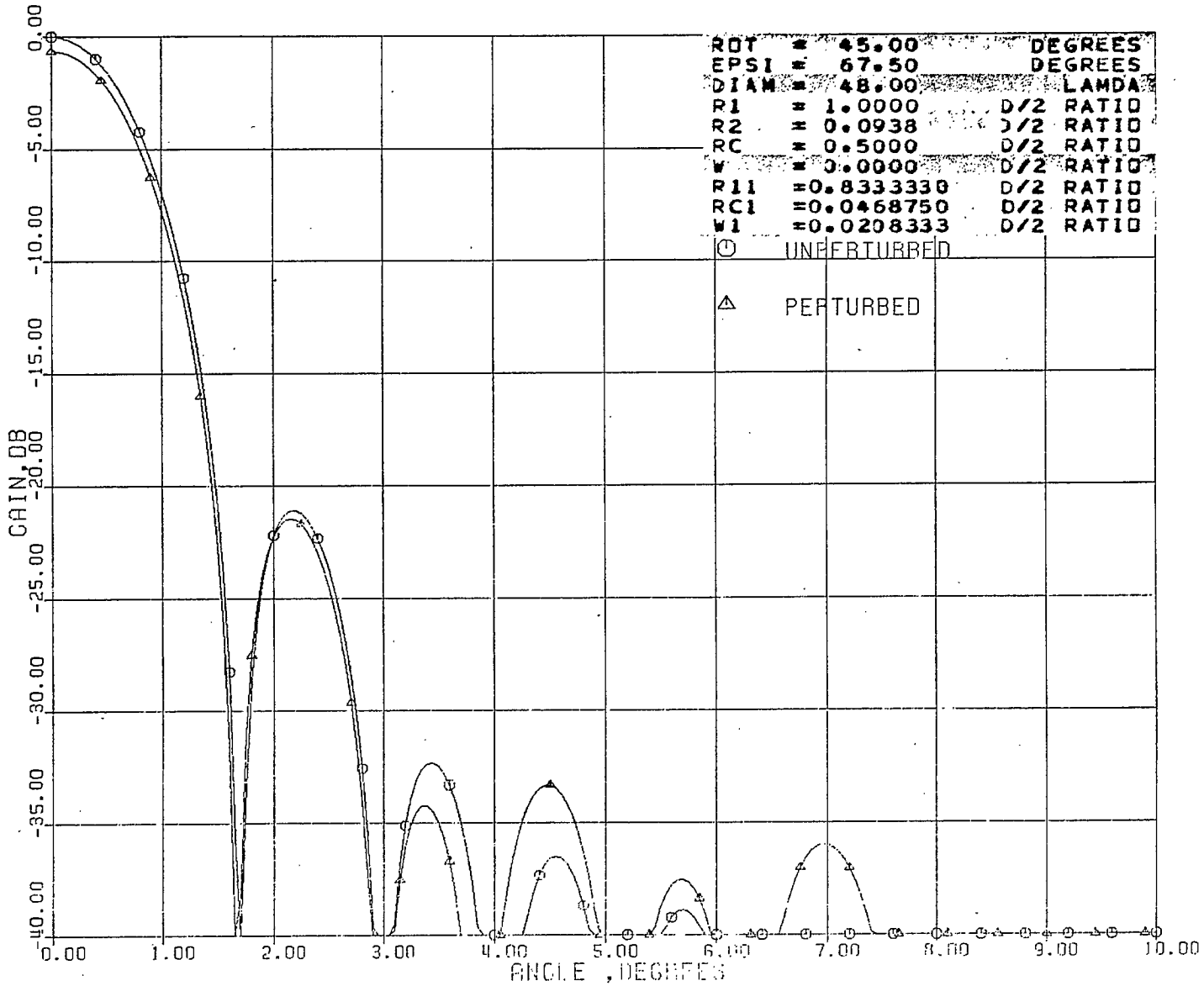

Figure 67. Radiation pattern with quad (C40845)

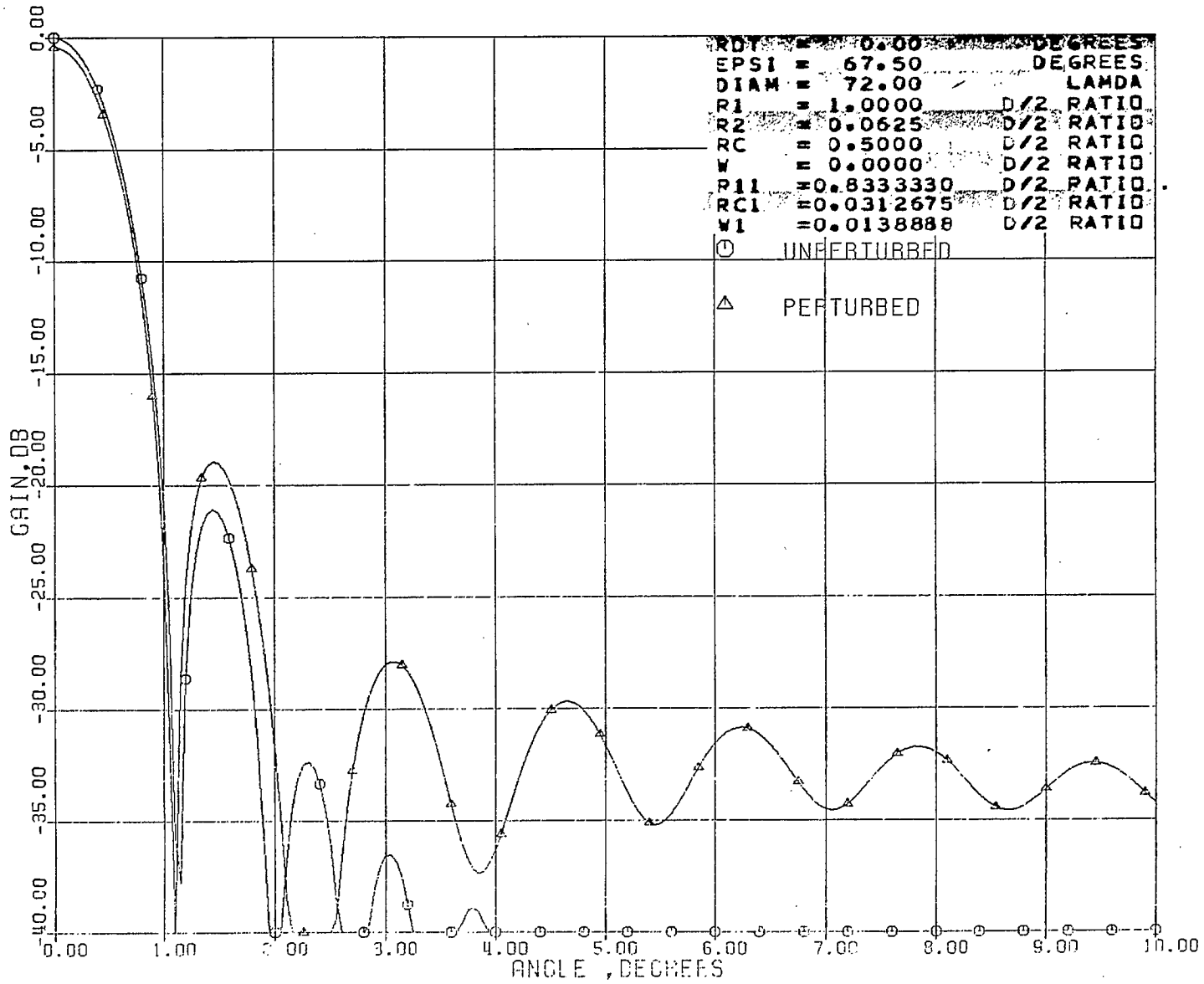

Figure 68. Radiation pattern with quad (D40800)

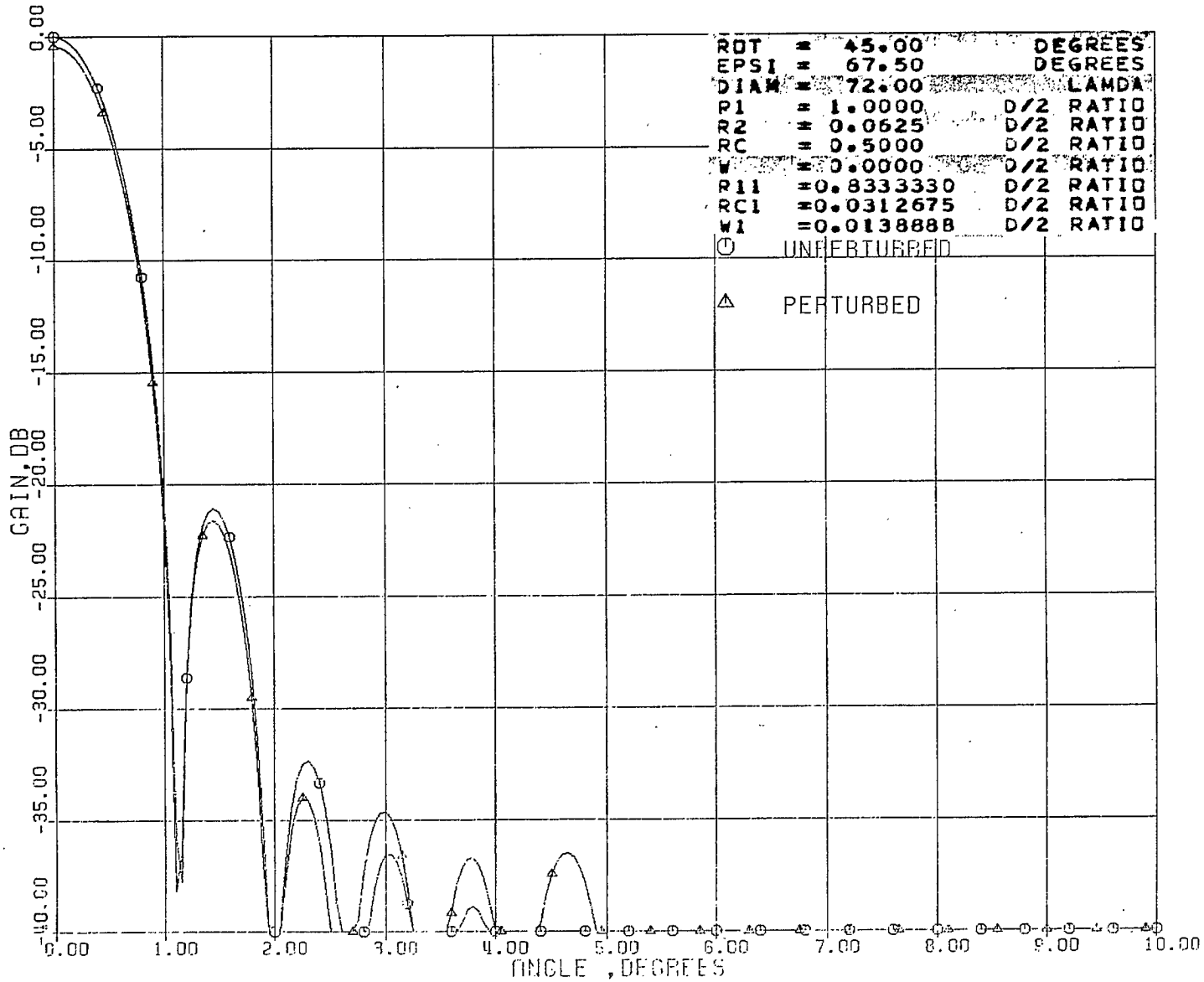

Figure 69. Radiation pattern with quad (D40845)

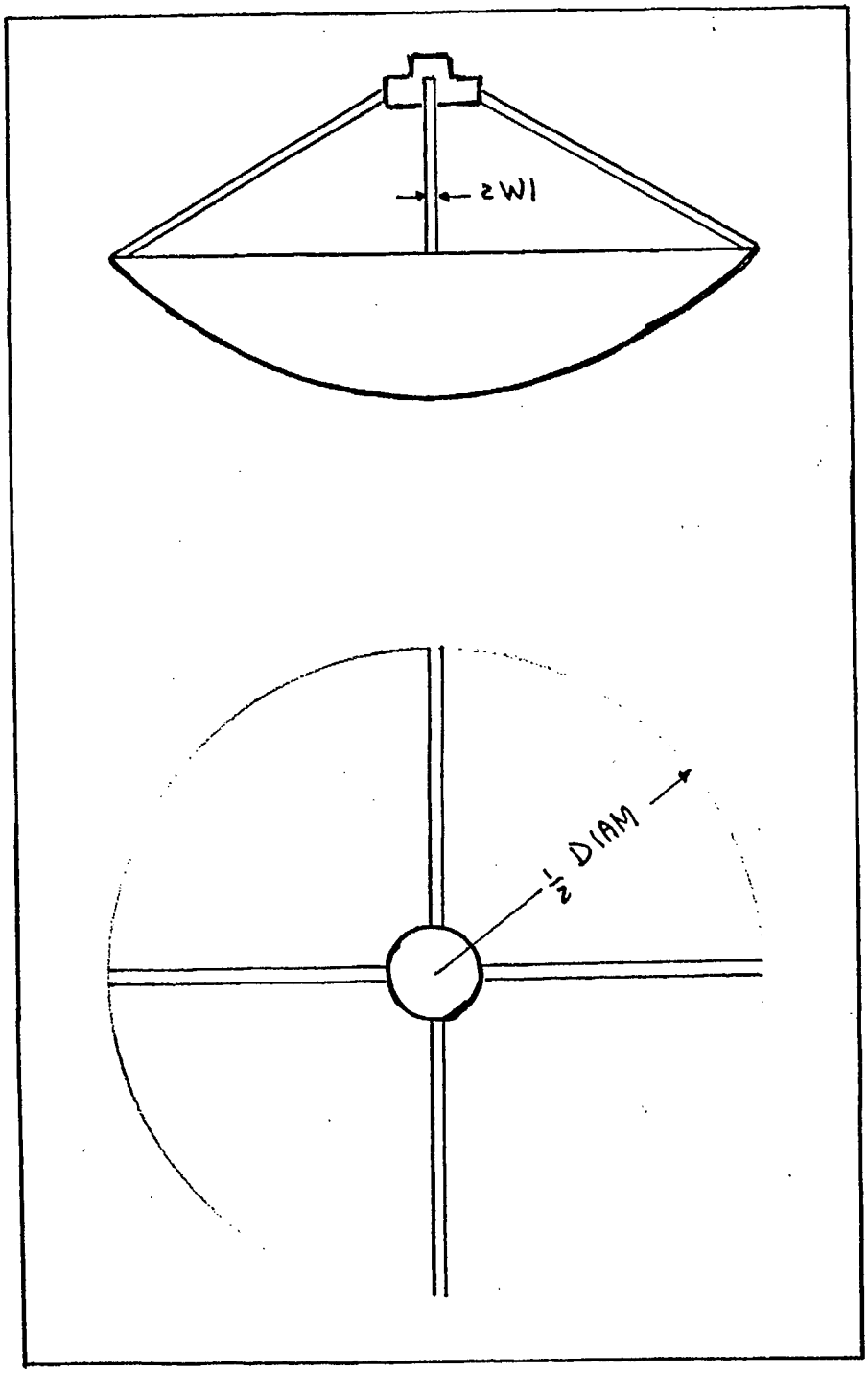

Figure 70. Geometry of quad located at the rim of reflector

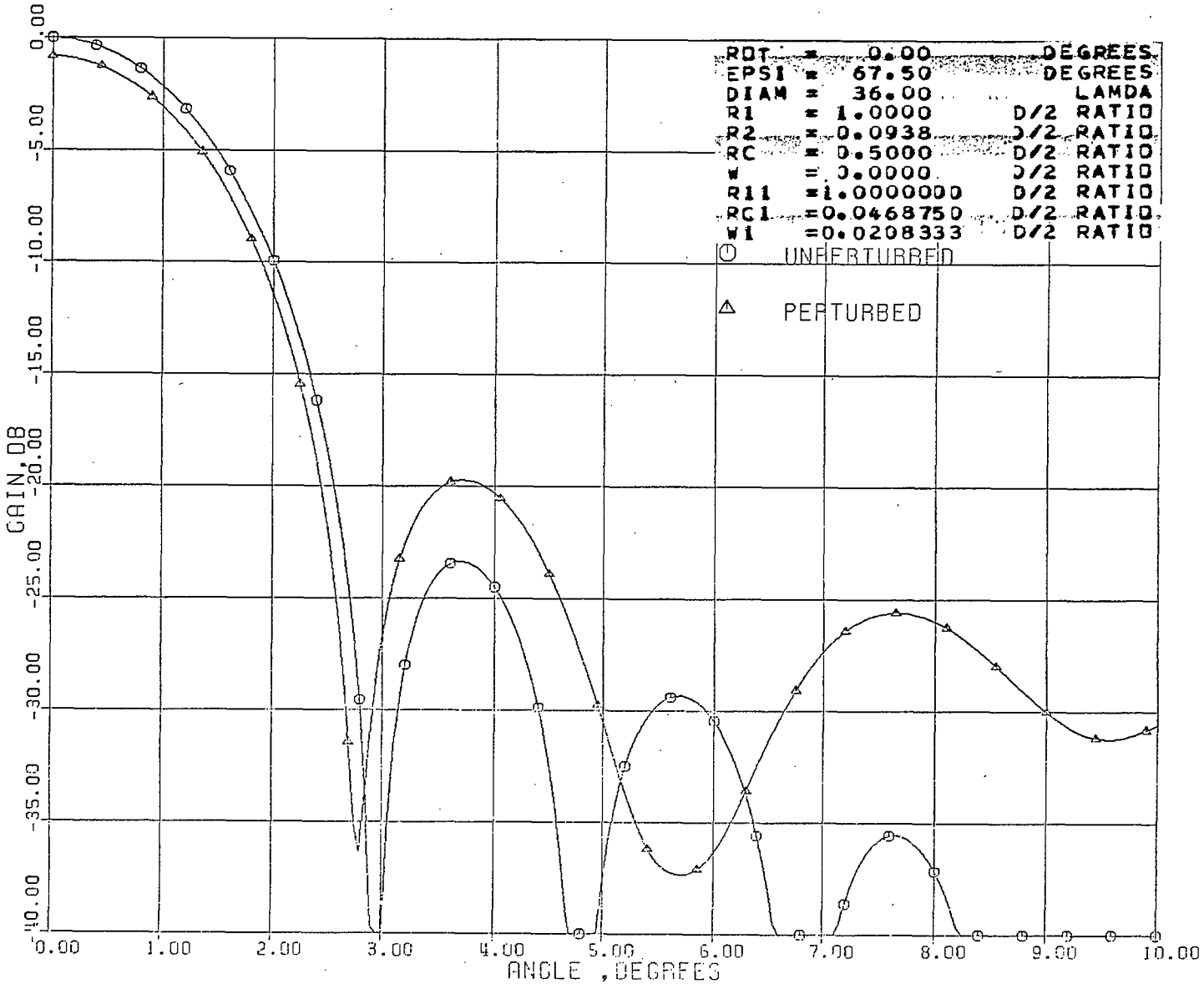

Figure 71. Radiation pattern with quad (B41000)

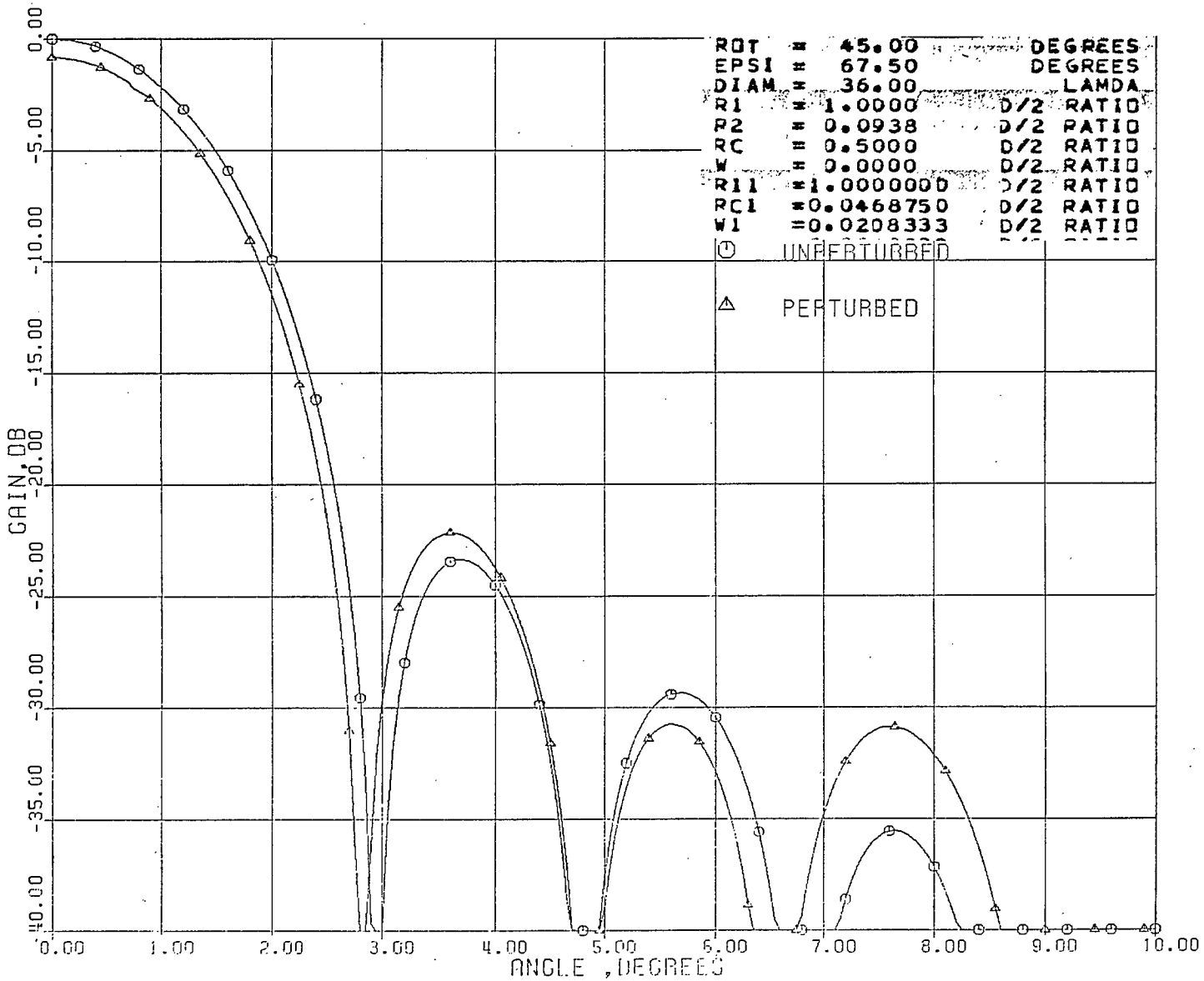

Figure 72. Radiation pattern with B41045)

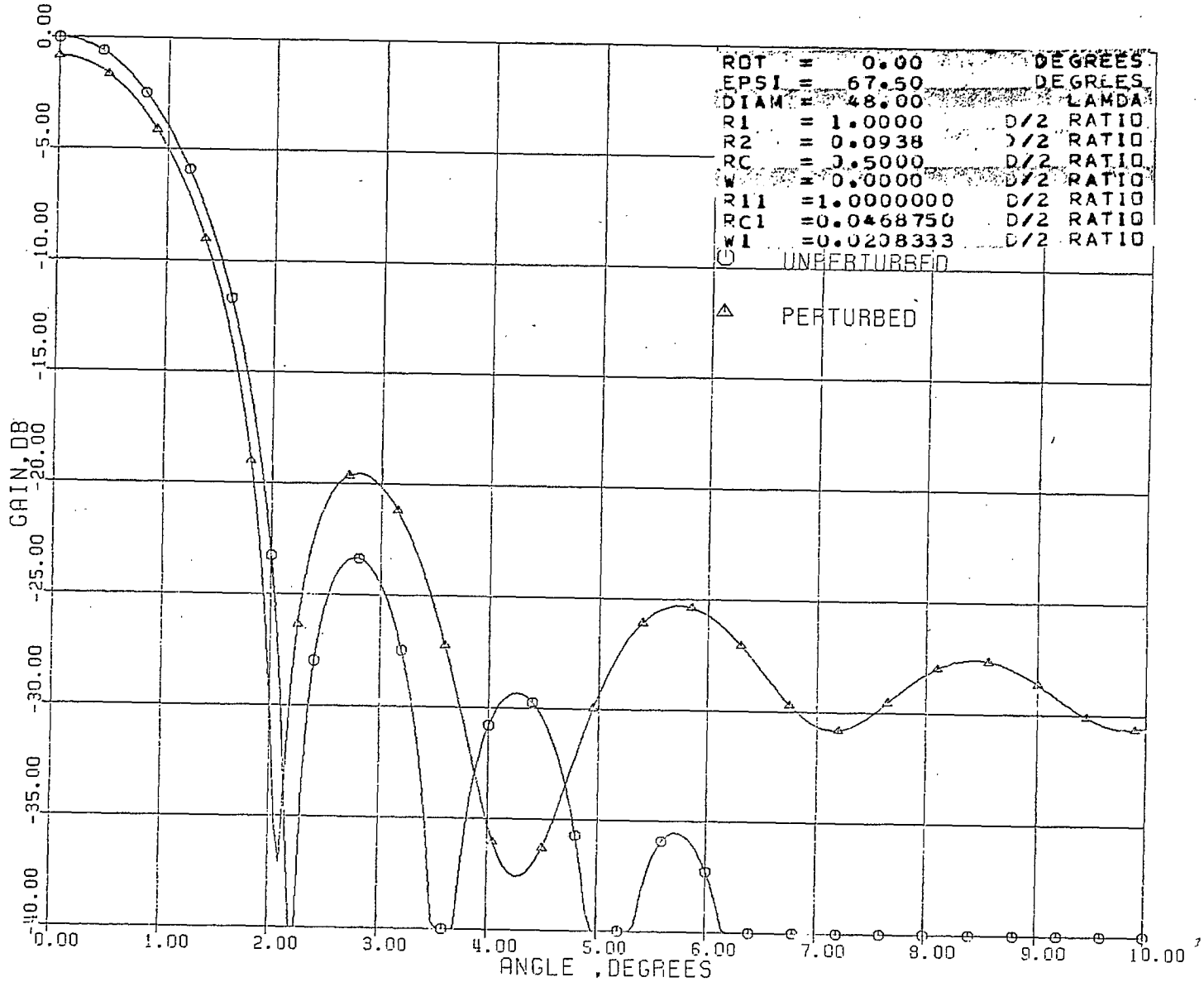

Figure 73. Radiation pattern with quad (C41000)

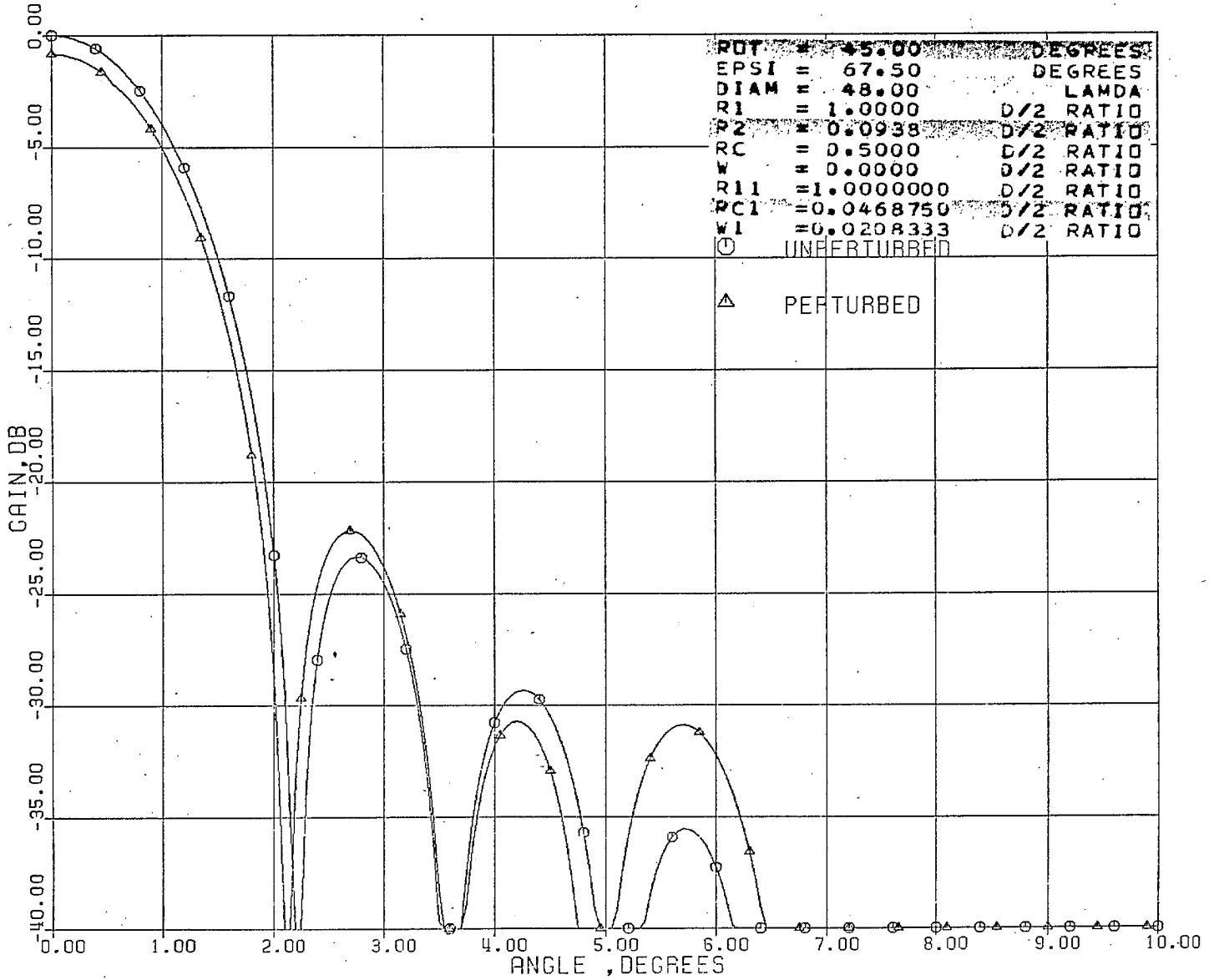

Figure 74. Radiation pattern with quad (C41045)

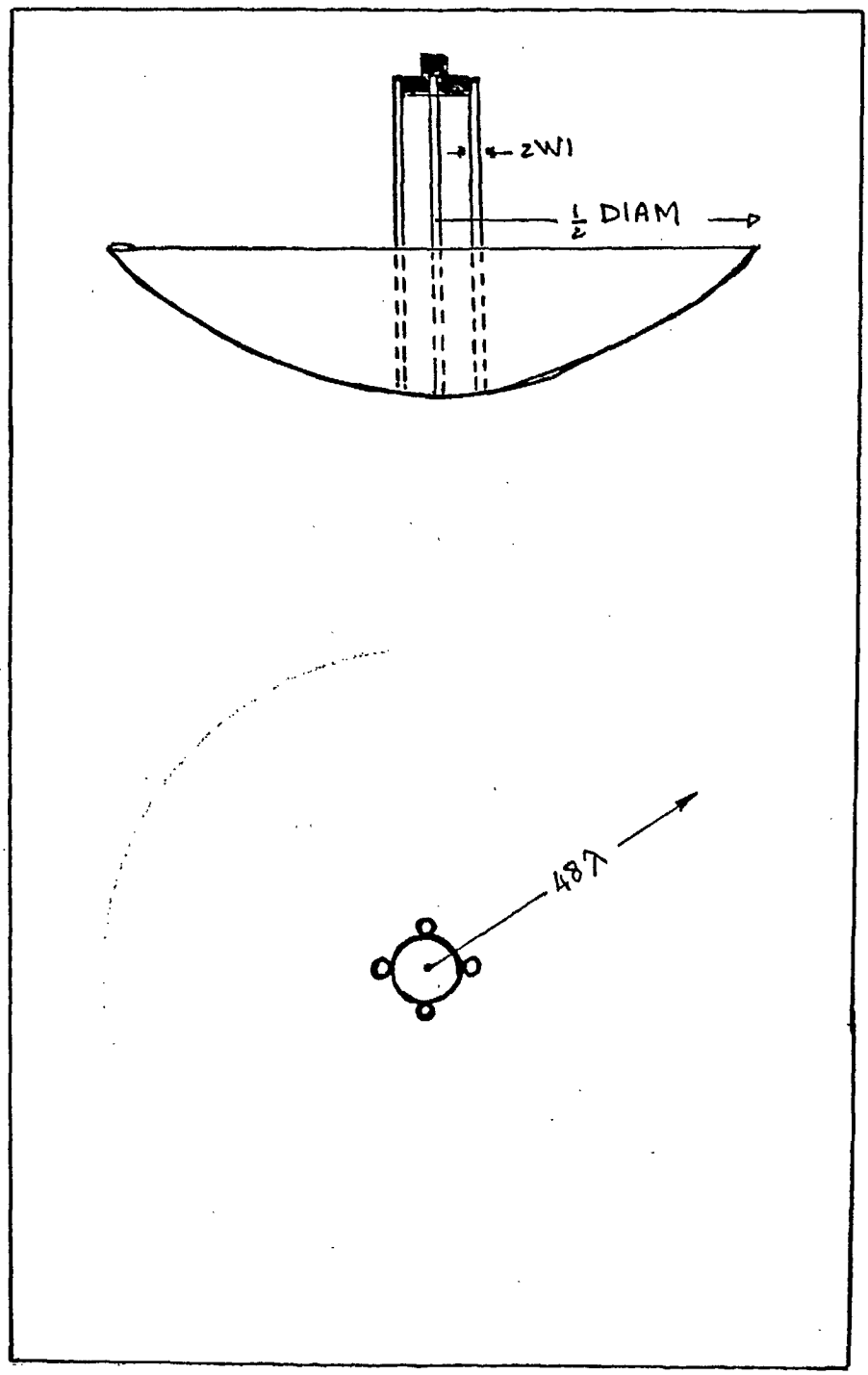

Figure 75. New quad geometry

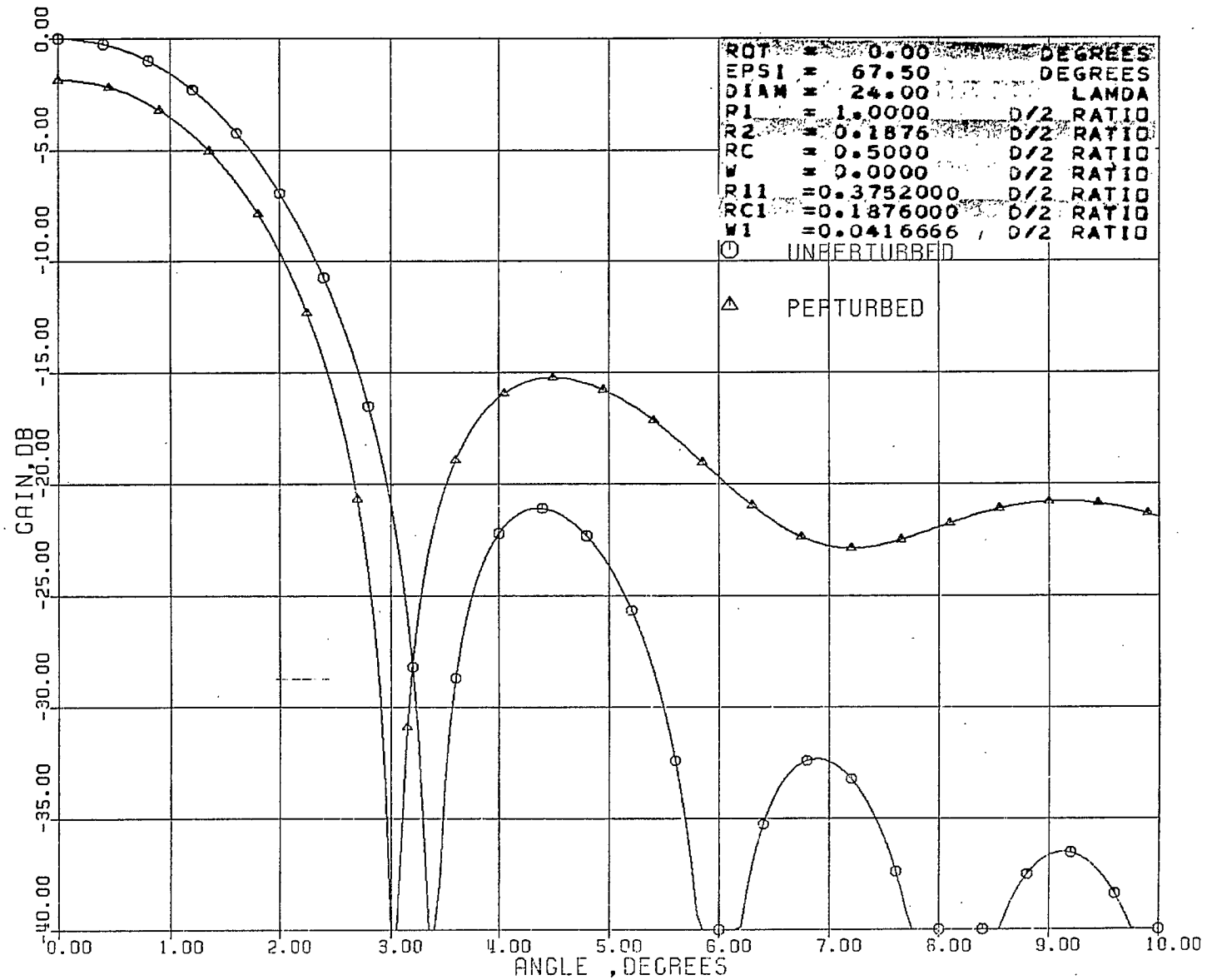

Figure 76. Radiation pattern with new quad struts (A40300)

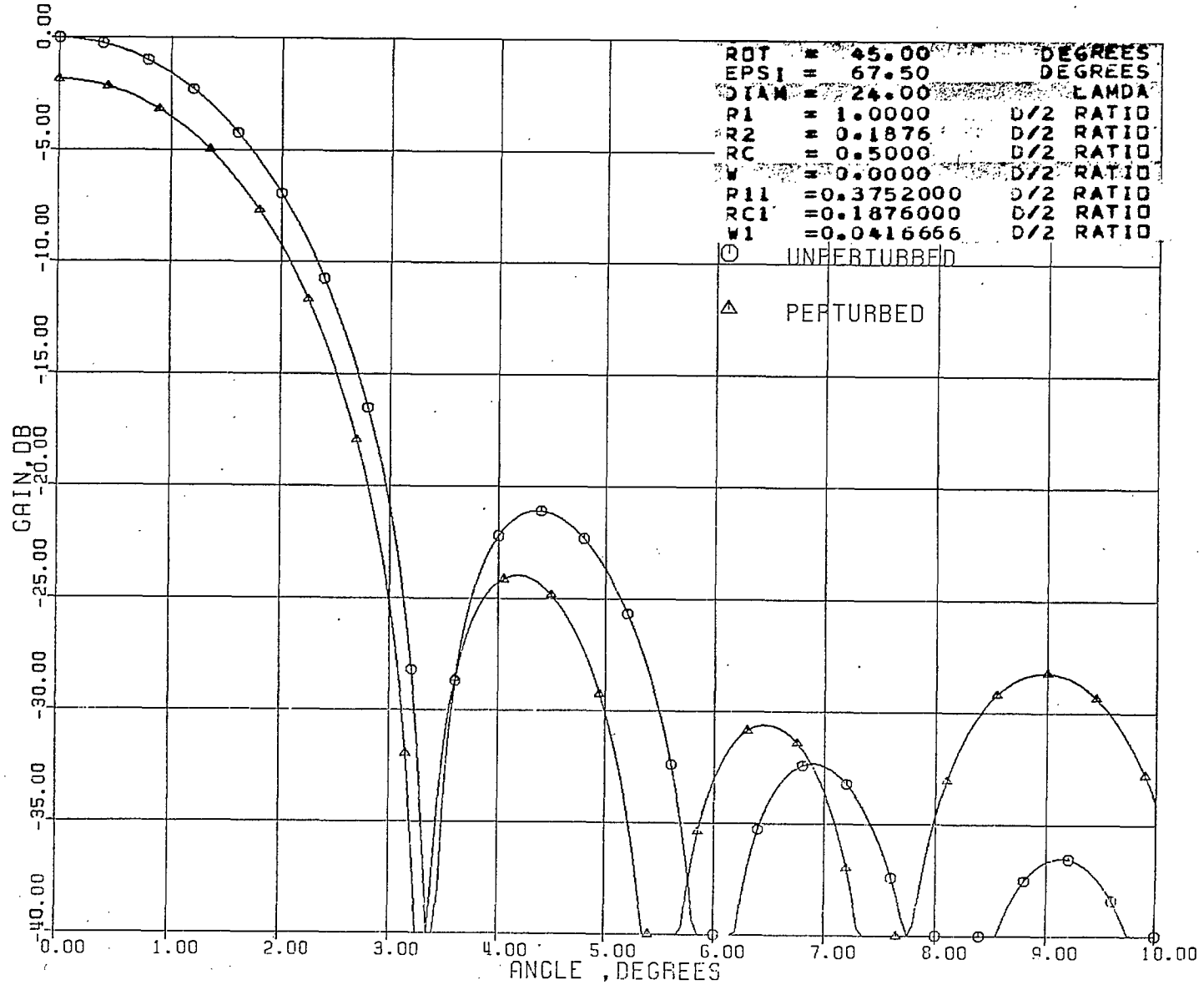

Figure 77. Radiation pattern with new quad struts (A40345)

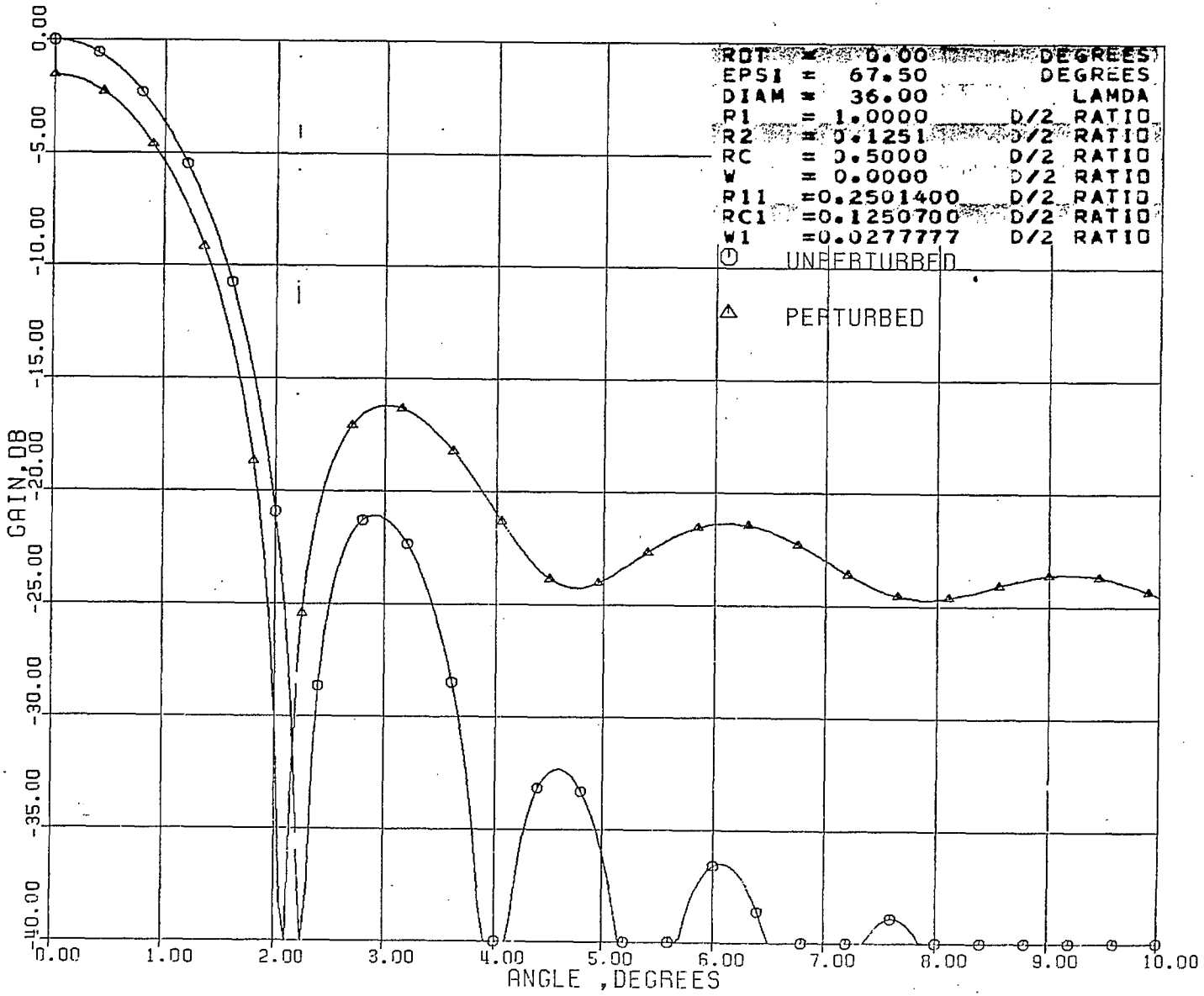

Figure 78. Radiation pattern with new quad struts (B40200)

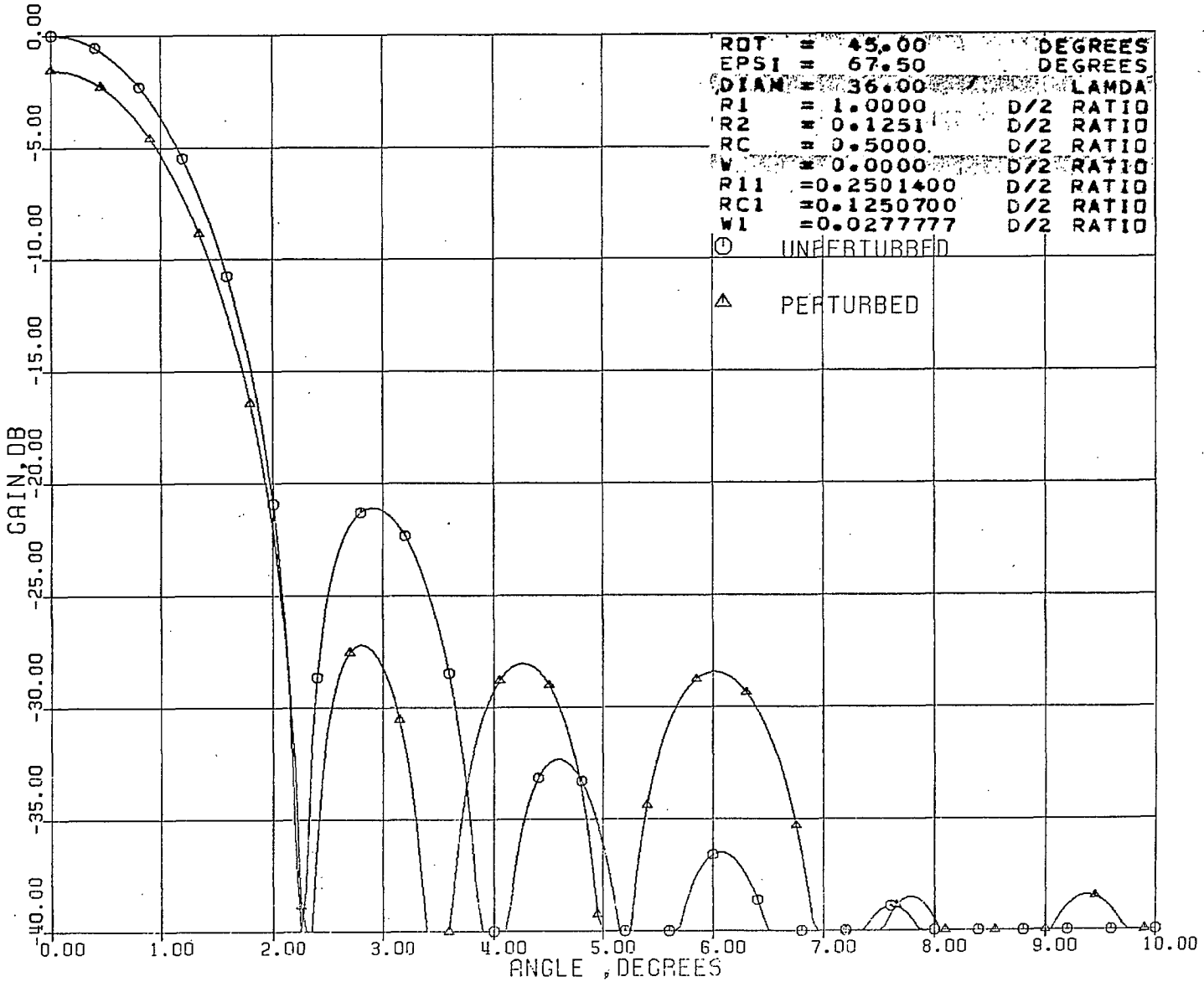

Figure 79. Radiation pattern with new quad struts (B40245)

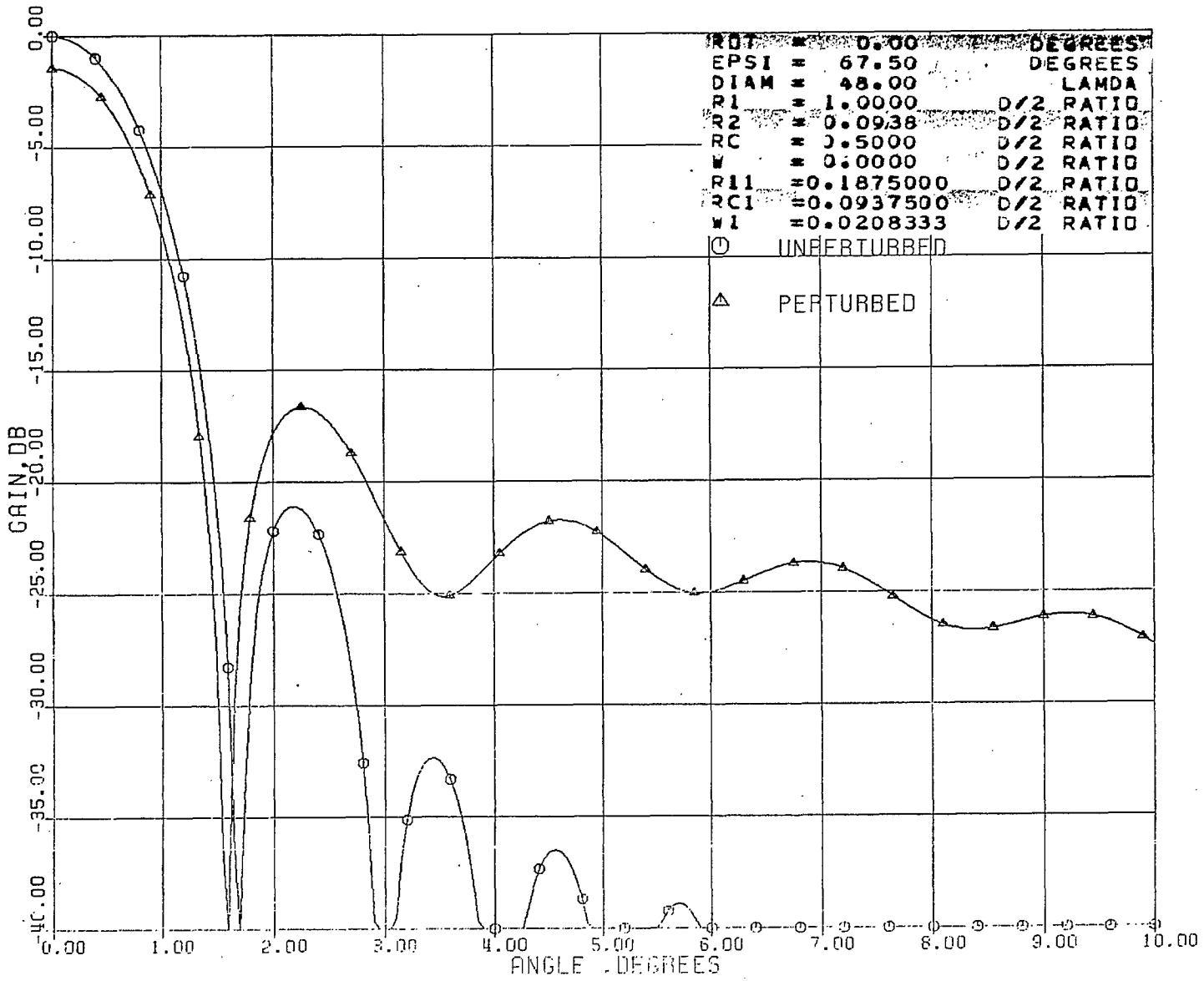

Figure 80. Radiation pattern with new quad struts (C40100)

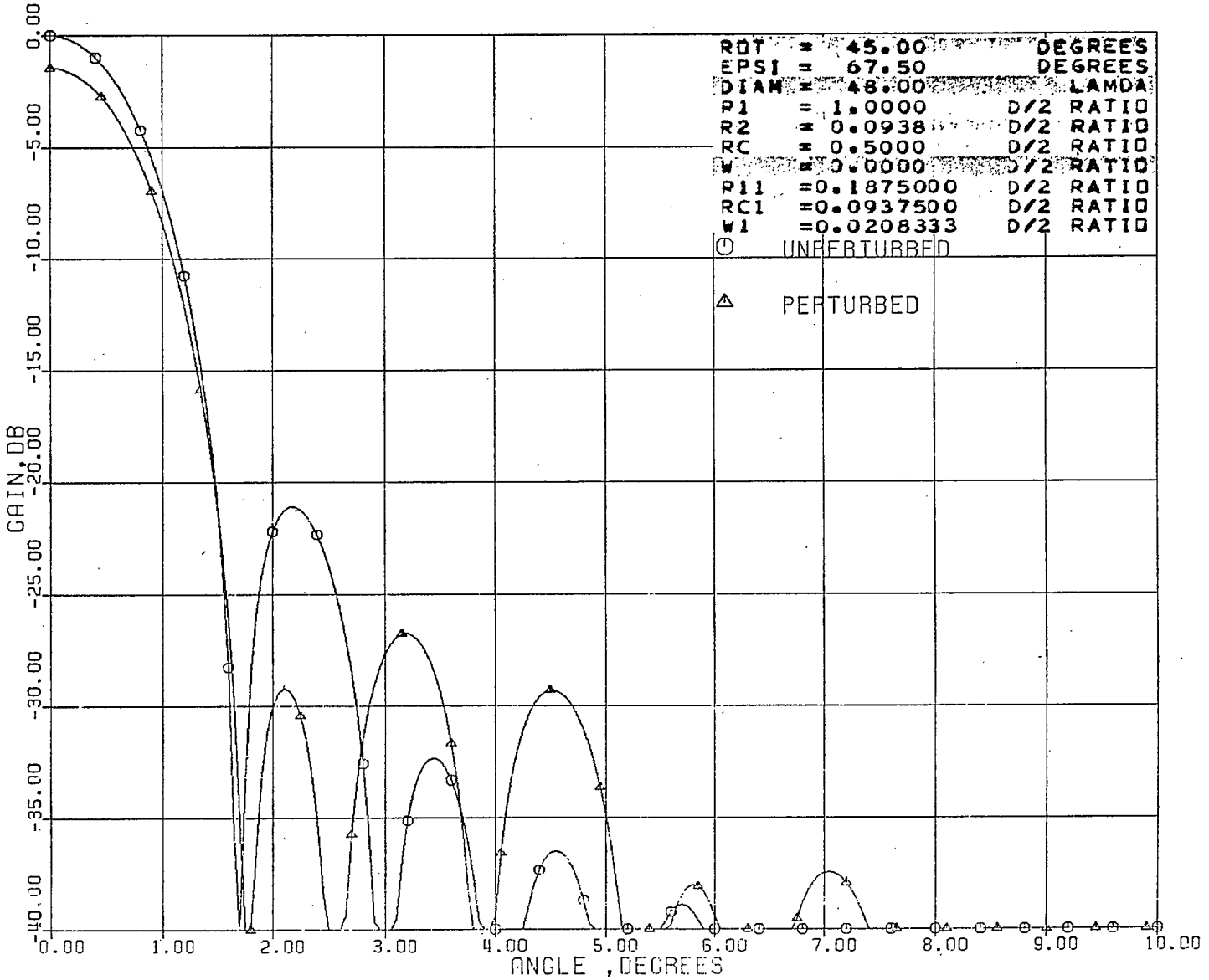

Figure 81. Radiation pattern with new quad struts (C40145)

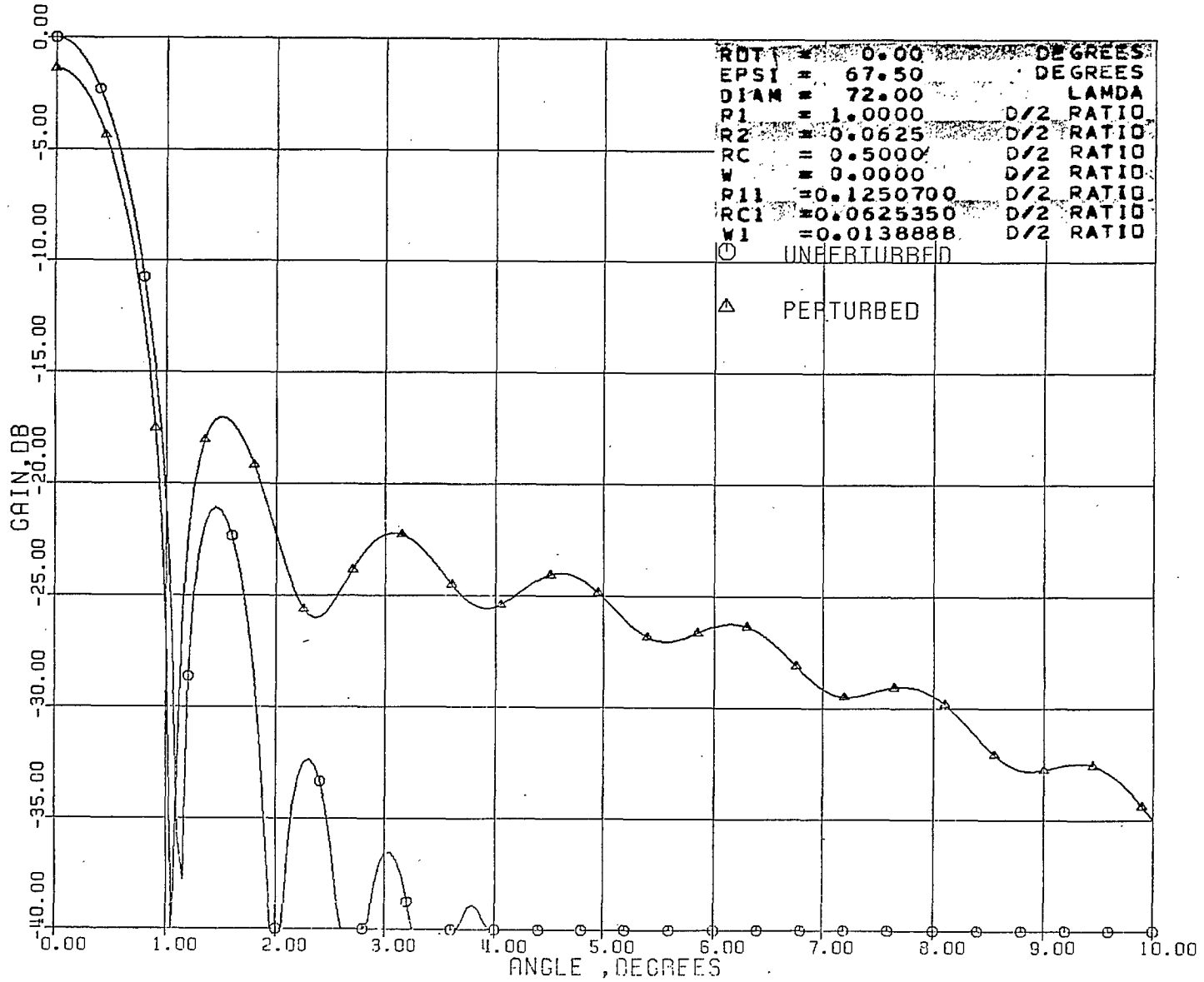

Figure 82. Radiation pattern with new quad struts (D40100)

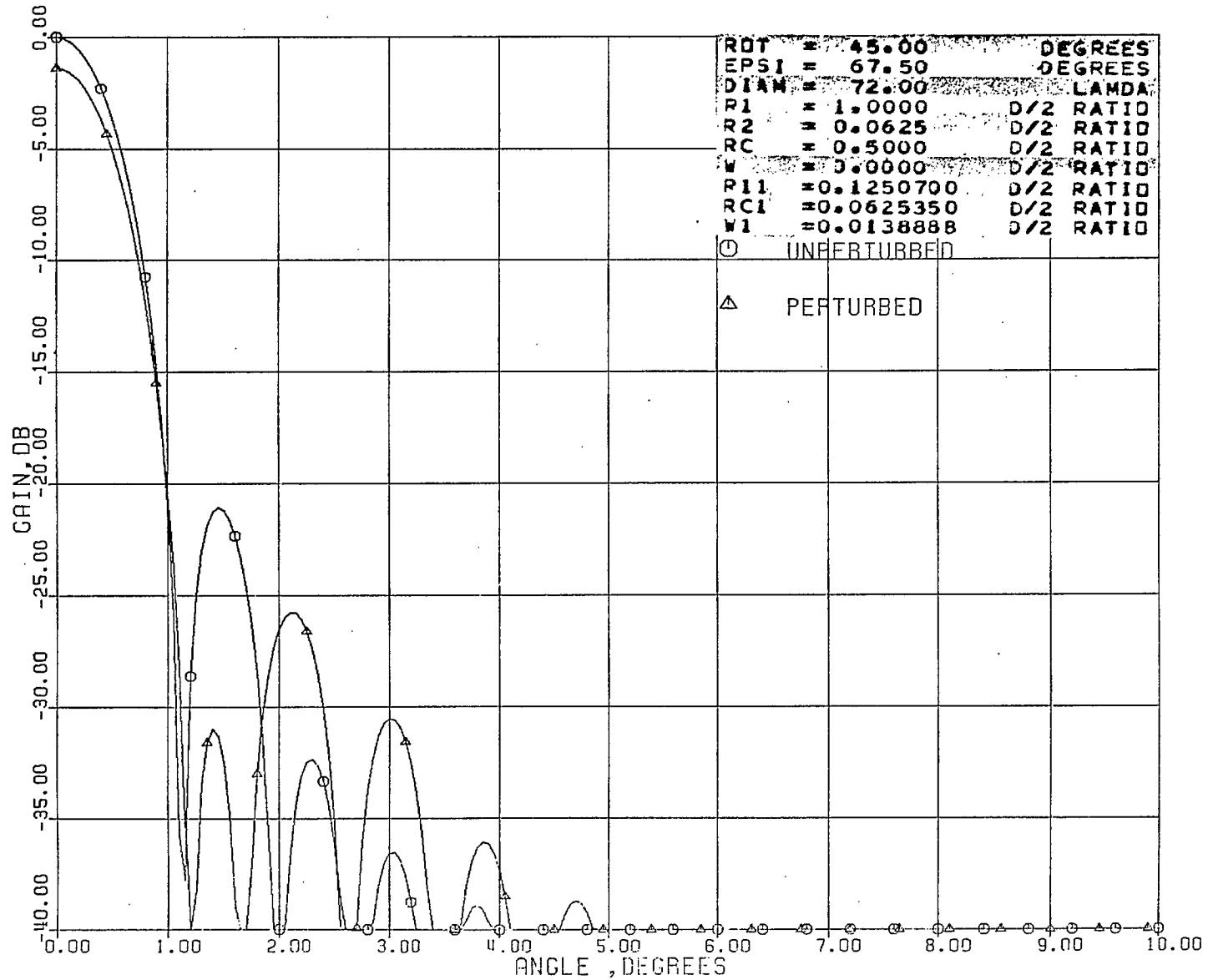

Figure 83. Radiation pattern with new quad struts (D40145)

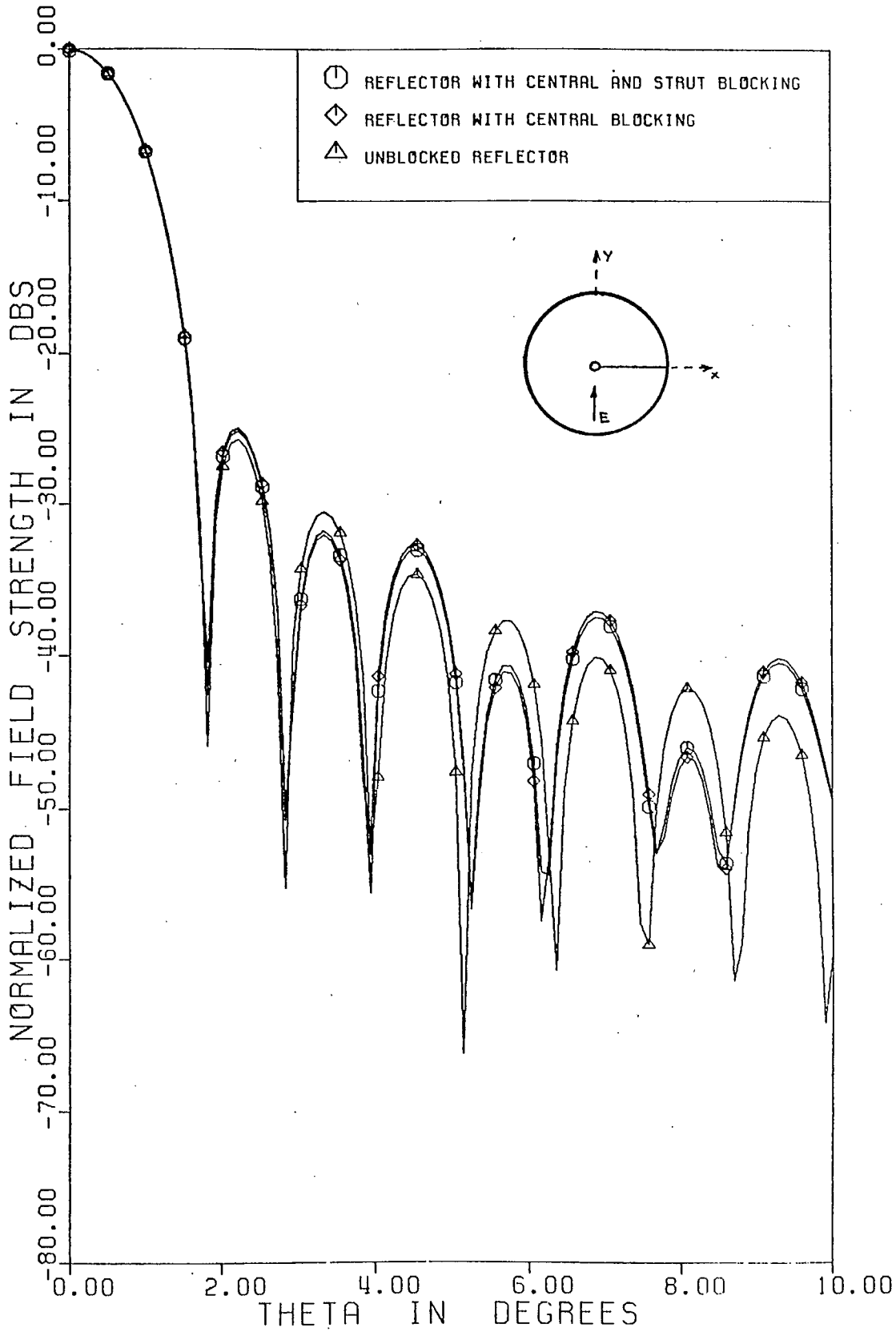

Figure 84. Single strut copolar patterns with cosθ illumination, $\phi = 0^{o}$ plane, w = 0.25λ

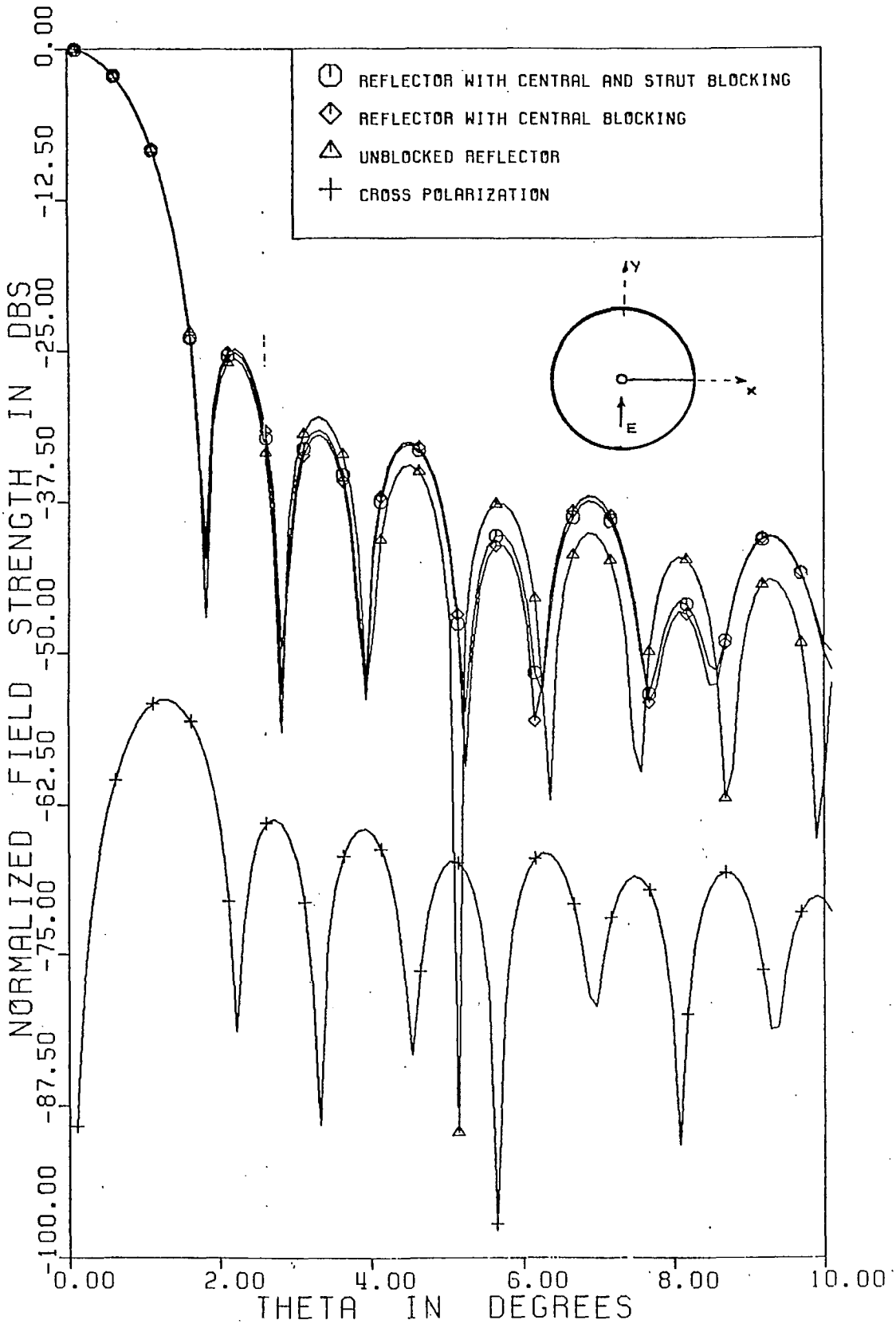

Figure 85. Single strut copolar and cross-polar patterns with cosθ illumination, ϕ = 45° plane, w = 0.25λ

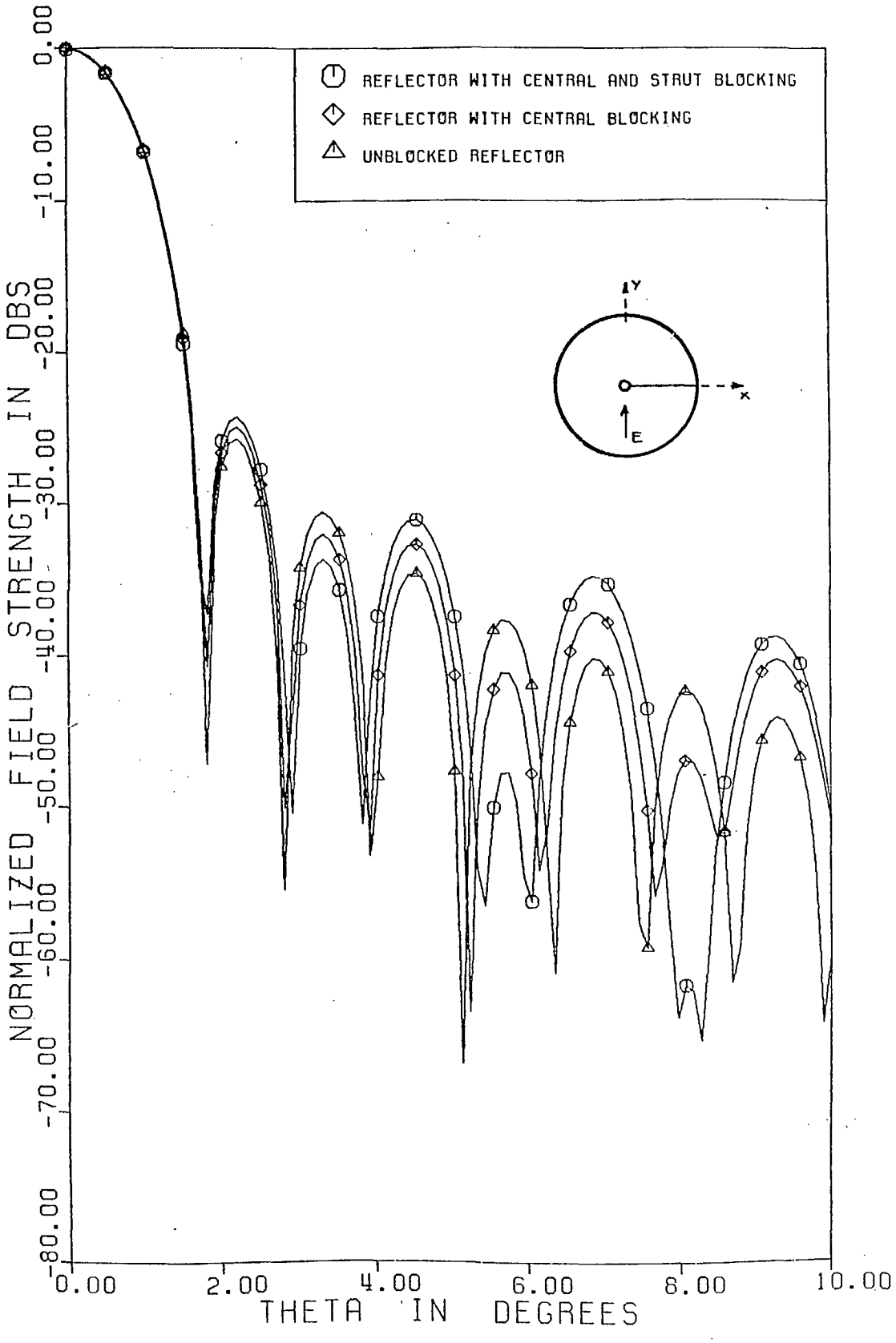

Figure 86. Single strut copolar patterns with cosθ illumination, $\phi = 90^{o}$ plane, $w = 0.25\lambda$

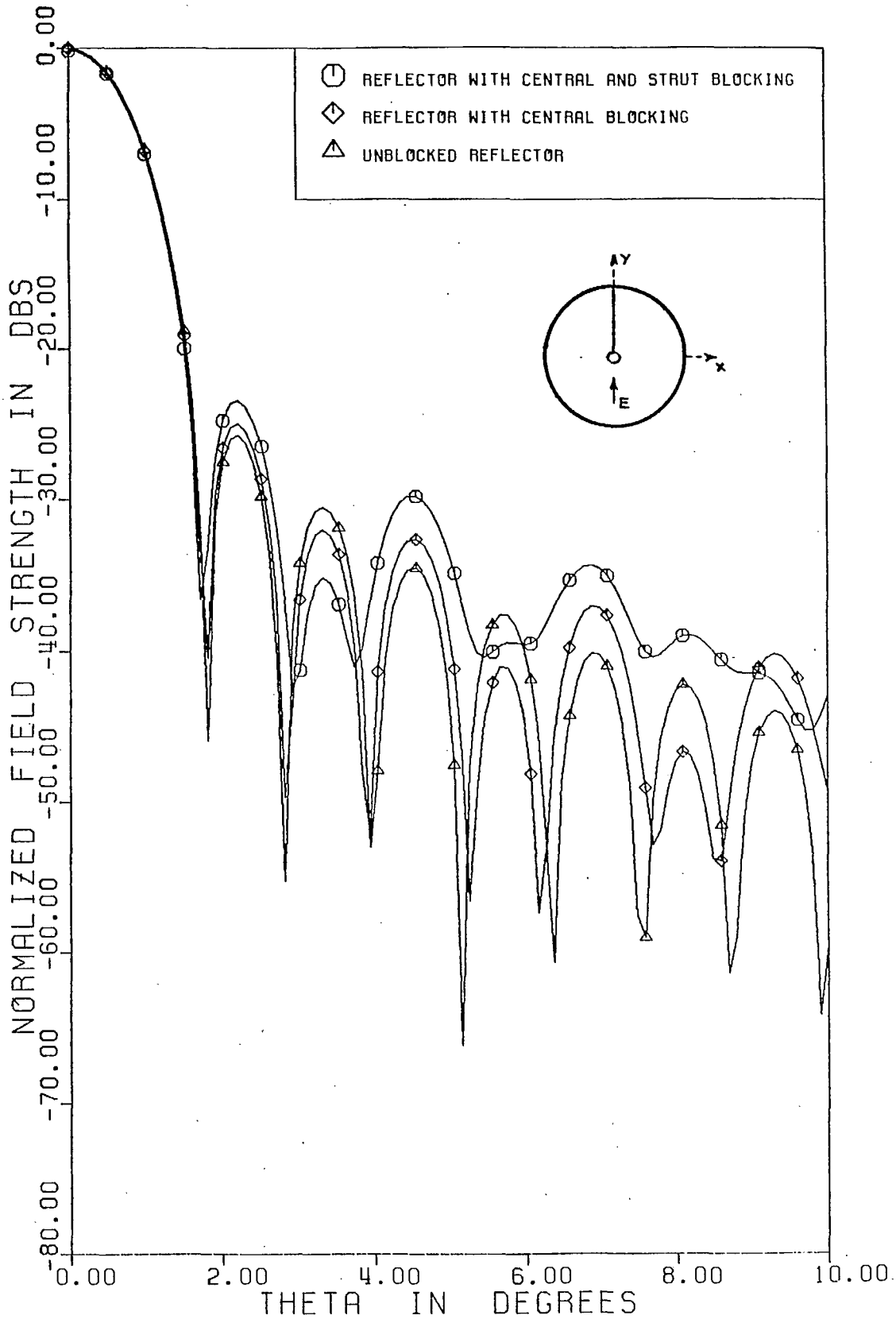

Figure 87. Single strut copolar patterns with cosθ illumination, $\phi = 0^{o}$ plane, $w = 0.25\lambda$

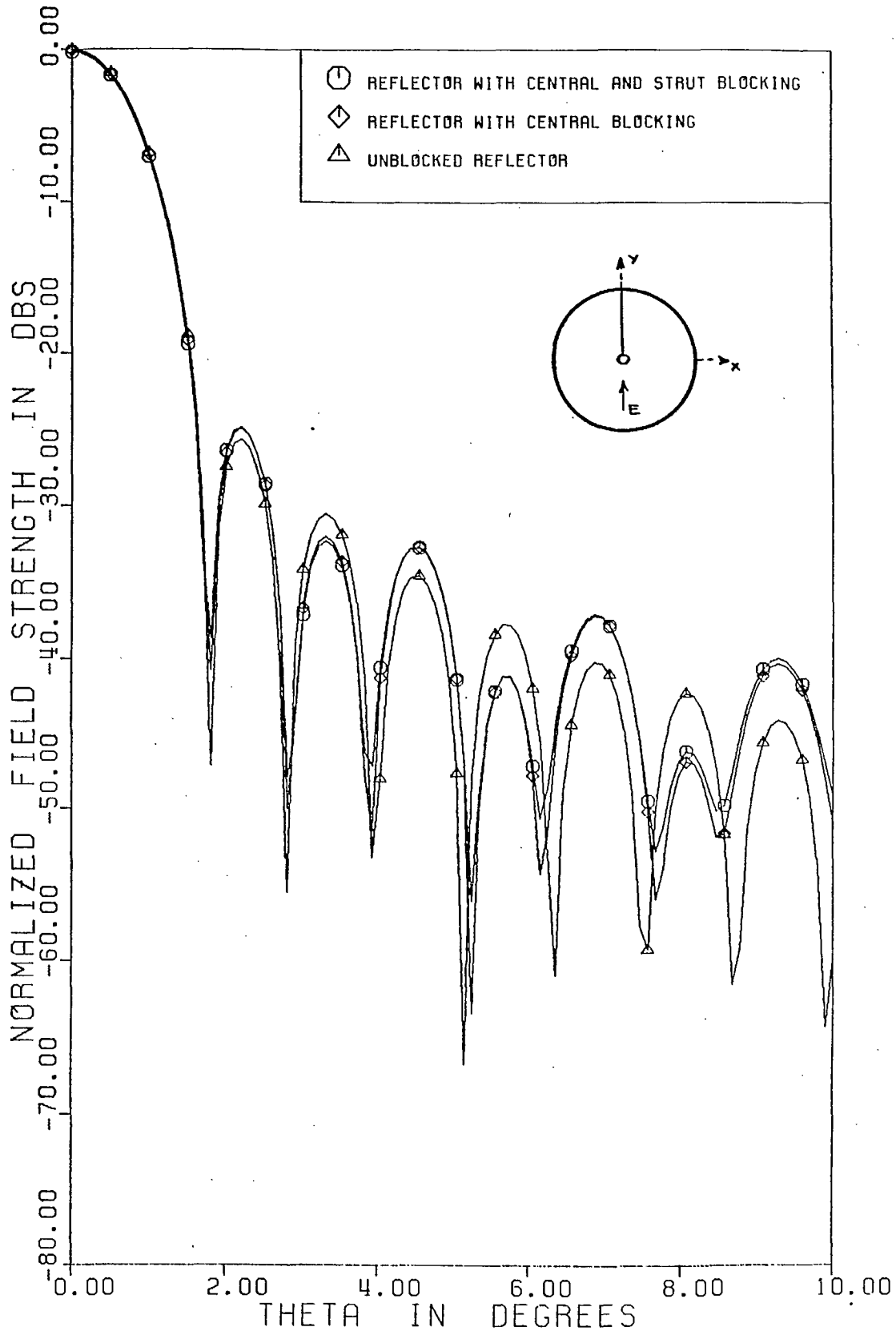

Figure 88. Single strut copolar patterns with cose illumination, $\phi = 90^{o}$ plane, $w = 0.25\lambda$

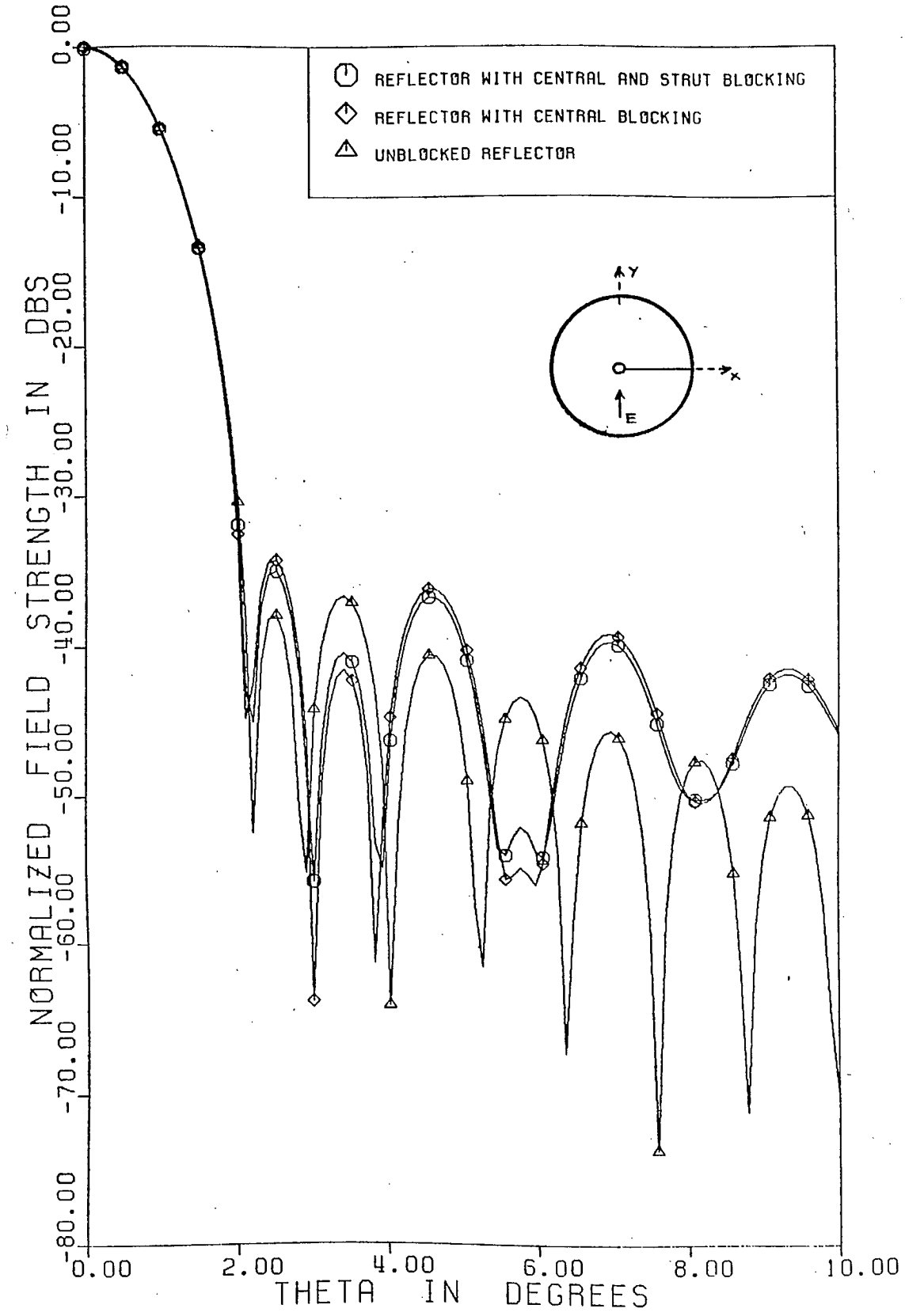

Figure 89. Single strut copolar patterns with $\cos^2\theta$ illumination, $\phi = 0^o$ plane, W = 0.25λ

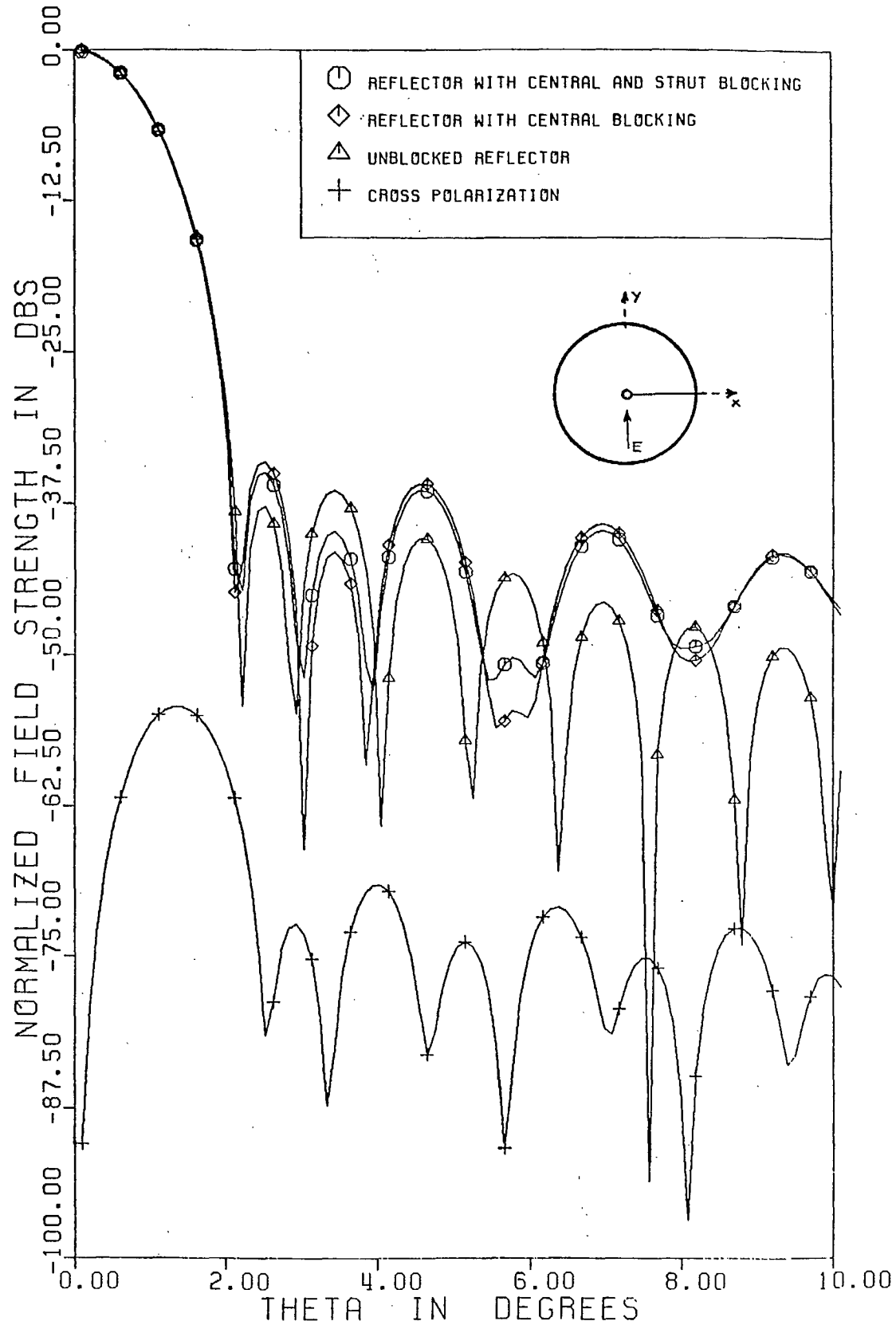

Figure 90. Single strut copolar and cross-polar patterns with $\cos^2\theta$ illumination, ϕ = 45° plane, w = 0.25λ

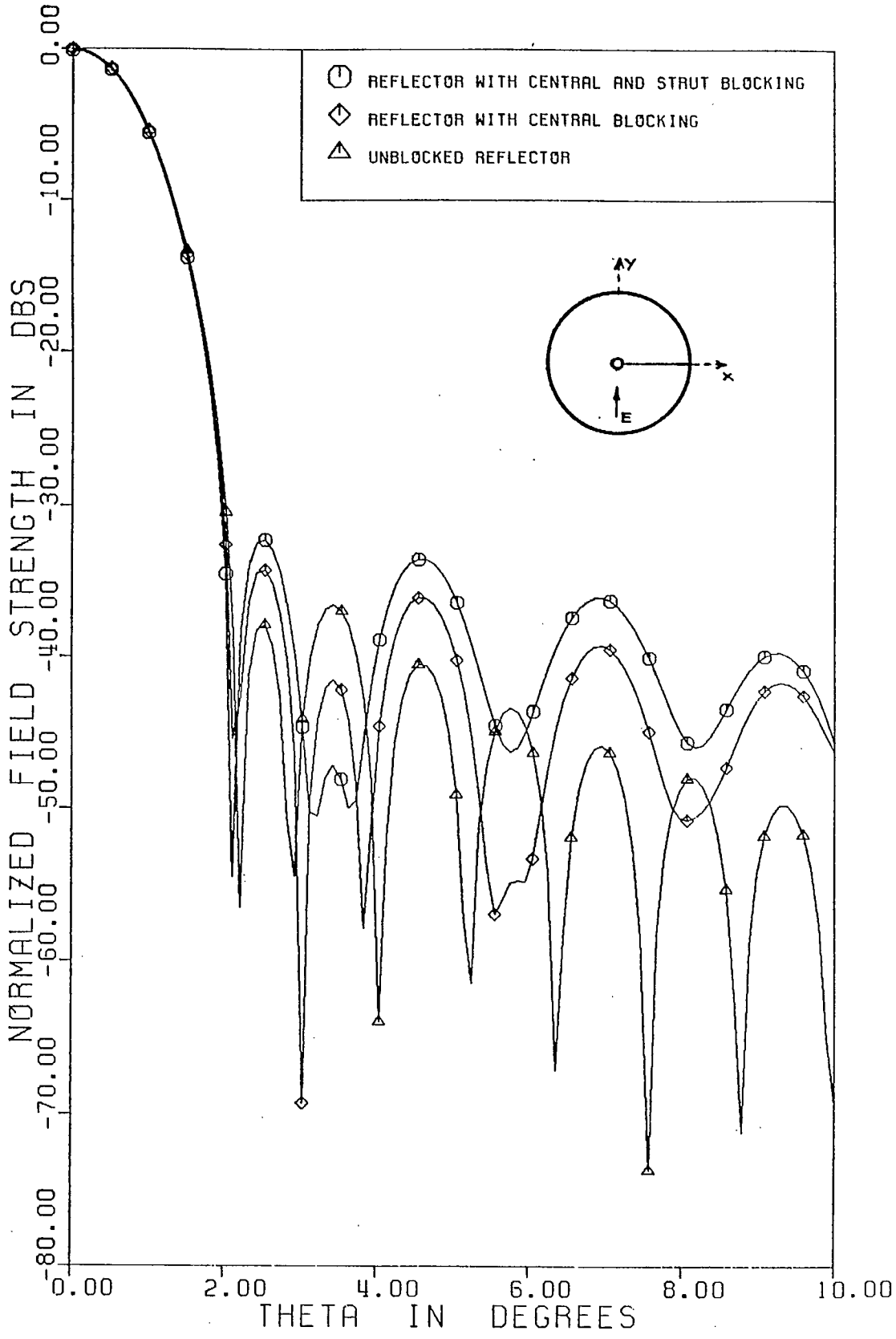

Figure 91. Single strut copolar patterns with $\cos^2\theta$ illumination, $\phi = 90^\circ$ plane, $w = 0.25\lambda$

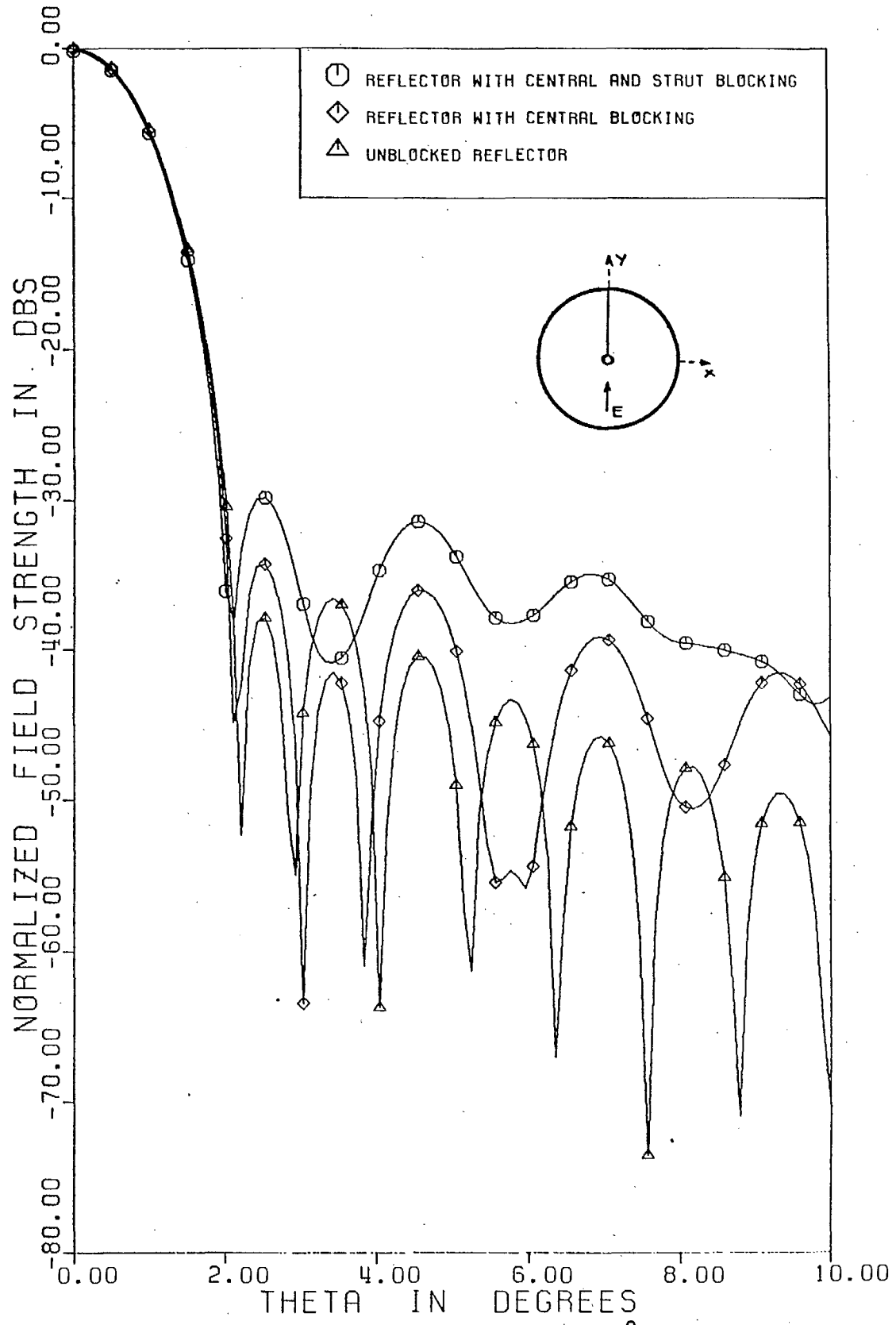

Figure 92. Single strut copolar patterns with $\cos^2\theta$ illumination, $\phi = 0^o$ plane, $w = 0.25\lambda$

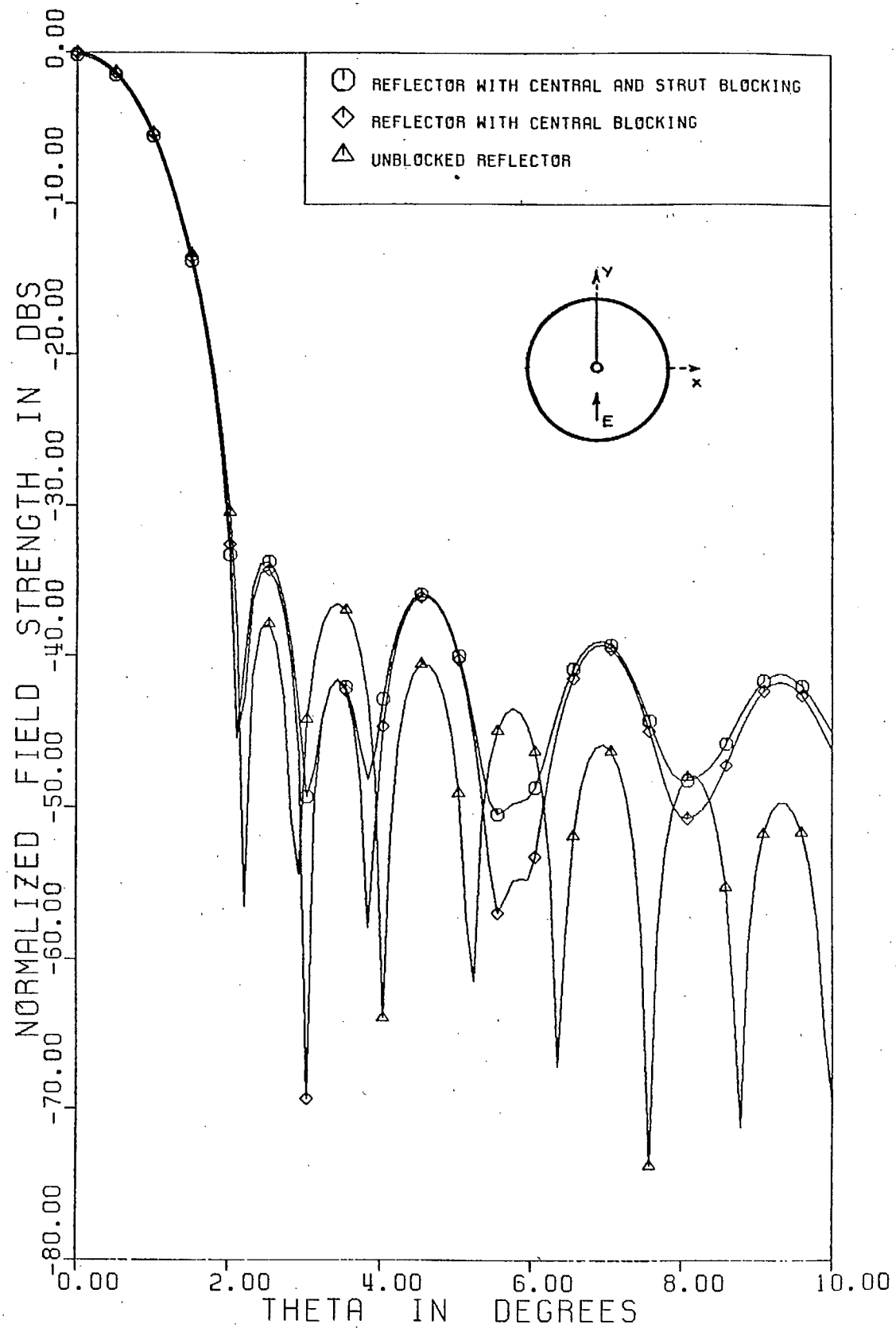

Figure 93. Single strut copolar patterns with $\cos^2\theta$ illumination, $\phi = 90^\circ$ plane, $w = 0.25\lambda$

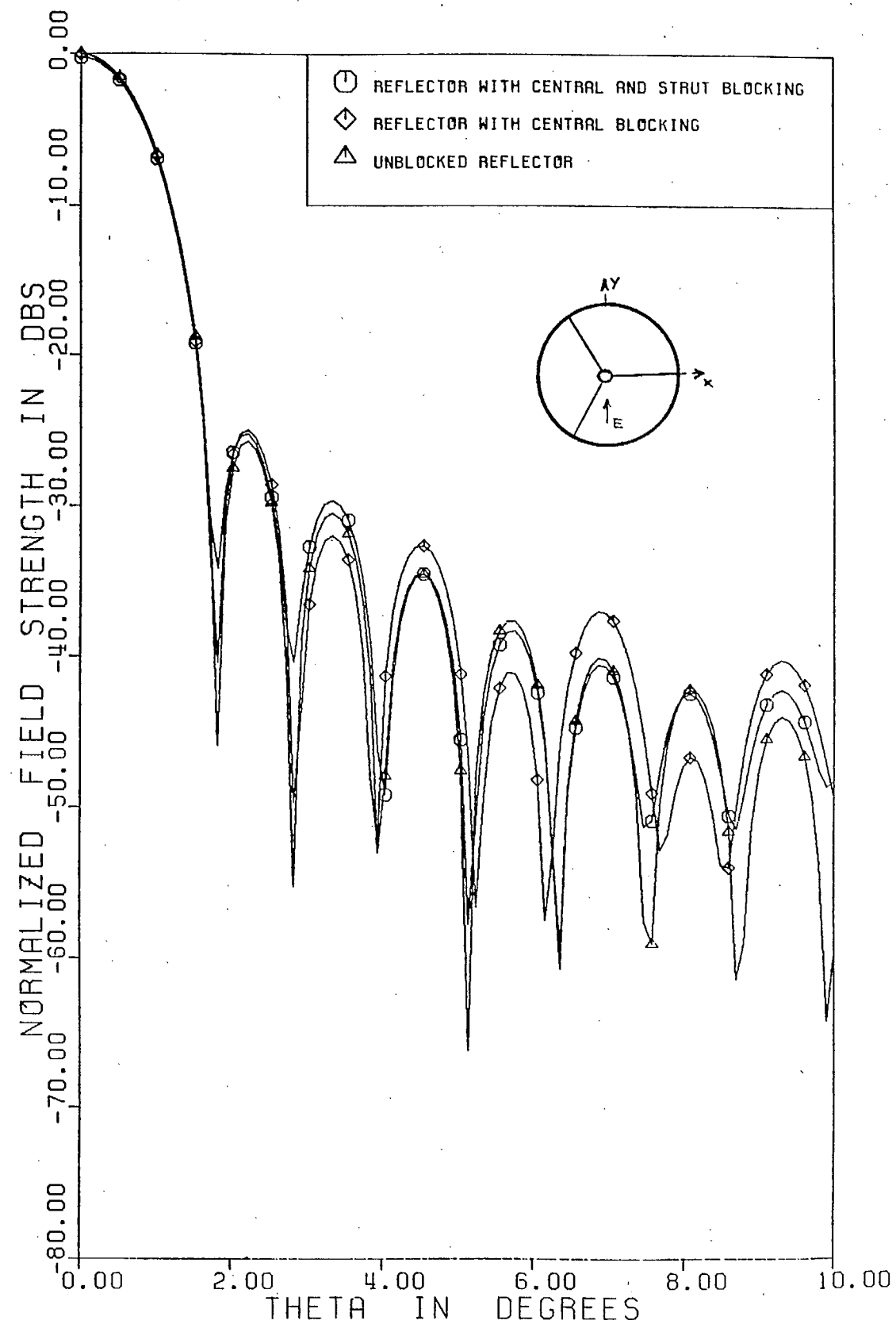

Figure 94. Tripod copolar patterns with cosθ illumination, $\phi = 0^{o}$ plane, $w = 0.25\lambda$

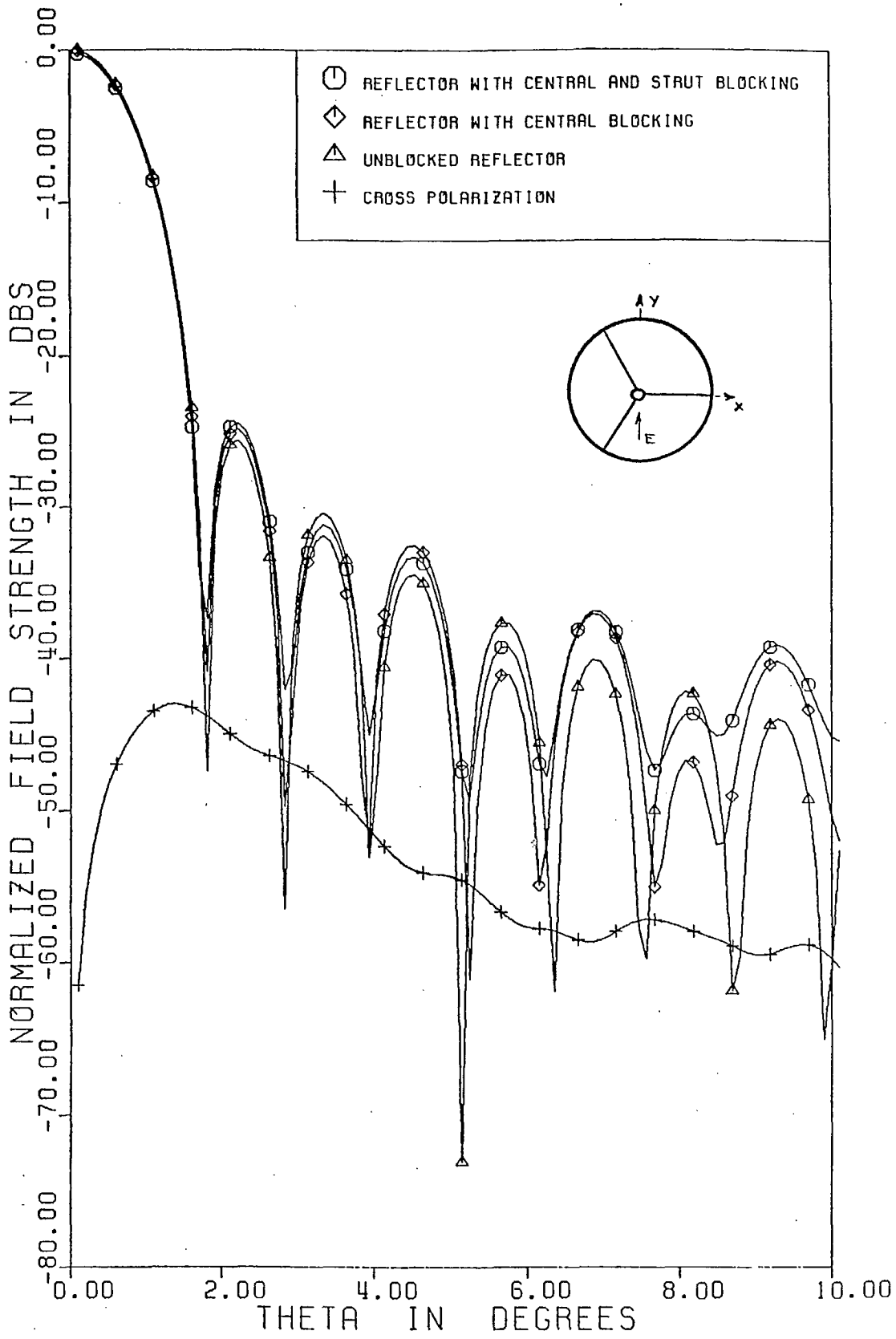

Figure 95. Tripod copolar and cross-polar patterns with $\cos_\theta$ illumination, $\phi = 60^o$ plane, $w = 0.25\lambda$

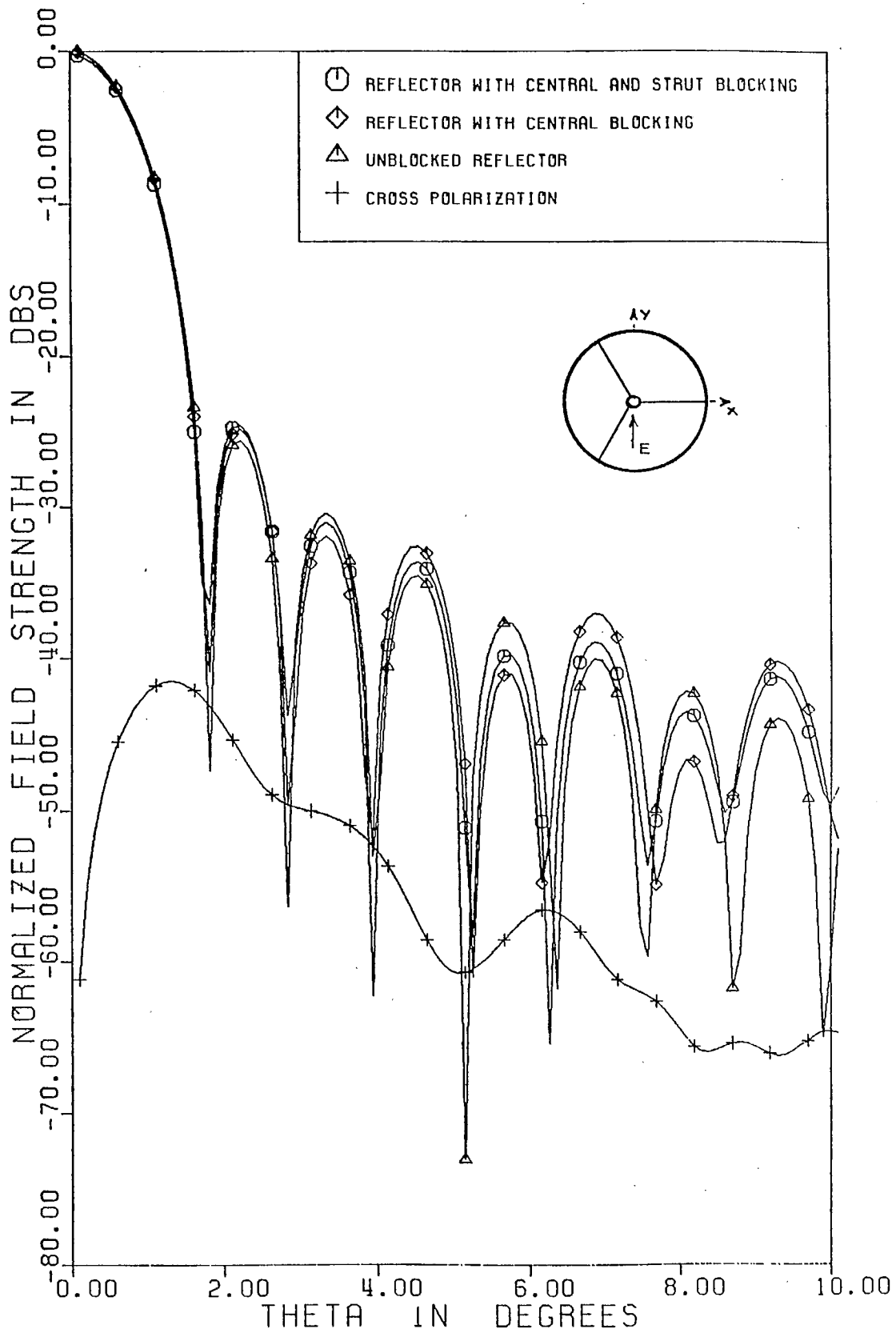

Figure 96. Tripod copolar and cross-polar patterns with $\cos\theta$ illumination, $\phi = 120^{o}$ plane, $w = 0.25\lambda$

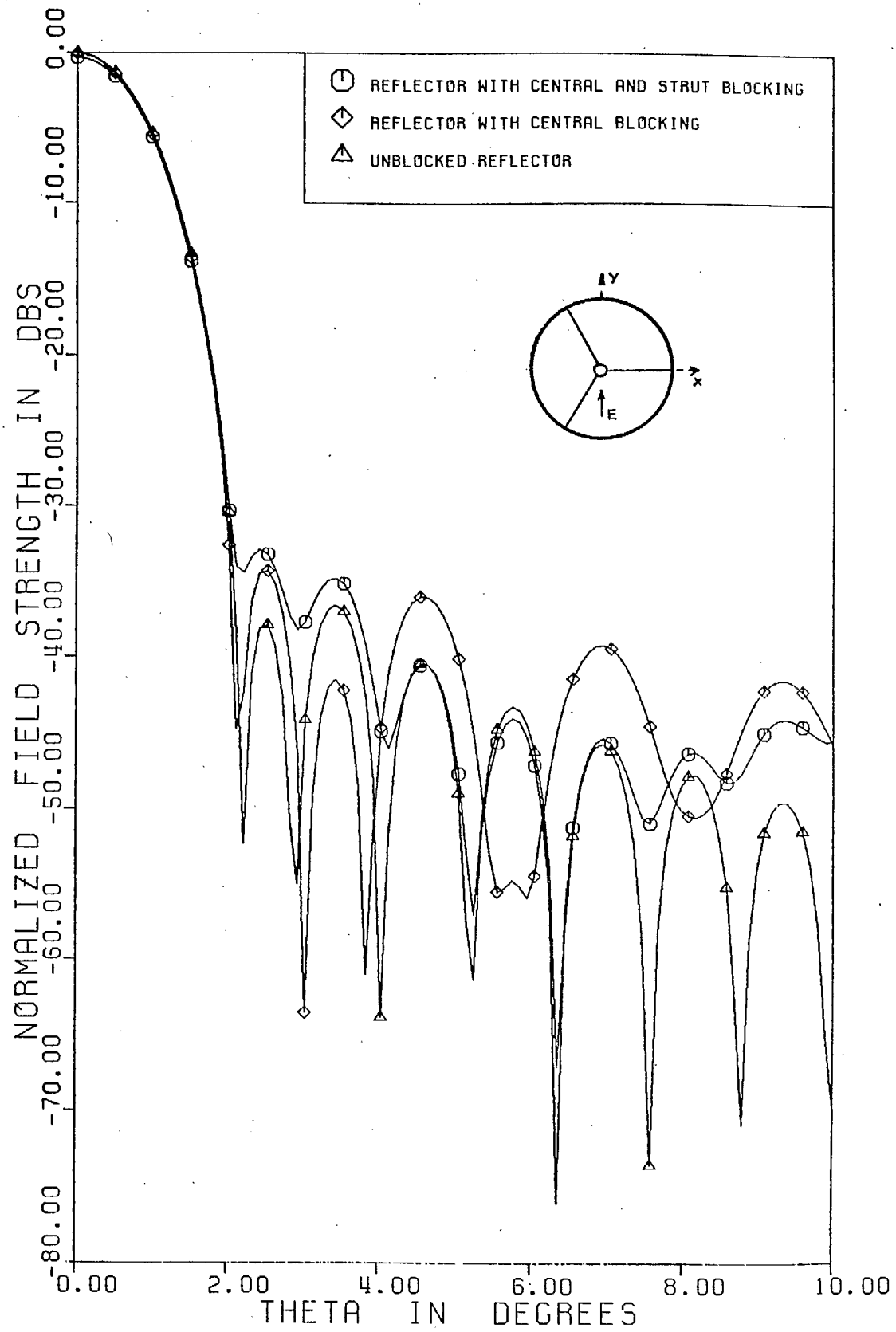

Figure 97. Tripod copolar and cross-polar patterns with $\cos^2\theta$ illumination, $\phi = 0^o$ plane, $w = 0.25\lambda$

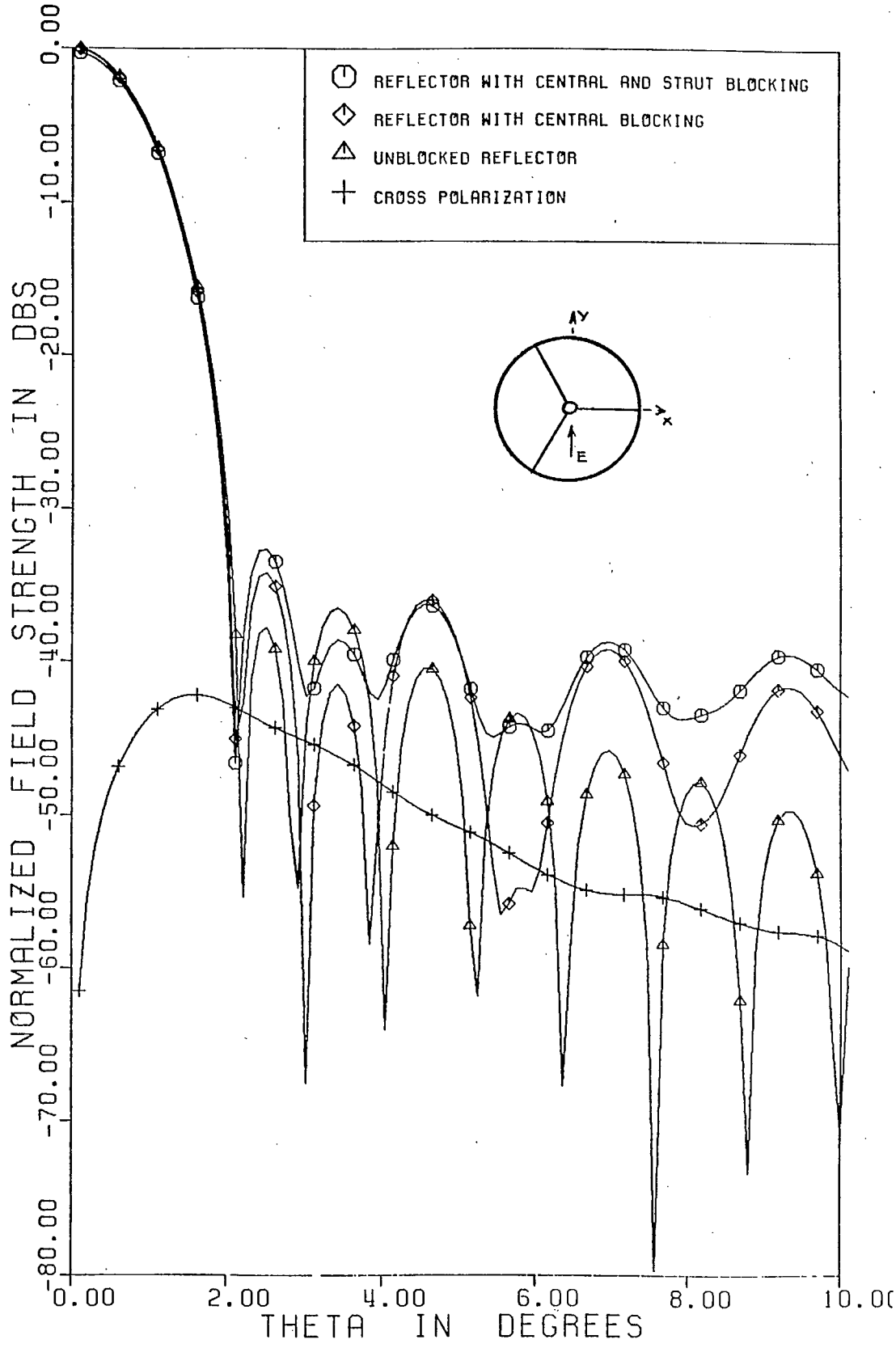

Figure 98. Tripod copolar and cross-polar patterns with $\cos^2\theta$ illumination, $\phi = 60^o$ plane, $w = 0.25\lambda$

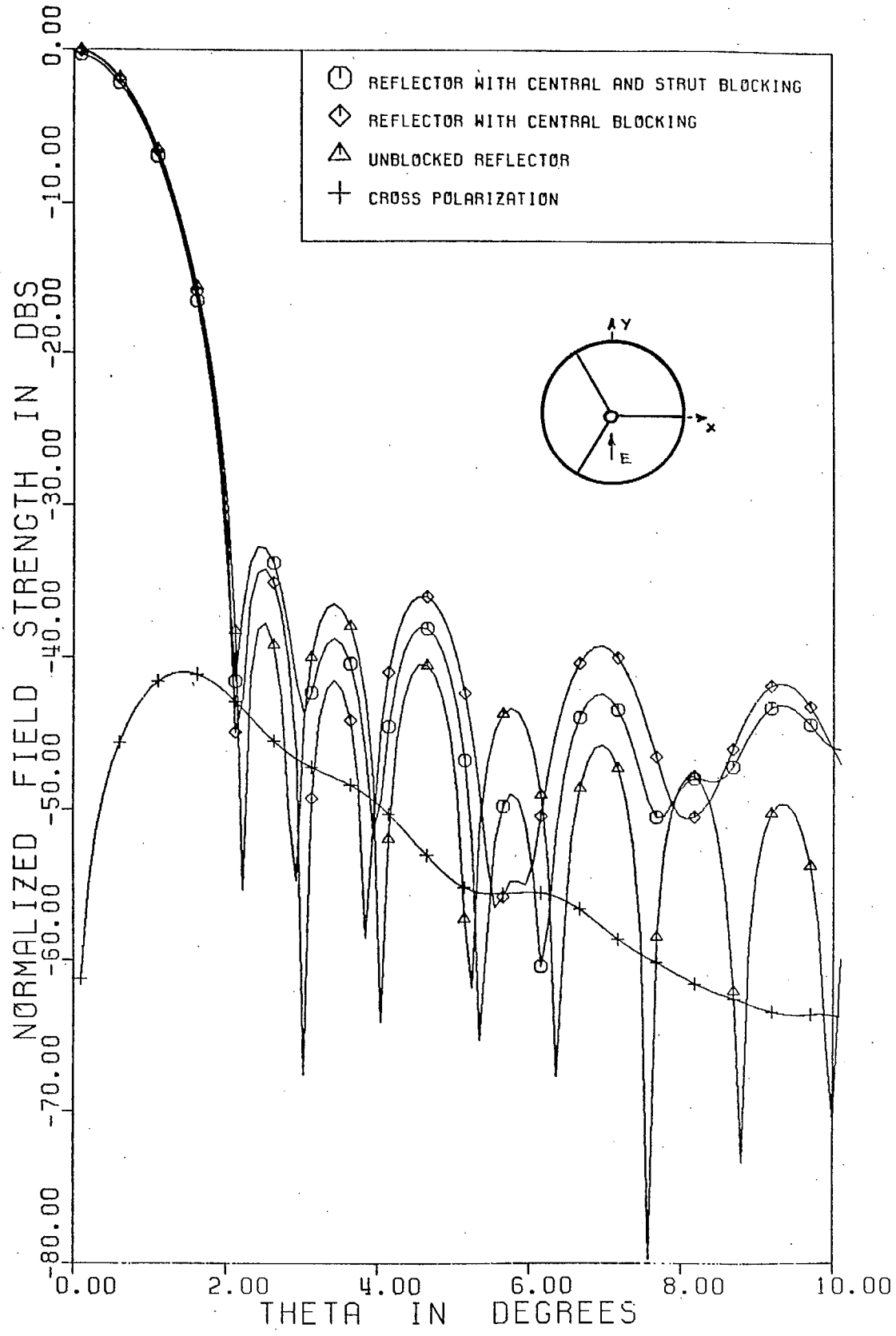

Figure 99. Tripod copolar and cross-polar patterns with $\cos^2\theta$ illumination, $\phi = 120^{o}$ plane, $w = 0.25\lambda$

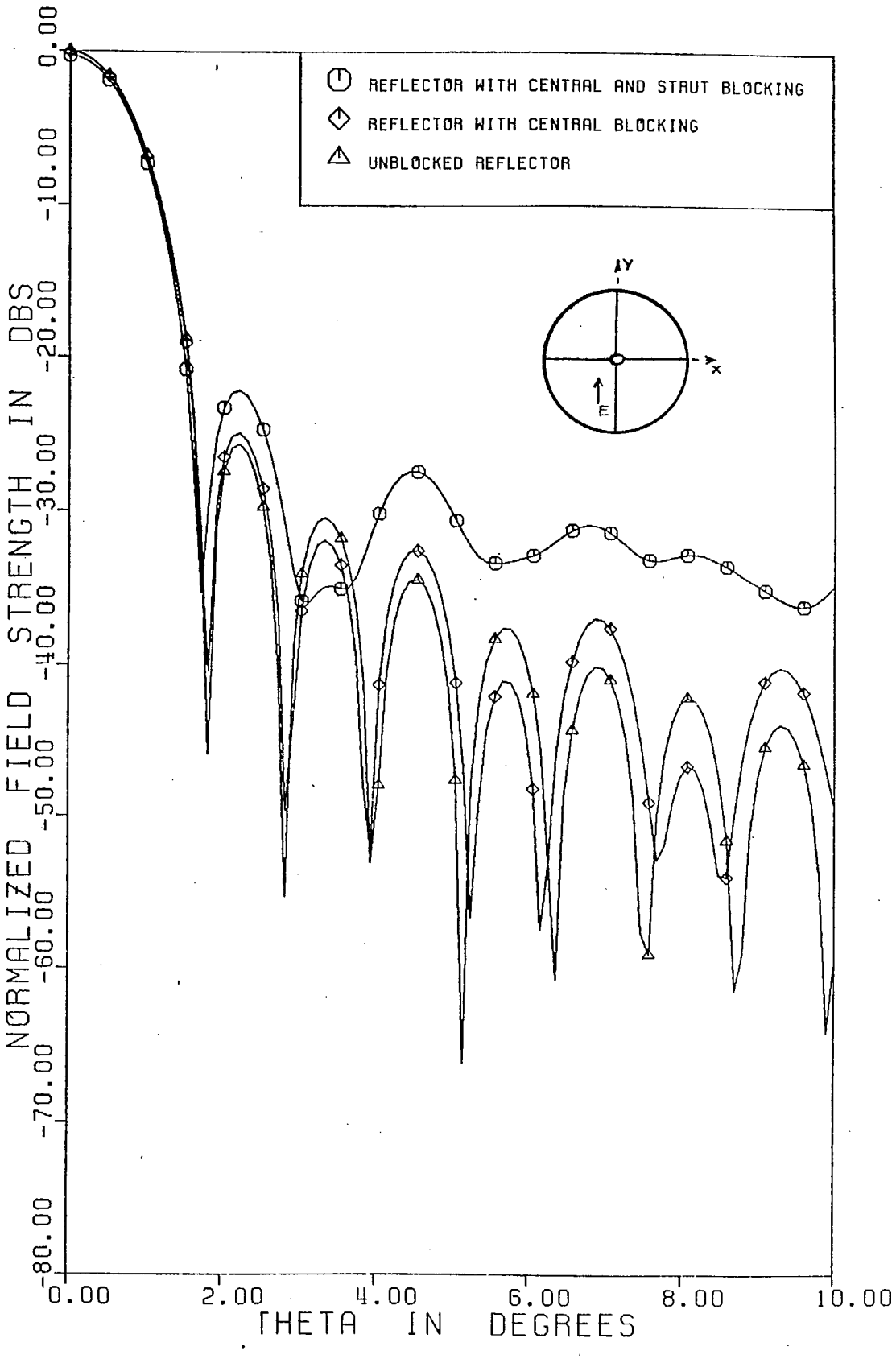

Figure 100. Quad copolar patterns with cosθ illumination, $\phi = 0^{o}$ plane, w = 0.25λ

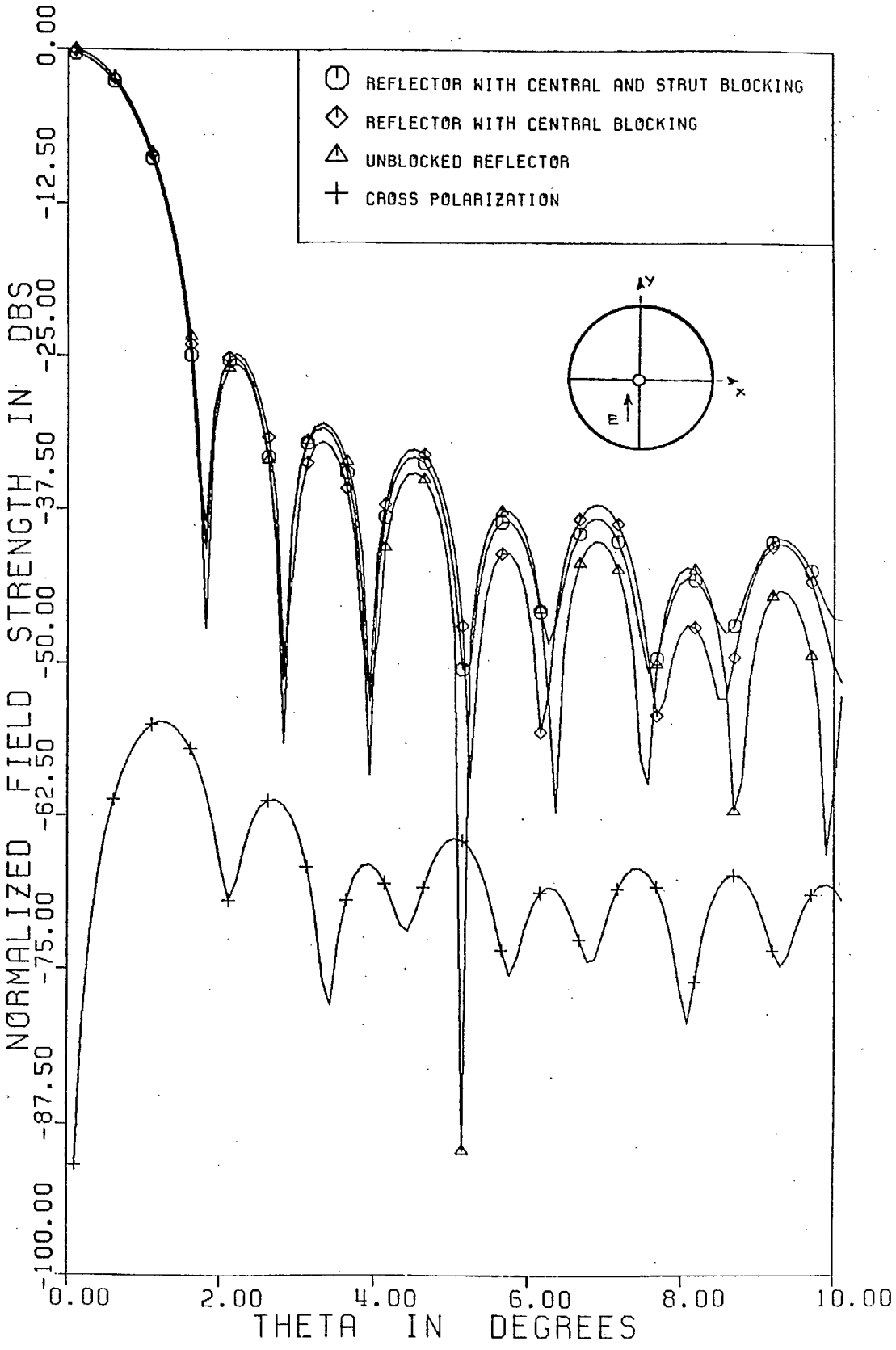

Figure 101. Quad copolar and cross-polar patterns with cosθ illumination, $\phi = 45^{o}$ plane, $w = 0.25\lambda$

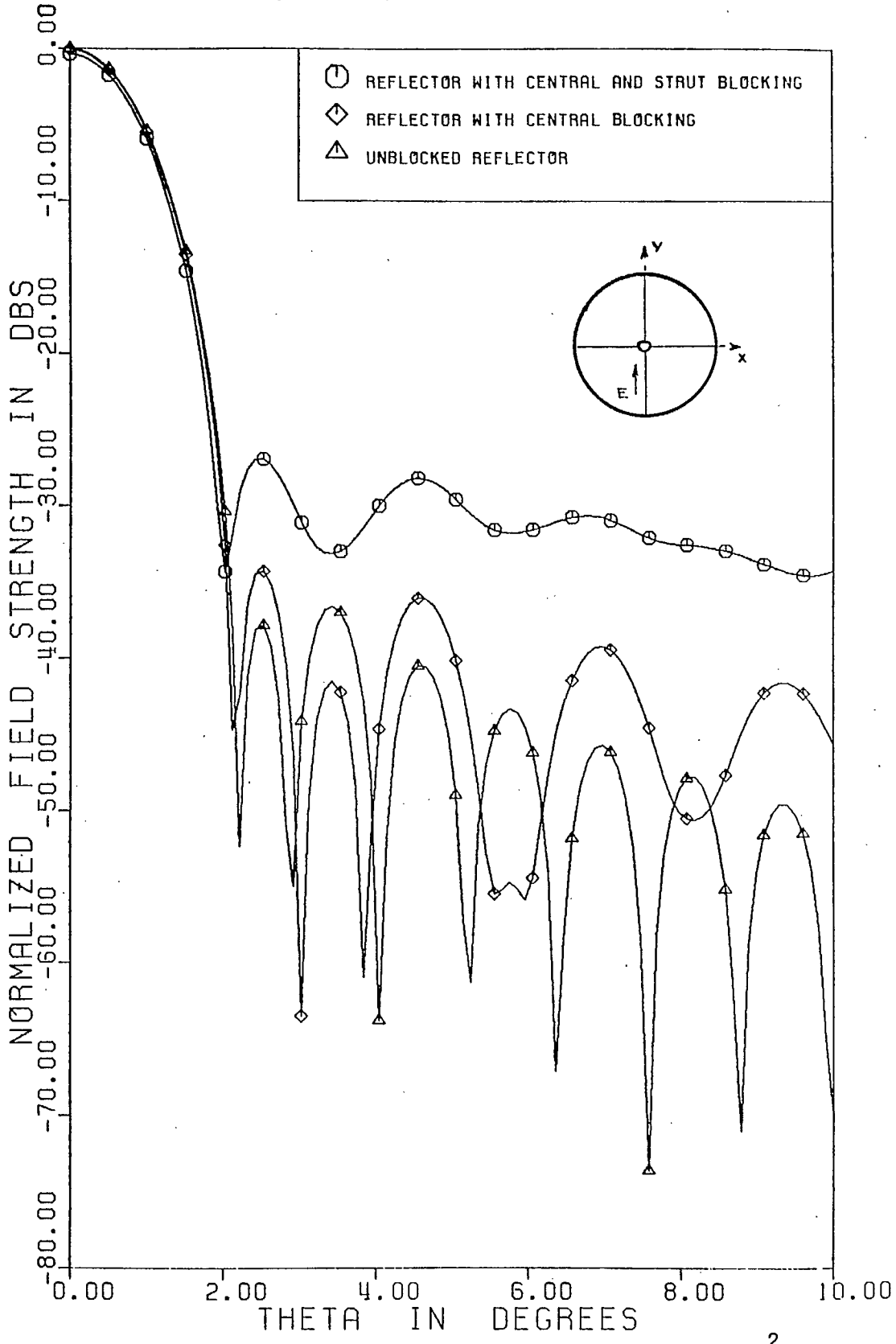

Figure 102. Quad copolar and cross-polar patterns with $\cos^2\theta$ illumination, $\phi = 0^o$ plane, $w = 0.25\lambda$

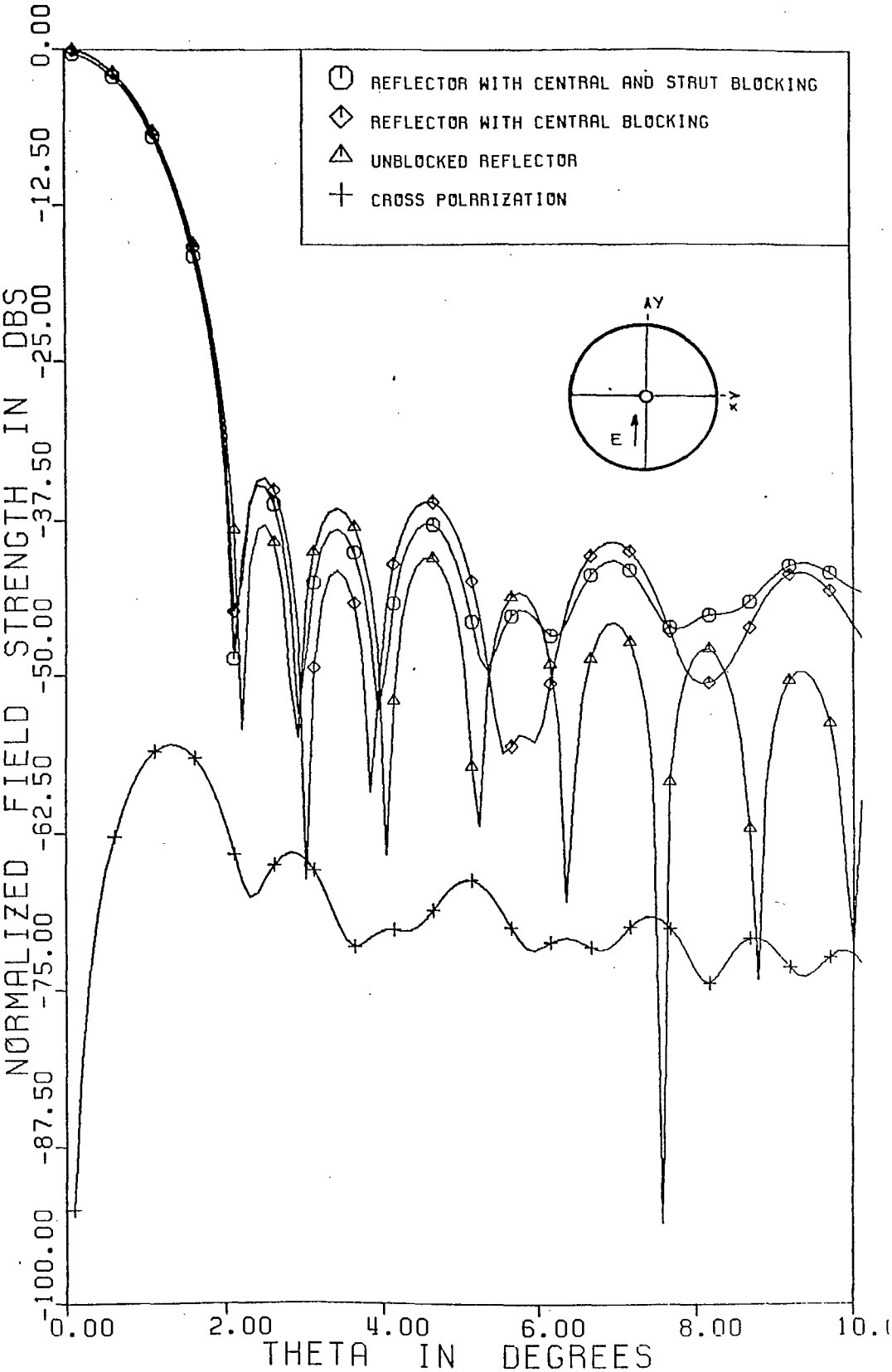

Figure 103. Quad copolar and cross-polar patterns with $\cos^2\theta$ illumination, $\phi = 45^{o}$ plane, $w = 0.25\lambda$

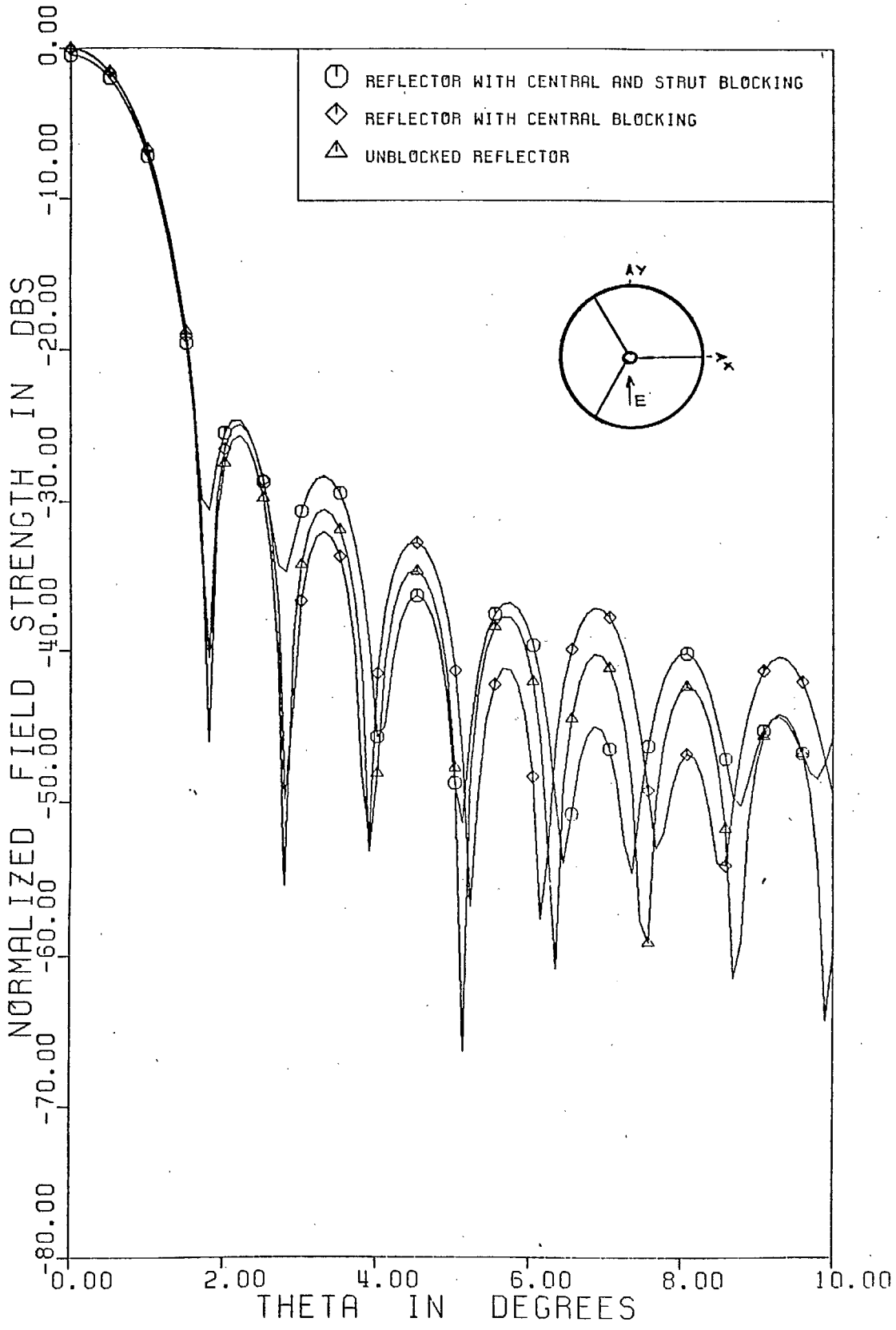

Figure 104. Tripod coloar patterns with cosθ illumination, $\phi = 0^{o}$ plane, $w = 0.5\lambda$

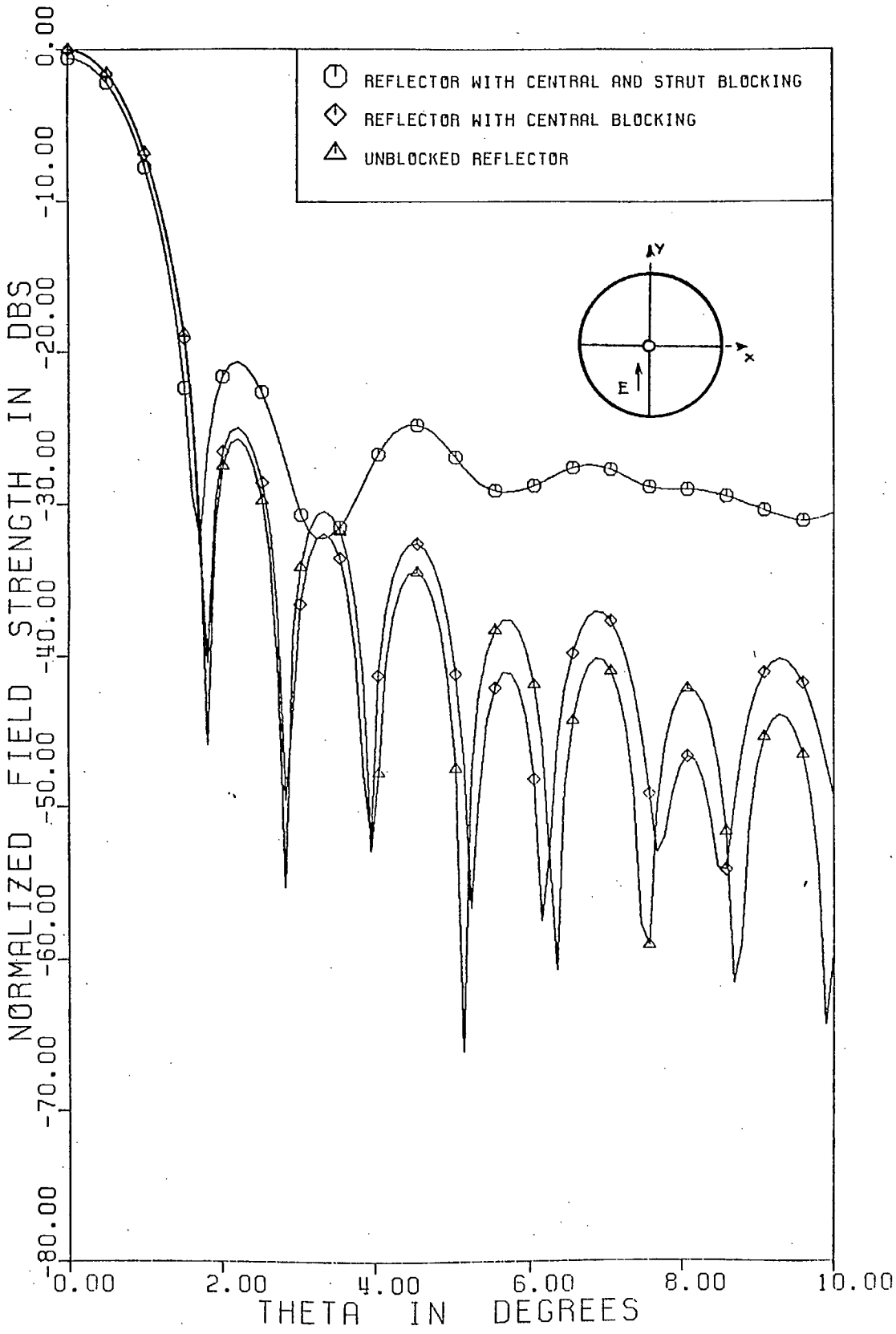

Figure 105. Quad copolar pattern with cosθ illumination, $\phi = 0^{o}$ plane, $w = 0.5\lambda$

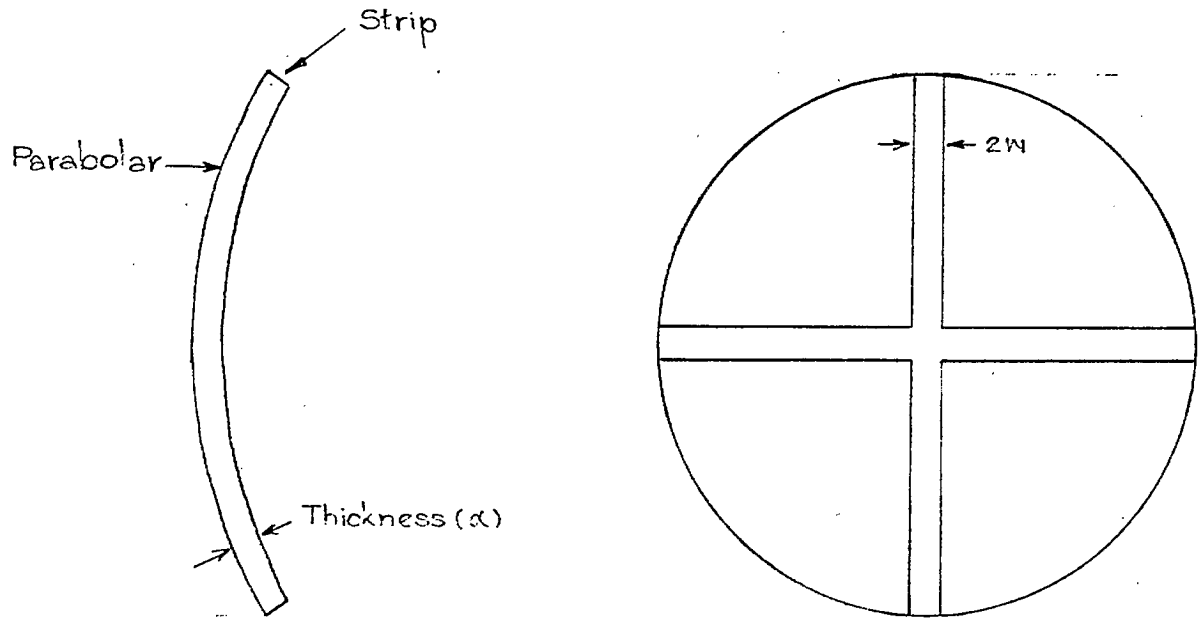

Figure 106. Geometry of the strip loaded reflector for a quad-strut configuration

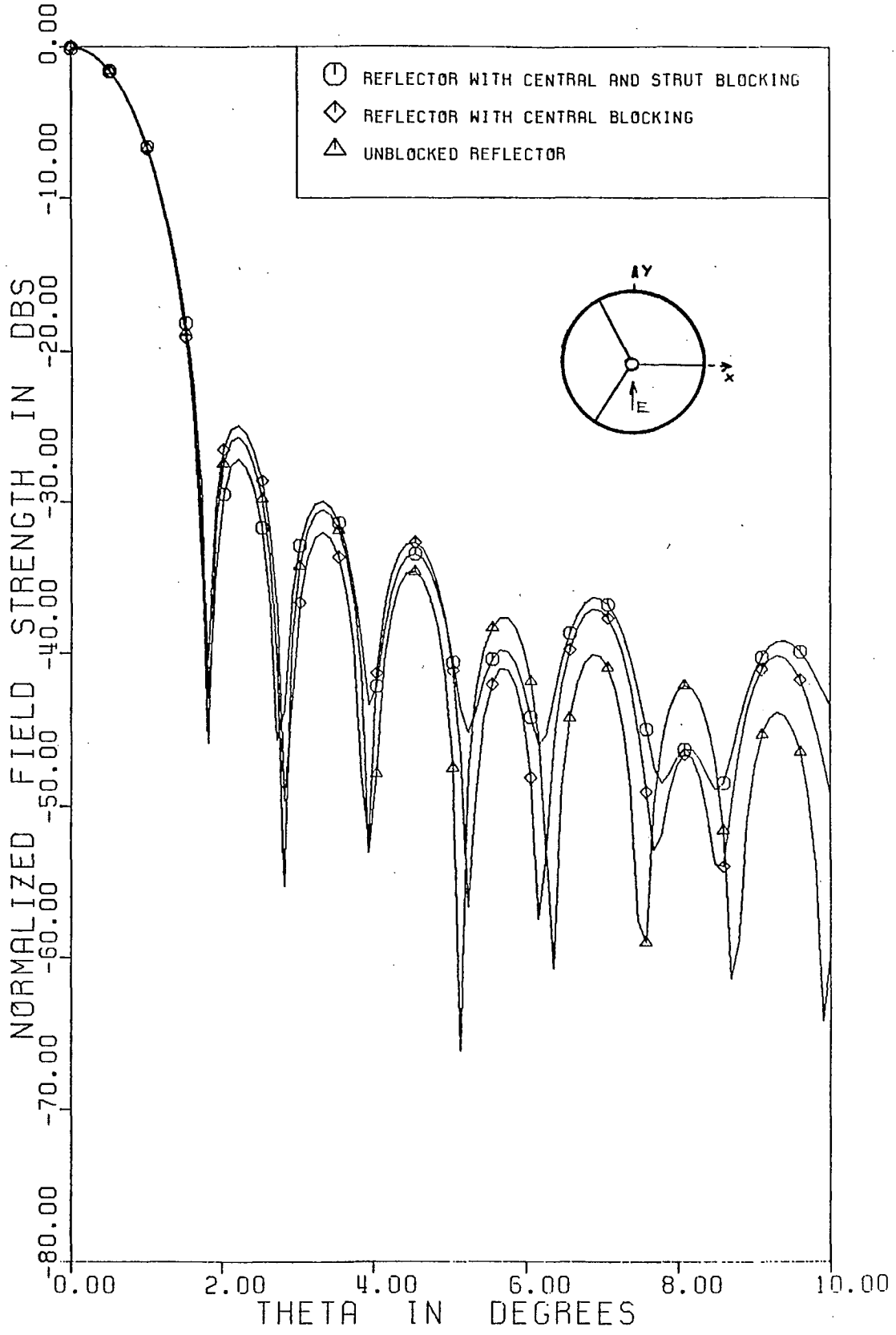

Figure 107. Patterns of tripod struts with strip corrected reflector, $\alpha = 0.35\lambda$, $\phi = 0^{o}$ plane

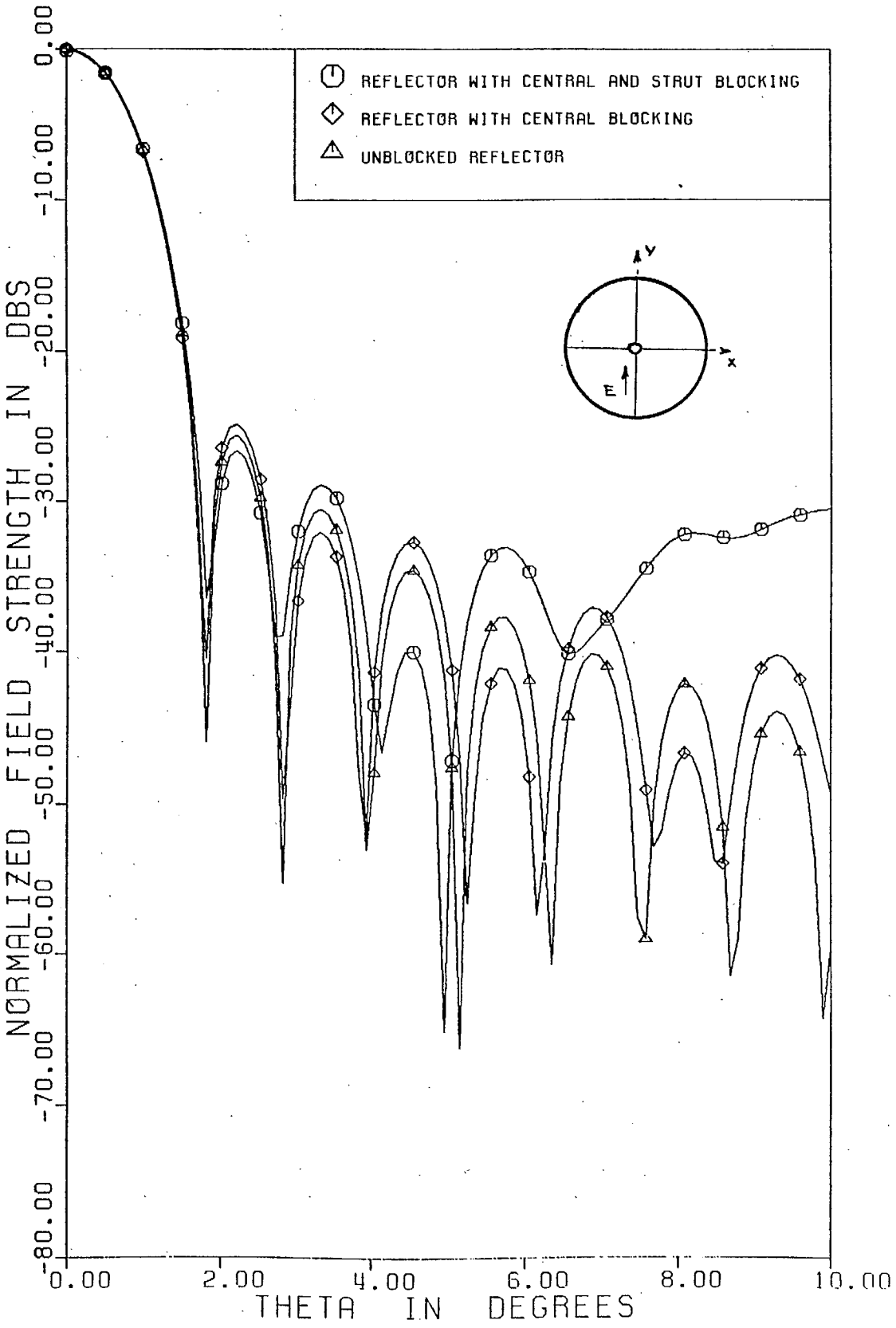

Figure 108. Patterns of quad struts with strip corrected reflector, $\alpha = 0.35\lambda$, $\phi = 0^{o}$ plane

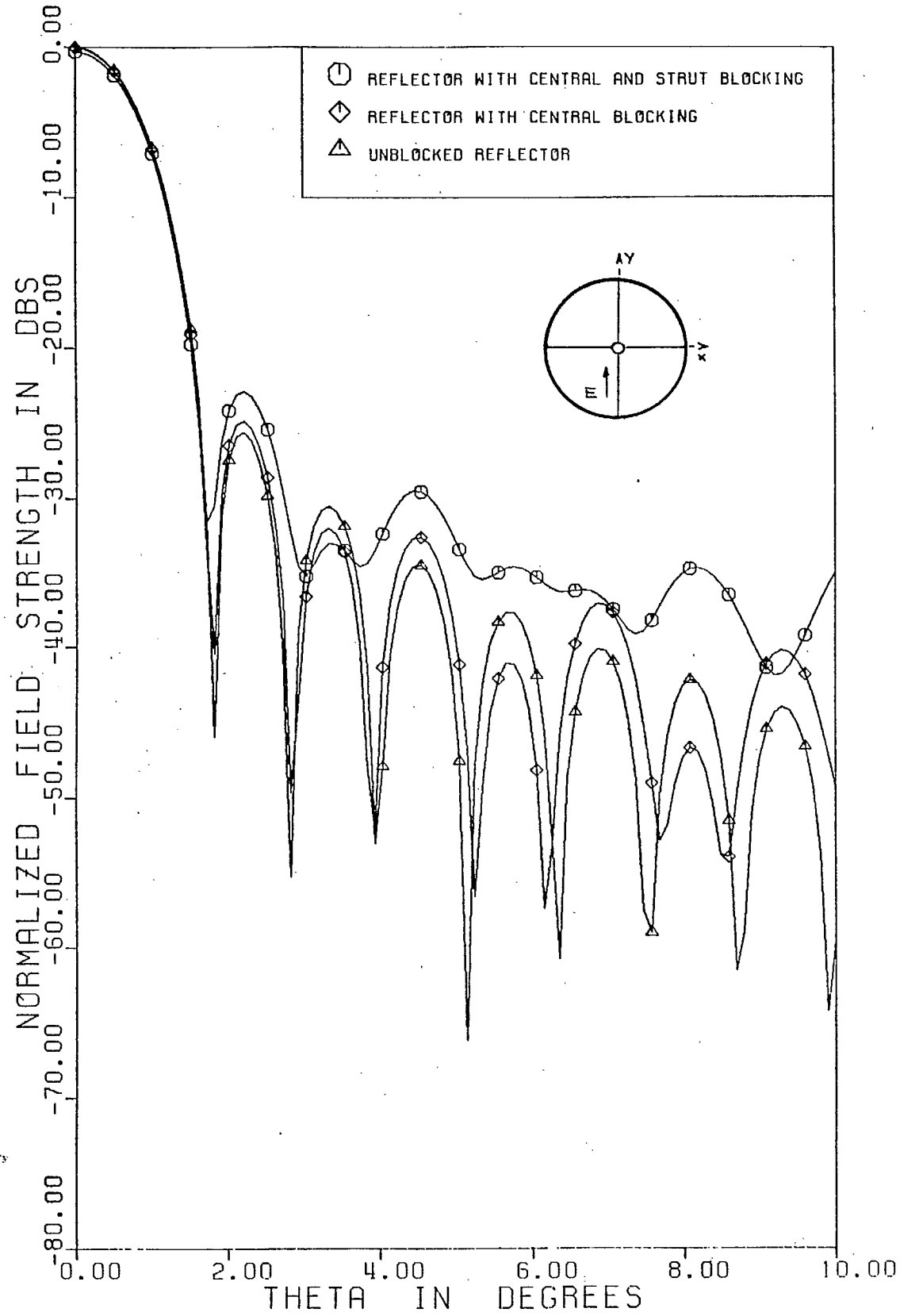

Figure 109. Patterns of quad struts with strip corrected reflector, $\alpha = 0.45\lambda$, $\phi = 0^{o}$ plane

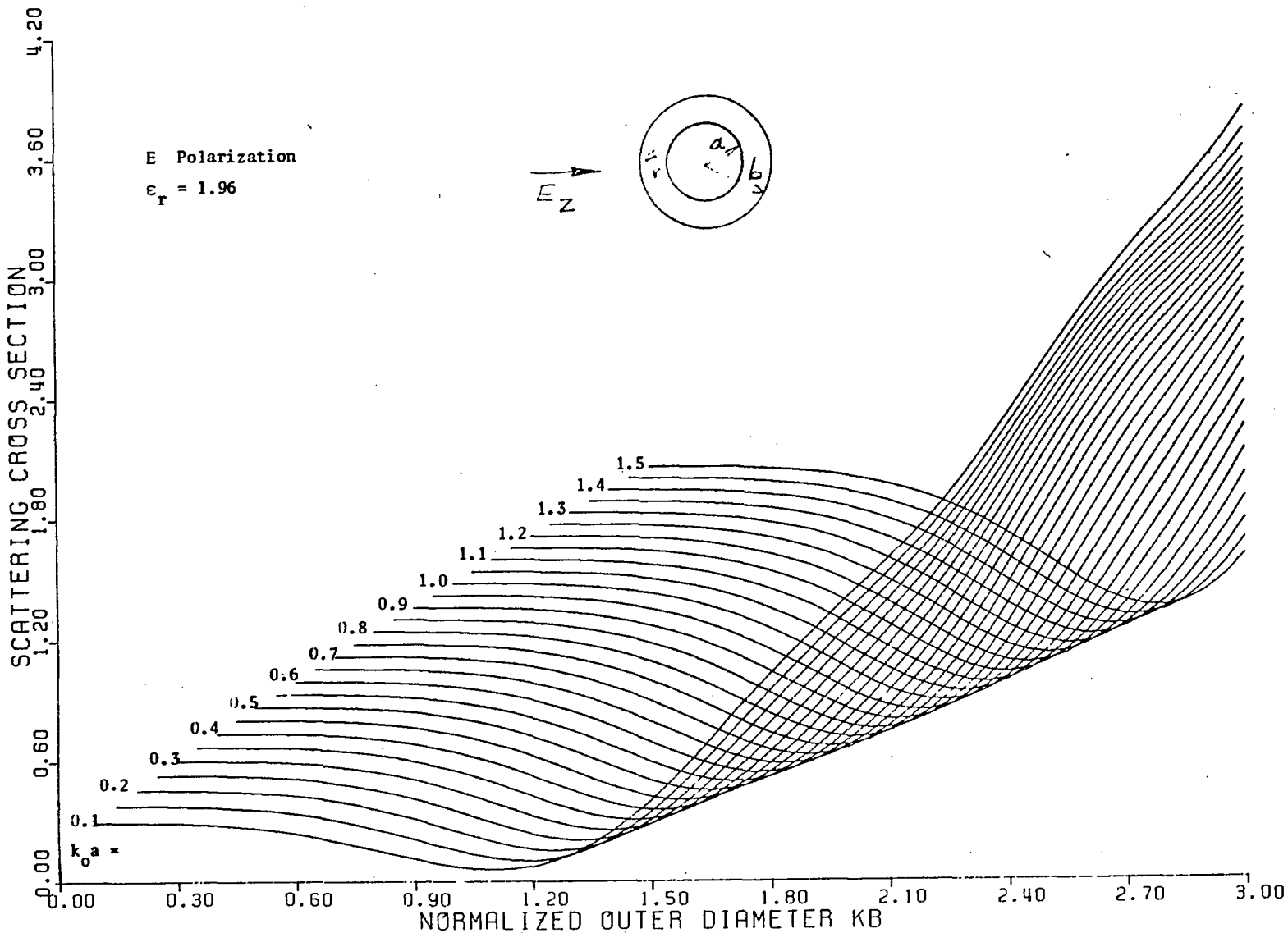

Figure 110. Variation of scattering cross-section of a dielectric coated cylinder

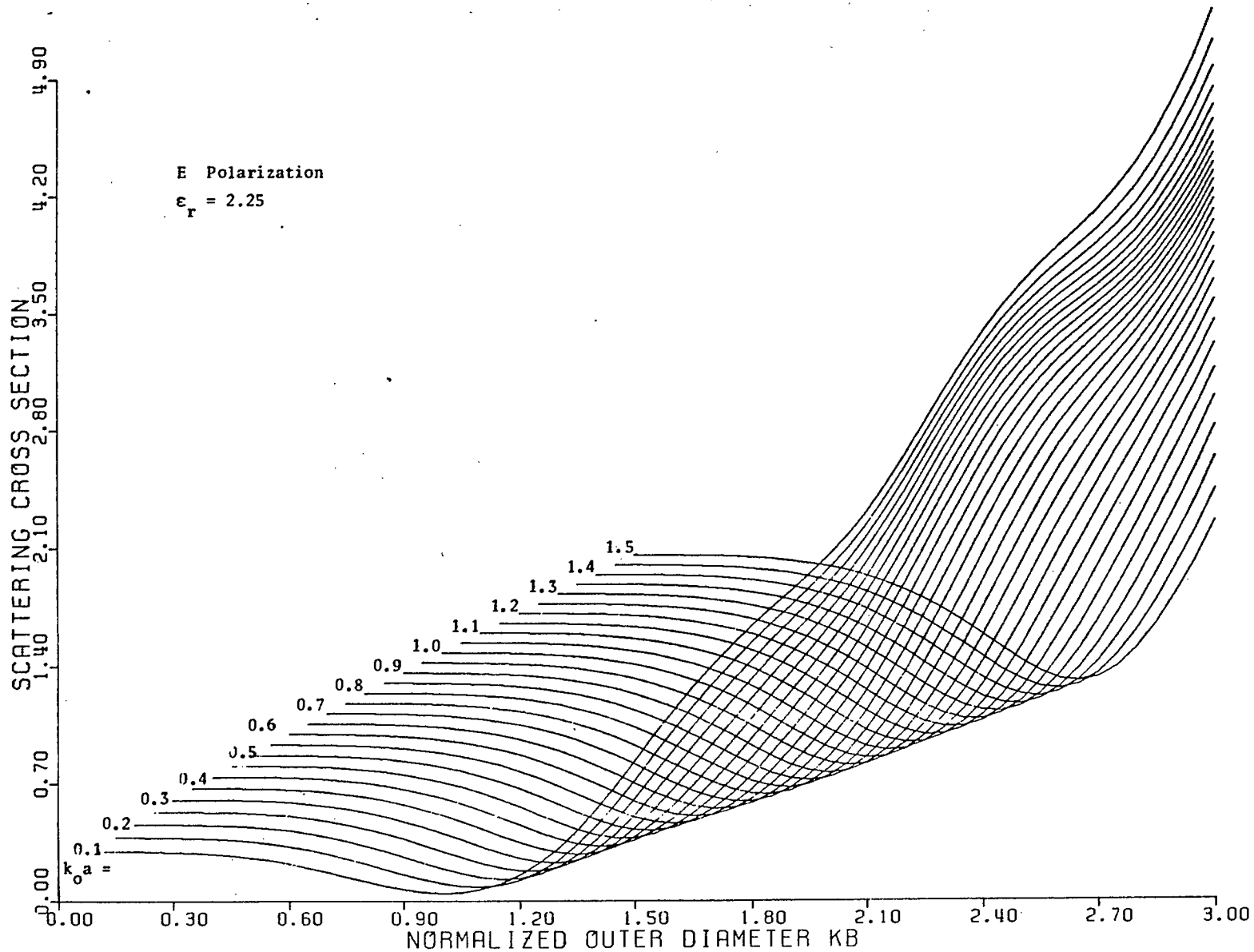

Figure 111. Variation of scattering cross-section of a dielectric coated cylinder

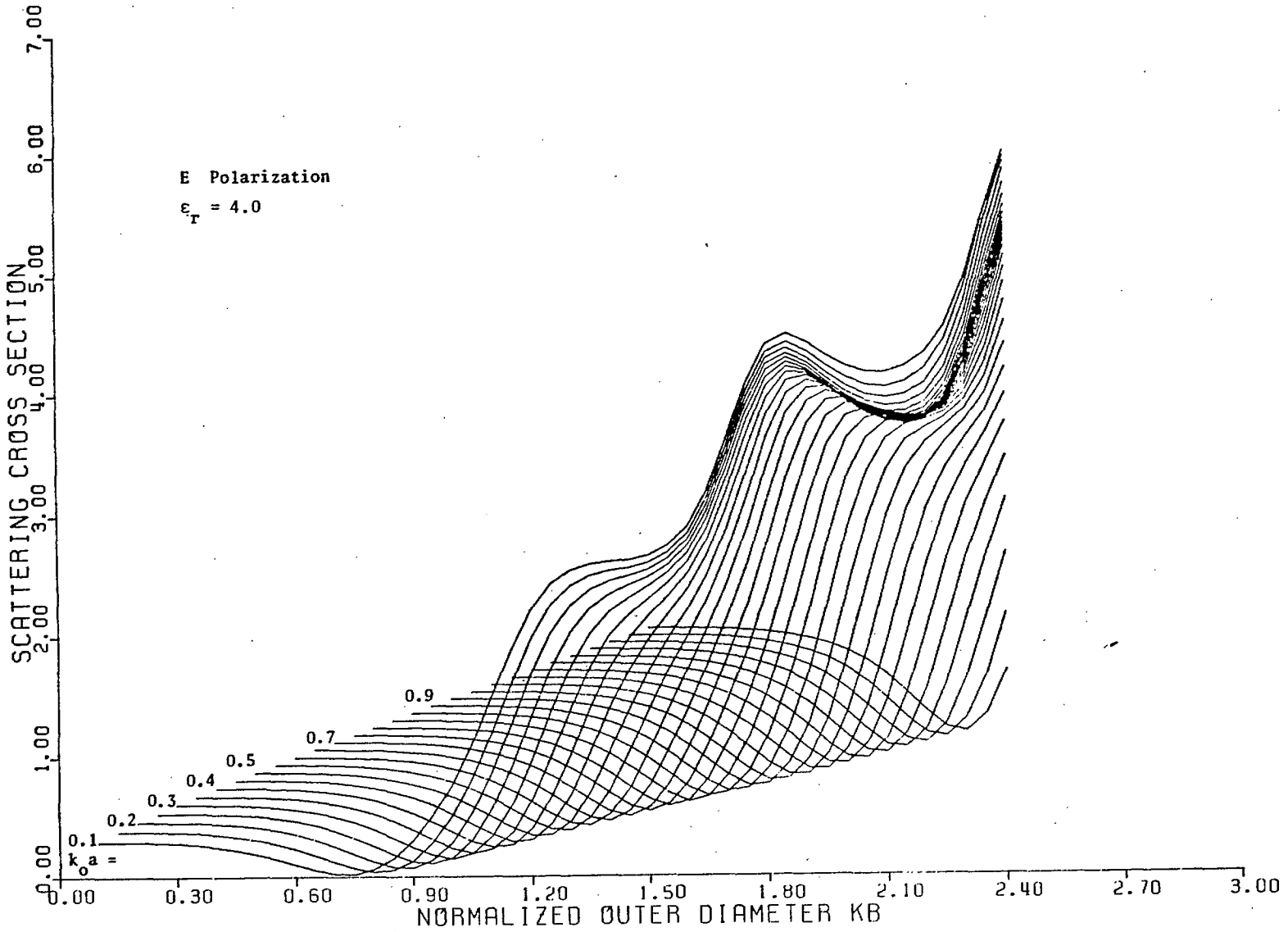

Figure 112. Variation of scattering cross-section of a dielectric coated cylinder

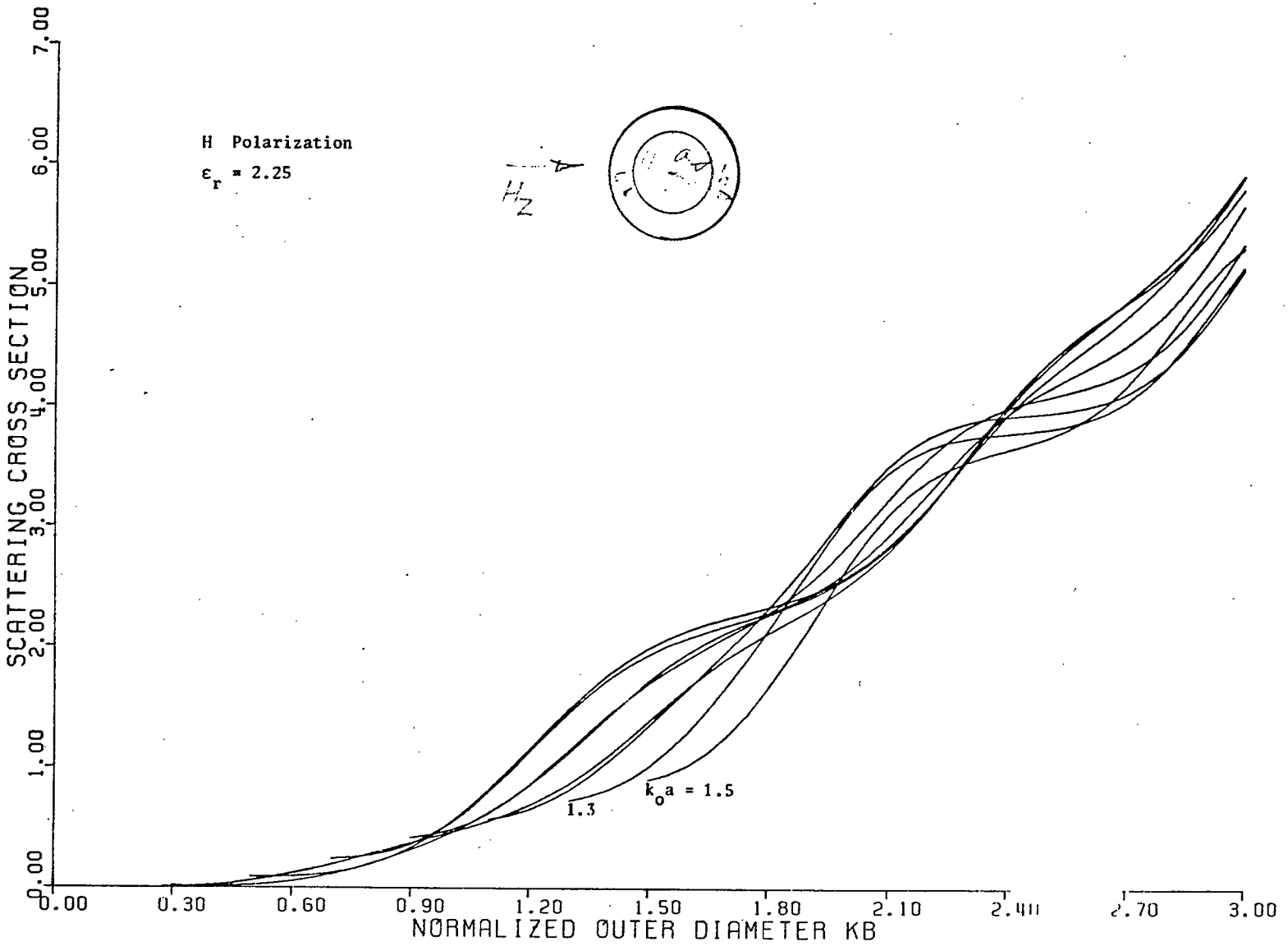

Figure 113. Variation of scattering cross-section of a dielectric coated cylinder

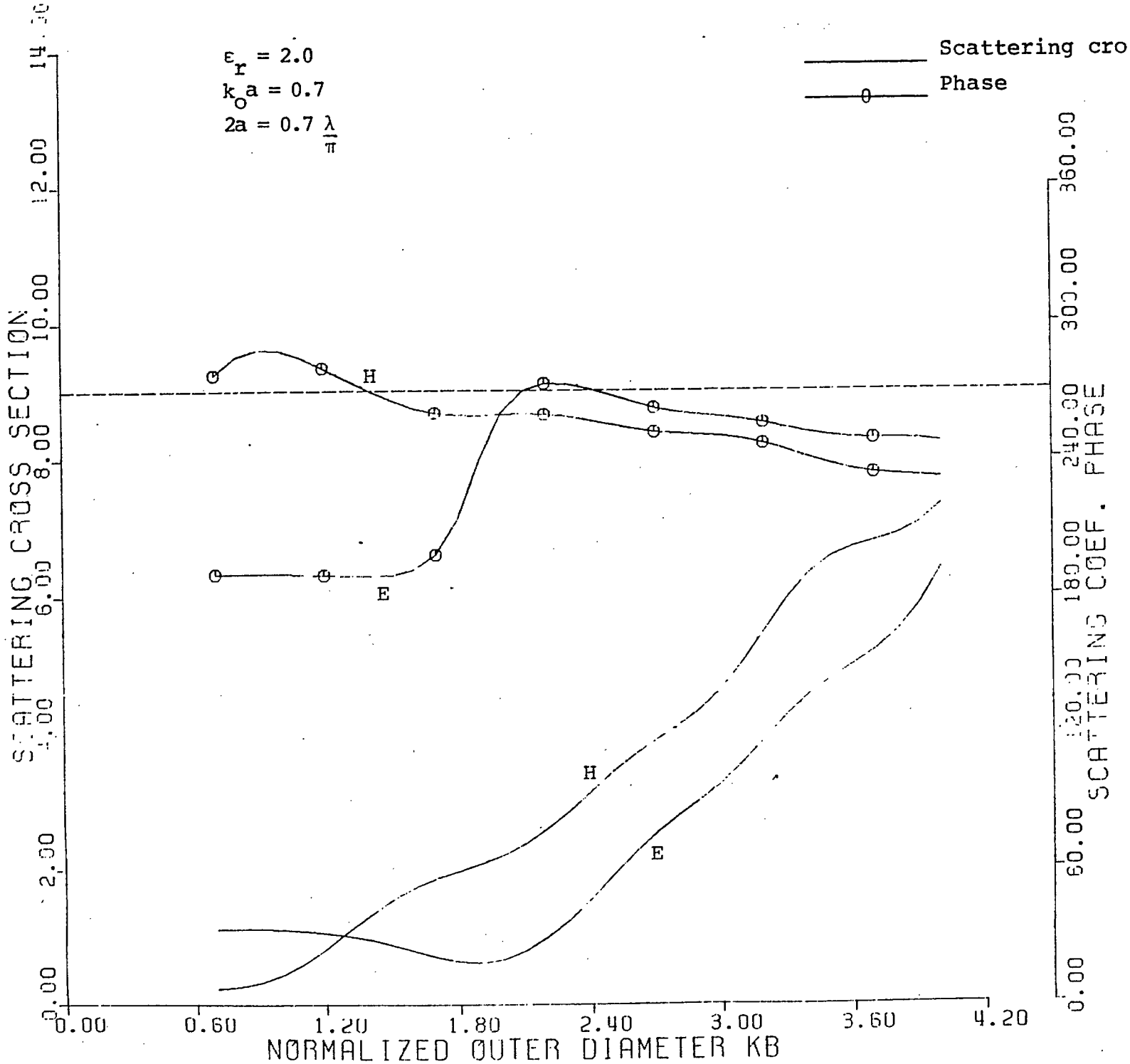

Figure 114. Magnitude and phase of the forward scattered fields

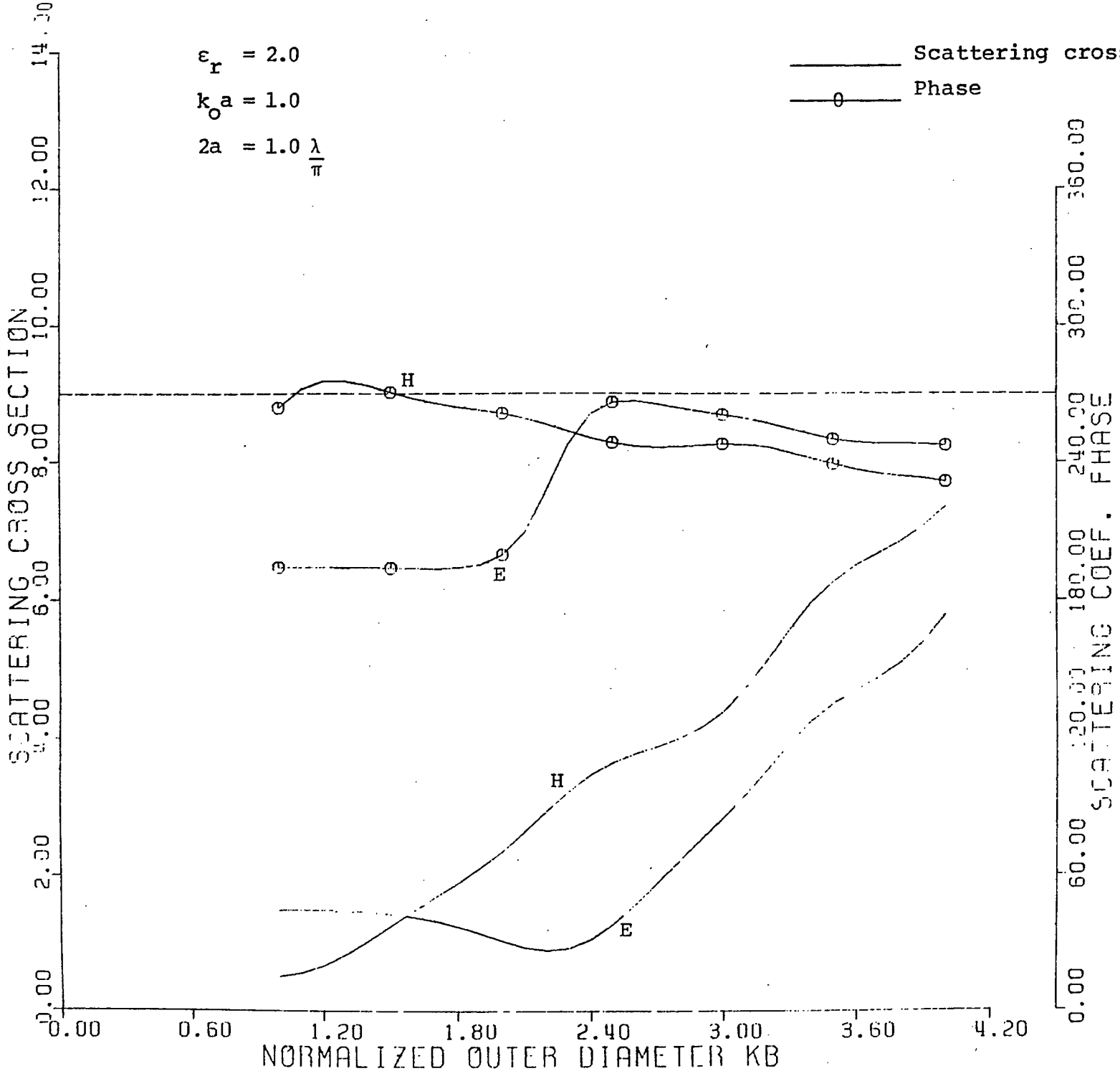

Figure 115. Magnitude and phase of the forward scattered field

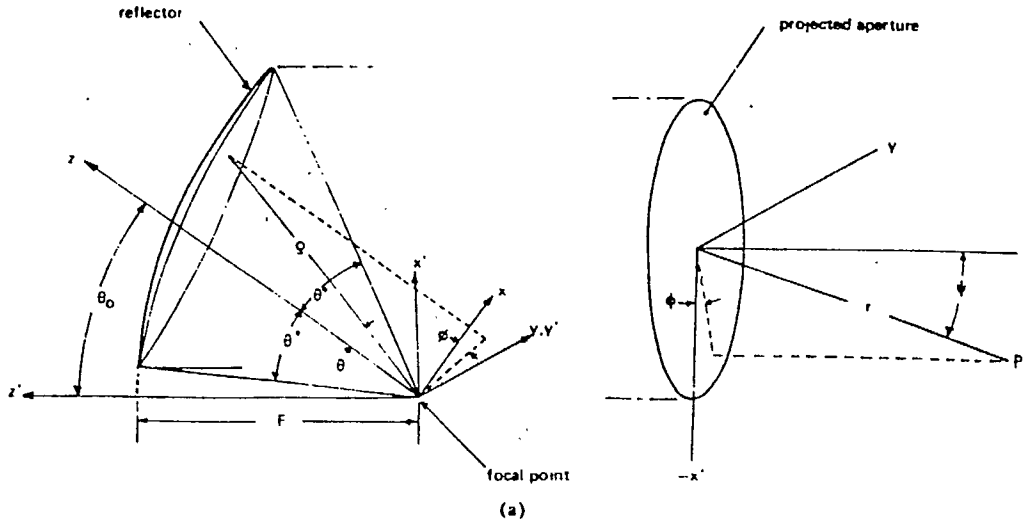

Figure 116. Offset-reflector coordinate system

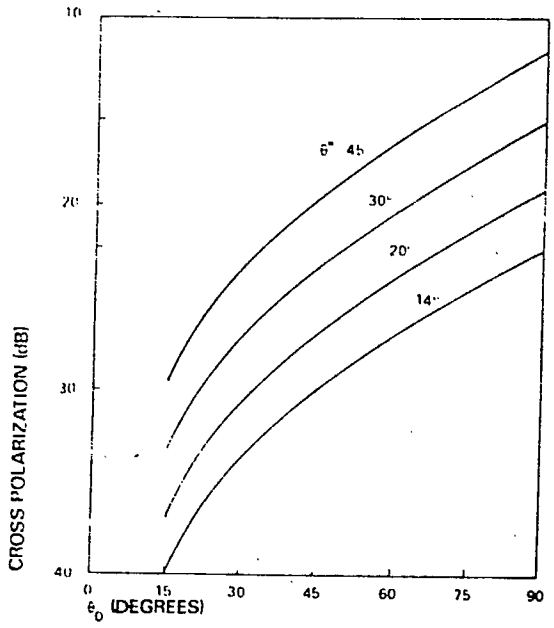

Figure 117. Peak cross-polar levels radiated in the plane of asymmetry ($\Phi = \pi/2$) as a function of the offset-reflector parameters θ_o and θ^* (from A.W. Rudge, Proc. IEEE, vol. 66)

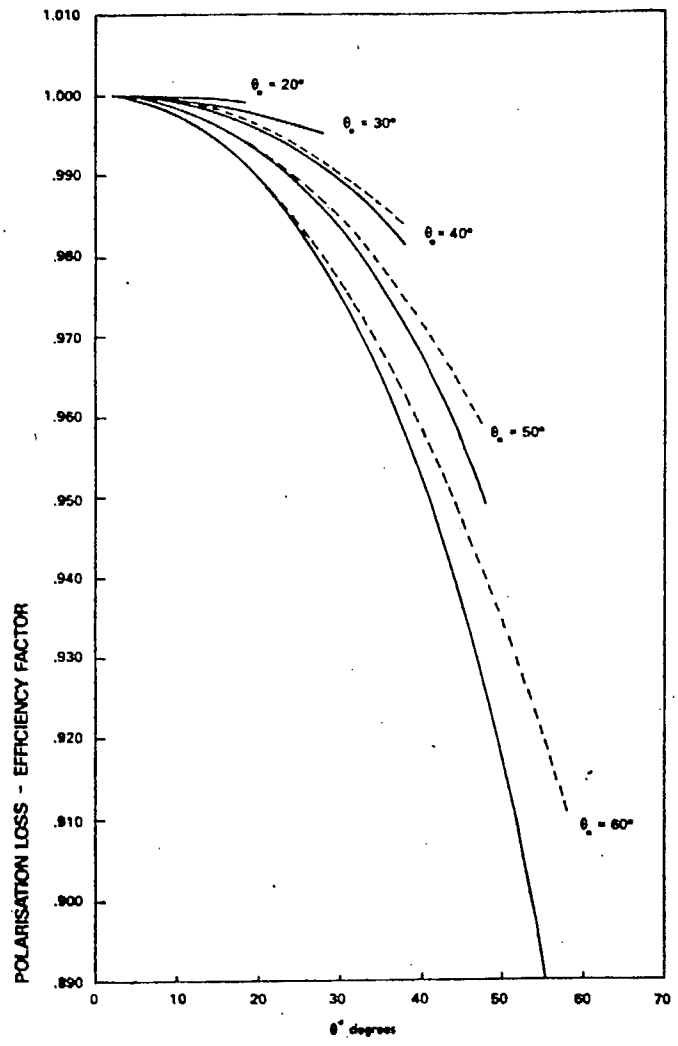

Figure 118. Polarization loss-efficiency factor of offset paraboloid reflector, illuminated by electric dipole oriented along x' axis and Huygens source and ---- electric dipole oriented along y' axis. (From A.W. Rudge,Proc.IEEE,vol.66)

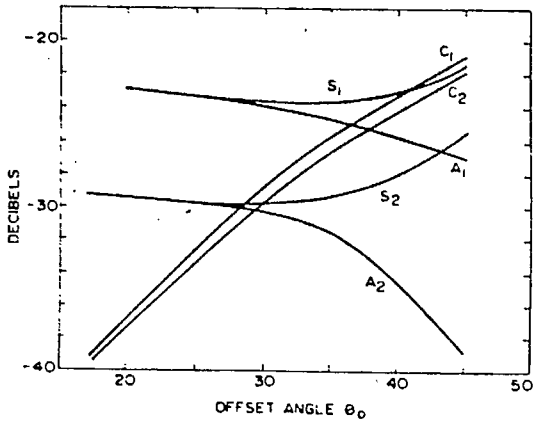

Figure 119. Peak copolar sidelobe levels in planes of symmetry (s) and asymmetry (A) for offset reflectors with $\theta o = \theta^* + 5^o$, fed by uniformly illuminated circular aperture feeds producing - 10 dB (subscript 1) and - 20 dB (subscript 2) illumination tapers at $\theta = \theta^*$. Peak cross-polar levels (c) occur in plane of asymmetry. (From A.W. Rudge, Proc. IEEE, vol. 66)

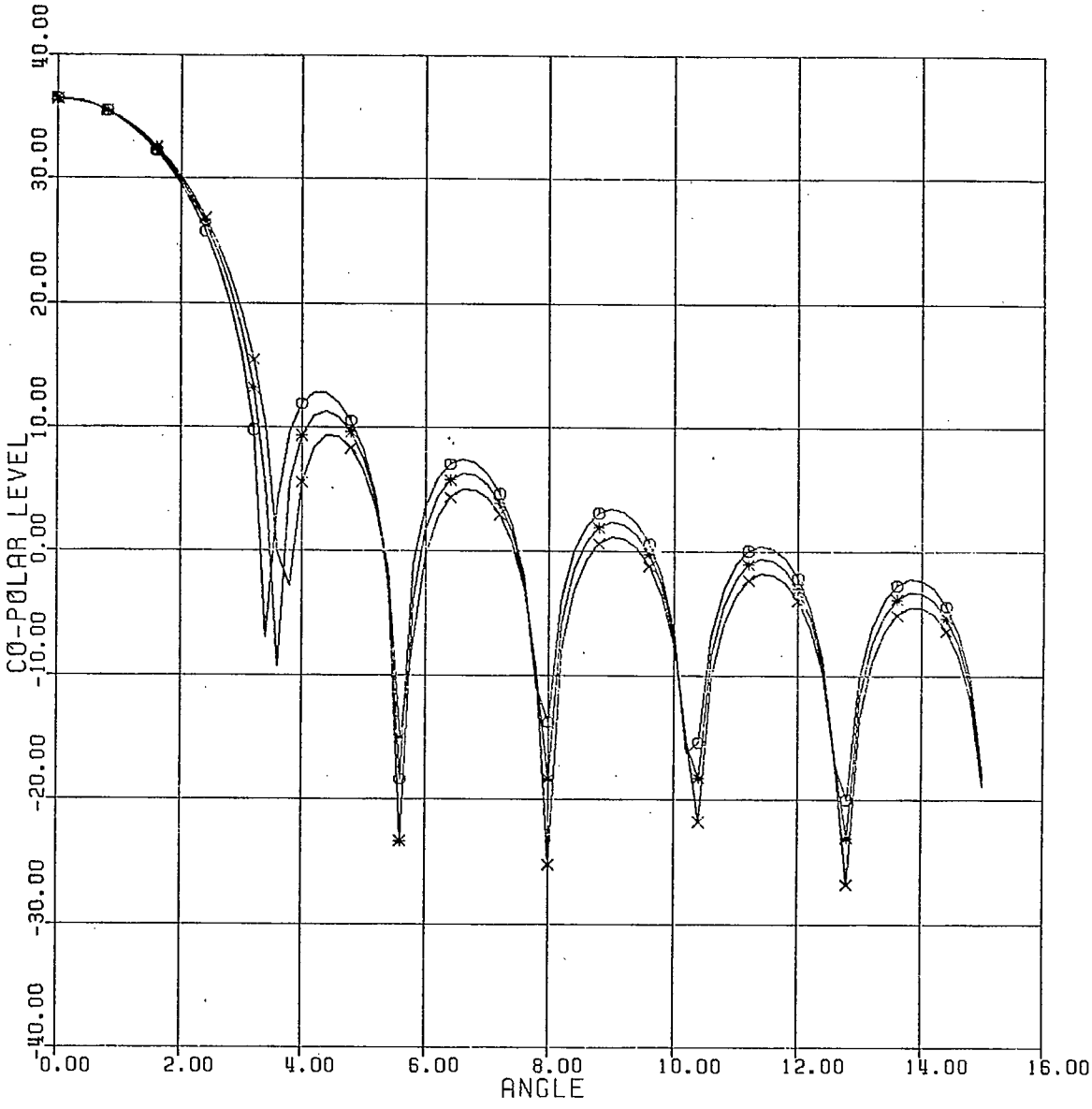

D M = 10

× M = 12

X M = 14

LAMDA=0.025 MT.

PLANE OF ASYMMETRY

X POLARIZATION

Figure 120

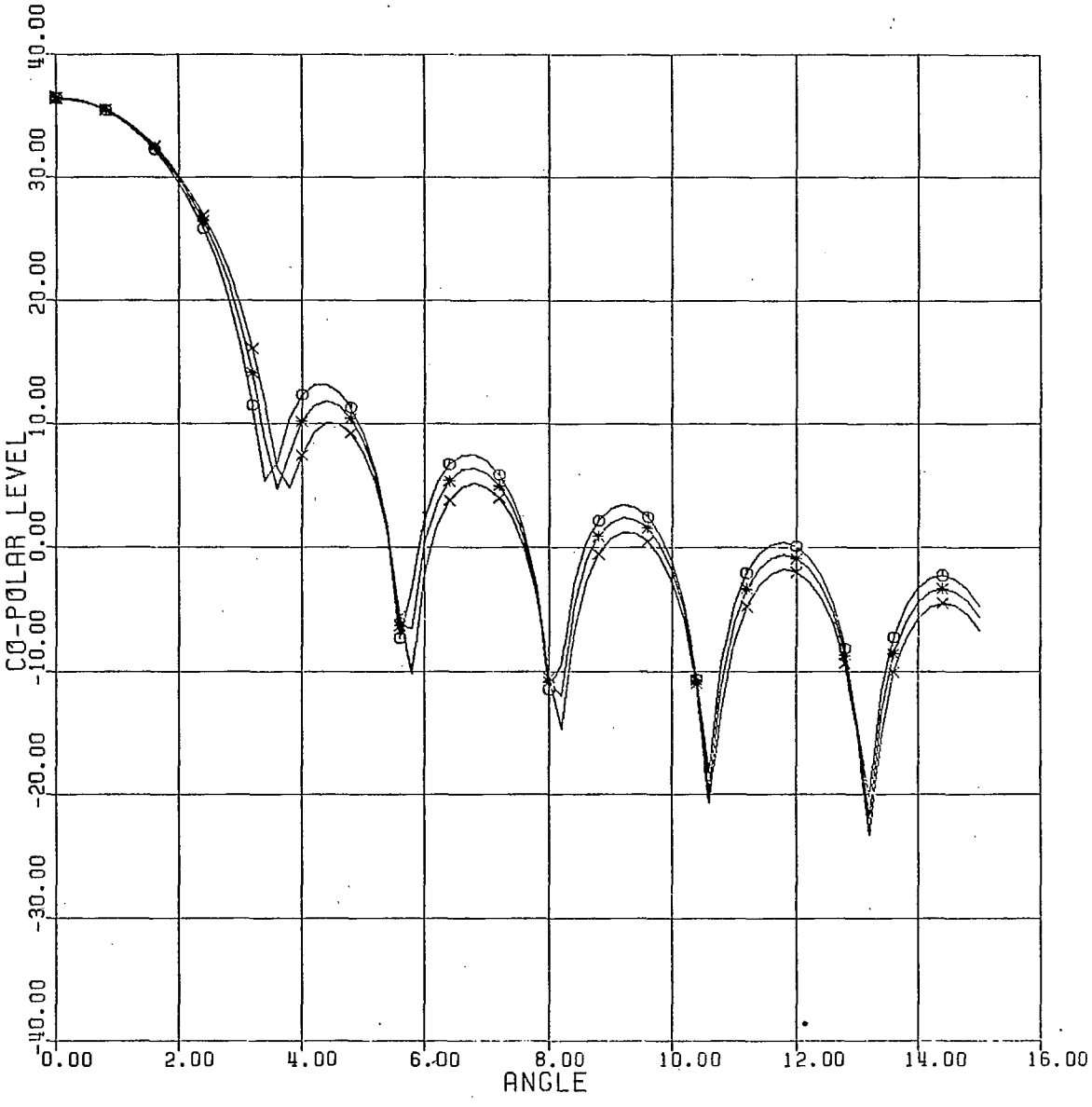
40.00
30.00
20.00
10.00
0.00
-10.00
-20.00
-30.00
-40.00
CO-POLAR LEVEL
0.00
2.00
4.00
6.00
8.00
10.00
12.00
14.00
16.00
ANGLE
O M = 10
* M = 12
X M = 14
LAMDA=0.025 MT.
PLANE OF SYMMETRY
X POLARIZATION

Figure 121.

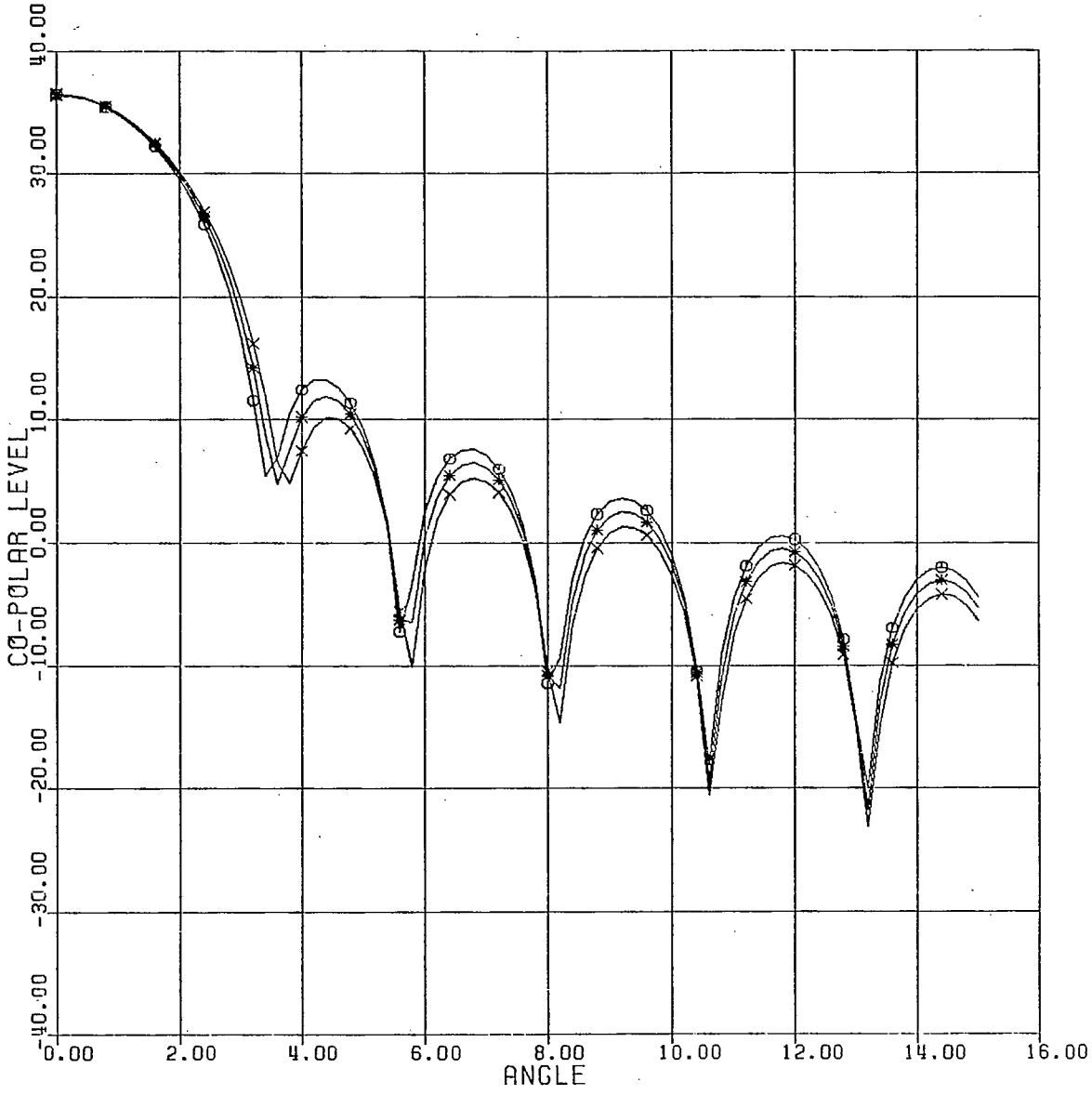
40.00
30.00
20.00
10.00
0.00
-10.00
-20.00
-30.00
-40.00
CØ-PØLAR LEVEL
0.00
2.00
4.00
6.00
8.00
10.00
12.00
14.00
16.00
ANGLE
O M = 10
* M = 12
X M = 14
LAMDA=0.025 MT.
PLANE OF SIMMETRI
Y POLARIZATION

Figure 122.

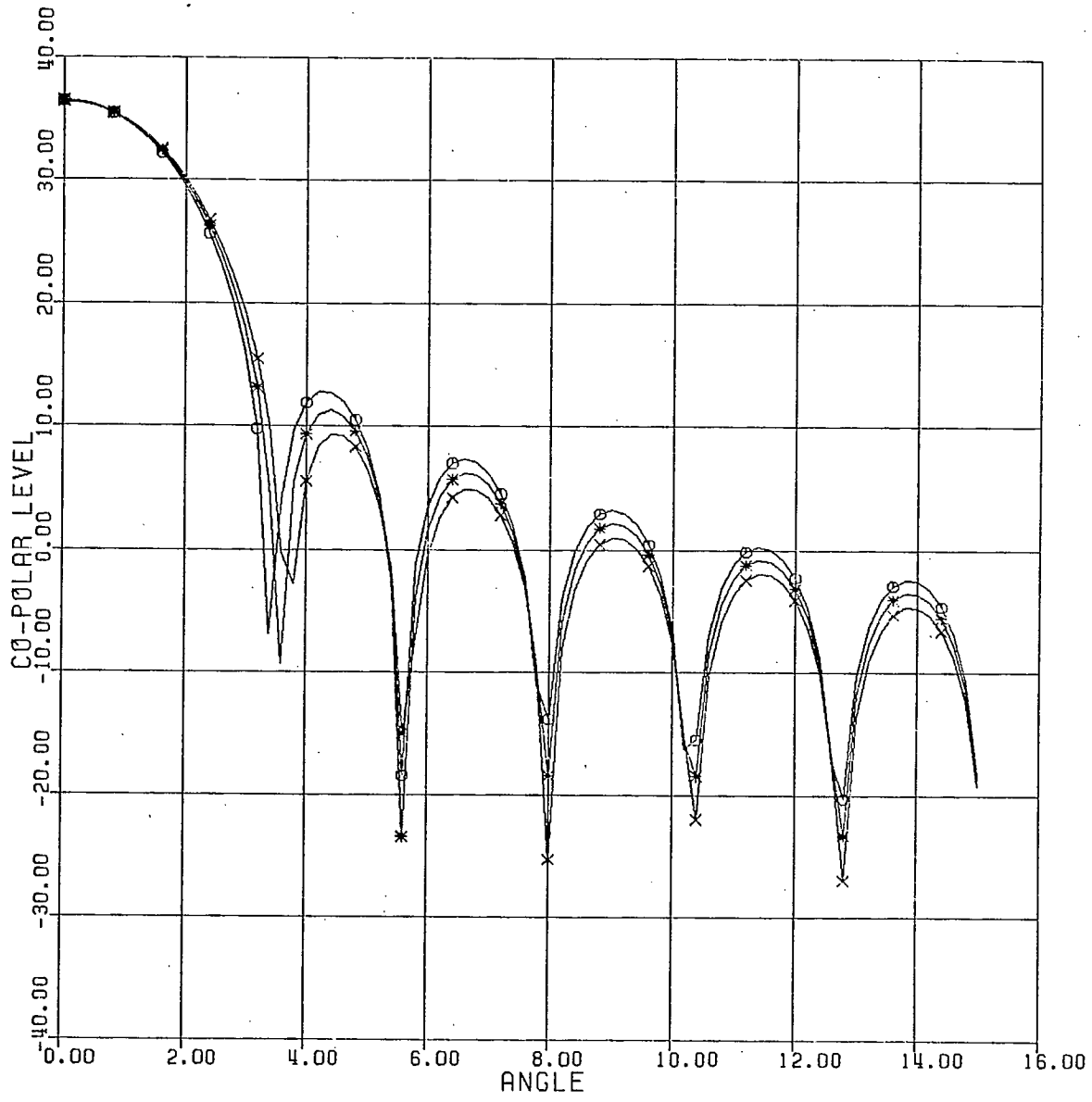
40.00
30.00
20.00
10.00
0.00
-10.00
-20.00
-30.00
-40.00
CØ-PØLAR LEVEL
0.00
2.00
4.00
6.00
8.00
10.00
12.00
14.00
16.00
ANGLE
O M = 10
* M = 12
X M = 14
LAMDA=0.025 MT.
PLANE OF ASYMMETRY
Y POLARIZATION

Figure 123.

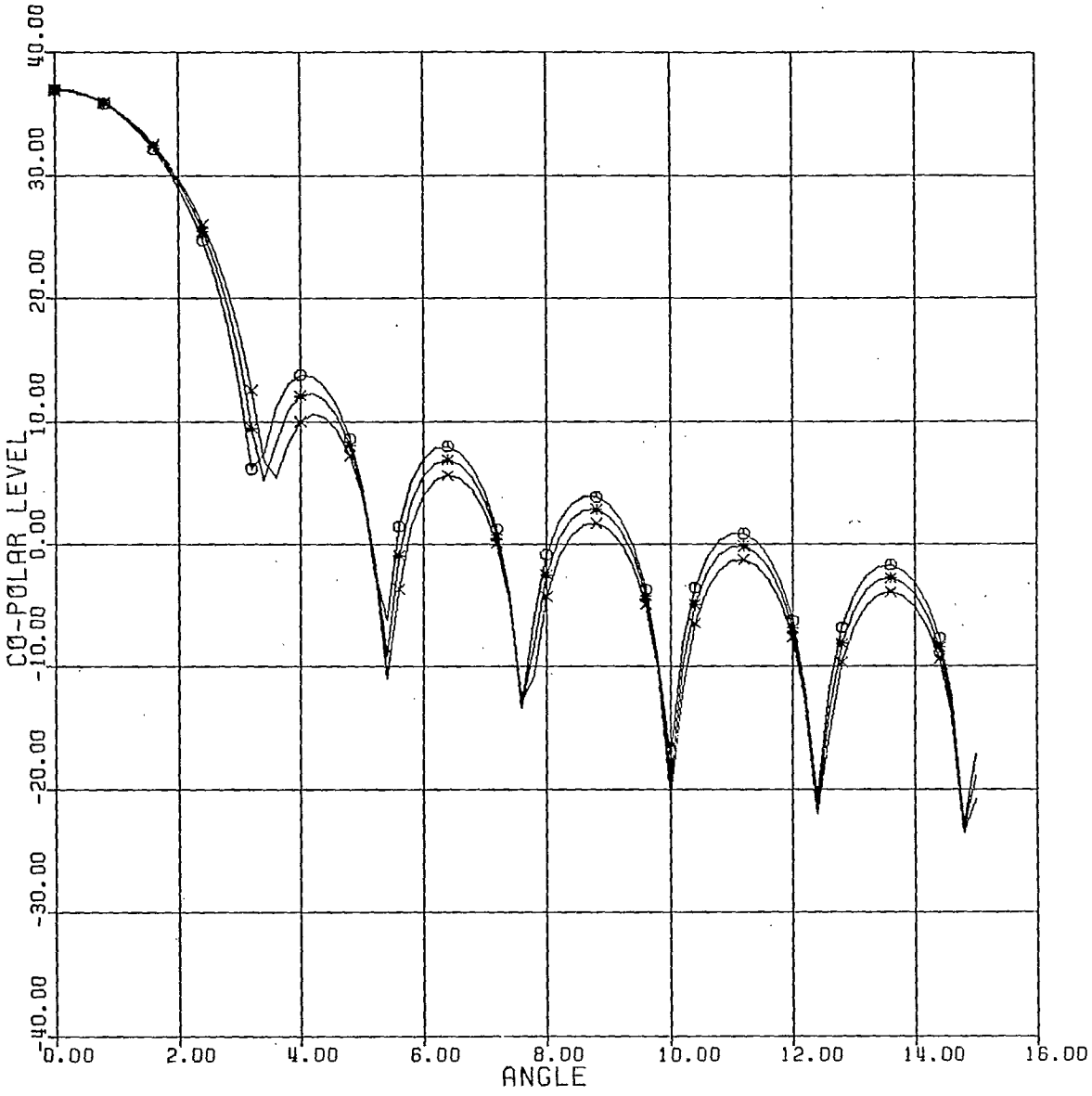
CØ-PØLAR LEVEL
40.00
30.00
20.00
10.00
0.00
-10.00
-20.00
-30.00
-40.00
0.00
2.00
4.00
6.00
8.00
10.00
12.00
14.00
16.00
ANGLE
O M = 10
* M = 12
X M = 14
LAMDA=0.02362 MT.
PLANE OF SYMMETRY
X POLARIZATION

Figure 124.

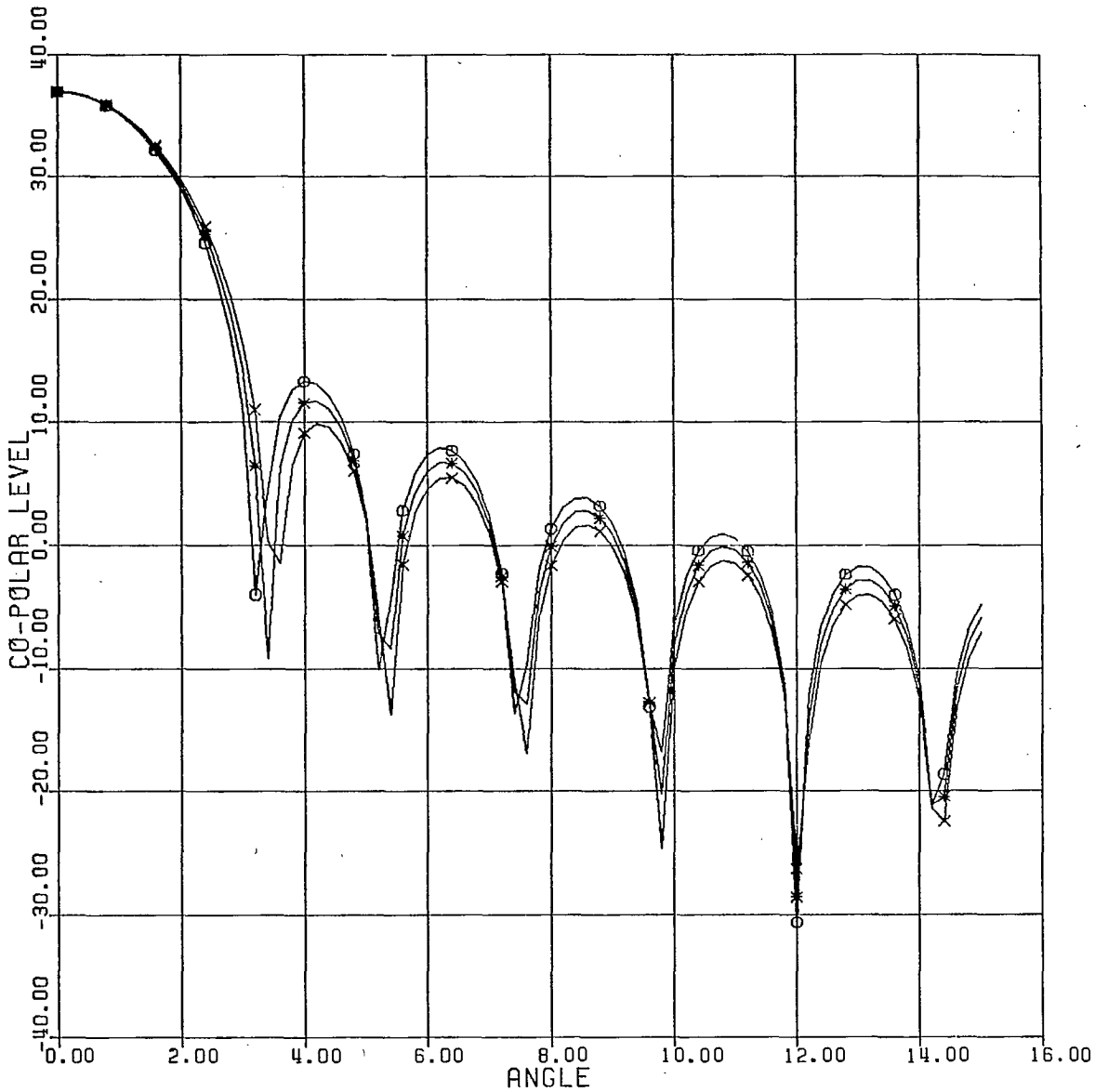

O M = 10

* M = 12

X M = 14

LAMDA=0.02962 MT.

PLANE OF ASYMMETRY

X POLARIZATION

Figure 125.

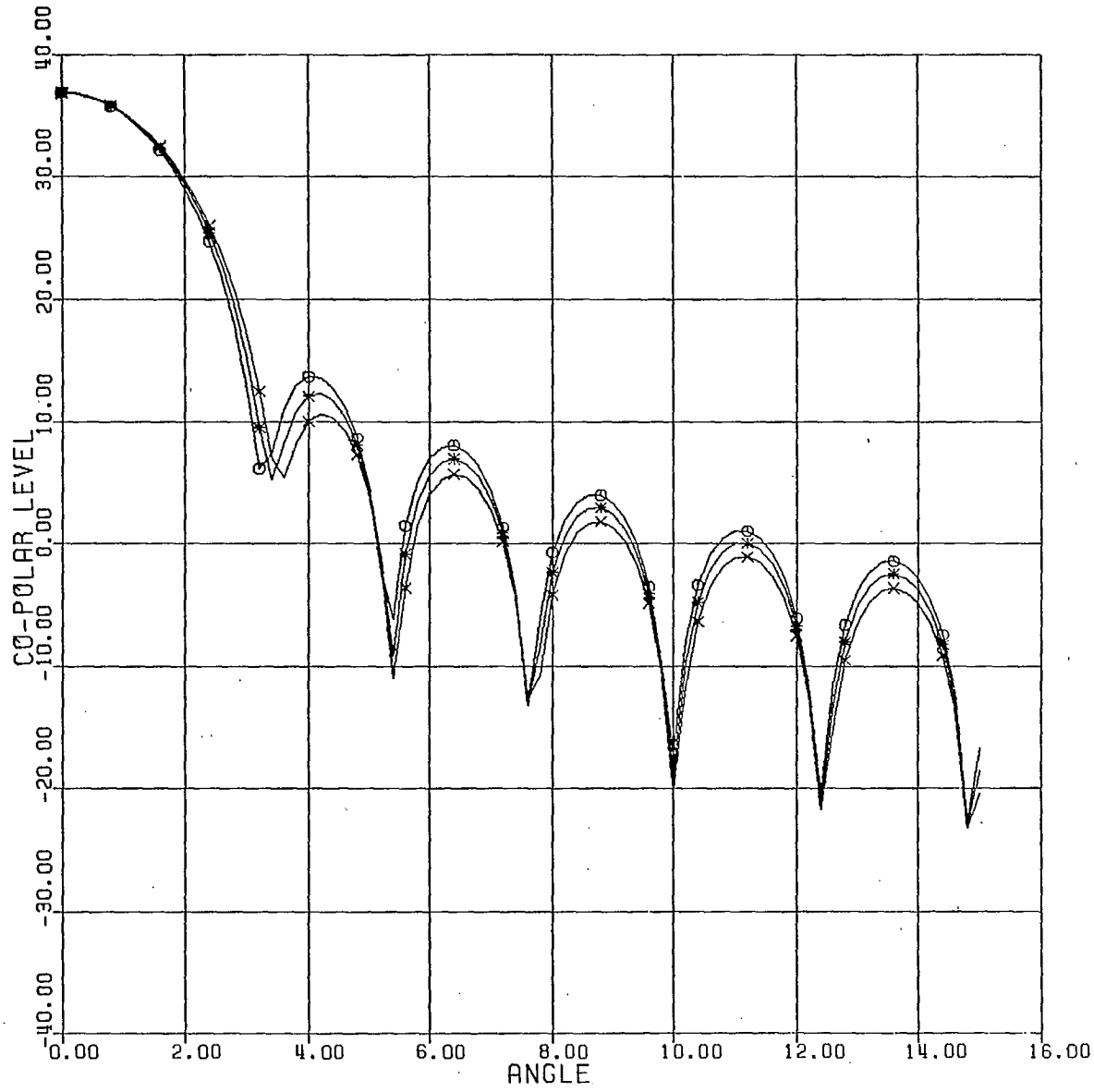
40.00
30.00
20.00
10.00
0.00
-10.00
-20.00
-30.00
-40.00
CO-POLAR LEVEL
0.00
2.00
4.00
6.00
8.00
10.00
12.00
14.00
16.00
ANGLE
O M = 10
* M = 12
X M = 14
LAMDA=0.02362 MT.
PLANE OF SYMMETRY
Y POLARIZATION

Figure 126.

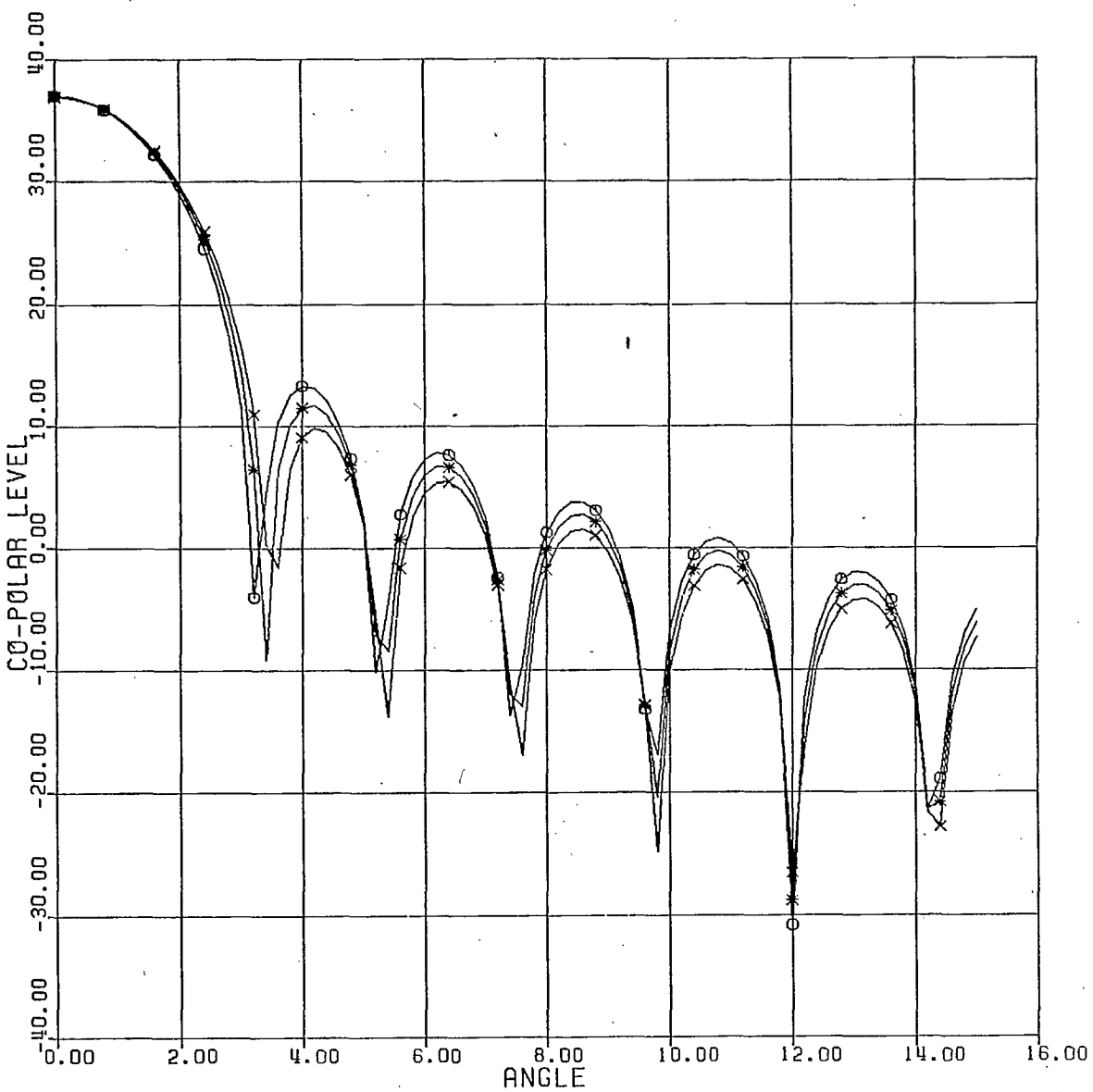
40.00
30.00
20.00
10.00
0.00
-10.00
-20.00
-30.00
-40.00
CØ-PØLAR LEVEL
0.00
2.00
4.00
6.00
8.00
10.00
12.00
14.00
16.00
ANGLE
O M = 10
* M = 12
X M = 14
LAMDA=0.02382 MT.
PLANE OF ASYMMETRY
Y POLARIZATION

Figure 127.

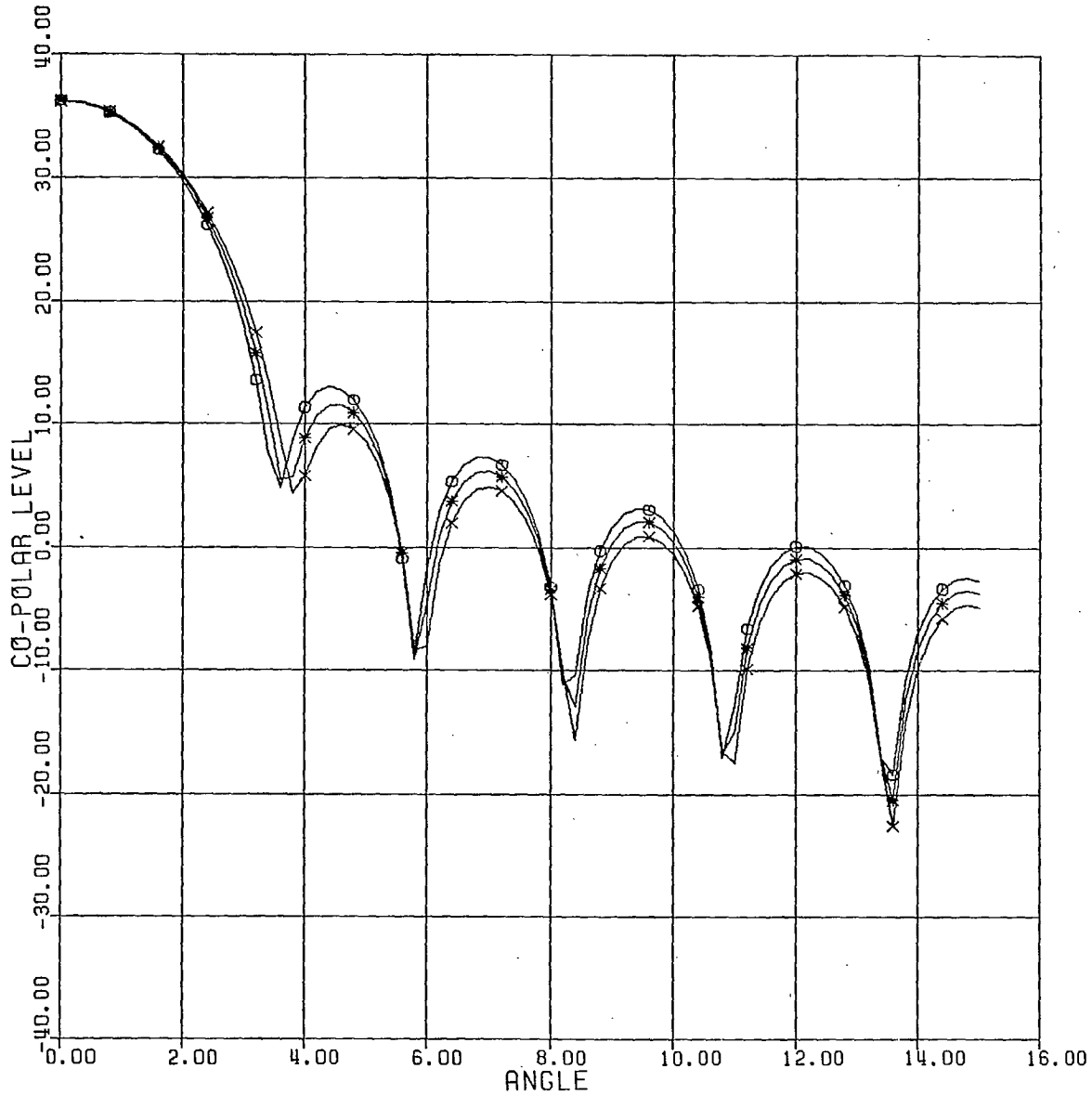
CØ-PØLAR LEVEL
40.00
30.00
20.00
10.00
0.00
-10.00
-20.00
-30.00
-40.00
0.00
2.00
4.00
6.00
8.00
10.00
12.00
14.00
16.00
ANGLE
O M = 10
* M = 12
X M = 14
LAMDA=0.02564 MT.
PLANE OF SYMMETRY
X POLARIZATION

Figure 128.

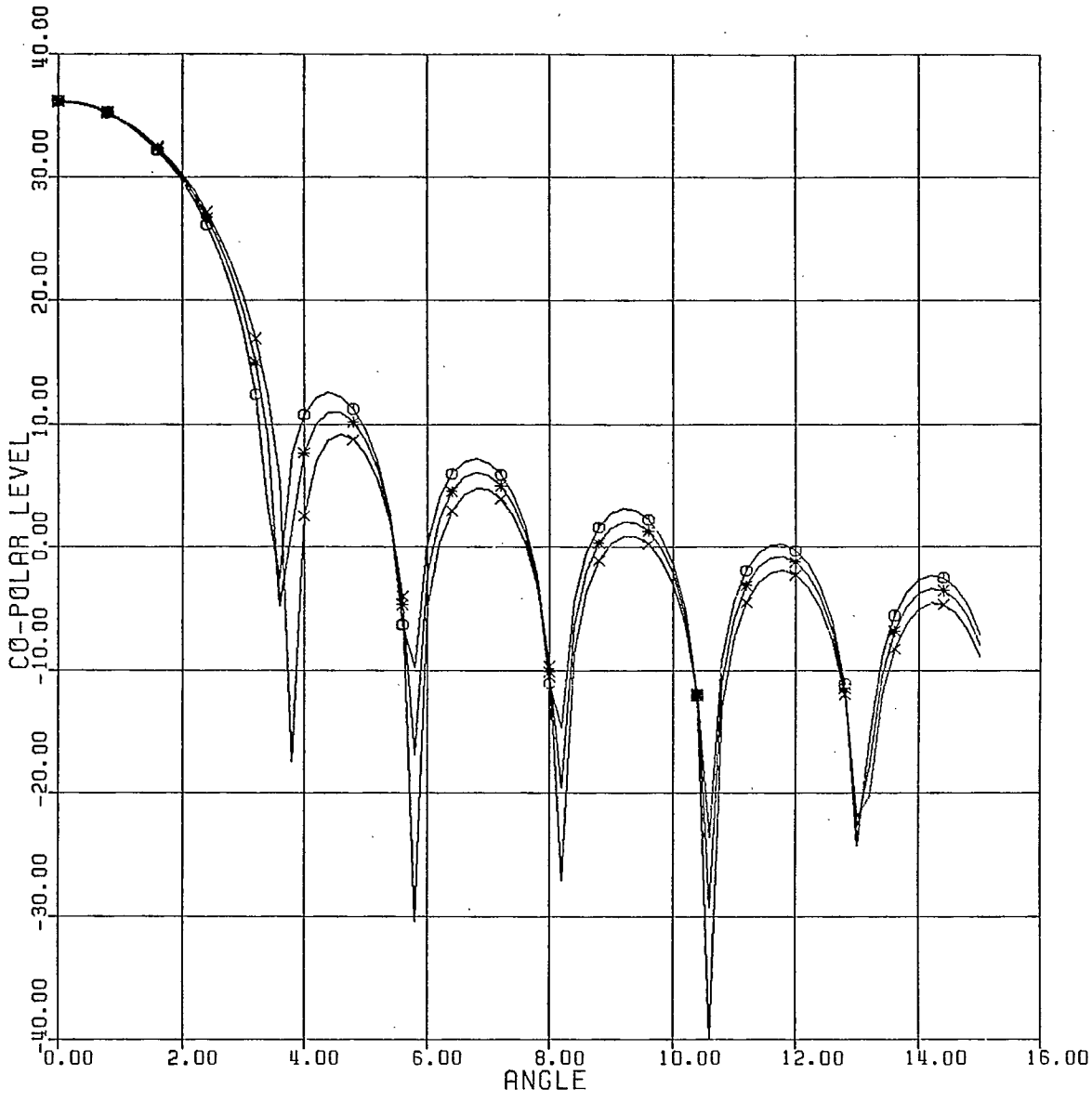
40.00
30.00
20.00
10.00
0.00
-10.00
-20.00
-30.00
-40.00
CØ-PØLAR LEVEL
0.00
2.00
4.00
6.00
8.00
10.00
12.00
14.00
16.00
ANGLE
O M = 10
* M = 12
X M = 14
LAMDA=0.02564 MT.
PLANE OF ASYMMETRY
X POLARIZATION

Figure 129.

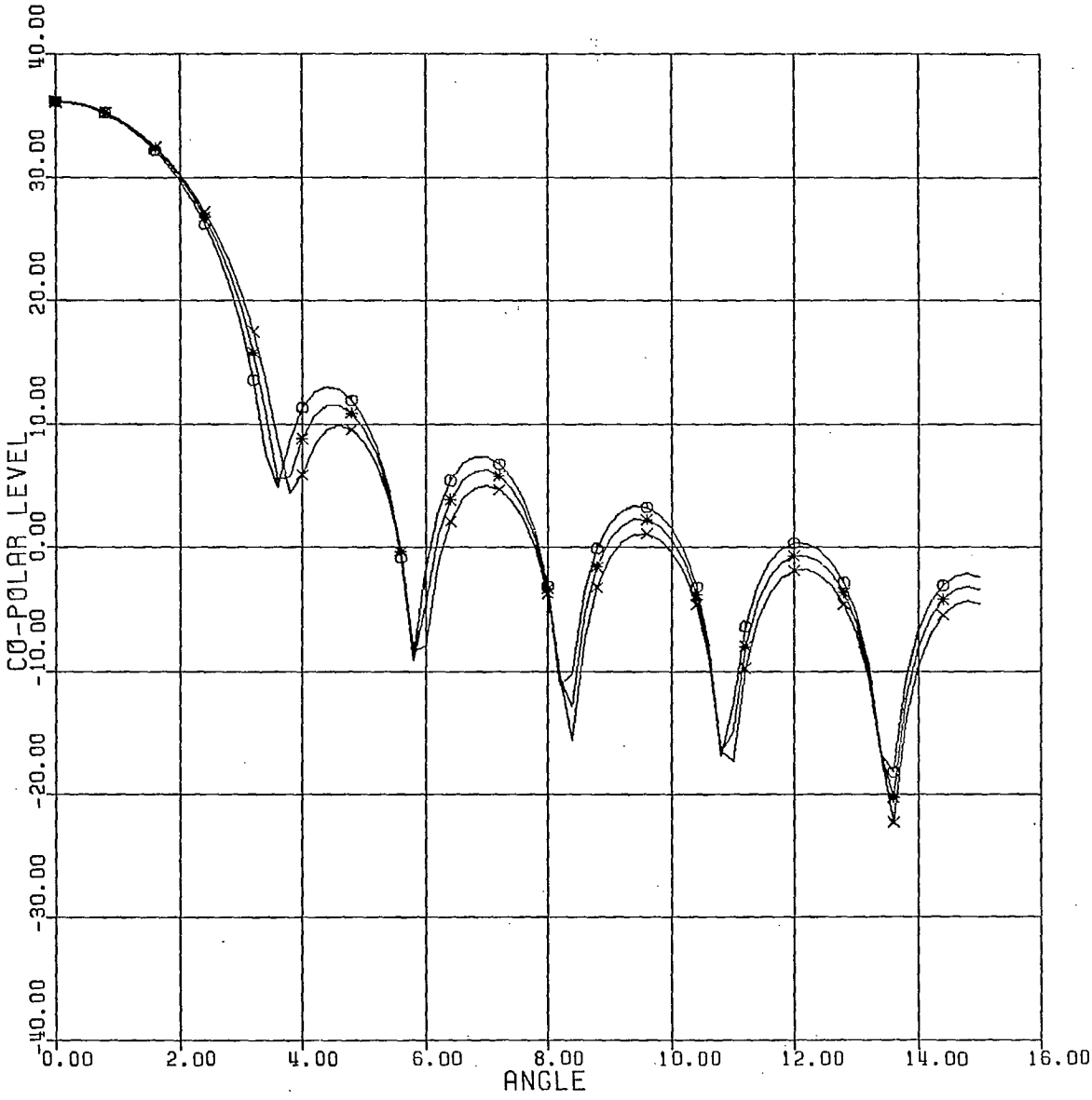
40.00
30.00
20.00
10.00
0.00
-10.00
-20.00
-30.00
-40.00
CØ-PØLAR LEVEL
0.00
2.00
4.00
6.00
8.00
10.00
12.00
14.00
16.00
ANGLE
0 M = 10
* M = 12
X M = 14
LAMDA=0.02584 MT.
PLANE OF SYMMETRY
Y POLARIZATION

Figure 130.

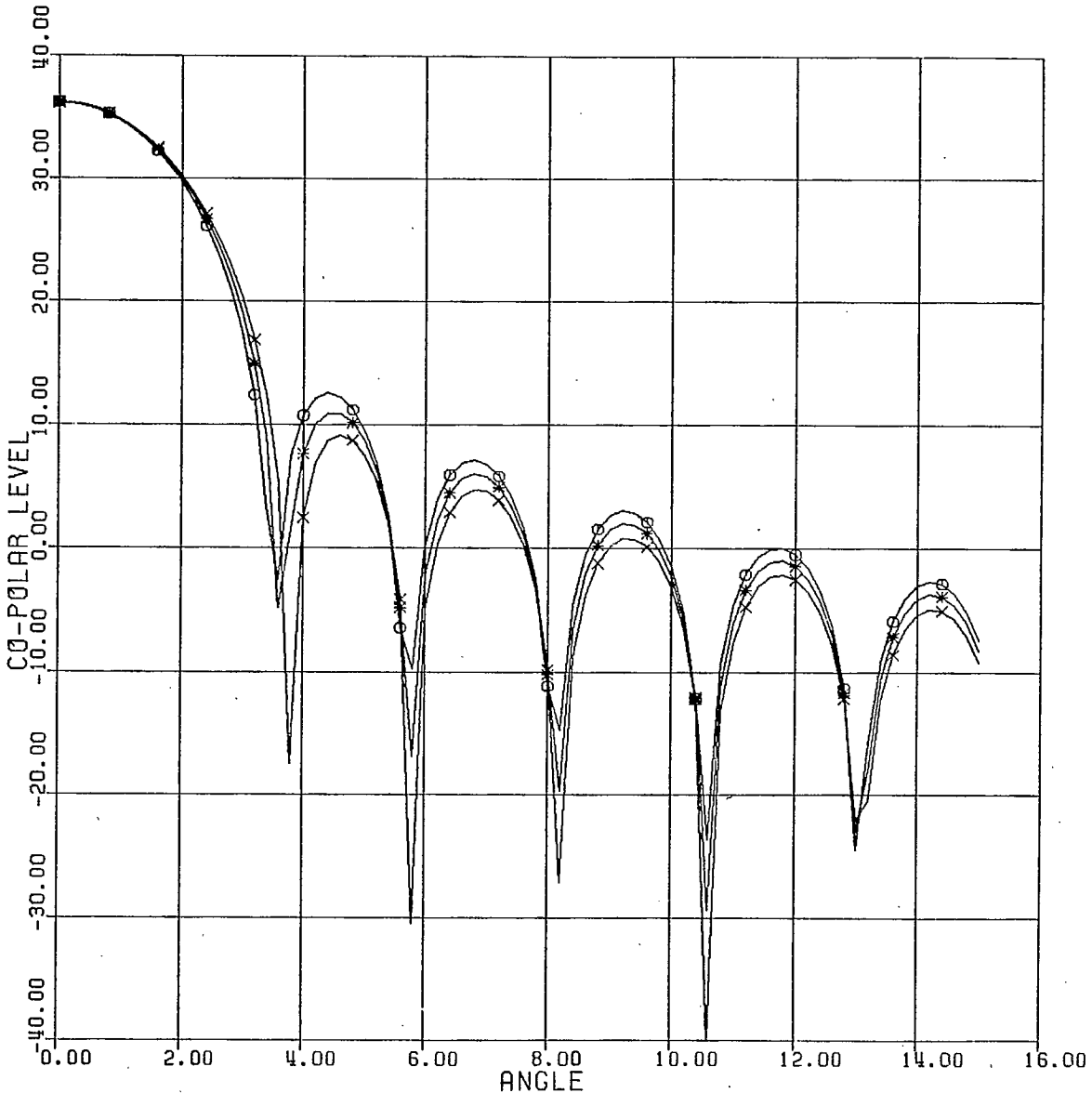
40.00
30.00
20.00
10.00
0.00
-10.00
-20.00
-30.00
-40.00
CØ-PØLAR LEVEL
0.00
2.00
4.00
6.00
8.00
10.00
12.00
14.00
16.00
ANGLE
O M = 10
* M = 12
X M = 14
LAMDA=0.02584 MT.
PLANE OF ASYMMETRY
Y POLARIZATION

Figure 131.

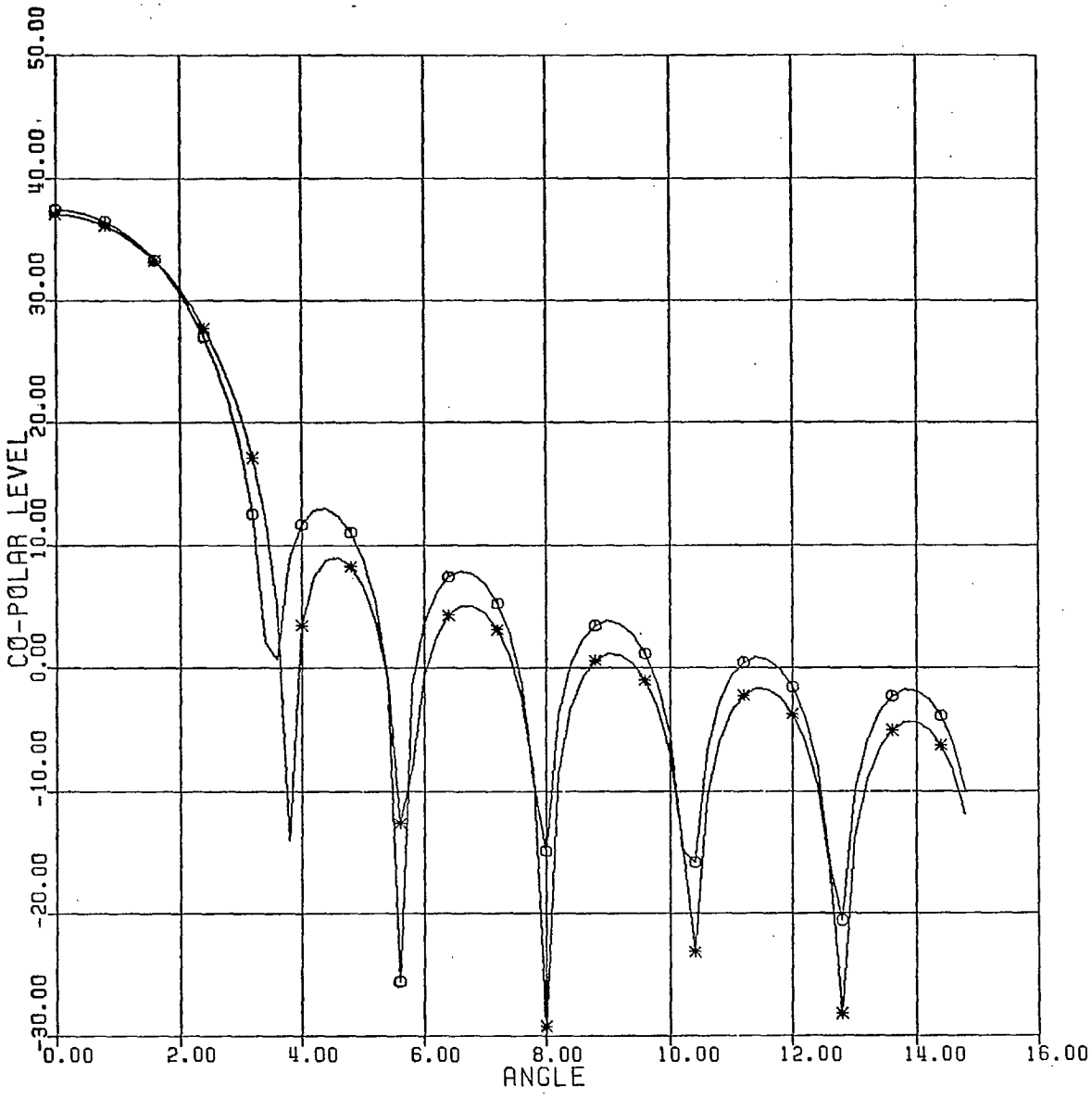
50.00
40.00
30.00
20.00
10.00
0.00
-10.00
-20.00
-30.00
CO-POLAR LEVEL
0.00
2.00
4.00
6.00
8.00
10.00
12.00
14.00
16.00
ANGLE
o M = 11
x M = 15
LAMDA=0.02962 MT.
PLANE OF ASYMMETRY
CIRCULAR POLARIZATION

Figure 132.

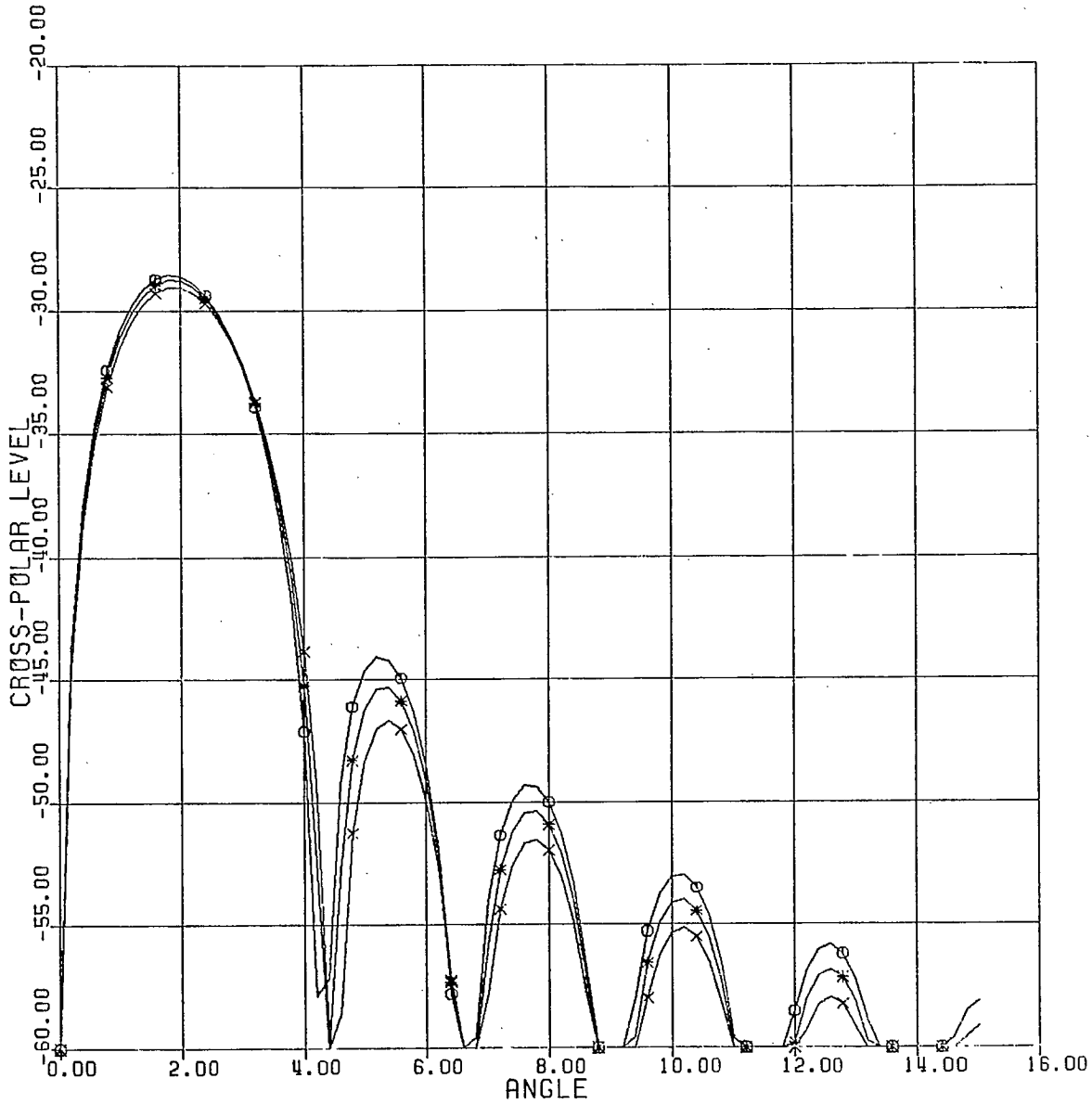
CROSS-POLAR LEVEL
-20.00
-25.00
-30.00
-35.00
-40.00
-45.00
-50.00
-55.00
-60.00
0.00
2.00
4.00
6.00
8.00
10.00
12.00
14.00
16.00
ANGLE
O M = 10
* M = 12
X M = 14
LAMDA=0.025 MT.
PLANE OF ASYMMETRY
X POLARIZATION

Figure 133.

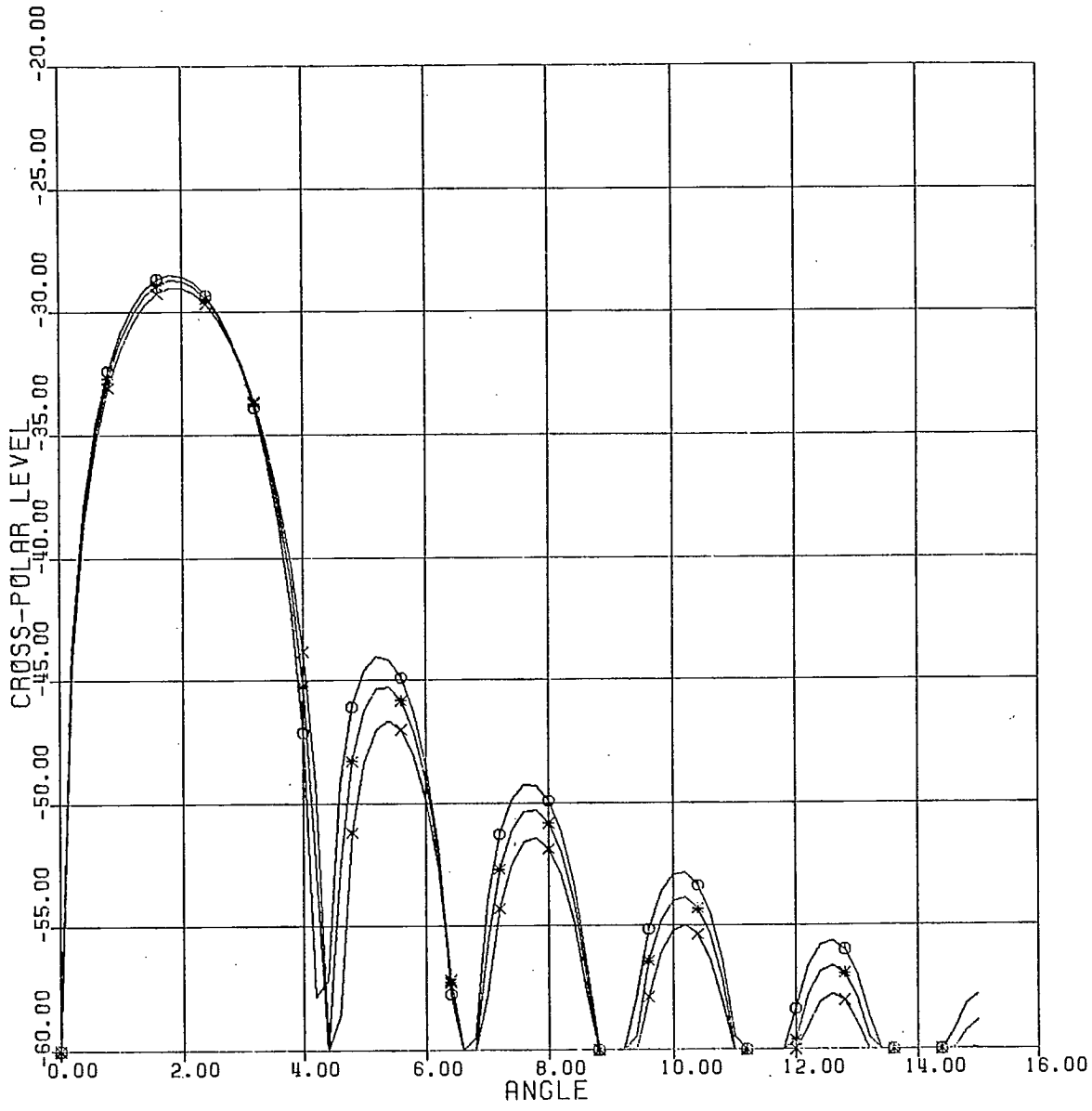
CROSS-POLAR LEVEL
-20.00
-25.00
-30.00
-35.00
-40.00
-45.00
-50.00
-55.00
-60.00
0.00
2.00
4.00
6.00
8.00
10.00
12.00
14.00
16.00
ANGLE
O M = 10
* M = 12
X M = 14
LAMDA=0.025 MT.
PLANE OF ASYMMETRY
Y POLARIZATION

Figure 134.

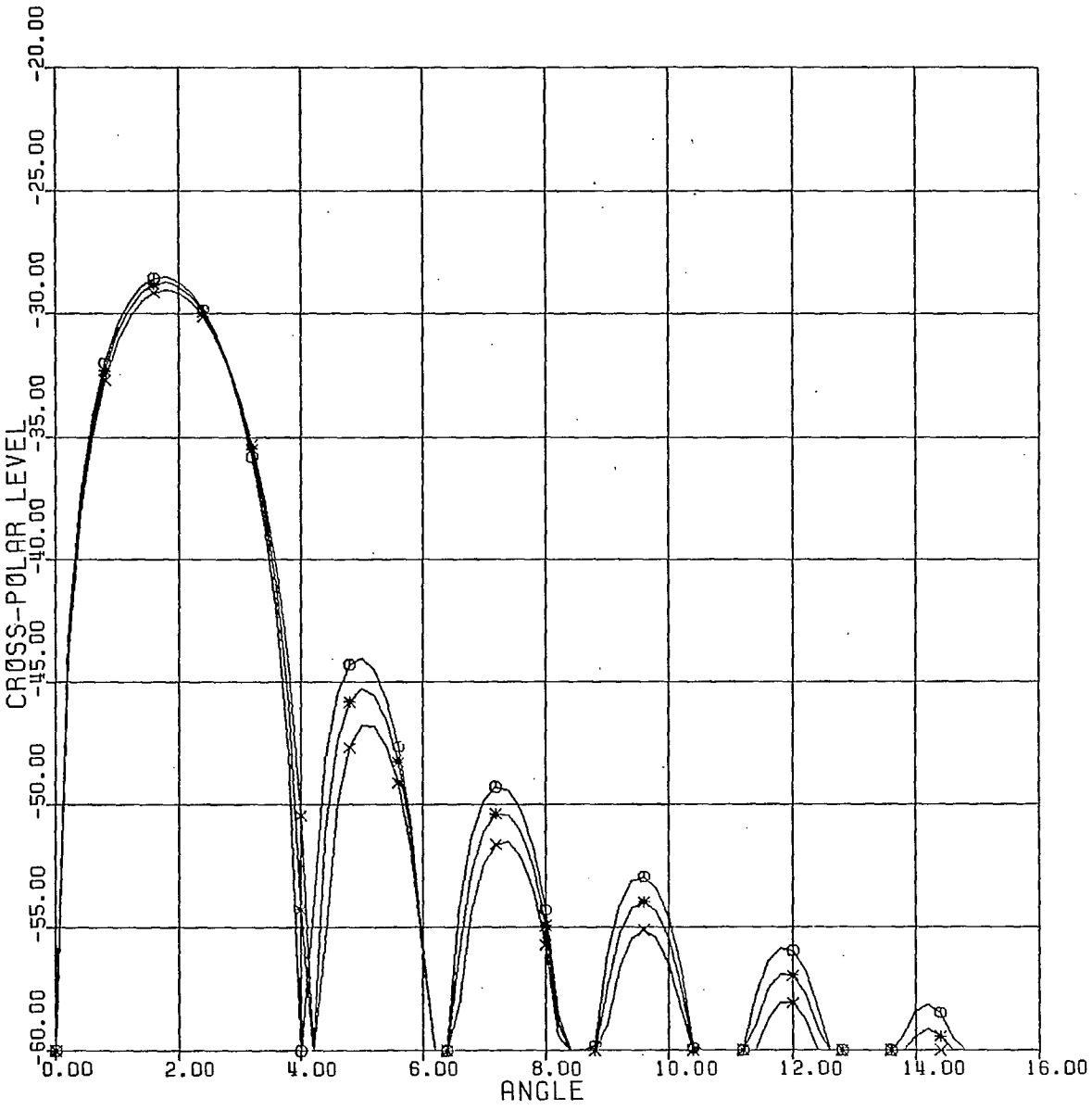
CRØSS-PØLAR LEVEL
-20.00
-25.00
-30.00
-35.00
-40.00
-45.00
-50.00
-55.00
-60.00
0.00
2.00
4.00
6.00
8.00
10.00
12.00
14.00
16.00
ANGLE
O M = 10
* M = 12
X M = 14
LAMDA=0.02982 MT.
PLANE OF ASYMMETRY
X POLARIZATION

Figure 135.

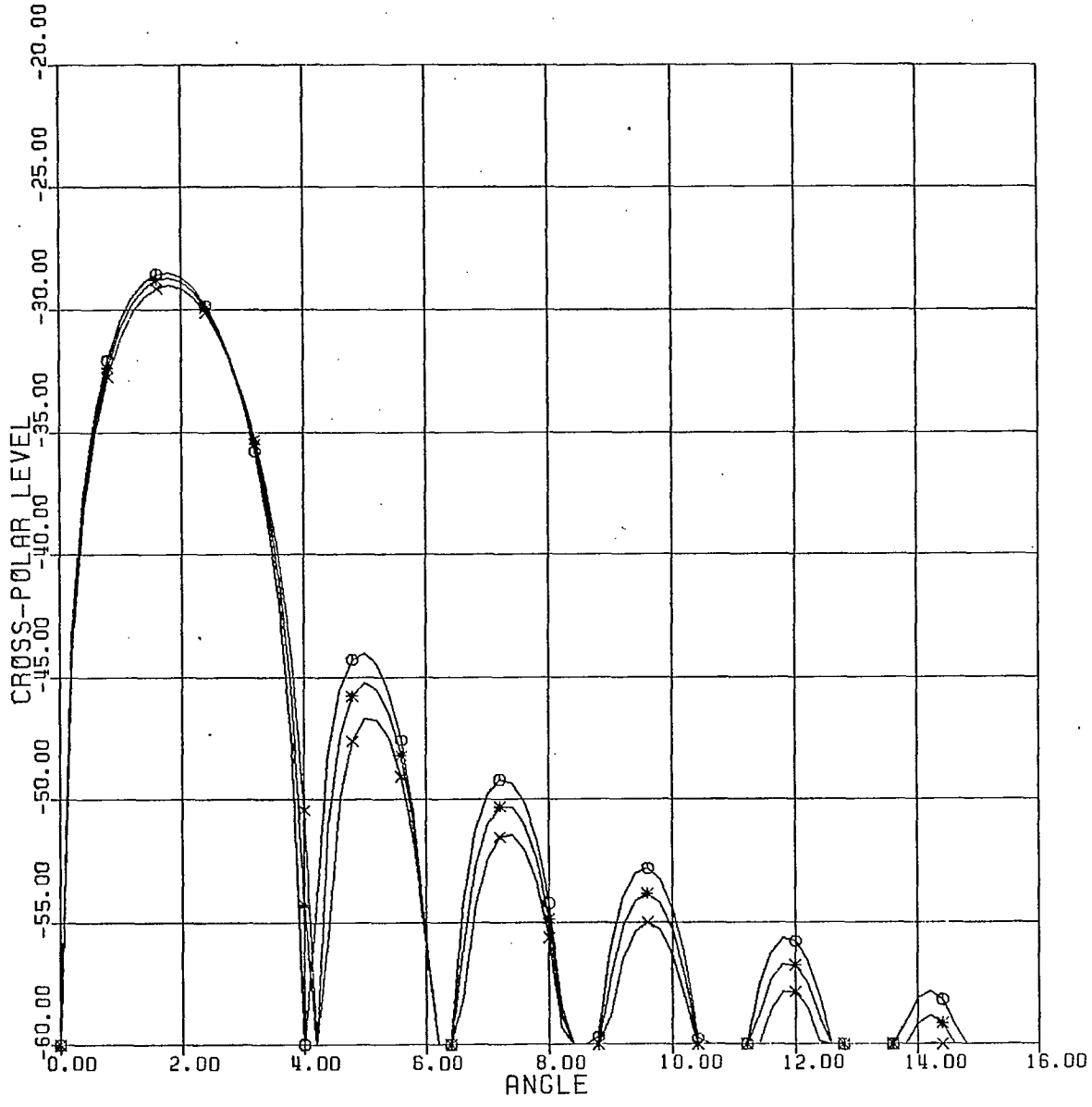
CROSS-POLAR LEVEL
-20.00
-25.00
-30.00
-35.00
-40.00
-45.00
-50.00
-55.00
-60.00
0.00
2.00
4.00
6.00
8.00
10.00
12.00
14.00
16.00
ANGLE
O M = 10
* M = 12
X M = 14
LAMDA=0.02382 MT.
PLANE OF ASYMMETRY
Y POLARIZATION

Figure 136.

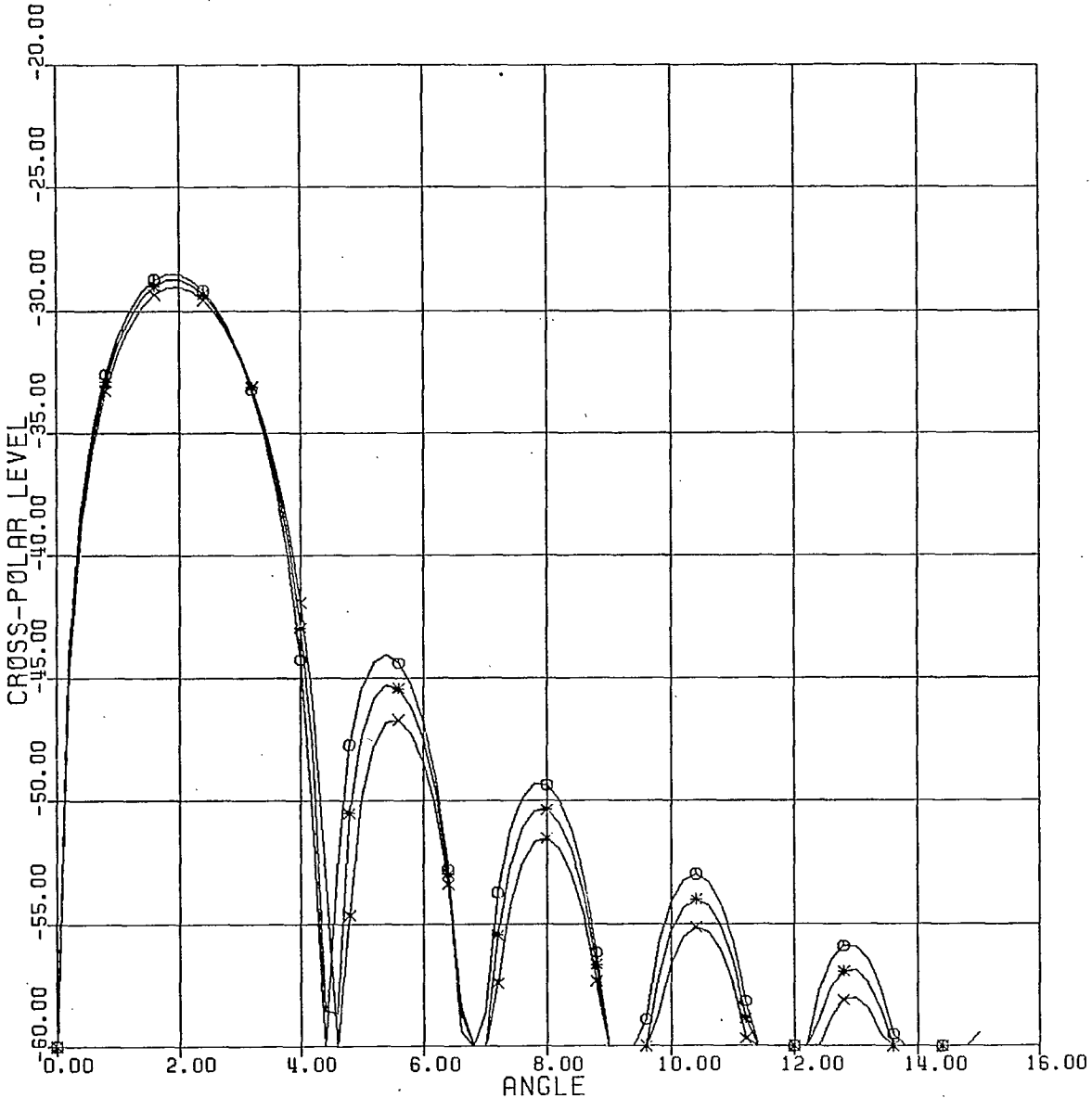
CROSS-POLAR LEVEL
-20.00
-25.00
-30.00
-35.00
-40.00
-45.00
-50.00
-55.00
-60.00
0.00
2.00
4.00
6.00
8.00
10.00
12.00
14.00
16.00
ANGLE
O M = 10
* M = 12
X M = 14
LAMDA=0.02584 MT.
PLANE OF ASYMMETRY
X POLARIZATION

Figure 137.

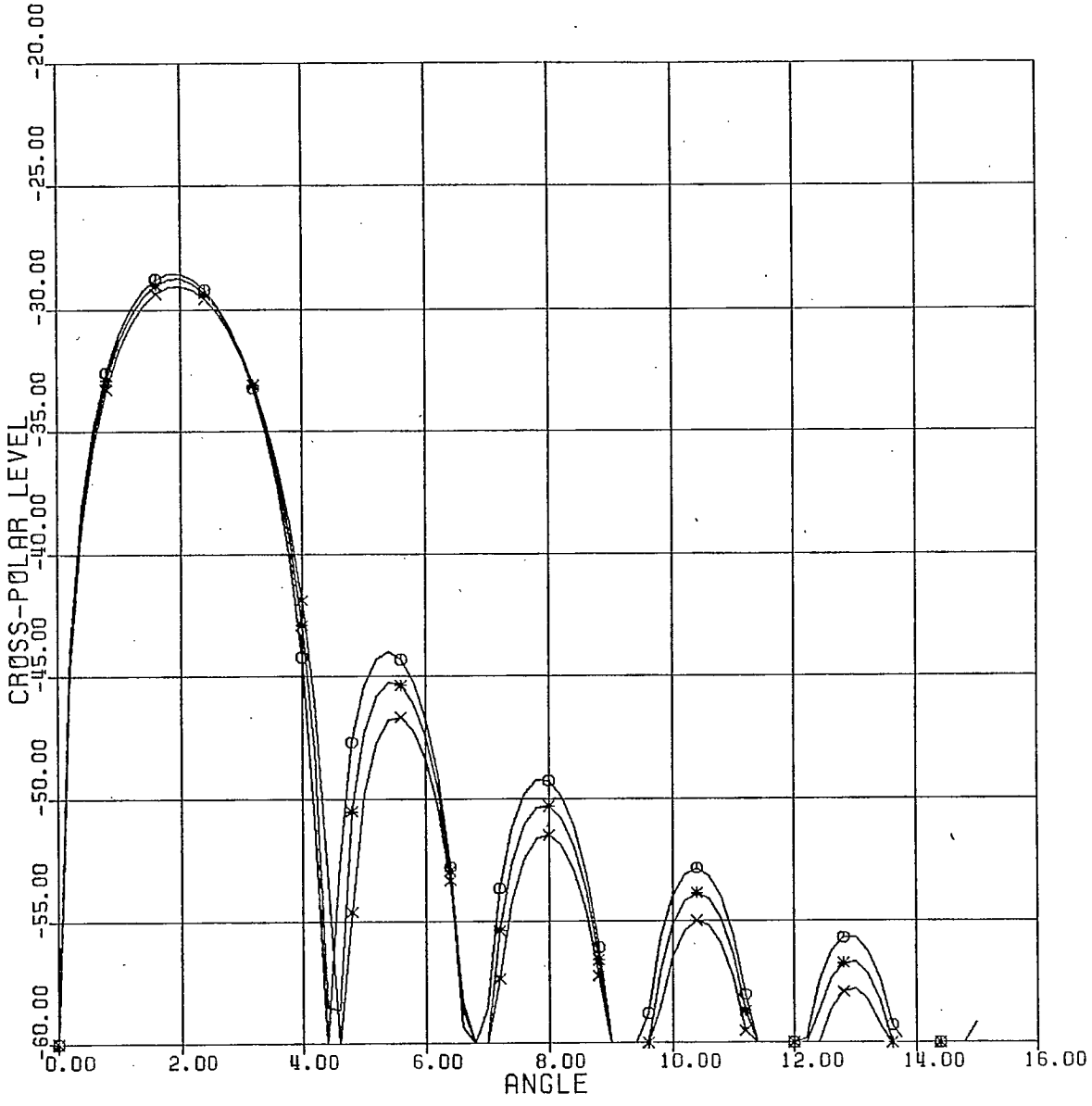
CROSS-POLAR LEVEL
-20.00
-25.00
-30.00
-35.00
-40.00
-45.00
-50.00
-55.00
-60.00
0.00
2.00
4.00
6.00
8.00
10.00
12.00
14.00
16.00
ANGLE
O M = 10
* M = 12
X M = 14
LAMDA=0.02584 MT.
PLANE OF ASYMMETRY
Y POLARIZATION

Figure 138.

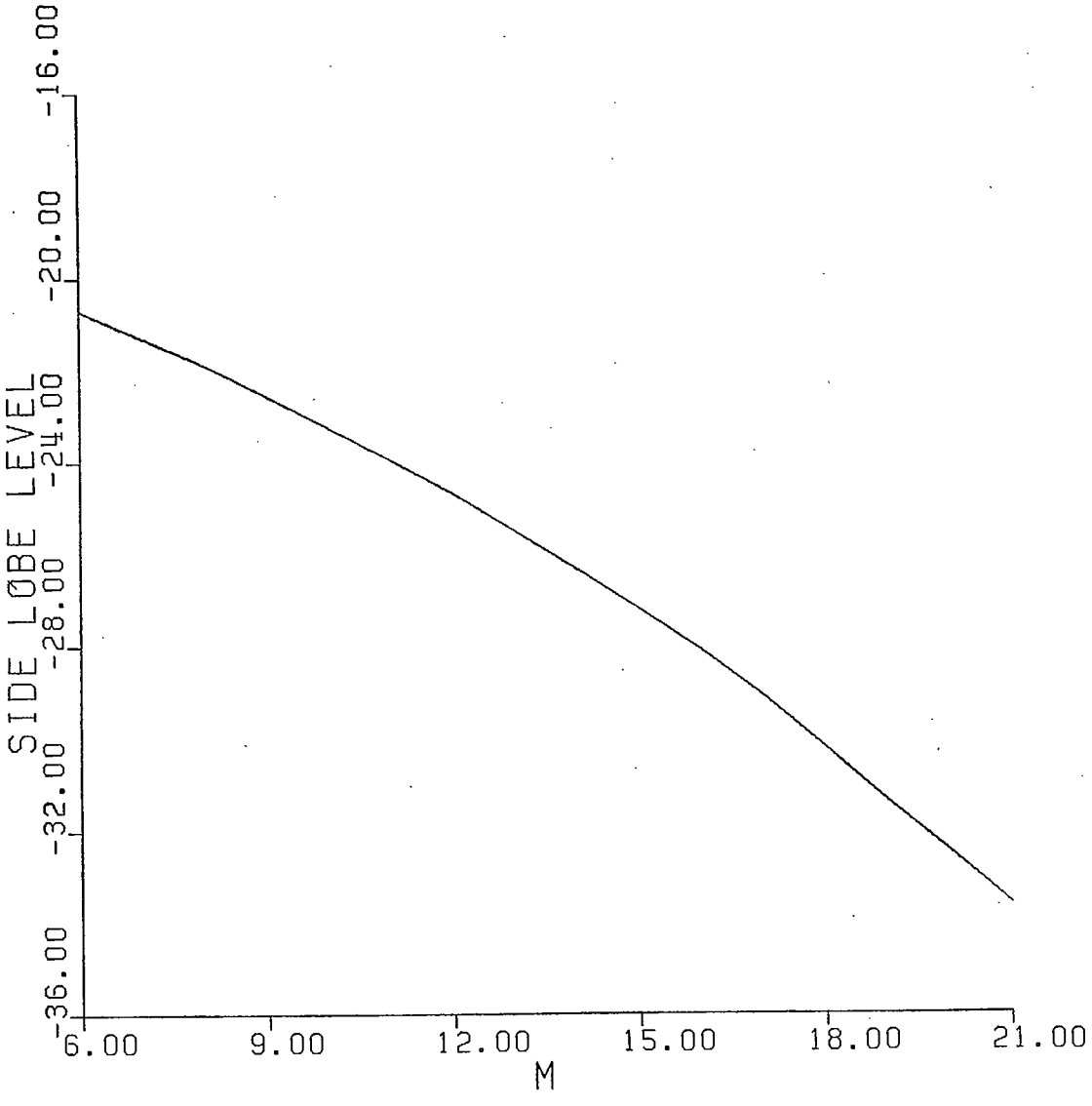

Figure 139. Sidelobe level as a function of feed illumination $\cos^{M}\theta$

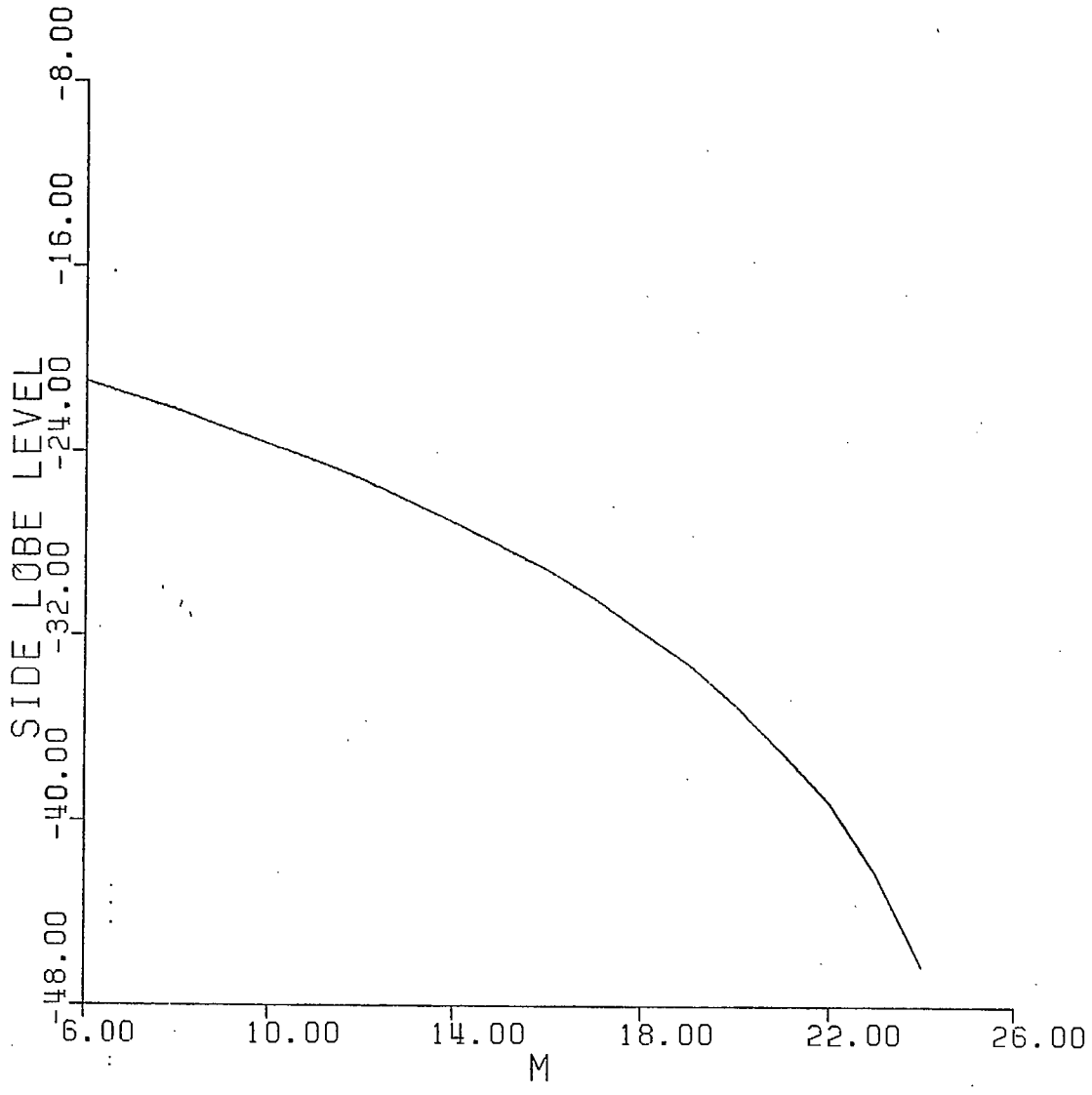

Figure 140. Sidelobe level as a function of feed illumination $\cos^{M}\theta$

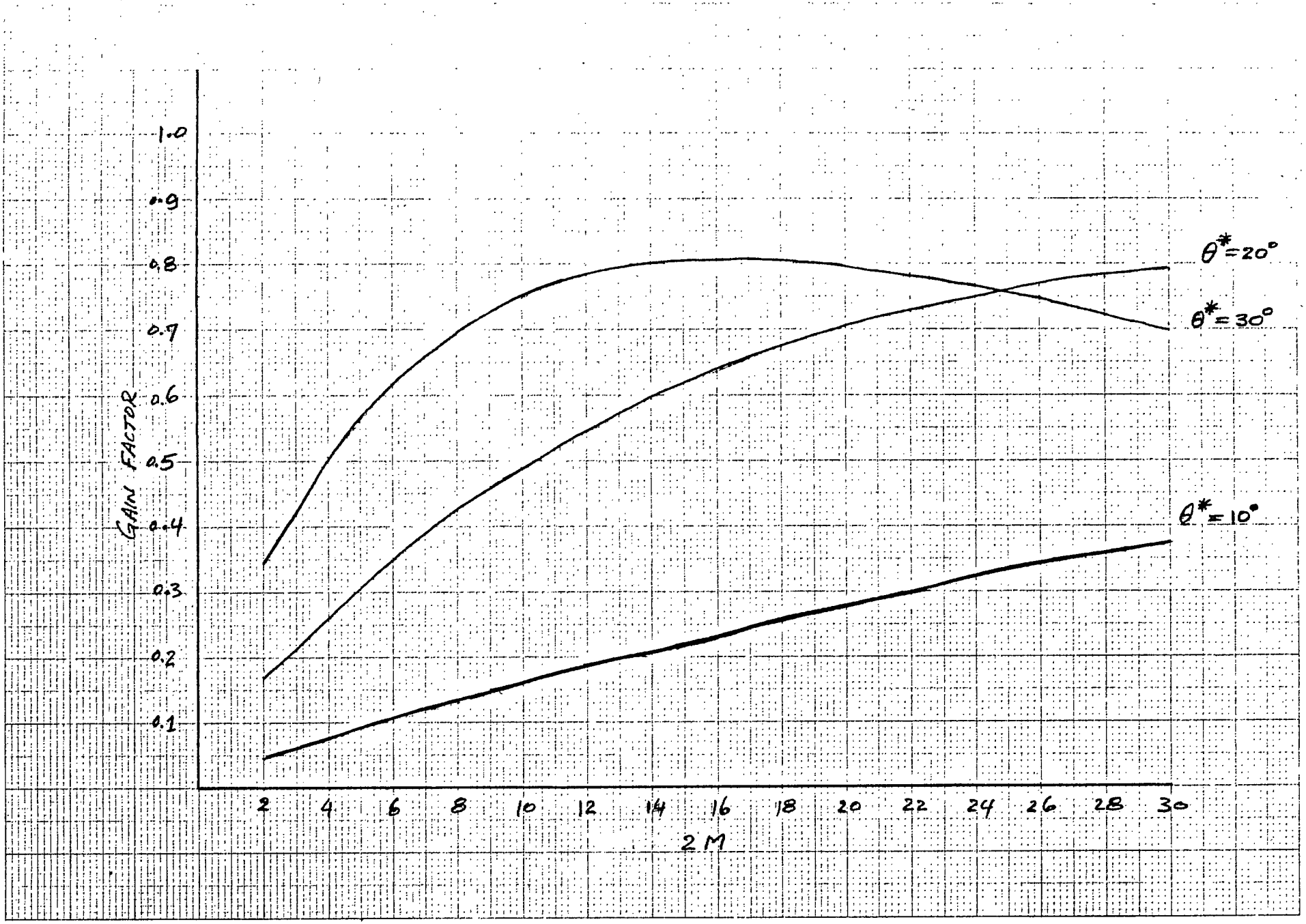

Figure 141(a). Dependance of the gain factor on angular aperture and feed pattern θo = 35°

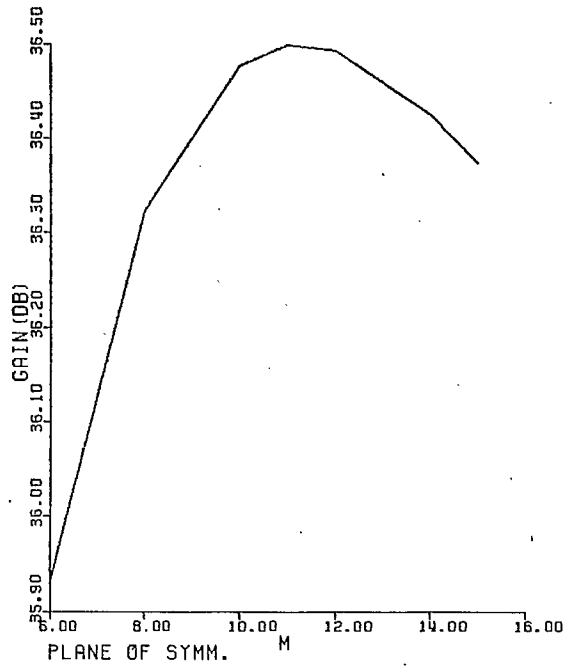

Figure 141(b). Dependence of the gain on feed illumination, $\cos^{m}\theta$

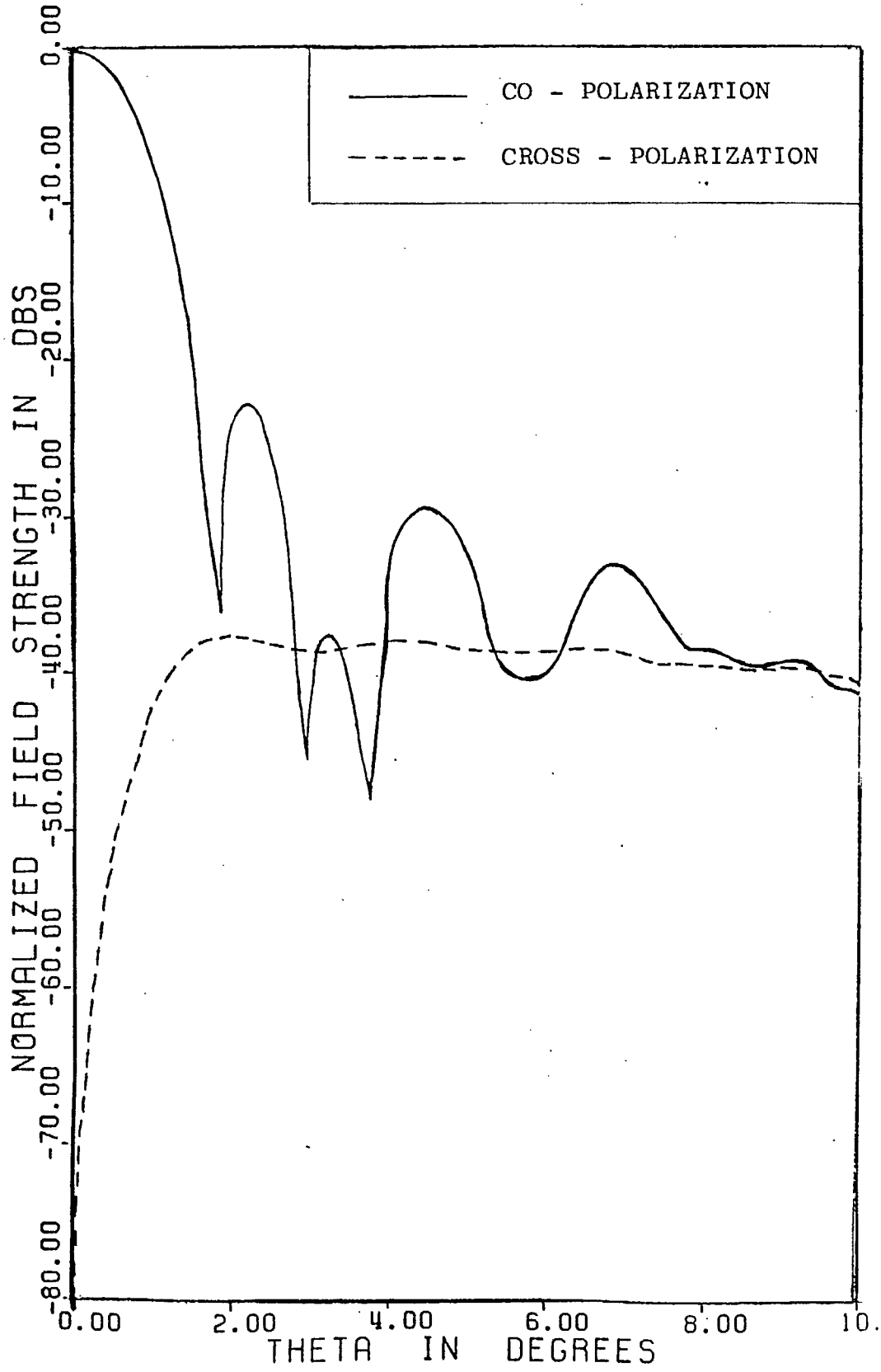

Figure 142. Quad copolar and cross-polar patterns of circular polarization feed with cosθ illumination, $\phi = 0^{o}$ and 90^{o}